

# Tissue-Engineered Liver Microreactor as an In Vitro Surrogate Assay for Gene Delivery

by

**Artemis Kalezi**

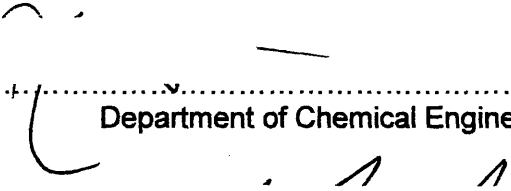
Diploma, Chemical Engineering  
National Technical University of Athens, 1997

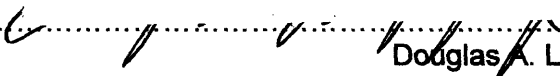
SUBMITTED TO THE DEPARTMENT OF CHEMICAL ENGINEERING IN PARTIAL  
FULFILLMENT OF THE REQUIREMENTS FOR THE DEGREE OF

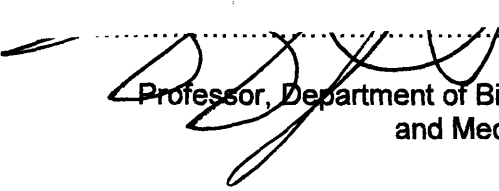
DOCTOR OF PHILOSOPHY IN CHEMICAL ENGINEERING  
AT THE  
MASSACHUSETTS INSTITUTE OF TECHNOLOGY

JUNE 2007

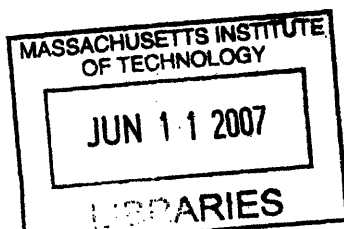
© 2007 Massachusetts Institute of Technology  
All rights reserved

Signature of Author:.....  
  
Department of Chemical Engineering, May 2007

Certified by:.....  
  
Douglas A. Lauffenburger  
Professor, Department of Chemical Engineering,  
Biological Engineering and Biology  
Thesis Supervisor

Certified by:.....  
  
Linda G. Griffith  
Professor, Department of Biological Engineering  
and Mechanical Engineering  
Thesis supervisor

Accepted by:.....  
William M. Deen  
Professor, Department of Chemical Engineering  
Chairman, Committee for Graduate Students



**ARCHIVES**

# **Tissue-Engineered Liver Microreactor as an In Vitro Surrogate Assay for Gene Delivery**

by

**Artemis Kalezi**

Submitted to the Department of Chemical Engineering  
on June 3, 2007 in Partial Fulfillment of the  
Requirements for the Degree of Doctor of Philosophy in  
Chemical Engineering

## **ABSTRACT**

The lack of correlation between in vitro and in vivo gene delivery experiments presents a significant obstacle in the progress of gene therapy studies by preventing the extrapolation of successful cell culture results into animals. This phenomenon has also been documented in the specific case of liver where standard hepatocyte culture systems fail to reliably predict the in vivo performance of gene delivery vectors. This is possibly a consequence of the loss of differentiated phenotype that these cells undergo when they are dissociated from their in vivo environment and cultured in vitro. This problem underscores the necessity for better in vitro models that can mimic the physiological environment and responses of in vivo liver tissue.

This thesis aimed at developing an alternative in vitro gene delivery assay based on the Tissue-Engineered Liver Microreactor, a culture system designed to facilitate the morphogenesis of three-dimensional tissue-like structures from isolated liver cells under continuous perfusion, maintain cell viability and hepatic functionality for long-term culture periods and enable repeated in situ observation with microscopy. We developed experimental assays to non-invasively detect and quantify gene delivery efficiency in the 3D environment of the microreactor culture based on the application of 2-photon microscopy and spectroscopy. These techniques provide a convenient platform for comparative analysis of different vectors.

Our main objective was to compare the gene delivery efficiency of an adenoviral vector (Ad5-CMV-EGFP) in the microreactor system and 2D hepatocyte monolayer culture. Quantitative assays were developed based on Real-Time PCR and RT-PCR to measure the levels of Ad vector uptake and transgene expression. The Ad mass transport in both systems was mathematically modeled to estimate the Ad uptake constant as a basis for comparison of delivery efficiency. This parameter was found to be significantly higher in the microreactor system, suggesting a more efficient mechanism of Ad internalization. Moreover, gene expression was measured in terms of transgene mRNA levels; the ratio of gene expression relative to Ad uptake was estimated as the basis for comparison of vector transcription efficiency. No significant difference was found between the 2 systems. These results provide some evidence that a more physiological culture system can yield different information (potentially more relevant to the in vivo situation) compared to standard in vitro culture.

Thesis supervisor: Linda G. Griffith

Title: Professor of Biological Engineering and Mechanical Engineering

Thesis supervisor: Douglas A. Lauffenburger

Title: Professor of Chemical Engineering, Biological Engineering and Biology



# Acknowledgements

First of all I would like to thank my advisors, Prof. Linda Griffith and Prof. Douglas Lauffenburger, for giving me the opportunity to work on this exciting project and for their invaluable guidance and support throughout my thesis. I would also like to thank my thesis committee members: Prof. William Deen for his valuable input on the mathematical modeling, Prof. Peter So for important feedback on the 2-photon microscopy experiments and Dr. Jack Wands for his expert advice on adenoviral gene delivery in liver and for providing the adenovirus vector for the preliminary experiments in this thesis.

There are several people that I must acknowledge whose contribution was important for the completion of this thesis. I am grateful to Dr. Karel Domansky who designed and built the miniaturized fiber optic spectrometer and the environmental control system, which were essential for several of my experiments; also for his help with the design and fabrication of the microreactor components and for many helpful discussions. Dr. Mark Powers, Dena Janigian and Carolyn Baker for teaching me the basics of the microreactor culture when I first joined the lab. Dan Bauer, Emily Larson and Albert Hwa for their technical assistance with the rat liver perfusions. Adam Capitano from the Griffith group and Tim Ragan from Prof. So's lab for their help with imaging during the preliminary 2-photon microscopy experiments presented in this thesis. All the members of the BPEC lab: Mark, Albert, Nate, Anand, Alexandria, Karel, Dena, Katy, Ben, Emily, Megan, Joe M., Joe S., Dan and many others for helpful discussions and a friendly working environment as well as the other members of the Griffith and Lauffenburger groups.

I would also like to thank Dr. Simon Watkins and Dr. Donna Stolz for hosting me in the Center for Biological Imaging at the University of Pittsburgh for almost a year, where I performed a large part of the 2-photon microscopy experiments presented in this work. I am grateful to Dr. Glenn Papworth for his help with the 2-photon imaging and to Mark Ross for his technical assistance with the rat liver perfusions. During that time Dr. Alan Wells hosted me in his lab and provided office space for me and I want to thank him and all the members of his group who made my stay in Pittsburgh very enjoyable.

Last but not least I want to thank my parents for their love and support throughout the good and the difficult times. I owe to them everything I have achieved.

Artemis Kalezi

# Table of Contents

<b>Abstract</b> .....	<b>2</b>
<b>Acknowledgements</b> .....	<b>3</b>
<b>Chapter 1: Background and Motivation</b> .....	<b>8</b>
1.1 Gene Delivery.....	9
1.1.1 Introduction.....	9
1.1.2 In vitro – in vivo lack of correlation.....	11
1.2 Gene Delivery in Liver.....	12
1.2.1 Liver as a target for gene delivery.....	12
1.2.2 In vitro – in vivo lack of correlation in liver gene delivery.....	13
1.3 Primary Hepatocytes Under In Vivo and In Vitro Conditions.....	14
1.3.1 Hepatocytes in vivo.....	14
1.3.2 Hepatocytes in vitro.....	15
1.4 The Tissue-Engineered Liver Microreactor: An Alternative In Vitro Assay for Gene Delivery?-Motivation and Overall Objective of Thesis.....	17
1.5 Adenovirus as a Gene Delivery Vector.....	19
1.6 Thesis Outline.....	22
1.7 References.....	24
<b>Chapter 2: The Tissue-Engineered Liver Microreactor</b> .....	<b>31</b>
2.1 Introduction.....	32
2.2 Microreactor Components and Assembly.....	34
2.3 Microreactor Design Parameters. Fluid Flow and Shear Stress Properties.....	38
2.4 Tissue Morphogenesis in the Liver Microreactor.....	39
2.5 Functional Behavior of Cells in the Liver Microreactor.....	42
2.6 Gene Delivery Experiments in the Microreactor.....	43
2.6.1 Experimental variables for gene delivery in the microreactor vs. 2D monolayer culture.....	43
2.6.2 Modification of the microreactor fluidic system design.....	44
2.6.3 Experimental procedure for Ad gene delivery in the microreactor.....	45
2.7 References.....	47
<b>Chapter 3: Materials and Methods</b> .....	<b>48</b>
3.1. Cell Culture.....	49

3.1.1 Rat Liver Perfusion and Hepatocyte Isolation.....	49
3.1.2 Composition of Hepatocyte Growth Medium (HGM) and DAPS Solution.....	49
3.1.3 Monolayer Hepatocyte Culture.....	50
3.1.4 Tissue-Engineered Liver Microreactor Culture.....	51
3.2 Adenoviral Gene Delivery.....	53
3.2.1 Adenovirus vector.....	53
3.2.2 Adenoviral Vector Infection in Monolayer Hepatocyte Cultures.....	54
3.2.3 Adenoviral Vector Infection in Liver Microreactor Cultures.....	57
3.3 DNA Extraction and Quantification.....	58
3.3.1 DNA Extraction and Purification.....	58
3.3.2 Quantification of Total DNA Content in Hepatocyte Culture Samples.....	58
3.3.3 Cellular DNA Content Measurements for Rat Hepatocytes.....	59
3.4 Quantitative Real-Time TaqMan PCR.....	62
3.4.1 Introduction.....	62
3.4.2 TaqMan PCR Assay Design and Optimization for Quantification of Adenoviral Vector Gene Delivery.....	65
3.5 RNA Extraction and Total RNA Quantification.....	75
3.5.1 RNA Extraction and Purification.....	75
3.5.2 DNase Treatment of RNA Samples.....	76
3.5.3 Quantification of Total RNA Content in Hepatocyte Culture Samples.....	76
3.5.4 Cellular RNA Content Measurements for Rat Hepatocytes.....	78
3.6 Quantitative Real-Time RT-PCR.....	80
3.6.1 Introduction.....	80
3.6.2 Quantitative real-time RT-PCR Assay Design for Quantification of EGFP mRNA Levels after Ad Vector Gene Delivery.....	82
3.7 Miniaturized Spectrometer System for Detection and Quantification of EGFP Expression in Microreactor Cultures.....	89
3.7.1 Introduction.....	89
3.7.2 Detection of EGFP expression with the Spectrometer.....	91
3.7.3 Monitoring the time course of EGFP expression in microreactor cultures with spectrometer measurements.....	91
3.7.4 Quantification of EGFP expression with spectrometer measurements.....	95
3.8 Two-Photon Laser Scanning Fluorescence Microscopy in Microreactor Cultures...	96

3.8.1 Introduction.....	96
3.8.2 Two-photon imaging in Hepatocyte Microreactor Cultures: Detection of EGFP expression; spatial distribution and temporal variations.....	98
3.8.3 Two-photon imaging of EGFP expression in Hepatocyte Microreactor Cultures: Quantification of Ad gene delivery efficiency in terms of % EGFP-expressing cells.....	101
3.9 References.....	110
<b>Chapter 4: Ad Gene Delivery in Hepatocyte Monolayer Cultures.....</b>	<b>114</b>
4.1 Introduction.....	115
4.2 Extracellular Mass Transfer and Cellular Uptake of AdEGFP Vector.....	116
4.2.1 Mathematical Model description.....	116
4.2.2 Experimental Approach to Evaluate the Uptake Rate Constant $k_u$ .....	123
4.2.3 Experimental Results and Analysis.....	127
4.3 Transgene (EGFP) Expression.....	134
4.3.1 Quantification of AdEGFP Gene Delivery Efficiency and Cell Viability with Fluorescence Microscopy.....	134
4.3.2 Quantification of EGFP mRNA Levels with Real-Time TaqMan RT-PCR.....	138
4.4 References.....	143
Appendix 4.1.....	144
Appendix 4.2.....	147
Appendix 4.3.....	155
Appendix 4.4.....	157
<b>Chapter 5: Ad Gene Delivery in Hepatocyte Microreactor Cultures.....</b>	<b>159</b>
5.1. Introduction.....	160
5.2 Extracellular Mass Transfer and Cellular Uptake of AdEGFP Vector.....	160
5.2.1 Tissue morphology and spatial distribution of Ad-infected hepatocytes in microreactor cultures.....	162
5.2.2 Mathematical Model Description.....	164
5.2.3 Experimental Results and Analysis.....	171
5.3 Transgene (EGFP) Expression.....	174
5.3.1 Quantification of EGFP expression with the Miniaturized Spectrometer System.....	176

5.3.2 Quantification of EGFP mRNA Levels with Real-Time TaqMan RT-PCR.....	178
5.3.3 Quantification of AdEGFP Gene Delivery Efficiency and Cell Viability with 2-photon microscopy.....	179
<b>Chapter 6: Conclusions and Future Directions.....</b>	<b>186</b>
6.1 Summary of Results-Conclusions.....	187
6.2 The Liver Microreactor as an in Vitro Assay for Gene Delivery.....	188
6.3 Future Directions.....	189
6.4 References.....	189

# **CHAPTER 1**

## **Background and Motivation**

## **1.1 Gene delivery**

### **1.1.1 Introduction**

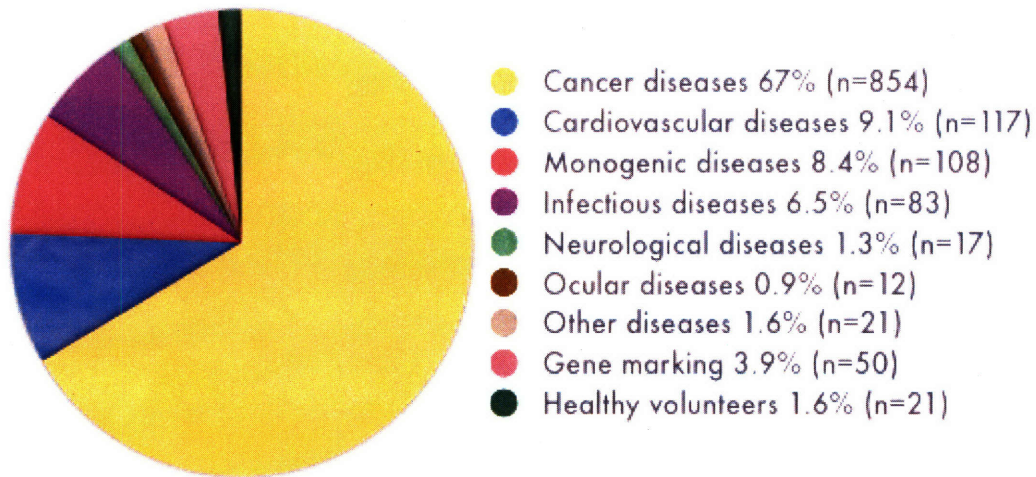
Human gene therapy aims at the treatment of inherited and acquired genetic diseases by delivering therapeutic genes into somatic cells. Consequently, it involves the identification and isolation of the appropriate genes, the selection of the target cells and the development of a technique to deliver the DNA to these cells. The advent of recombinant DNA technology and the identification of the genetic defects responsible for many disorders have made gene therapy become a reality and move from feasibility and safety studies in animals to clinical applications (Crystal, 1995). The first clinical trials began in 1990 and since then 1283 protocols have been approved for the treatment of a variety of diseases (Figure 1.1). Today about 600 protocols are underway involving thousands of patients.

However, although simple as a theoretical concept, gene therapy faces significant obstacles in practice. Clinical trials have demonstrated that gene transfer to humans is indeed feasible, but there is still no result that can be considered as a major success. Additionally, gene therapy has suffered major setbacks due to adverse effects on patients. First in 1999, with the death of 18-year-old Jesse Gelsinger, a participant in a gene therapy trial for ornithine transcarboxylase deficiency (OTCD); his death was the result of a severe immune response to an adenovirus vector. Then in 2003, two children successfully treated by gene therapy for X-linked severe combined immunodeficiency disease (X-SCID) with a retroviral vector, developed a leukemia-like condition, prompting the FDA to place a temporary halt on all gene therapy trials using retroviral vectors in blood stem cells.

An important problem that prevents gene therapy from becoming an established therapeutic strategy is gene delivery, namely the lack of efficient delivery systems and of sustained transgene expression (Verma and Somia, 1997). Ideally, a gene delivery vector should be capable of efficiently and stably transferring the gene(s) of interest specifically to the target cells, without inducing inflammation or host immune responses; moreover it should be easy to produce and purify (Crystal, 1995). Currently existing vectors can be divided into two classes: viral (e.g. retroviral, adenoviral) and nonviral vectors (naked DNA, liposomes, molecular conjugates). Unfortunately, none of these satisfy all of the above mentioned requirements. Retroviruses cannot transduce non-dividing cells and are mostly used in ex vivo strategies; moreover the random integration to the host genome involves the risk of insertional

(a)

### Indications Addressed by Gene Therapy Clinical Trials

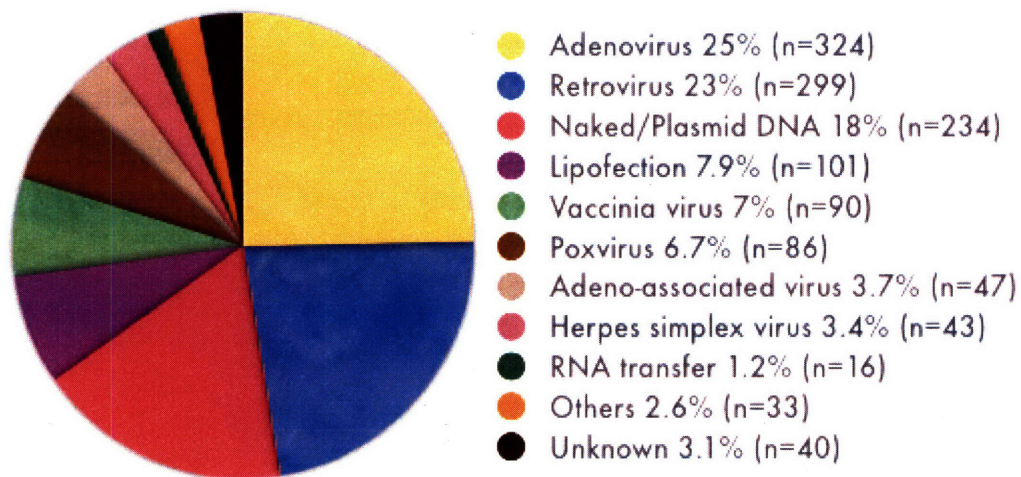


The Journal of Gene Medicine, © 2007 John Wiley and Sons Ltd

[www.wiley.co.uk/genmed/clinical](http://www.wiley.co.uk/genmed/clinical)

(b)

### Vectors Used in Gene Therapy Clinical Trials



The Journal of Gene Medicine, © 2007 John Wiley and Sons Ltd

[www.wiley.co.uk/genmed/clinical](http://www.wiley.co.uk/genmed/clinical)

**Figure 1.1.** Gene therapy clinical trials since 1989 categorized by: (a) indication and (b) vector type.



mutagenesis (as was the case in the above mentioned X-SCID trial). Adenoviral vectors, although very efficient, typically induce strong immune responses (which was the cause of the fatality in the OTCD trial). Nonviral vectors are less immunogenic and are able to carry genes of unlimited size but they have very low transfection efficiency compared to viral vectors. Moreover, there are problems that need to be overcome for all vectors, such as the lack of target specificity, transgene regulation, and efficient, large-scale production methods (Crystal, 1995).

Therefore, current efforts in gene therapy research focus to a large extent on vector design, namely the manipulation and modification of already existing systems in order to improve their properties and circumvent their limitations (mainly through the combination of features of different vectors), as well as the development of new synthetic systems.

### ***1.1.2 In vitro – in vivo lack of correlation***

In order for a new gene delivery system to reach the stage of human trials, extensive tests have to be performed that provide strong evidence of its potential clinical effectiveness and demonstrate that it can be used safely with no serious adverse effects. The first step in this process involves in vitro experiments, typically in monolayer cell cultures. Reporter genes are used (such as green fluorescent protein, luciferase,  $\beta$ -galactosidase) to allow the detection and quantification of gene expression. In this way the in vitro performance of the gene delivery vector can be determined in terms of its transduction efficiency (percentage of transduced cells) and the levels of transgene expression. The ability of the vector to provide stable transduction can also be studied by determining the persistence of gene expression with time.

The intermediate step between in vitro experiments and clinical trials consists of animal studies, where the in vivo performance of the vector is tested using a reporter gene or the therapeutic gene of interest. Gene expression can be assayed for example in the former case by removing and examining tissue sections or by whole animal imaging, or in the latter case, by measuring the levels of the therapeutic protein in the blood circulation, immunostaining of tissue sections, DNA, RNA and protein assays, etc.

In this stepwise experimental process, successful results are the necessary condition in order to proceed to the next stage. However, it is not a sufficient condition to guarantee an equally successful outcome. There have been several examples in which promising results from animal studies failed to be reproduced in humans or even the toxicity of the vector could not be

predicted (Crystal, 1995). Likewise, transfection efficiency in vitro and in vivo do not always correlate, making translation of positive results in cell culture into animals difficult (Luo and Saltzman, 2000). In general, many parameters could be responsible for the in vitro-in vivo lack of correlation. Typical in vitro cultures cannot duplicate the complexity of the whole organism; the interaction of the vector with blood components and the immune system, the dynamic flow conditions and possible anatomical barriers can affect gene delivery efficiency.

Moreover, the isolation and culture of cells in vitro alter the structural and functional properties that they exhibit as part of an organized tissue. For example, loss of differentiated phenotype can affect gene transfer efficiency; well-differentiated airway epithelial cells in vivo are more difficult to transfect with cationic liposomes than poorly differentiated primary cells in culture or certain cell lines (Matsui et al., 1997). Similarly, although adenoviral vectors (Ad) developed for the treatment of cystic fibrosis can deliver very efficiently transgenes to respiratory epithelial cells grown in culture, experiments in vivo indicated that the murine and human respiratory epithelium is poorly transduced by Ad (Pickles et al., 1996); a probable explanation is the absence, from well-differentiated airway epithelial cells, of the specific receptor and integrins that mediate attachment and internalization of Ad (Pickles et al., 1998).

Since the focus of this thesis is on liver, the following section will describe in more detail the particular aspects of liver gene therapy.

## **1.2 Gene Delivery in Liver.**

### ***1.2.1 Liver as a target for gene therapy***

The liver is an attractive target for gene therapy due to its unique morphological and functional characteristics. The liver is a highly vascularized organ, with 30 per cent of the cardiac output flowing through every minute (Guyton, 1981); therefore, intravenously injected gene delivery vectors can be rapidly delivered to it and the therapeutic proteins that are subsequently produced and secreted in the blood can be efficiently distributed systemically (Chiou et al., 1994). Due to its sinusoidal structure and its unusually permeable endothelium (cell lining with large fenestrations as opposed to a continuous layer) the parenchymal cells (hepatocytes) are in direct contact with the plasma and its constituents. This structure allows

direct access of large molecules and particles, such as adenoviral vectors, to hepatocytes (Ledley, 1995).

The liver is also the site of essential metabolic pathways; briefly, its metabolic functions include carbohydrate, fat and protein metabolism, storage of vitamins, as well as detoxification or removal of drugs, hormones and other substances (Guyton, 1981). As such, the liver is involved in many hereditary metabolic diseases (e.g. familial hypercholesterolemia,  $\alpha_1$ -antitrypsin deficiency, phenylketonuria), possible candidates for gene therapy. Moreover, it is responsible for the production and secretion of a large proportion of all plasma proteins, the major of which is albumin, followed by glycoproteins (e.g. coagulation factors) and lipoproteins. Of the 70g of proteins per liter of plasma in humans, approximately 55g are produced by hepatocytes, which, in contrast to other secretory cells, release them immediately (Feldman, 1994). Therefore, the liver is an ideal site for high level expression of therapeutic proteins (Chiou et al., 1994). An additional feature that makes hepatocytes attractive for gene therapy applications, is the ability for targeted gene delivery by taking advantage of the presence of a variety of liver-specific receptors (such as the asialoglycoprotein receptor) or by using hepatocyte-specific promoters (Ledley, 1995).

### ***1.2.2 In vitro – in vivo lack of correlation in liver gene delivery***

Many attempts have been made to deliver genes to the liver using a variety of approaches, ranging from naked plasmid DNA to sophisticated recombinant viral vectors. There have been no successful results in humans so far and the design of a method providing efficient and stable gene transfer and expression in human hepatocytes is still a challenging problem. The lack of in vitro vs. in vivo and animal vs. human experiment correlation is an important issue here too. Ferry and Heard (1998) mention some interesting examples. In one case, where DNA was complexed with polylysine coupled to an asialoglycoprotein moiety for liver-targeted gene delivery, the system was efficient in vitro and retained its targeting capability in vivo, but in vivo expression was low and transient. When an adenovirus particle was linked to the receptor-based DNA carrier to increase transfection efficiency, high expression was observed in primary hepatocyte cultures but improvements were limited in vivo.

In another case, where retrovirus-mediated gene delivery was combined with the stimulation of liver regeneration, high levels of efficiency and stability were obtained in rats; however liver regeneration kinetics differ between rodents and larger mammals leading to poor

results in dogs. Another example that demonstrates the inability of in vitro systems to predict correctly the performance of gene delivery vectors in vivo, involves ecotropic retroviral vectors which fail to transfect rat hepatocytes in vivo because the ecotropic receptor is not expressed by hepatocytes in vivo, even though it is expressed under normal culture conditions in vitro (Ledley, 1995). Moreover, in vitro studies aiming at the evaluation of vectors carrying hepatocyte-specific promoters for liver-targeted gene delivery are likely to be affected by the decrease in the rates of liver-specific transcription observed in culture systems of primary hepatocytes (Ponder et al., 1991). Similarly, hepatoma cell lines cannot be used because they fail to reproduce normal hepatic transcription patterns.

All the above mentioned examples lead to the conclusion that typical in vitro hepatocyte culture systems provide inadequate and sometimes unreliable information for accurate predictions of in vivo gene delivery performance. This is possibly a consequence of the changes in structure and function that these cells undergo when they are dissociated from their in vivo environment and cultured in 2D monolayers.

In order to further clarify this point, the following section describes in more detail the characteristic structure of hepatocytes, how it is tightly related to their unique functions, the effect of in vitro conditions on both, as well as the various in vitro methodologies developed to study and minimize this effect.

## **1.3 Primary Hepatocytes Under In Vivo and In Vitro Conditions.**

### ***1.3.1 Hepatocytes in vivo.***

Hepatocytes are large, cuboidal, epithelial cells (20-30 $\mu$ m diameter), which, in the liver, are arranged in one cell-thick plates. These plates are separated from each other by specialized capillaries called the sinusoids. In this configuration, the lateral sides of a hepatocyte establish contact with the neighboring hepatocytes and form the bile canaliculi, whereas the other sides face the sinusoids. A narrow space containing extracellular matrix components (space of Disse) separates the hepatocytes from the endothelial layer that lines the sinusoids (Maher and Bissell,

1993). This arrangement establishes the polarity of hepatocytes by dividing their plasma membrane into three, morphologically and functionally different regions: the sinusoidal (contact with blood, e.g. secretion of plasma proteins), the lateral (contact with neighboring hepatocytes through various kinds of junctions) and the canalicular or apical region (excretion of bile) (Le Bail et al., 1992; Feldman, 1994) (schematic in Figure 1.2). The maintenance of this architecture is essential for the hepatocyte's role in xenobiotic metabolism and biliary excretion.

The specialized morphology and function of hepatocytes is a consequence of the expression of a variety of liver-specific genes, which are regulated by a combination of transcription factors; the latter are believed to be determined and regulated by extracellular signals, soluble (hormones) and insoluble (extracellular matrix, cell-cell interactions).

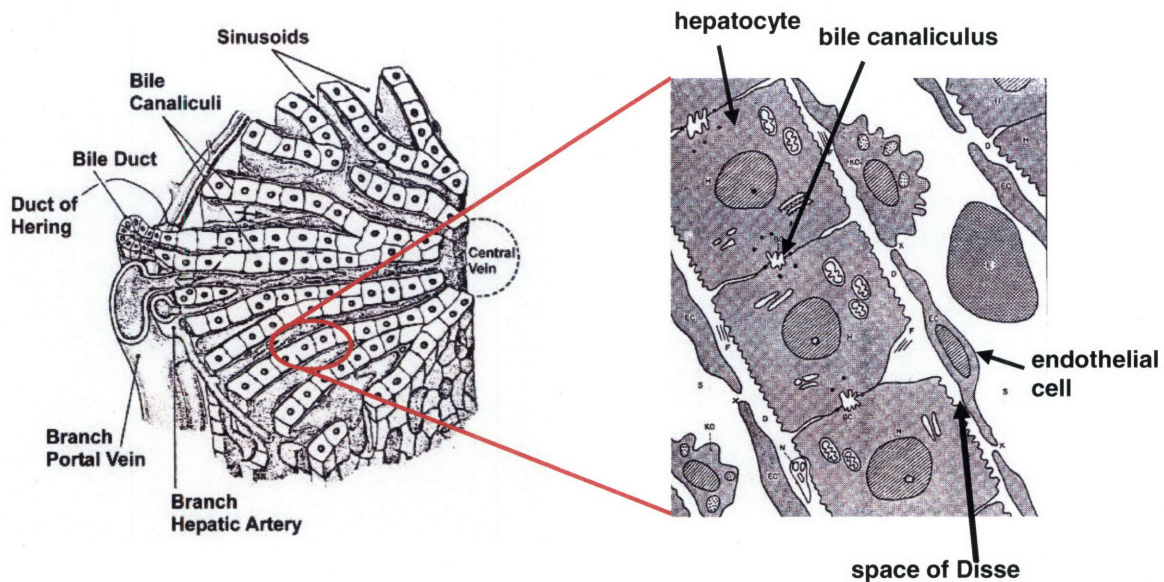


**Figure 1.2** Schematic of liver tissue architecture and hepatocyte microenvironment.

### 1.3.2 Hepatocytes *in vitro*.

When hepatocytes are isolated from the liver and maintained under conventional culture conditions, their recovery and adaptation to the *in vitro* environment is followed by the rapid loss of liver-specific functions (protein synthesis, xenobiotic metabolism, cytochrome P-450 induction), the failure to reestablish normal cell polarity and architecture, and the deterioration of

cell viability (Le Cluyse et al., 1996). As a result, the utility of in vitro hepatocyte cultures for pharmacological and toxicological studies is significantly reduced.

The progress in understanding the factors responsible for the hepatocyte phenotype has led to the development of various methods that aim at maintaining liver-specific function in vitro by providing suitable culture conditions. The four parameters that are considered to play an important role are: the culture medium and extracellular matrix composition, cell-cell interactions and, cell shape and tissue organization.

The design of alternative, more complex culture systems by manipulation of one or more of these parameters has led to considerable improvements in cell viability and function. These approaches range from determining an optimal combination and composition of culture medium and extracellular matrix, to the more sophisticated co-cultures, sandwich configurations and spheroidal aggregate cultures. Although the results have been very encouraging, none of these systems completely restores all liver-specific functions and structure. Moreover, their utility for various applications might be limited. For example, systems using complex substrata or sandwich configurations are not amenable to transfection with DNA constructs (Le Cluyse et al., 1996).

Among the culture systems mentioned above, spheroidal aggregates provide a three-dimensional cyto-architecture. Landry et al. (1985) first reported that, when rat liver cells are cultured on a non-adhesive substratum, they tend to aggregate into spheroids, where the different cell types sort out and reorganize, and extracellular matrix is deposited around each cell population. Moreover, they showed that these conditions enhance cell viability and allow the maintenance of some differentiated functions (albumin secretion, tyrosine aminotransferase induction) for an extended period of time. In addition to this, in spheroid cultures, DNA synthesis is suppressed even in the presence of growth factors, which suggests that hepatocytes remain in the  $G_0$  phase. This indicates the maintenance of differentiated function, given the reciprocal relationship between differentiation and growth. On the contrary, when the spheroids are dissociated to form a monolayer, cells enter the  $G_1$  phase and proceed through the cell cycle (Yuasa et al., 1993). Spheroids can also form in spinner flask cultures, a method significantly more efficient than formation in static dishes and which does not have any adverse effects in their functional properties (Wu et al., 1996).

The beneficial effect of spheroid culture on hepatocyte function has been attributed to the three-dimensional structure that approximates in vivo morphology, the production and deposition by the cells of ECM components, and the establishment of cell-cell interactions. This hypothesis is re-enforced by experimental evidence. TEM experiments indicate the presence of

tight junctions and microvilli-lined bile canaliculus-like channels (Wu et al., 1996). Moreover, another study suggests a correlation between cytoskeleton organization and cytochrome P-450 activity, a marker for the level of hepatocyte differentiated function (Hansen et al., 1998).

## **1.4 The Tissue-Engineered Liver Microreactor: A Promising In Vitro Assay for Gene Delivery? - Motivation and Overall Objective of Thesis.**

The information presented so far can be summarized into the following main points:

- There is a lack of correlation between in vitro and in vivo gene delivery experiments which prevents the extrapolation of successful cell culture results into animals and therefore presents a significant obstacle in the progress of gene therapy studies.
- In the particular case of liver, typical in vitro hepatocyte culture systems provide inadequate and sometimes unreliable information for accurate predictions of in vivo gene delivery performance. This is possibly a consequence of the loss of differentiated phenotype (exhibited by drastic changes in structure and function) that these cells undergo when they are dissociated from their in vivo environment and cultured in vitro.
- A variety of culture methods have been developed to foster the maintenance of the hepatocytic phenotype, but still, not all of the important functions of liver can be replicated at desired levels, prompting continued efforts to develop new methods. The culture of liver cells in 3D conditions has been shown to promote histotypic reorganization and maintenance of differentiated functions.

**The above statements underscore the necessity for better in vitro models in liver gene therapy studies, models that can mimic the physiological conditions and responses of in vivo liver tissue.**

This problem provided the motivation for this thesis. We are particularly interested in developing an alternative in vitro assay for gene delivery to hepatocytes, based on a three-dimensional tissue-engineered perfusion culture system, the 'liver microreactor'.

The liver microreactor, which was developed in the Griffith lab at MIT, supports the culture of liver cells in a 3D tissue-like environment that is continuously perfused with medium. Additionally, the design of this system allows repeated in situ observation with microscopy. It has been demonstrated that the microreactor facilitates the formation of hepatocellular aggregates reminiscent of the structures observed in vivo and that this leads to an enhanced and sustained maintenance of key liver-specific functions (Powers et al, *Biotech. Bioeng.* 2002 and *Tissue Eng.* 2002, Sivaraman et al., 2005).

**Therefore the liver microreactor provides a promising platform for in vitro studies of in vivo hepatocyte responses and consequently a promising platform for predicting the performance of gene delivery vectors in vivo.**

With the above statement as our premise we hypothesize that the liver microreactor, being a more in vivo-like culture, can yield qualitatively and quantitatively different (and possibly more relevant to the in vivo situation) information regarding the efficiency of gene delivery, compared to conventional hepatocyte culture.

The overall objective of this thesis is to test this hypothesis by comparing the performance of a gene delivery vector in the microreactor system and in standard 2D hepatocyte culture. For this study a first generation adenoviral vector carrying the gene for Enhanced Green Fluorescent Protein (EGFP) under the control of a CMV promoter was selected as the gene delivery vector. The following section describes the properties of Ad and EGFP as well as the reasons that make them appropriate choices for the experiments in this thesis.



## 1.5 Adenovirus as a Gene Delivery Vector.

The adenovirus (Ad) is a DNA virus that infects a wide range of mammalian and avian hosts and causes respiratory disease in humans. Among the at least 50 different human adenovirus serotypes that have been identified (Shenk, 1996), type 2 (Ad2) and type 5 (Ad5) have been most extensively studied and their genome has been completely sequenced; consequently they are the most widely used as gene delivery vectors (Douglas and Curiel, 1997).

Adenoviruses are icosahedral particles (20 triangular surfaces and 12 vertices), 70-100nm in diameter and consist of a protein shell (capsid) which surrounds a DNA-containing core. The capsid is composed of 240 hexons and 12 pentons (corresponding to the vertices). Pentons and hexons are surrounded by 5 and 6 neighbours respectively. Each penton contains a base which forms part of the surface of the capsid and a projecting fiber made up of a tail, a rodlike shaft and a terminal globular structure (knob) (Shenk, 1996; Douglas and Curiel, 1997).

Infection of cells with Ad is a stepwise process. Initially, the virus binds to a specific cell-surface receptor, the Coxsackievirus and Adenovirus Receptor (CAR) (Bergelson et al., 1997). It has also been reported that MHC class I can mediate Ad attachment via the fiber (Hong et al., 1997). Internalization of the Ad is mediated by the interaction of RGD sequences in the penton base with integrins  $\alpha_v\beta_3$  and  $\alpha_v\beta_5$ . After internalization, the Ad is localized within clathrin-coated vesicles and later in endosomes. Acidification of the endosomes allows the rapid movement to the cytoplasm. The transport of the virus across the cytoplasm to the nucleus is mediated by microtubules and is followed by a gradual disassembly of the capsid. When the Ad reaches the nucleus it attaches to the cytoplasmic side of the nuclear pore complex and releases the DNA inside the nucleus (Greber et al., 1999; Shenk, 1996; Douglas and Curiel, 1997). The mechanism of Ad entry in cells is remarkably efficient and has been extensively exploited to facilitate conjugate-mediated gene delivery (Curiel, 1994; Diebold et al., 1999; Horwitz, 1996).

The Ad genome consists of a single linear, double stranded DNA molecule (~36kb) and its expression consists of two phases. The early phase involves the early genes E1, E2, E3 and E4 (essential for DNA replication except for E3), whereas the late phase begins after the onset of DNA replication and involves the expression of Ad structural proteins. The Ad genome can be manipulated by recombinant technology. Therefore, Ad vectors for gene therapy can be constructed by substitution of the E1 region with a transgene. The deletion of the E1A and E1B early genes is required for safety reasons so that the recombinant Ad vector is replication

deficient. These vectors can be produced in complementary cell lines such as the 293 cells (Kovesdi et al, 1997). The recombinant adenoviruses are fully competent to infect human cells without the E1 region and transcribe the inserted sequences (Horwitz, 1996).

Adenoviral vectors have been extensively studied for their ability to deliver therapeutic genes *in vitro* and *in vivo* (Becker et al. 1994, Ferry and Heard, 1998), and their advantages and limitations have been identified. Moreover, they represent 25% of approved clinical trial protocols since 1989 (Figure 1.1b). The major advantages are their ability to deliver genes very efficiently to a wide variety of both dividing and non-dividing cells, their ability to accommodate up to ~7.5kb foreign DNA (when E1 and E3 regions are deleted) and the ease of production in high titers. Moreover, they have been previously used in humans as vaccines without any side effects (Kovesdi et al., 1997) and their stability in the bloodstream allows administration by intravenous injection (Douglas and Curiel, 1997).

However, the adenovirus DNA does not integrate into the host genome and remains inside the cell nucleus in an episomal state resulting in transient transgene expression and the need for repeated administration. In addition to this, the induction of host cellular and humoral immune responses leads to the rejection of the transduced cells and precludes the possibility of readministration of the same vector. Finally, a very important limitation of Ad vectors is the lack of cell-specific targeting. Several studies are directed towards the identification of the specific mechanisms responsible for these problems (Muruve et al., 1999; Harvey et al., 1999; Christ et al., 2000) and the development of various approaches to circumvent them and make Ad vectors more suitable for gene delivery. Such approaches include the development of “gutless” Ad vectors (i.e. in which all viral coding sequences have been deleted) to reduce immunogenicity, and the specific targeting of Ad by genetic or immunological modification of the fiber knob or by using cell-type-specific promoters (Douglas and Curiel, 1997; Kovesdi et al., 1997; Ferry and Heard, 1998; Sandig et al., 2000; Pastore et al., 1999; Sandig et al., 1996).

Although Ad vectors are able to infect a variety of cell types *in vitro*, when administered systemically *in vivo*, they accumulate predominantly in the liver. In fact the clearance of Ad5 from the bloodstream and its accumulation in the liver occur within minutes (Alemany et al. 2000). This phenomenon is attributed to the tissue architecture of the liver. The Ad particles reach the liver via the portal vein and come in contact with the hepatocytes only after passing through the liver sinusoids, which are lined by fenestrated endothelium. The sinusoidal fenestrations which have a size of about 100nm allow the access of the Ad particles (average diameter of 80nm) into the space of Disse and subsequently to the hepatocytes and Kupffer

cells (located on the inside of the sinusoids). Ad is efficiently taken up by both hepatocytes and Kupffer cells (Alemany et al. 2000; Schiedner et al. 2003).

As mentioned earlier, Ad vectors use a two-step mechanism to infect cells in vitro. The first step involves the attachment of the Ad fiber knob to the CAR receptor. The second step involves binding of the penton base RGD motifs to cellular integrins, leading to Ad internalization. In vivo however, other mechanisms have been found to play a more important role in the Ad infection of liver cells. It has been shown that when the interactions of Ad with CAR and integrins are ablated, transduction in the liver is not eliminated (Alemany and Curiel, 2001; Martin et al., 2003; Smith et al., 2002). Moreover, the Ad5 fiber shaft has been found to bind to heparan sulfate proteoglycans (HSPGs), resulting in liver transduction (Smith et al., 2003).

**Therefore, adenovirus appears to be an interesting vector choice for the experiments in this study and relevant to the hypothesis we want to examine.**

#### EGFP: Non-invasive reporter of gene expression

The choice of Enhanced Green Fluorescence Protein as a reporter for gene delivery is based on several properties. EGFP is a stable fluorophore, with excitation and emission spectra similar to those of fluorescein, therefore it is easy to use in fluorescence microscopy. It can be followed non-invasively in living cells, allowing the study of dynamic systems, in contrast to other reporters (chloramphenicol acetyltransferase, alkaline phosphatase,  $\beta$ -galactosidase, firefly luciferase) which require cell fixation and permeabilization or lack single cell resolution. Moreover, EGFP can be fused to promoters or proteins and expressed in cells as a reporter for gene expression or protein localization without any effect on the fluorescence properties or the protein function (*Spector et al., Cells: A laboratory manual*). GFP has been used extensively as a reporter in gene transfer studies in order to obtain quantitative information on transduction efficiency and levels of expression for different gene delivery vectors (Schaffer et al., 1997; Muldoon et al., 1997; Schaffer and Lauffenburger, 1998; Protzer et al., 1999) or to monitor gene expression in time relative to the different steps of the intracellular pathway of the vector (Leopold et al., 1998; Zelphati et al., 1999; Godbey et al., 1999; Schaffer et al., 2000).

## 1.6 Thesis Outline.

The main goal of this thesis is to compare adenoviral gene delivery in two in vitro hepatocyte culture systems, the 3D liver microreactor and 2D cell monolayers. As described in the previous section, Ad delivery (and in general gene delivery) is a stepwise process including attachment to the cell membrane, internalization, translocation to the nucleus and gene expression. The efficiency of any of these steps could potentially be dependent on the conditions of the culture environment, ultimately resulting in differences in the overall efficiency of gene delivery between the 2 culture systems. The approach that was followed in this thesis was to define Ad delivery efficiency in terms of two processes: the Ad vector uptake and the transgene expression (transcription and translation).

The Ad vector uptake process essentially lumps the steps of cell membrane attachment and internalization into one. Ad uptake is quantified by measuring the number of Ad genomic copies present inside the cells. The efficiency of this process is defined in terms of the 'uptake rate constant', a mathematical model parameter that incorporates the effects of extracellular Ad mass transfer. This parameter is fitted to the experimental data and becomes the basis of comparison between the 2 culture systems. This approach is essential due to the fact that in the liver microreactor the hepatocytes are cultured in a 3-dimensional environment continuously perfused with medium, whereas the monolayer culture is a 2-dimensional static system; therefore the differences in extracellular mass transfer need be taken into account.

The transgene expression is what ultimately determines the overall efficiency of gene delivery. In this thesis, gene expression is quantified in terms of the transgene (EGFP) mRNA levels. The ratio of mRNA levels over uptake levels is calculated as a measure of the efficiency of Ad delivery steps that follow the Ad uptake and as the basis of comparison between the 2 systems.

In order to carry out the above approach, mathematical models were developed to describe the Ad extracellular mass transfer and Ad uptake in the two culture systems. In the case of the liver microreactor, due to the complexity of the system, experimental methods were required to provide the necessary information for mathematical modeling of Ad mass transfer; in particular, a 2-photon microscopy protocol was developed to image the 3D tissue in order to detect and track Ad delivery via EGFP expression and provide spatial information. Finally, experimental assays were developed to measure (a) Ad genomic DNA levels (Quantitative

Real-Time PCR) and (b) Ad mRNA levels (Quantitative Real-Time RT-PCR). In addition to this, a spectrometric assay was developed to track the time course of EGFP expression in the microreactor and determine the optimum time point to conduct gene expression measurements.

The remainder of this thesis is organized as follows:

**CHAPTER 2 (The Tissue-Engineered Liver Microreactor):** the liver microreactor system is presented in detail. The design parameters and fabrication details are described, as well as the tissue morphogenesis, and functional behavior of the cells. Finally, the specific details related to the application of the microreactor for gene delivery experiments are presented.

**CHAPTER 3 (Materials and Methods):** comprises all the experimental procedures and protocols. The sections about PCR, RT-PCR, Spectrometry and Two-Photon Microscopy include theoretical background, assay design and optimization details, as well as experimental data (spectrometry, 2-photon microscopy).

**CHAPTER 4 (Quantitative Analysis of Ad Gene Delivery in Hepatocyte Monolayer Cultures):** The first part describes the mathematical model for Ad delivery in monolayer hepatocyte cultures and presents the experimental results and data analysis. The second part presents the gene expression results.

**CHAPTER 5 (Quantitative Analysis of Ad Gene Delivery in Hepatocyte Microreactor Cultures):** The first part presents the mathematical model development for Ad delivery in microreactor cultures and the experimental results and data analysis. The second part presents the gene expression results.

**CHAPTER 6 (Discussion and Future Directions):** This chapter summarizes the results obtained in this thesis and discusses the conclusions derived from the experimental data analysis as well as potential future directions for this research.

## 1.7 References

Alemaný, R. and Curiel D.T. (2001). CAR-binding ablation does not change biodistribution and toxicity of adenoviral vectors. *Gene Therapy*. **8**:1347–1353.

Alemaný, R., K. Suzuki, and D. T. Curiel. 2000. Blood clearance rates of adenovirus type 5 in mice. *J. Gen. Virol.* **81**:2605–2609.

Becker T.C., Noel R.J., Coats W.S., Gomez-Foix A.M., Alam T., Gerard R.D., and Newgard C.B., 1994. Use of Recombinant Adenovirus for Metabolic Engineering of Mammalian Cells. *Methods in Cell Biology*, Vol. 43, Academic Press Inc., p.161

Bergelson J.M., Cunningham J.A., Droguett G, Kurt-Jones E.A., Krithivas A., Hong J.S., Horwitz M.S., Crowell R.L., Finberg R.W., 1997. Isolation of a Common Receptor for Coxsackie B Viruses and Adenoviruses 2 and 5. *Science*, Vol. 275: 1320-1323

Block G.D., Locker J., Bowen W.C., Petersen B.E., Katyal S., Strom S.C., Riley T., Howard T.A., Michalopoulos G.K., 1996. Population Expansion, Clonal Growth, and Specific Differentiation Patterns in Primary Cultures of Hepatocytes Induced by HGF/SF, EGF and TGF $\alpha$  in a Chemically Defined (HGM) Medium. *The Journal of Cell Biology*, Vol.132, No.6, p.1133-1149

Chiou H.C., Spitalny G.L., Merwin J.R. and Findeis M.A., 1994. In Vivo Gene Therapy via Receptor-Mediated DNA Delivery. *Gene Therapeutics: Methods and Applications of Direct Gene Transfer*. Jon A. Wolff, Editor. Birkhauser Boston, p. 143

Christ M., Louis B., Stoeckel F., Dieterle A., Grave L., Dreyer D., Kintz J., Hadji D.A., Lusky M., Mehtali M., 2000. Modulation of the Inflammatory Properties and Hepatotoxicity of Recombinant Adenovirus Vectors by the Viral E4 Gene Products. *Human Gene Therapy*, 11: 415-427

Crystal, R.G., 1995. Transfer of Genes to Humans: Early Lessons and Obstacles to Success. *Science*, Vol. 270: 404-410

Curiel D.T., 1994. Receptor-Mediated Gene Delivery Employing Adenovirus-Polylysine-DNA Complexes. *Gene Therapeutics: Methods and Applications of Direct Gene Transfer*, Jon A. Wolff, Editor, Birkhauser Boston, p. 99-117

Davis I., Girdham C.H., O'Farrell P.H., 1995. A Nuclear GFP That Marks Nuclei in Living Drosophila Embryos; Maternal Supply Overcomes a Delay in the Appearance of Zygotic Fluorescence. *Developmental Biology*, 170: 726-729

Denk W., Strickler J.H., Webb W.W., 1990. Two-Photon Laser Scanning Fluorescence Microscopy. *Science*, Vol. 248: 73-76

Denk W., Piston D.W., Webb W.W., 1995. Two-Photon Molecular Excitation in Laser-Scanning Microscopy. *Handbook of Biological Confocal Microscopy*, edited by J.B. Pawley, Plenum Press, pp. 445-458

Diebold S.S., Lehrmann H., Kursa M., Wagner E., Cotten M., Zenke M., 1999. Efficient Gene Delivery into Human Dendritic Cells by Adenovirus Polyethylenimine Transfection. *Human Gene Therapy*, 10: 775-786

Douglas J.T. and Curiel D.T., 1997. Adenoviruses as Vectors for Gene Therapy. *Science and Medicine*, March/April 1997, p. 44-53

Feldman G, 1994. Tissue and Cellular Organization of the Liver. *Liver Gene Expression*, edited by Francois Tronche and Moshe Yaniv. R.G. Landes Company, p. 17

Ferry N and Heard J.M., 1998. Liver-Directed Gene Transfer Vectors. *Human Gene Therapy*, 9: 1975-1981

Godbey W.T., Wu K.K., Mikos A.G., 1999. Tracking the intracellular path of poly(ethylenimine)/DNA complexes for gene delivery. *Proc. Natl. Acad. Sci. USA*, Vol. 96, pp. 5177- 5181

Greber U.F., Nakano M.Y., and Suomalainen M., 1999. Adenovirus entry into cells. *Methods in Molecular Medicine, Vol. 21: Adenovirus Methods and Protocols*, Edited by: W.S.M. Wold, Humana Press Inc., p.217

Guyton A.C., 1981. The Liver as an Organ, *Textbook of Medical Physiology*, Philadelphia, W.B. Saunders Company, p. 771

Hansen L.K., Hsiao C.-C., Friend J.R., Wu F.J., Bridge G.A., Remmel R.P., Cerra F.B., Hu W.-S., 1998. Enhanced Morphology and Function in Hepatocyte Spheroids: A Model of Tissue Self-Assembly. *Tissue Engineering*, Vol. 4, pp. 65-74

Harvey B.-G., Worgall S., Ely S., Leopold P.L., Crystal R.G., 1999. Cellular Immune Responses to Healthy Individuals to Intradermal Administration of an E1<sup>-</sup> E3<sup>-</sup> Adenovirus Gene Transfer Vector. *Human Gene Therapy*, 10: 2823-2837

Hegenbarth S., Gerolami R., Protzer U., Tran P.L., Brechot C., Gerken G., Knolle P.A., 2000. Liver Sinusoidal Endothelial Cells Are Not Permissive for Adenovirus Type 5. *Human Gene Therapy*, 11: 481-486

Hong S.S., Karayan L., Tournier J., Curiel D.T., Boulanger P.A., 1997. Adenovirus type 5 fiber knob binds to MHC class I  $\alpha_2$  domain at the surface of human epithelial and B lymphoblastoid cells. *EMBO Journal*, 16: 2294-2306

Horwitz M.S., 1996. Adenoviruses. *Fields Virology*, Third Edition, p. 2149

Kovesdi I., Brough D.E., Bruder J.T. and Wickham T.J., 1997. Adenoviral vectors for gene transfer. *Current Opinion in Biotechnology*, 8: 583-589

Landry J., Bernier D., Ouellet C., Goyette R., Marceau N., 1985. Spheroidal Aggregate Culture of Rat Liver Cells: Histotypic Reorganization, Biomatrix Deposition, and Maintenance of Functional Activities. *The Journal of Cell Biology*, Vol. 101: 914-923

Le Bail B., Balabaud C., Bioulac-Sage P., 1992. 1. Anatomy and Structure of the Liver and Biliary Tree. *Hepatobiliary Diseases*, Springer-Verlag, pp. 1-38



LeCluyse E.L., Bullock P.L., Parkinson A., 1996. Strategies for restoration and maintenance of normal hepatic structure and function in long-term cultures of rat hepatocytes. *Advanced drug delivery reviews*, 22: 133-186.

Ledley F.D., 1995. Hepatic Gene Therapy. *Somatic Gene Therapy*, CRC Press, p.61

Leopold P.L., Ferris B., Grinberg I., Worgall S., Hackett N.R., Crystal R.G., 1998. Fluorescent Virions: Dynamic Tracking of the Pathway of Adenoviral Gene Transfer Vectors in Living Cells. *Human Gene Therapy*, 9: 367-378

Luo D. and W. Mark Saltzman, 2000. Synthetic DNA delivery systems. *Nature Biotechnology*, Vol. 18: 33-37.

Maher J.J. and Bissell D.M., 1993. Cell-matrix interactions in liver. *Seminars in Cell Biology*, Vol. 4, pp. 189-201

Martin, K., A. Brie, P. Saulnier, M. Perricaudet, P. Yeh, and E. Vigne. 2003. Simultaneous CAR- and  $\alpha_5\beta_1$  integrin-binding ablation fails to reduce Ad5 liver tropism. *Molecular Therapy* 8:485–494.

Matsui H., Johnson L.G., Randell S.H., and Boucher R.C., 1997. Loss of Binding and Entry of Liposome-DNA Complexes Decreases Transfection Efficiency in Differentiated Airway Epithelial Cells. *The Journal of Biological Chemistry*, Vol. 272, No. 2: 1117-1126.

Muldoon R.R., Levy J.P., Kain S.R., Kitts P.A., Link Jr. C.J., 1997. Tracking and Quantitation of Retroviral-Mediated Transfer Using a Completely Humanized, Red-Shifted Green Fluorescent Protein Gene. *BioTechniques*, 22: 162-167

Muruve D.A., Barnes M.J., Stillman I.E., Libermann T.A., 1999. Adenoviral Gene Therapy Leads to Rapid Induction of Multiple Chemokines and Acute Neutrophil-Dependent Hepatic Injury in Vivo. *Human Gene Therapy*, 10: 965-976

Pastore L., Morral N., Zhou H., Garcia R., Parks R.J., Kochanek S., Graham F.L., Lee B., Beaudet A.L., 1999. Use of a Liver-Specific Promoter Reduces Immune Response to the Transgene in Adenoviral Vectors. *Human Gene Therapy*, 10: 1773-1781

Pickles R.J., Barker P.M., Ye H., Boucher R.C., 1996. Efficient adenovirus-mediated gene transfer to basal but not columnar cells of cartilaginous airway epithelia. *Human Gene Therapy*, 7: 921-931

Pickles R.J., McCarty D., Matsui H., Hart P.J., Randell S.H., Boucher R.C., 1998. Limited entry of adenovirus vectors into well-differentiated airway epithelium is responsible for inefficient gene transfer. *Journal of Virology*, 72: 6014-6023

Piston D.W., 1999. Imaging living cells and tissues by two-photon excitation microscopy. *Trends in Cell Biology*, Vol. 9: 66-69

Ponder K.P., Dunbar R.P., Wilson D.R., Darlington G.J., Woo S.L.C., 1991. Evaluation of Relative Promoter Strength in Primary Hepatocytes Using Optimized Lipofection. *Human Gene Therapy*, 2: 41-52.

Powers, M.J., Domansky, K., Kaazempur-Mofrad, M.R., Kalezi, A., Capitano, A., Upadhyaya, A., Kurzawski, P., Wack, K.E., Beer-Stolz, D., Kamm, R., Griffith, L.G. (2002). A Microfabricated Array Bioreactor for Perfused 3D Liver Culture. *Biotechnology and Bioengineering* 78 (3), 257-269.

Powers, M.J., Janigian, D.M., Wack, K.E., Baker, C.S., Beer-Stolz, D., Griffith, L.G. (2002). Functional Behavior of Primary Rat Liver Cells in a Three-Dimensional Perfused Microarray Bioreactor. *Tissue Engineering* 8 (3), 499-513.

Protzer U., Nassal M., Chiang P.-W., Kirschfink M., Schaller H., 1999. Interferon gene transfer by a hepatitis B virus vector efficiently suppresses wild-type virus infection., *Proc. Natl. Acad. Sci. USA*, Vol. 96, pp. 10818-10823

Putnam D. and Langer R., 1999. Poly(4-hydroxy-L-proline ester): Low-Temperature Polycondensation and Plasmid DNA Complexation. *Macromolecules*, Vol. 32, No 11, pp. 3658-3662

Sandig V., Loser P., Lieber A., Kay M.A., Strauss M., 1996. HBV-derived promoters direct liver-specific expression of an adenovirally transduced LDL receptor gene. *Gene Therapy*, 3: 1003-1009

Sandig V., Youil R., Bett A.J., Franlin L.L., Oshima M., Maione D., Wang F., Metzker M.L., Savino R., Caskey C.T., 2000. Optimization of the helper-dependent adenovirus system for production and potency in vivo. *PNAS*, Vol. 97, No. 3, pp.1002-1007

Schaffer D.V., Neve R.L., Lauffenburger D.A., 1997. Use of the Green Fluorescent Protein as a Quantitative Reporter of Epidermal Growth Factor Receptor-Mediated Gene Delivery. *Tissue Engineering*, Vol. 3, No. 1, pp.53-63

Schaffer D.V. and Lauffenburger D.A., 1998. Optimization of Cell Surface Binding Enhances Efficiency and Specificity of Molecular Conjugate Gene Delivery. *The Journal of Biological Chemistry*, Vol. 273, No. 43, pp. 28004-28009

Schaffer D.V., Fidelman N.A., Dan N., Lauffenburger D.A., 2000. Vector Unpacking as a Potential Barrier for Receptor-Mediated Polyplex Gene Delivery. *Biotechnology and Bioengineering*, Vol. 67, No 5, pp. 598-606

Schiedner, G., S. Hertel, M. Johnston, V. Dries, N. van Rooijen, and S. Kochanek. 2003. Selective depletion or blockade of Kupffer cells leads to enhanced and prolonged hepatic transgene expression using high-capacity adenoviral vectors. *Mol. Ther.* 7:35–43.

Seglen P.O., 1976. Preparation of Isolated Rat Liver Cells. *Mehtods in Cell Biology*, 13: 29-83.

Shayakhmetov, D. M., S. Ni, A. Gaggar, V. Krasnykh, and A. Lieber. 2003. Binding of adenovirus knob to blood coagulation factors mediates CAR independent liver tropism. *Molecular Therapy* 7: S165.

Shenk T., 1996. Adenoviridae: The Viruses and Their Replication, *Fields Virology*, Third Edition, p. 2111

Sheppard C.J.R. and Shotton D.M., 1997. Confocal Laser Scanning Microscopy. BIOS Scientific Publishers Limited, pp. 87-90.

Sivaraman, A., Leach, J.K., Townsend, S., Iida, T., Hogan, B.J., Stolz, D.B., Fry, R., Samson, L.D., Tannenbaum, S.R., Griffith, L.G. (2005). A Microscale In Vitro Physiological Model of the Liver: Predictive Screens for Drug Metabolism and Enzyme Induction. *Current Drug Metabolism* **6**, 569-592.

Smith, T., N. Idamakanti, H. Kylefjord, M. Rollence, L. King, M. Kaloss, M. Kaleko, and S. C. Stevenson. 2002. In vivo hepatic adenoviral gene delivery occurs independently of the coxsackievirus-adenovirus receptor. *Molecular Therapy* **5**: 770–779.

Smith, T. A., N. Idamakanti, M. L. Rollence, J. Marshall-Neff, J. Kim, K. Mulgrew, G. R. Nemerow, M. Kaleko, and S. C. Stevenson. 2003. Adenovirus serotype 5 fiber shaft influences in vivo gene transfer in mice. *Human Gene Therapy*. **14**: 777–787.

Spector D.L., Goldman R.D., Leinwand L.A. Heterologous Expression of the Green Fluorescent Protein. *Cells: A Laboratory Manual. Volume 1*, Cold Spring Harbor Laboratory Press, pp. 78.1-78.21.

Verma, I.M. and Somia N., 1997. Gene therapy-promises, problems and prospects. *Nature*, Vol. 389: 239-242.

Wu F.J., Friend J.R, Hsiao C.C., Zilliox M.J., Ko W.-J., Cerra F.B., Hu W.-S., 1996. Efficient Assembly of Rat Hepatocyte Spheroids for Tissue Engineering Applications. *Biotechnology and Bioengineering*, Vol. 50, pp. 404-415

Yuasa C., Tomita Y., Shono M., Ishimura K., Ichihara A., 1993. Importance of Cell Aggregation for Expression of Liver Functions and Regeneration Demonstrated With Primary Cultured Hepatocytes. *Journal of Cellular Physiology*, 156: 522-530

Zelphati O., Liang X., Hobart P., Felgner P.L., 1999. Gene Chemistry: Functionally and Conformationally Intact Fluorescent Plasmid DNA. *Human Gene Therapy*, 10: 15-24

# **CHAPTER 2**

## **The Tissue-Engineered Liver Microreactor**

## 2.1 Introduction

The liver microreactor was developed in the Griffith lab at the Biotechnology Process Engineering Center at MIT (Powers et al, Biotechn. Bioeng. 2002, Tissue Eng. 2002). It is a microfabricated bioreactor designed to: 1) facilitate the morphogenesis of three-dimensional tissue-like structures from isolated liver cells under continuous perfusion, 2) maintain cell viability and hepatic functionality for long-term culture periods and 3) enable repeated in situ observation with microscopy and spectroscopy.

The basic component of this system is the cell scaffold, a thin (230 $\mu$ m) silicon sheet permeated from top to bottom by a regular array of channels and placed on top of a microporous filter. The filter is mechanically supported by a second scaffold (schematic shown in Figure 2.1a). The scaffold assembly is placed between the upper and lower compartments of a flow-through chamber. Each compartment has a pair of ports to allow the flow of culture medium. The medium flow is driven by a peristaltic pump into the upper compartment. The pressure drop between the upper and lower compartments is the driving force for perfusion flow through the scaffold channels and out of the lower compartment (Figure 2.1b). The chamber is connected to a medium reservoir and the medium is continuously re-circulated (Figure 2.1c). The design of the chamber includes an optical window for in situ optical imaging and spectroscopy during cell culture.

The cells are seeded into the channels of the cell scaffold where they are initially held in place by the filter. Aided by the adhesive properties of the channel wall surface, the cells attach to the walls and within 24-48 hours reorganize into 3D tissue structures, as described in more detail later in this chapter. Each channel represents an individual functional unit of the microreactor designed to mimic the acinus, the basic functional unit of the liver. All channels are uniform in size, are exposed to the same culture conditions and contain approximately the same number of cells. The total number of cells in a microreactor can be adjusted by increasing or decreasing the number of channels on the scaffold and by scaling up or down the dimensions of the chamber.

In the following sections of this chapter, the microreactor system is described in detail, including the scaffold and chamber design and fabrication, the fluid flow and shear stress properties, the morphogenesis of the tissue structures and the functional behavior of the cells. Finally, the specific details related to the application of the microreactor for gene delivery

experiments are presented, including an alternative design of the fluidic system, developed to maintain constant crossflow rates.

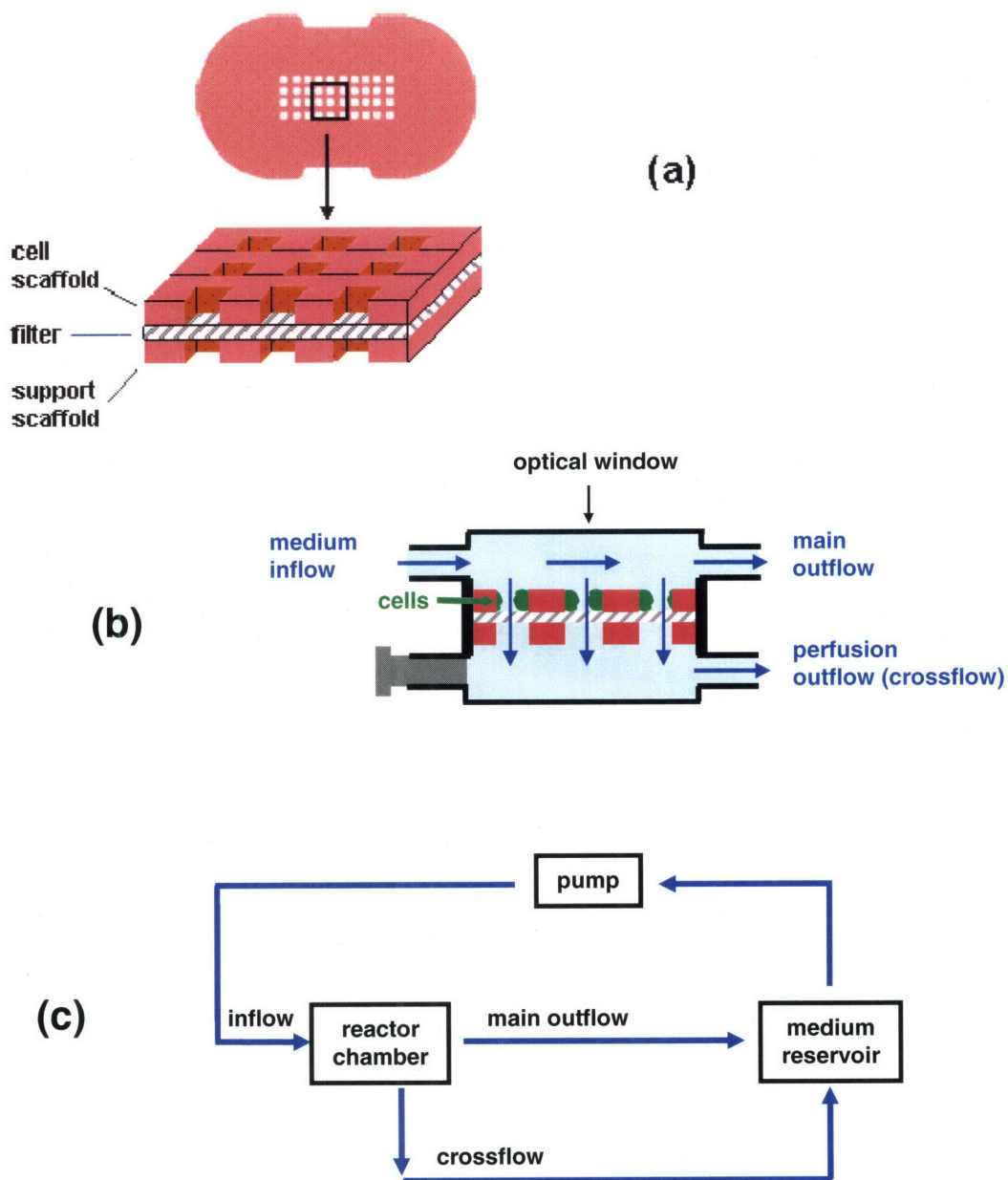
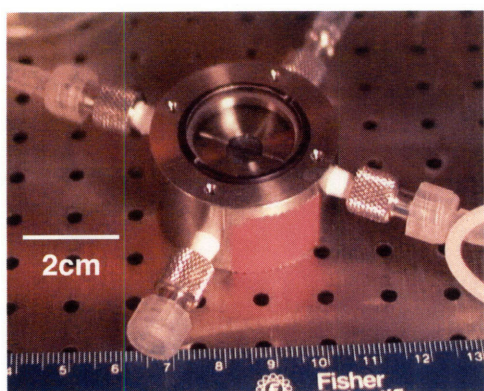


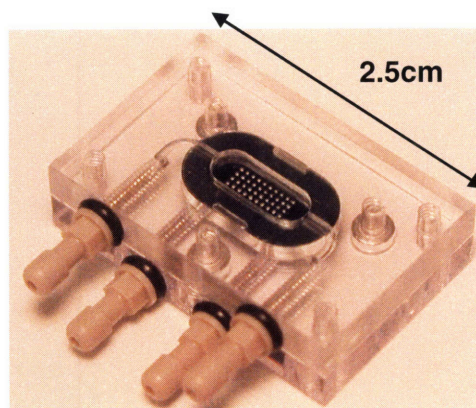
**Figure 2.1** Schematic of (a) scaffold, (b) microreactor chamber (cross-section) and (c) fluid circuit.

## 2.2 Microreactor Components and Assembly

Two different microreactor versions were used in this thesis. In the original version (Figure 2.2a) the chamber is fabricated from stainless steel and features cylindrical upper and lower compartments; additionally, the scaffold is circular with a diameter of 12.7mm and has 100 channels (10x10 array). The initial experiments of this project were performed with the original version. Those were preliminary experiments focused mainly on protocol development and optimization and are not all shown in this thesis. Some, of particular interest are included in Chapter 3 (sections 3.7 and 3.8). The remainder of the experiments presented in this thesis including the ones in Chapter 5 (quantitative analysis of gene delivery efficiency), were performed with the final version of the microreactor (Figure 2.2b). In this case the chamber is fabricated from polycarbonate and features oblong upper and lower compartments. The silicon scaffold is also oblong-shaped (12 x 7mm) and has 40 channels (4x10 array). The final version was designed for better control of fluid flow properties.



(a)



(b)

**Figure 2.2** Microreactor chamber (a) original version, (b) final version.



**The cell scaffold:** The scaffolds are fabricated by deep reactive ion etching (DRIE) of double-side polished 230 $\mu\text{m}$  thick  $\langle 100 \rangle$  boron-doped silicon wafers using standard methods as shown in Figure 2.3. During step 4 of the DRIE process the microchannel pattern is etched through the wafer with  $\text{SF}_6$  followed by passivation in  $\text{C}_4\text{F}_8$ . As a result the sidewalls of the channels are covered with a thin layer of fluoropolymer.

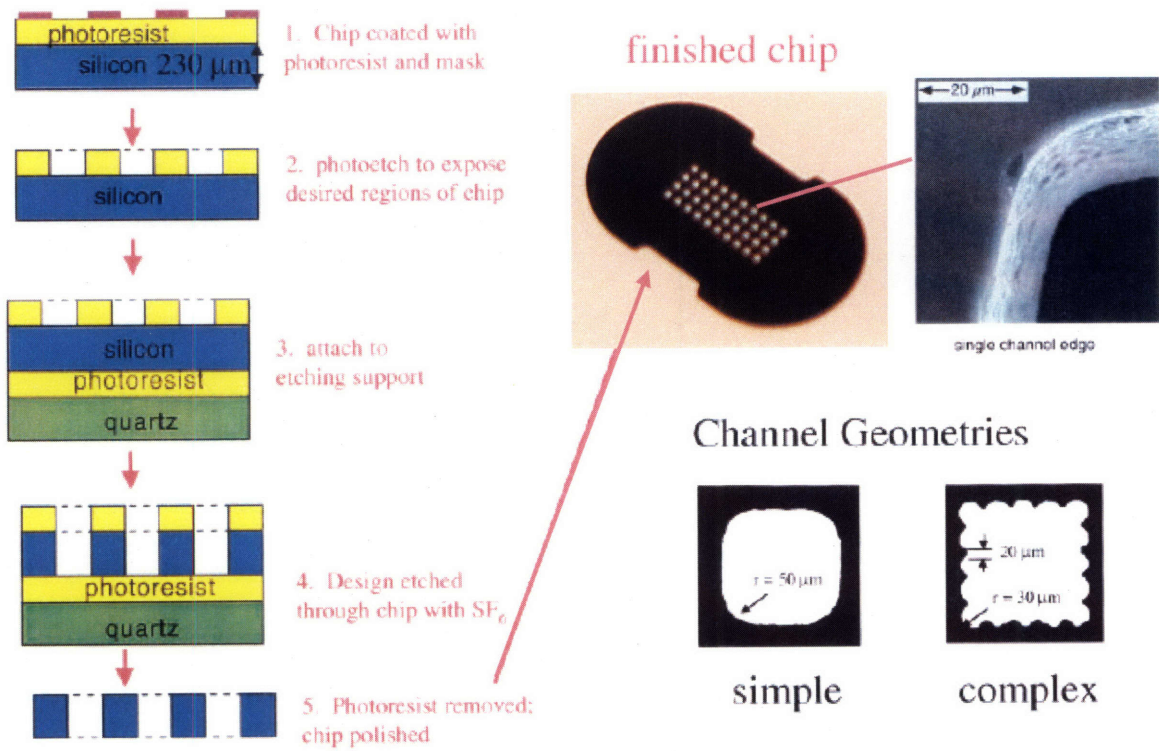


**Figure 2.3** Silicon scaffold fabrication by deep reactive ion etching (DRIE). Schematic of the DRIE process (left) and photos of the channel structure and geometries showing resolution (right). The upper photos include a photo of the overall scaffold structure (scaffold for the final version of the microreactor is shown) and a scanning electron micrograph depicting the texture of the channel walls. The lower micrographs show the resolution of features in two different channel geometries. The simple channel geometry was used in this thesis. (Figure adapted from Powers et al., *Biotechnol. Bioeng.*, 2002)

**The filter:** The microporous filter that is placed between the cell scaffold and the support scaffold is made from 5µm pore-size Durapore filter (Millipore Corp.) cut to the dimensions of the cell scaffold.

**The support scaffold:** In the case of the original version of the microreactor chamber, the support scaffold is cylindrical with a 12.7mm diameter and a 350µm thickness. It is fabricated from 316 stainless steel, using a combination of a wire and die-sinking electro-discharge machining (EDM) technique to create an array of channels complementary to the cell scaffold. In the case of the final version of the microreactor chamber, a second silicon scaffold (identical to the cell scaffold) served as the support scaffold.

**The microreactor chamber (original version):** The chamber is fabricated by conventional machining from stainless steel. The upper and lower compartments are cylindrical with an inner diameter of 7.6mm and both have a glass viewing window. The internal volume of the chamber is 1.9ml and its total weight including the scaffold assembly and the inlet connectors is 159g.

**The microreactor chamber (final version):** The chamber is custom-fabricated from polycarbonate by micromechanical milling and thermal diffusion bonding to create an 8 x 3mm oblong upper compartment with a 125µm thick optical window. The internal volume of the chamber is 102µl and its total weight including the scaffold assembly and the connectors (as shown in Figure 2.2) is 3.5g.

#### **Assembly of the microreactor:**

All microreactor components are sterilized by autoclaving except for the polycarbonate chamber compartments which are sterilized in 70% ethanol. Cell scaffolds are coated with 30µg/ml type I collagen (Vitrogen, Cohesion Technologies) and then rinsed in PBS. The filter is coated with 1% BSA (bovine serum albumin) in PBS. The scaffold assembly (cell scaffold - filter - support scaffold) is placed inside the pocket of the upper polycarbonate compartment together with other components such as gaskets and O-rings (as shown in Figure 2.4) and is secured by screwing together the two polycarbonate compartments.

The original version of the microreactor is assembled in a similar manner. The scaffold assembly is secured inside the stainless steel chamber with gaskets and O-rings and the upper and lower compartments are closed by securing the glass windows.

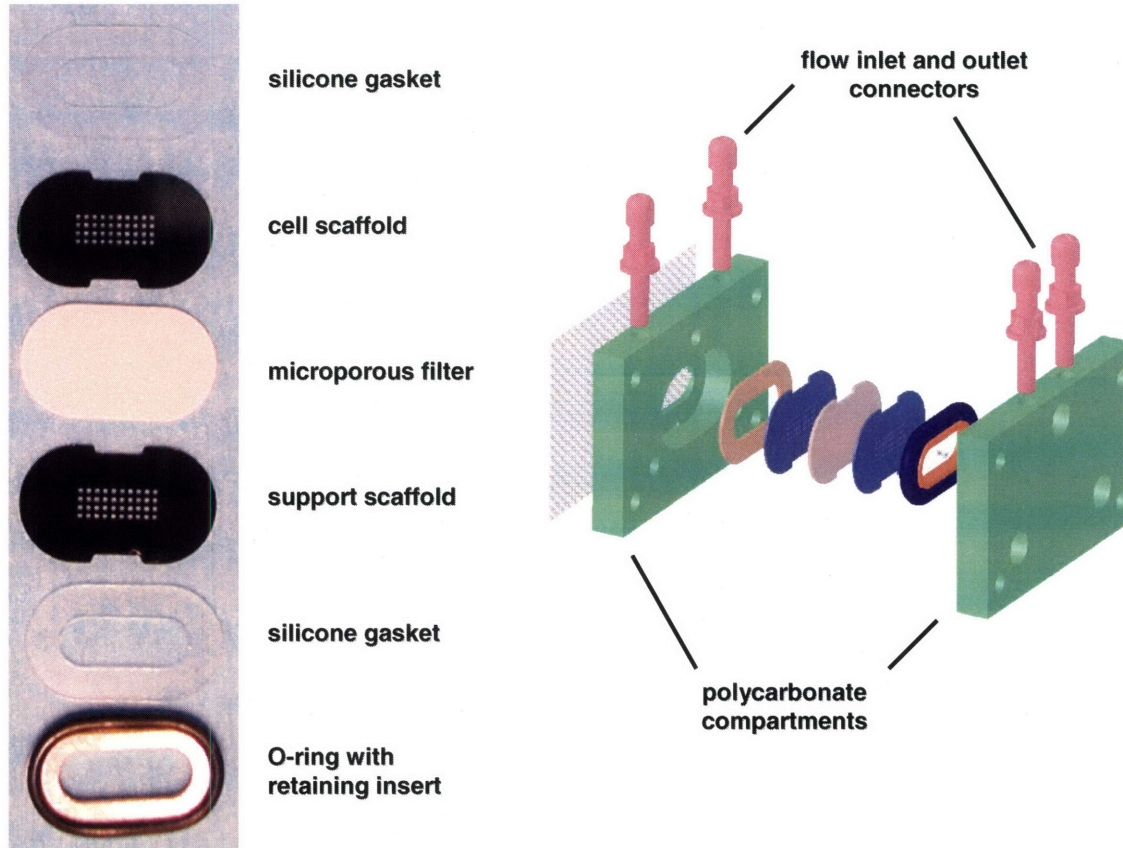


**Figure 2.4** Microreactor assembly (final version). Photo of the complete list of scaffold assembly components (left) and schematic of the assembly procedure (photograph and schematic by Dr. Karel Domansky).

### **The fluidic circuit:**

The microreactor chamber is connected to a medium reservoir with Silastic tubing (Dow Corning). The reservoir is made of glass in the case of the original version of the microreactor system and of polypropylene in the case of the final version. A mini peristaltic pump (Instech Inc.) is used to circulate the culture medium continuously as shown in the schematic of Figure 2.1. All the components of the fluid circuit are sterilized with autoclaving. The total volume of medium circulating in the system is 30ml for the original version and 20ml for the final version of the microreactor.

## 2.3 Microreactor Design Parameters. Fluid Flow and Shear Stress Properties

As mentioned earlier, one of the primary goals of the liver microreactor system is to enable the formation of structures with tissue-like morphology; that goal guided the selection of key design parameters. The dimensions of the scaffold channel cross section were selected as  $300\mu\text{m} \times 300\mu\text{m}$ , a sufficient length scale for tissue reorganization (Powers and Griffith, 1998). These dimensions were also empirically determined to support formation of 3D structures and fluid flow conduits (Powers et al., *Biotechn. Bioeng.* 2002). The channel depth ( $230\mu\text{m}$ ) was set to approximate the size of a hepatic capillary bed, the functional unit of *in vivo* liver tissue. Additionally, it ensures sufficient mass transport of oxygen and other nutrients to the cells even under conditions of zero perfusion flow (diffusion limitations arise at a depth of  $150\mu\text{m}$ ). The medium flow rate into the upper compartment of the chamber was set to  $1.0\text{ml}/\text{min}$  for the original microreactor version and  $0.5\text{ml}/\text{min}$  for the final version. These flow rates were chosen to minimize changes in oxygen concentration throughout the upper compartment. The crossflow rate at the start of the culture was measured as  $\sim 0.7\mu\text{l}/\text{min}$  per channel, a value that ensures sufficient nutrient supply to the tissue structures via convective transport. Another key characteristic of the microreactor design is the choice of a filter with low hydraulic permeability (in comparison to the tissue inside the channels). This means that the filter provides much higher resistance to the medium flow through the channels than the cell mass, ensuring homogeneous flow rate and mass transfer throughout the channel array.

Finite element modeling of fluid flow and shear stress distribution for the flow rates mentioned above showed relatively uniform velocity and shear stress values in the upper chamber compartment at the surface of the cell scaffold, especially in the case of the final microreactor version (oblong-shaped flow compartment). Fluid flow inside the scaffold channels was also mathematically modeled; the maximum shear stress the cells are exposed to is about  $0.7\text{dynes}/\text{cm}^2$  ( $0.07\text{Pa}$ ), a value that approaches the lower limit of the range of physiological values for *in vivo* endothelium (Powers et al., *Biotechn. Bioeng.* 2002).

## 2.4 Tissue Morphogenesis in the Liver Microreactor

The morphogenesis of the 3D tissue structures in the microreactor channels is determined by the adhesive properties of the surface of the channel walls as well as by the geometry and dimensions of the channels. As mentioned earlier, the silicon scaffold is coated with type I collagen before the chamber is assembled. Collagen adsorbed on hydrophobic substrates can be used to control hepatocyte adhesion as well as cell morphology (Powers and Griffith, 1998; Powers and Griffith-Cima, 1996). Due to the fabrication process of the silicon scaffolds, the channel walls are coated with a thin layer of fluoropolymer. Hepatocytes were found to attach and spread on fluoropolymer-covered silicon surfaces coated with collagen I but not in the absence of collagen. Additionally, hepatocytes did not adhere strongly to silicon surfaces, with or without adsorbed collagen (Powers et al., *Biotechn Bioeng.* 2002). Therefore adsorption of collagen on the silicon scaffolds enhances preferential adhesion of hepatocytes to the channel walls.

In this thesis, microreactor cultures were established from primary rat hepatocytes pre-aggregated into spheroids. The process is shown in the schematic of Figure 2.5. Primary hepatocytes are harvested from rat liver using the 2-step collagenase perfusion procedure; a hepatocyte enriched fraction is isolated and seeded in spinner flasks. Three days later, the spheroids that have formed are harvested and seeded into the microreactor channels which have been coated with collagen (seeding procedure described in detail in Chapter 3). Within 24-48hrs the spheroids attach to the channel walls, and reorganize to form large structures throughout the depth of each channel. These tissue structures remain stable for several days undergoing only minor changes.

Figure 2.6a shows a light micrograph of hepatocyte tissue structures in microreactor channels 3 days after spheroid seeding. The image is taken by focusing at the top of the silicon scaffold with a 5X objective lens. The silicon scaffold appears black, the cells are grey and the areas devoid of cells are bright. A variety of 3D structures are formed. Very often these structures have a doughnut-like shape with a fluid flow conduit in the middle of the channel; in other cases there are structures that span the middle of the channel creating more than one flow conduit as shown in Figure 2.6b. This is a fluorescence micrograph of microreactor structures stained with Calcein AM (green cytoplasm – live cells) and ethidium homodimer (red nuclei – dead cells) after 2 weeks of culture which shows that the cells display high viability



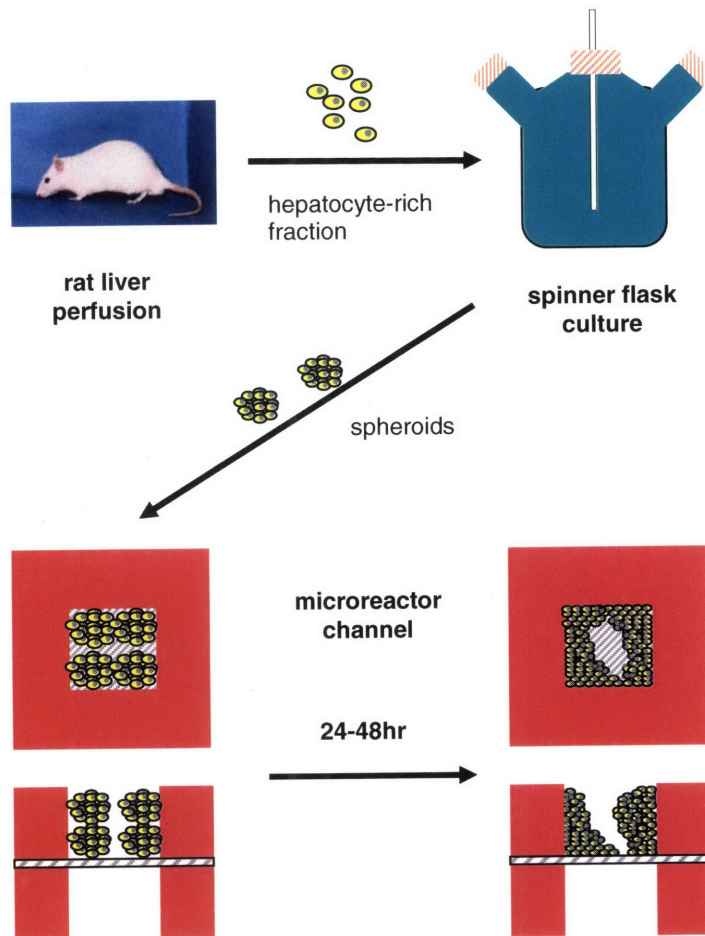


**Figure 2.5** Schematic of 3D tissue structure formation in microreactor channels from hepatocytes isolated from rat liver with collagenase perfusion.

(Powers et al., Tissue Eng. 2002). Viable, healthy cells (colored dark blue) are also observed in toluidine blue-stained histological sections of tissue structures in the microreactor channels (Figure 2.6c). Although a hepatocyte-enriched fraction was used to form the spheroids that were seeded in microreactors, scanning electron micrographs of 3D structures inside the channels suggested the presence of a heterogeneous cell population at the fluid-tissue interface. Cells with the cobblestone morphology of vessel endothelium have also been observed (Figure 2.6 d and e).

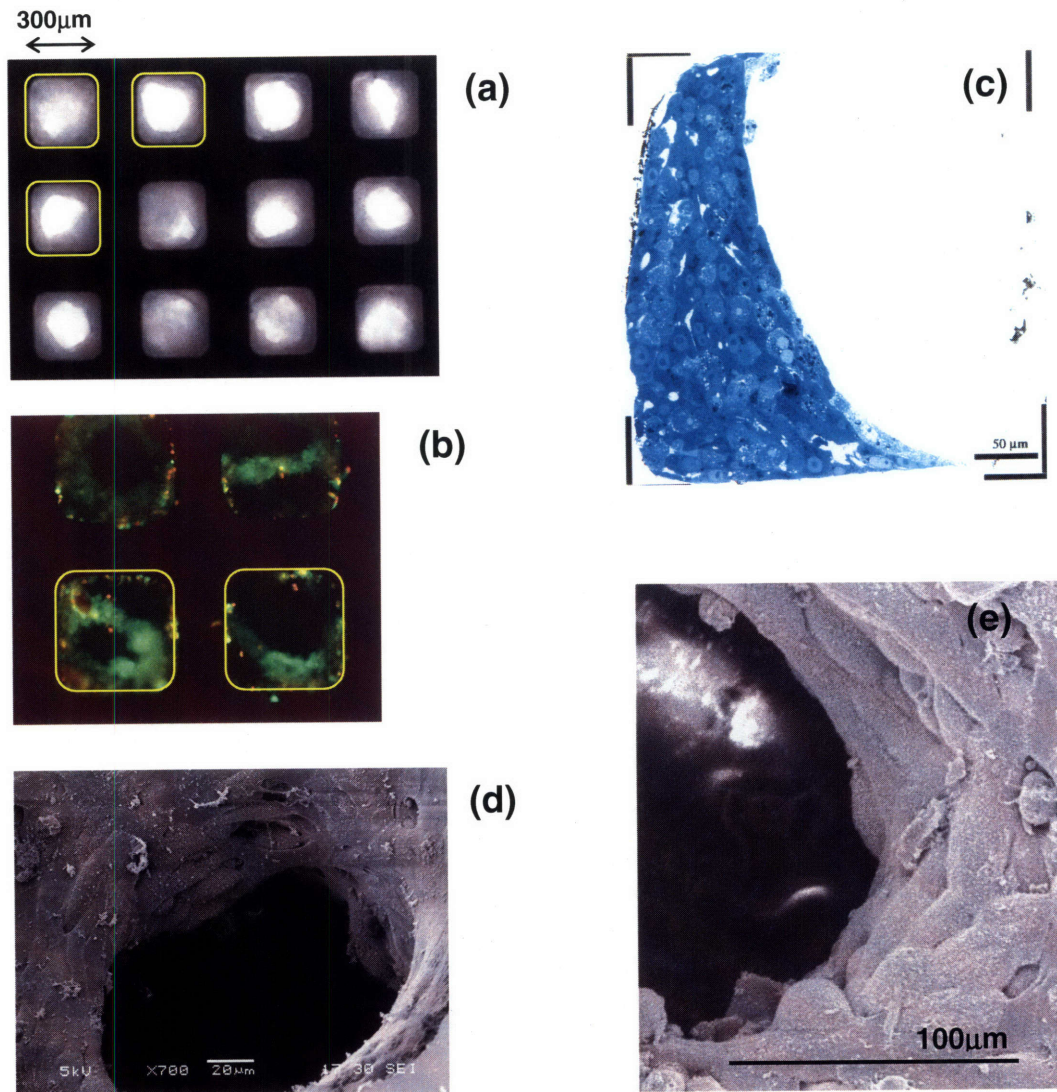


**Figure 2.6** Morphological behavior and viability of hepatocytes maintained in microreactors observed with: **(a)** light microscopy (3 day culture), **(b)** fluorescence microscopy (live-dead assay in 13 day culture), **(c)** toluidine blue-staining of histological sections, **(d)** scanning electron microscopy (2 day culture), **(e)** SEM (7 day culture).

## 2.5 Functional Behavior of Cells in the Liver Microreactor

Based on the above results and observations, the culture of hepatocytes in the 3D perfused environment of the microreactor appears to approximate to a certain extent the physiological conditions and morphological properties of native *in vivo* liver tissue. To determine whether this translates to improved liver-specific functional behavior of the culture, qualitative observations of cellular features and quantitative measurements of key hepatocyte properties such as albumin secretion and urea production were performed (Powers et al., Tissue Eng. 2002). Transmission electron micrographs of the tissue structures revealed typical features observed *in vivo*, such as tight junctions and desmosomes between adjacent cells, complex bile canaliculi with microvilli, as well as numerous mitochondria, rough endoplasmic reticulum and glycogen storage areas. These characteristics are indicative of well maintained metabolic functions. The rates of albumin secretion (~150pg/cell/day) and urea genesis (~700-900pg/cell/day) in microreactor cultures were maintained at constant levels for at least two weeks. Additionally, these levels were one order of magnitude higher than those measured for static cultures of spheroids prepared from the same cell population. These results offer further evidence that the microreactor culture environment promotes increased and sustained functional responses of hepatocytes

More recent studies using a broad spectrum of gene expression, protein expression and biochemical activity metrics, have shown that in the microreactor cultures the liver-specific phenotype is maintained at levels closer to those of *in vivo* liver tissue, compared to standard *in vitro* cultures such as 2D collagen gel sandwich cultures. The expression levels of key hepatic nuclear receptors and transcription factors that regulate the genes responsible for hepatic drug metabolism (e.g. cytochrome P450 genes) and other liver-specific functions were found to be better maintained in the liver microreactor. Additionally, the levels of basal and drug-induced expression of several drug metabolism genes themselves, as well as the biochemical activity of the corresponding proteins were found to approximate *in vivo* levels in 7 day-old microreactor cultures (Sivaraman et al., 2005).

Finally, recent work has shown that the 3D microreactor environment can support the survival and proliferation of sinusoidal endothelial cells cultured with hepatocytes for 2 weeks, whereas these cells disappear within a few days in a 2D co-culture system (Hwa et al., 2007).



## 2.6 Gene Delivery Experiments in the Microreactor.

### ***2.6.1 Experimental variables for gene delivery in the microreactor vs. 2D monolayer culture.***

In standard in vitro gene delivery experiments on adherent cells, the vector is dispersed in the medium overlaying the cell monolayer. Its uptake by the cells is a process that is dependent on the relative rates of diffusion and internalization; the parameters that can be varied to control gene delivery include the initial concentration of the vector and the duration of exposure (Chapter 4). As described in Chapter 1 the vector that was chosen for the experiments in this thesis is an adenoviral (Ad) vector expressing EGFP. Preliminary experiments indicated that a concentration of  $4 \times 10^6$  pfu/ml (pfu=plaque forming units, a measure for the number of infectious Ad particles) and a 24h exposure were sufficient for Ad infection of almost 100% of hepatocytes cultured in confluent monolayers on collagen-coated plates, as determined by the expression of EGFP with fluorescence microscopy. Therefore these conditions were selected as the maximum Ad concentration and duration of infection applied in this thesis. The concentration was varied within a range of one order of magnitude and the infection duration between 2 and 24 hours.

In the liver microreactor system, the Ad vector is dispersed in the culture medium inside the reservoir and circulates through the fluidic circuit and into the chamber. The crossflow transports the vector through the scaffold channels where it interacts with the tissue structures. Therefore in this case the delivery of the vector to the cells is more likely controlled by convective transport. These conditions mimic more closely those of in vivo gene delivery where, after administration into the bloodstream, the vector is transported to the hepatocytes via flow through the liver sinusoids. For a constant crossflow rate and total volume of circulating medium, the initial concentration and duration of infection are the parameters that can be varied to control the levels of Ad delivery. The maximum values of these parameters selected for the experiments in this thesis were the same as for the 2D monolayer cultures. Preliminary experiments indicated that these conditions resulted in EGFP expression levels easily detectable with 2-photon scanning fluorescence microscopy. The concentration was varied within a range of one order of magnitude and the duration of infection was set at 24h for the experiments in this thesis.

It needs to be underscored that selecting the same initial Ad concentration and infection duration in both cases does not correspond to equivalent Ad exposure of the cells because of the differences in the mechanism of extracellular vector transfer (diffusion vs. convection) and tissue morphology (2D vs. 3D). These differences will be factored in by means of mathematical modeling of the Ad mass transfer, before comparing the Ad gene delivery efficiency between the two in vitro culture systems.

### ***2.6.2 Modification of the microreactor fluidic system design.***

As described earlier, a peristaltic pump is used to drive medium flow into the upper compartment of the microreactor chamber and the pressure drop between the upper and lower compartments creates perfusion flow (crossflow) through the scaffold channels. The crossflow rate is controlled by the resistance of the microporous filter between the cell scaffold and the support scaffold and was measured at  $\sim 0.7 \mu\text{l}/\text{min}$  per channel at the start of the culture. However, the crossflow rate gradually decreases with time and usually within 24-48 hours reaches zero. This poses a problem not only in terms of insufficient oxygen and nutrient supply to the cells deep inside the channels, but also affects the transport of the gene delivery vector. The crossflow rate is an important parameter that determines the concentration profile and therefore the rate of cellular uptake of the vector. At zero crossflow rate the transfer of the vector inside the channels is diffusion limited, whereas at the value mentioned above convective transport dominates (Pe number is in the order of  $10^3$ ). In order to conduct quantitative experiments and measure the efficiency of gene delivery in the microreactor cultures the crossflow rate needs to be maintained at a known constant value.

A second peristaltic pump was connected to the crossflow line to force medium flow through the channels at a constant rate but did not solve the problem, which indicated crossflow was stopped due to debris blocking the pores of the filter. When the direction of the flow was reversed (medium flowing into the lower compartment of the chamber and through the channels to the upper compartment), the debris was removed from the filter and crossflow was reestablished. However, due to the continuous recirculation of medium (and debris) in the system the filter was clogged from the opposite side and crossflow had stopped again within 24 hours. The debris is probably the result of the spheroid reorganization that takes place during the first 24 hours in the microreactor channels releasing dead cells and cell fragments.

In order to circumvent this problem, the fluidic system operation is modified as follows: after the spheroids are seeded in the microreactor channels, the crossflow rate is controlled by a peristaltic pump at  $\sim 0.7\mu\text{l}/\text{min}$  per channel (Figure 2.7a). 24 hours later the crossflow direction is reversed and a Durapore syringe filter (PallGelman) with a  $0.45\mu\text{m}$  pore size is connected to the crossflow tubing (Figure 2.7b). When the flow is reversed, the debris in the scaffold filter is removed and released into the medium circulation; however it is prevented from blocking the scaffold filter again by the presence of the crossflow line filter. Additionally, the tissue structures inside the cell scaffold have already attached to channel walls and are not affected by the change in the flow direction. 2 hours after the reversal of the flow, the medium in the reservoir is replaced to remove the bulk of the released debris. The crossflow filter and the medium in the reservoir are replaced every 3-4 days.

This modification in the fluidic system allows the unobstructed flow of medium through the microreactor chamber at constant rates. It also ensures that gene delivery experiments are conducted under consistent conditions among different microreactor cultures.

### ***2.6.3 Experimental procedure for Ad gene delivery in the microreactor.***

As described earlier, the microreactors are seeded with 3-day hepatocyte spheroids which attach to the scaffold channel walls and reorganize within 24-48h. Day 3 after spheroid seeding (day 6 after rat liver perfusion) was selected as an appropriate time point for Ad infection. At that point the tissue has reorganized into stable structures and the albumin and urea production rates have stabilized (Powers et al., Tissue Eng. 2002). Additionally, conditions of constant crossflow rate have been established ( $\sim 0.7\mu\text{l}/\text{min}/\text{channel}$ ). The medium in the reservoir is then replaced with fresh medium containing the Ad vector, which is allowed to continuously flow in the system for 24h. During the infection the medium in the reservoir is kept under well-mixed conditions to ensure uniform concentration of the vector. For that purpose, a network of Air-Driven Turbine Magnetic Stirrers connected in parallel to an airflow supply line was installed inside the cell culture incubators. Each medium reservoir is equipped with a stir bar and positioned on top of a stirrer. The Ad infection is ended by replacing the medium and the entire fluid circuit (tubing, reservoir and crossflow filter) under sterile conditions (described in detail in Chapter 3). The cultures are then maintained until the end of the experiment under normal culture conditions.

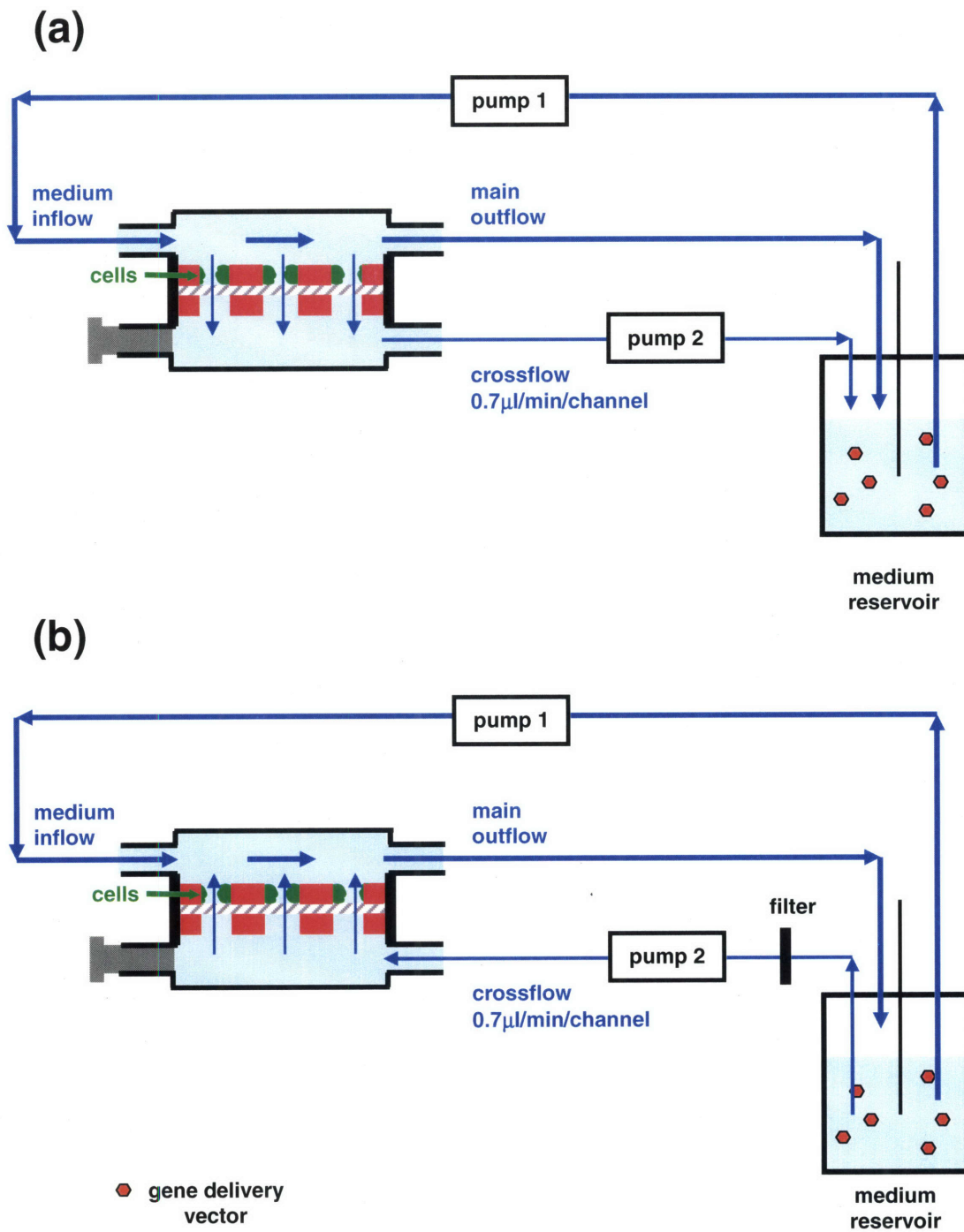


**Figure 2.7** Modification of the microreactor fluidic system design: (a) Operation after cell seeding ( $t=0$ ), (b) operation after  $t=24\text{h}$  and for the remainder of the culture.

## 2.7 References

Griffith, L.G., Wu, B., Cima, M.J., Powers, M.J. Chaignaud, B., Vacanti, J.P. (1997). *In Vitro* Organogenesis of Liver Tissue. *Annals of the New York Academy of Sciences* **831**, 382-397.

Hwa, A.J., Fry, R.C., Sivaraman, A., So, P.T., Samson, L.D., Stolz, D.B., Griffith, L.G. (2007). Rat liver sinusoidal endothelial cells survive without exogenous VEGF in 3D perfused co-cultures with hepatocytes. *The FASEB journal* **21**, published online April 10 2007.

Powers, M.J. and Griffith-Cima, L.G. (1996). Motility Behavior of Hepatocytes on Extracellular Matrix Substrata During Aggregation. *Biotechnology and Bioengineering* **50** (4), 392-403.

Powers, M.J., Rodriguez, R.E., Griffith, L.G. (1997). Cell-substratum Adhesion Strength as a Determinant of Hepatocyte Aggregate Morphology. *Biotechnology and Bioengineering* **53** (4), 415-426.

Powers, M.J. and Griffith, L.G. (1998). Adhesion-Guided In Vitro Morphogenesis in Pure and Mixed Cell Cultures. *Microscopy Research and Technique* **43**, 379-384.

Powers, M.J., Domansky, K., Kaazempur-Mofrad, M.R., Kalezi, A., Capitano, A., Upadhyaya, A., Kurzawski, P., Wack, K.E., Beer-Stolz, D., Kamm, R., Griffith, L.G. (2002). A Microfabricated Array Bioreactor for Perfused 3D Liver Culture. *Biotechnology and Bioengineering* **78** (3), 257-269.

Powers, M.J., Janigian, D.M., Wack, K.E., Baker, C.S., Beer-Stolz, D., Griffith, L.G. (2002). Functional Behavior of Primary Rat Liver Cells in a Three-Dimensional Perfused Microarray Bioreactor. *Tissue Engineering* **8** (3), 499-513.

Sivaraman, A., Leach, J.K., Townsend, S., Iida, T., Hogan, B.J., Stolz, D.B., Fry, R., Samson, L.D., Tannenbaum, S.R., Griffith, L.G. (2005). A Microscale In Vitro Physiological Model of the Liver: Predictive Screens for Drug Metabolism and Enzyme Induction. *Current Drug Metabolism* **6**, 569-592.

# **CHAPTER 3**

## **Materials and Methods**

## **3.1. Cell Culture**

### ***3.1.1 Rat Liver Perfusion and Hepatocyte Isolation***

Hepatocytes were harvested from 150-230g male Fisher rats with a modification of Seglen's two-step collagenase perfusion procedure (Seglen, 1976) as described in Powers et al., 2002. Briefly, the liver was initially perfused with  $\text{Ca}^{2+}$ -free buffer through a catheter inserted in the inferior vena cava at a flow rate of 25 ml/min for 6-7 min (until the blood was cleared from the liver and the liver had acquired a light caramel color); then the liver was perfused with collagenase solution at a flow rate of 15 ml/min for approximately 11 min (until the tissue had disintegrated enough to allow for the isolation of hepatocytes without compromising cell viability). The liver was then removed and gently shaken in a DMEM/Albumin/Penicillin-Streptomycin (DAPS) solution to break up the tissue and free the cells. The resulting cell suspension was filtered through a 100 $\mu\text{m}$  mesh filter to remove tissue debris and processed to isolate a hepatocyte-rich fraction. In particular, the cells were centrifuged twice at 50g for 3 min at 4 $^{\circ}\text{C}$  to remove debris, dead cells and non-parenchymal cells. To further increase the percentage of live hepatocytes in the preparation, the cells were subjected to a centrifugation in an isodensity Percoll solution followed by a washing step in DAPS solution and a 2 $^{\text{nd}}$  centrifugation. The resulting pellet was resuspended in Hepatocyte Growth Medium (HGM) (chemically defined medium as described by Block et al. 1996, but without hepatocyte growth factor and with modifications as described below). Hepatocyte viability was assessed with the trypan blue exclusion method and only cells from perfusions yielding greater than 85% viability were used for cell culture experiments.

### ***3.1.2 Composition of Hepatocyte Growth Medium (HGM) and DAPS Solution***

HGM consists of DMEM supplemented with L-proline (0.03 g/L), L-ornithine (0.1 g/L), niacinimide (0.305 g/L), glucose (2.25 g/L), galactose (2 g/L), bovine serum albumin (2 g/L), Hepes (10 mM),  $\text{ZnCl}_2$  (0.0544 mg/L),  $\text{ZnSO}_4 \cdot 7\text{H}_2\text{O}$  (0.075 mg/L),  $\text{CuSO}_4 \cdot 5\text{H}_2\text{O}$  (0.02 mg/L),  $\text{MnSO}_4$  (0.025 mg/L), penicillin-streptomycin (100 U/ml), L-glutamine (1 mM), insulin (5 mg/L), transferrin (5 mg/L), sodium selenite (5  $\mu\text{g/L}$ ), dexamethasone (0.1  $\mu\text{M}$ ) and epidermal growth factor (20 ng/ml). The above composition of HGM includes corrections of mistakes in Block et

al, as determined by personal communication with the Michalopoulos lab. The mixed HGM solution was sterilized by filtration through a 0.22  $\mu\text{m}$  low protein-binding Nalgene PES filter unit and stored at 4°C. The epidermal growth factor (EGF) was added to HGM right before use. The DAPS solution used during the hepatocyte isolation procedure consists of DMEM, albumin and penicillin-streptomycin at the same concentrations as HGM and was also sterilized by filtration before use. DMEM and glutamine were purchased from GIBCO/BRL, the insulin-transferrin-sodium selenite mixture from Roche, EGF from BD Biosciences and the rest of the components from Sigma.

### **3.1.3 Monolayer Hepatocyte Culture**

Non plasma-treated bacteriological polystyrene 12-well plates were coated with collagen I (Vitrogen) via adsorption from a 3  $\mu\text{g}/\text{ml}$  solution in PBS (GIBCO/BRL) at room temperature for one hour. Hepatocytes were plated at a density of  $3 \times 10^5$  cells per well, cultured in HGM and maintained in a humidified 8.5%  $\text{CO}_2$  atmosphere at 37°C inside an incubator.

#### Measurement of Cellular Surface Area, A

The average surface area (A) of a primary rat hepatocyte in the monolayer culture system described above was determined from phase contrast photomicrographs. Images were acquired with a Zeiss Axiocam HRc video camera attached to a Zeiss Axiovert 100 Microscope with a 10X objective lens and were processed with the Openlab v3 software on a Macintosh G4 computer. Cells were imaged 24 hours after plating. Images were acquired from two 12-well plates and four different wells (two per plate). A total of 11 regions of interest (ROI) were outlined in the acquired images and the surface area of each region was measured with the software; a hemocytometer grid was used for calibration. The number of hepatocytes in each region was counted manually. A total of 775 cells were counted and the average cellular surface area was determined to be approximately:

$$\mathbf{A = 1.7 \times 10^{-5} \text{ cm}^2 / \text{cell}}$$

The hepatocyte surface area measurements were required for the calculations with the mathematical model for adenoviral vector mass transfer and cellular uptake in monolayer cultures, as described in Chapter 4.



### **3.1.4 Tissue-Engineered Liver Microreactor Culture**

#### Assembly and Preparation of Microreactors

All microreactor components except for the polycarbonate chamber were sterilized by autoclaving. The two chamber parts were sterilized by soaking in 70% ethanol for 15 min and then washed in PBS. The silicon scaffolds were coated with collagen I (Vitrogen) via adsorption from a 30 µg/ml solution in PBS at room temperature for one hour (in a 6cm tissue culture plate with a volume of 10ml of collagen solution). The crossflow filters were soaked in a PBS-BSA (1%) solution (sterilized by filtration) to render them protein resistant and prevent adsorption of nutrients from the medium during the liver tissue culture. The microreactor chambers were assembled and connected to the fluid flow circuit and the medium reservoir under sterile conditions as described in Chapter 2. The microreactor systems were then operated in the absence of cells to establish continuous medium flow and neutralize the surfaces of the system. The medium in the reservoir was replaced with fresh HGM immediately before the hepatocyte seeding. The total volume of medium flowing in the microreactor system was 20 ml.

#### Hepatocyte Spheroid Cultures

Hepatocyte spheroids were formed in suspension using methods similar to Wu et al, 1996. After rat liver perfusion and hepatocyte isolation the cells were seeded in 250ml spinner flasks (BellCo Glass, Inc.) at a density of  $3 \times 10^7$  hepatocytes suspended in 100ml HGM per flask and were cultured under continuous stirring conditions for three days to form spheroids. The spinner flask cultures were maintained on a spinner table (BellCo Glass, Inc.) at a speed of 85 rpm in a humidified 8.5% CO<sub>2</sub> atmosphere at 37°C. On day 3 after hepatocyte isolation, the spheroid suspension was filtered through a 300µm mesh nylon filter (SEFAR America) to remove the spheroids that were larger than the microreactor channel dimensions (300x300µm cross section and 230µm depth). The flow-through suspension was then filtered through a 100µm mesh nylon filter (SEFAR America) to remove small cell clumps, dead cells and debris; the spheroids collected on the filter were re-suspended in 25ml rinse medium (DAPS) and centrifuged at 40g for 3min. The spheroid pellet was then re-suspended in 25-30ml HGM before seeding into the microreactors. The quality (size: majority of spheroids between 100-200µm; shape: tightly formed aggregates without dead cells protruding) and cell viability of the spheroids was qualitatively determined by observation under the microscope with the addition of

Trypan Blue. The quality of the spheroid culture is important for establishing healthy microreactor cultures.

### Microreactor seeding and culture maintenance

Each microreactor was seeded with hepatocyte spheroids under sterile conditions. The spheroid suspension was loaded into a 1 ml syringe. The medium flow in the system was stopped and the syringe was connected to the upper outlet of the microreactor chamber. The spheroid suspension was slowly injected into the reactor chamber; the tubing leading to the upper inlet of the reactor chamber was clamped to force fluid flow only through the silicon scaffold channels and out of the lower outlet of the chamber. This led to the spheroids settling inside the scaffold channels (the presence of the crossflow filter prevents them from flowing through). When the channels were filled with spheroids, the syringe was removed. HGM was pumped into the upper inlet at 0.4 ml/min and collected in a waste container for 2 min to clear spheroids from the top surface of the silicon scaffold. Then the upper inlet tubing was reconnected to the chamber and the medium flow was reestablished in the system as shown in Figure 2.7a. The microreactor cultures were maintained in a humidified 8.5% CO<sub>2</sub> atmosphere at 37°C.

At 24 hours after cell seeding (day 4 after hepatocyte isolation), the direction of the medium flow in the crossflow line of each microreactor was reversed (medium now flowing from the reservoir into the lower part of the chamber, through the scaffold channels to the upper part of the chamber) and a syringe filter was introduced in the crossflow line tubing (as shown in Figure 2.7b). The medium in the reservoir was also replaced. As explained in detail in Chapter 2, this procedure ensures the unobstructed flow of medium through the scaffold (and therefore through the tissue culture). At that time the spheroids had already attached to the collagen-coated scaffold channel walls and therefore were not dislodged by the change in the direction of fluid flow. Two hours later, the medium in the reservoir was replaced again to ensure the removal of debris that was released from the chamber filter due to the reversal of the direction of crossflow.

The syringe filter in the crossflow line (whose purpose was to prevent debris from reaching and clogging the chamber filter and consequently obstructing the flow) was replaced every three days as well as the medium in the reservoir. However, in the case of Ad gene delivery experiments, the medium was also replaced at the beginning and at the end of Ad infection.

## 3.2. Adenoviral Gene Delivery

### 3.2.1 Adenovirus vector

The vector used in this thesis for gene delivery experiments was an E1-, E3-deleted first generation human adenovirus 5 vector, which contained an expression cassette consisting of the cytomegalovirus (CMV) immediate/early promoter and enhancer, an artificial splice site (SV40 intron), the transgene and the polyadenylation site from SV40. The transgene encoded the enhanced green fluorescent protein (EGFP). This vector, labeled as H5.010CMVEGFP, was purchased from the Vector Core of the Institute for Human Gene Therapy at the University of Pennsylvania, School of Medicine. The genomic and infectious titers of the vector were measured by the supplier as  $4.7 \times 10^{12}$  particles/ml and  $2.8 \times 10^{11}$  pfu/ml (pfu: plaque forming units) respectively, establishing a particle over pfu ratio equal to 17. The Ad preparation was tested for the presence of RCA (replication competent adenovirus) and was found negative. This vector preparation was used for the experiments described in this thesis unless mentioned otherwise. The vector was aliquoted in adenovirus storage buffer (10% glycerol in PBS) and stored at  $-80^{\circ}\text{C}$ . Before each gene delivery experiment the Ad was diluted in HGM to give the required concentrations.

Another Ad vector, labeled H5.010CMVLacZ (expressing  $\beta$ -galactosidase), was used as a control in a microreactor experiment (see Chapter 5) as well as in the experiments testing the specificity of the primers/probe set designed for the TaqMan PCR assay (see section 3.4). This vector is identical to H5.010CMVEGFP apart from the transgene sequence. The genomic and infectious titers were  $5 \times 10^{12}$  particles/ml and  $1.67 \times 10^{11}$  pfu/ml respectively (particle over pfu ratio = 30). This vector was also purchased from the Vector Core at UPenn.

The construction of the above-mentioned vectors and the protocols for propagation, purification and genomic and infectious titer quantification are described in detail by Davis et al. (1998, 2001). However, since the methods applied for the quantification of the Ad titers have a significant effect on the quantitative analysis of gene delivery in both hepatocyte monolayer and microreactor systems (as it will be discussed in Chapter 4), a few details are mentioned here. The genomic titer (concentration of total Ad particles) was quantified by optical absorbance at 260 nm. The infectious titer (concentration of infectious Ad particles) was determined with the plaque assay on 293 cells, which support the replication of first generation adenoviral vectors (Graham et al. 1977). In this assay, detection of one Ad particle involves infection of a 293 cell

(cultured in a monolayer) by one Ad particle suspended in the medium, followed by viral replication and spread of infection to nearby cells sufficient to form a visible plaque.

According to the protocol followed by our vector suppliers, 293 cells were seeded in 6-well plates and incubated with dilutions of the Ad preparation (1 ml of Ad solution per well) for three to four hours. After removing the Ad-containing medium the cells were overlaid with agar. A second agar overlay was applied on day 7 and when plaques became visible (day 12) a third agar overlay mixed with Neutral Red was added. The plaques were counted in the wells corresponding to the Ad dilution that resulted in the formation of 10-90 plaques per well. The infectious titer (pfu/ml) was calculated by multiplying the average number of plaques with the dilution factor.

### ***3.2.2 Adenoviral Vector Infection in Monolayer Hepatocyte Cultures***

Primary hepatocytes were harvested from male Fisher rats, isolated from non-parenchymal cells with successive centrifugation steps and seeded on collagen-coated 12-well plates at a density of  $3 \times 10^5$  cells per well as described in section 3.1. The hepatocyte monolayers were cultured in HGM for 24 hours. Then ( $t = 0$ ) the medium in each well was replaced with 750 $\mu$ l HGM containing AdEGFP at three different concentrations:  $4 \times 10^5$ ,  $2 \times 10^6$  and  $4 \times 10^6$  pfu/ml. These Ad concentrations are based on the infectious titer of the original Ad preparation as measured by the vector supplier and correspond to MOI values of 1, 5 and 10 respectively. (MOI = multiplicity of infection = pfu/cell = [concentration] x [HGM volume] / [cell number])

At different time points ( $t = 2, 4, 8, 12$  and  $24$  hr), the Ad infection was terminated by removing the Ad-containing supernatant and washing twice with PBS (carefully so as not to disturb the cell monolayer). The hepatocytes were then either harvested immediately for DNA extraction (data set 1), or cultured in HGM until  $t=48$ hr. In the second case the cells were subsequently harvested for DNA extraction (data set 2), counterstained with Hoechst and Ethidium Homodimer for fluorescence imaging of EGFP expression (data set 3), or harvested in Trizol reagent for RNA extraction (data set 4). Triplicate wells were prepared for each initial Ad concentration, time point condition and data set. Additionally, negative controls (no Ad added to the medium) were prepared in each case.

### Nuclear Counterstaining of Monolayer Hepatocyte Cultures Infected with AdEGFP Vector

At time  $t=48\text{hr}$  after the beginning of the Ad infection, the hepatocyte monolayers were incubated with ethidium homodimer-1 (Molecular Probes) at a concentration of  $4\mu\text{M}$  in HGM for 10 minutes, followed by an incubation with Hoechst 33342 (Molecular Probes) at a concentration of  $20\mu\text{g/ml}$  in HGM for 20 minutes. Both ethidium homodimer and Hoechst are nucleic acid stains. Ethidium homodimer enters cells with damaged plasma membranes and upon binding to the DNA emits bright red fluorescence in dead cells (ex/em  $\sim 495\text{nm}/\sim 635\text{nm}$ ), while it is excluded by the intact membrane of living cells. Hoechst is cell-permeant and upon binding to the DNA emits bright blue fluorescence (ex/em  $\sim 350\text{nm}/\sim 461\text{nm}$ ). Therefore, the live and dead cells on the hepatocyte monolayers can be distinguished by visualizing their respective blue- or red-labeled nuclei with a fluorescence microscope.

### Imaging of Transgene (EGFP) Expression in Monolayer Hepatocyte Cultures and Quantification of AdEGFP Gene Delivery Efficiency and Cell Viability.

After staining, the hepatocyte monolayers were imaged with a Zeiss Axiovert 100 microscope equipped with Zeiss Achrostigmat dry lenses (5X with  $\text{NA}=0.12$ , 10X with  $\text{NA}=0.25$  and 20X with  $\text{NA}=0.30$ ; NA: numerical aperture) and a mercury-arc lamp (ebq 100). EGFP was detected with a FTIC filter set, Hoechst with a DAPI filter set and ethidium homodimer with a rhodamine filter set. The images were captured with a Zeiss AxioCam HRC camera and processed with the OpenLab v3 Software on a Macintosh G4 computer. The green, blue and red layers of each image were combined in a three-color overlay; an example is shown in Figure 3.2.1. As mentioned in a previous section, triplicate wells were prepared for each initial Ad concentration and infection time point condition. Images were acquired for 5-6 different regions of each 'Ad concentration & time point' combination (for example  $\text{MOI}=10$  & 24hr infection,  $\text{MOI}=10$  & 12hr infection, etc...).

The total number of cells was determined by counting manually the number of blue nuclei (stained with Hoechst) and the number of dead cells by counting the red nuclei (stained with ethidium homodimer) on each image. Cell viability was calculated as the % ratio of the live cell number over the total cell number. The number of EGFP-expressing (green) cells was also counted manually. Control cultures (no Ad infection) did not display any visible levels of green fluorescence; therefore any cell on the acquired images of Ad infected monolayers that

displayed green fluorescence detectable by eye was scored as an EGFP positive cell. The efficiency of Ad gene delivery was calculated as the % ratio of EGFP-expressing cells over the total number of live cells. The sums of cell counts for all images corresponding to each 'Ad concentration & time point' combination were used for the viability and efficiency calculations. The results are presented in Chapter 4.

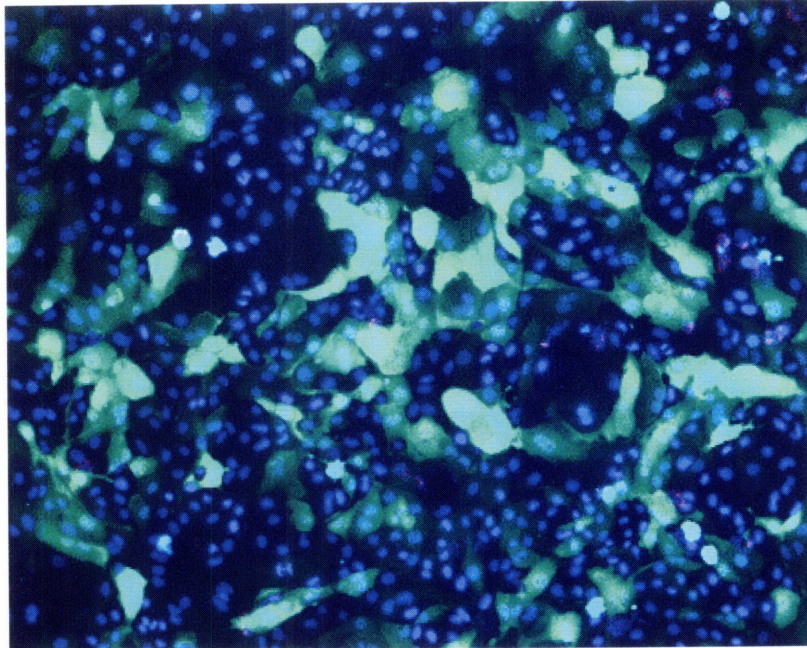


**Figure 3.2.1.** Fluorescence micrograph of rat hepatocyte monolayer infected with Ad5-CMV-EGFP at MOI=5\* for 24 hours. The cells were stained with Hoechst 33342 and Ethidium Homodimer 1 and imaged 24 hours after the end of the Ad infection with a Zeiss Axiovert 100 microscope and a 10X dry objective lens. EGFP was detected with a FTIC filter set, Hoechst with a DAPI filter set and Ethidium Homodimer with a Rhodamine filter set. The images were captured with a Zeiss AxioCam HRc camera and processed with the OpenLab v3 Software on a Macintosh G4 computer. An overlay of the green, blue and red images is shown here.

\*corresponds to the infectious Ad titer provided by the vector supplier.

### **3.2.3 Adenoviral Vector Infection in Liver Microreactor Cultures.**

On day 6 after the hepatocyte isolation, the medium inside the microreactor reservoir was replaced with fresh HGM containing the Ad5-CMV-EGFP vector. Three different Ad concentrations were used:  $4 \times 10^5$ ,  $2 \times 10^6$  and  $4 \times 10^6$  pfu/ml. These Ad concentration values refer to the entire medium volume in the microreactor system and are based on the infectious titer of the original Ad preparation as measured by the vector supplier. Typically in each experiment duplicate microreactors were prepared for each Ad concentration as well as control microreactors with no Ad added. The Ad vector circulated in the microreactor system for 24 hours. During the infection, the medium in the reservoir was kept under well-mixed conditions to ensure uniform concentration of the vector. For that purpose, a network of air-driven turbine magnetic stirrers connected in parallel to an airflow supply line was installed inside the cell culture incubators. Each medium reservoir was equipped with a stir bar and positioned on top of a stirrer.

At the end of the Ad infection ( $t=24h$ ) the microreactor chamber was disconnected from the rest of the system and connected to a new set of tubing and reservoir components with fresh HGM. The Ad particles inside the chamber were washed out by flowing fresh medium through the upper and lower inlets and collecting the first 2 ml flowing out of the upper outlet, before connecting the upper outlet tubing. Additionally, two hours after the removal of Ad, the medium in the reservoir was replaced again.

The liver microreactor cultures were then maintained until approximately  $t=70h$  after the beginning of Ad infection (day 9 after hepatocyte isolation) unless specified otherwise. At that time the silicon scaffolds containing the hepatocyte tissue were removed from the microreactor chambers and were stored either at  $-20^{\circ}C$  for DNA extraction or at  $-80^{\circ}C$  in Trizol reagent for RNA extraction.

### **3.3. DNA Extraction and Quantification**

#### ***3.3.1 DNA Extraction and Purification***

##### Hepatocyte Monolayer Cultures

Hepatocytes were harvested with a cell scraper in 200  $\mu$ l PBS per well (after the culture medium was removed). The DNA was extracted with the High Pure PCR Template Preparation Kit (Roche). During this process the cells are lysed by incubation with Proteinase K and a buffer containing a chaotropic salt, which inactivates nucleases. The samples are subsequently flown through filter tubes pre-packed with special glass fibers. DNA binds to the glass fibers and after a series of wash-and-spin steps in a microcentrifuge to remove PCR inhibitory contaminants and other cellular impurities, it is eluted with a low salt buffer. The resulting DNA solutions were stored at  $-20^{\circ}\text{C}$  until DNA quantification and real-time PCR analysis.

##### Liver Microreactor Cultures

The cells were harvested from the silicon scaffolds in 200  $\mu$ l of Tissue Lysis Buffer with repetitive pipeting to break up the tissue structures. The DNA was extracted with the High Pure PCR Template Preparation Kit as described in the previous paragraph. The resulting DNA solutions were stored at  $-20^{\circ}\text{C}$  until DNA quantification and real-time PCR analysis.

#### ***3.3.2 Quantification of Total DNA Content in Hepatocyte Culture Samples***

After DNA extraction and purification the samples (hepatocyte monolayer cultures and tissue-engineered microreactors) were assayed for total DNA content with the RediPlate™ 96 PicoGreen® dsDNA Microplate Assay (Molecular Probes). This assay is based on the ability of the nucleic acid stain PicoGreen to selectively bind to dsDNA and subsequently emit bright green fluorescence. The stain is predispensed in the wells of a 96-well microplate and is dissolved in TE buffer before the addition of the DNA samples; fluorescence is measured in a fluorescence microplate reader using excitation at 485 nm and detection at 530 nm. The



fluorescence of the sample of interest is compared to that of a standard curve of DNA. The assay has a linear range of 1-100 ng DNA in a 200  $\mu$ l assay volume according to the manufacturer.

The RediPlate PicoGreen assay was applied to all DNA samples that were also assayed for AdEGFP genomic copy number with quantitative real-time PCR. A standard curve was prepared for each microplate. The standard curve was derived from a series of dilutions of calf thymus DNA (Sigma) in TE buffer ranging from 0.2 to 10  $\mu$ g/ml (2 to 100 ng in a 200  $\mu$ l assay volume). All standards were assayed in triplicates. The slopes of the standard curves were comparable within a narrow range among microplates from the same production batch –the coefficient of variation was less than 10% (Figure 3.3.1). Among microplates from different batches the coefficient of variation for the standard curve slopes was less than 14%. All hepatocyte samples were assayed in triplicate and the total DNA content was determined from the standard curve by interpolation. The mean values were used for further calculations (normalization of real-time PCR data). The assay was repeated for samples for which the coefficient of variation exceeded 10%.

### ***3.3.3 Cellular DNA Content Measurements for Rat Hepatocytes***

To determine the DNA content of a rat hepatocyte (for data normalization purposes), samples of hepatocytes were needed containing known numbers of cells. After each rat liver perfusion and hepatocyte isolation though, the cell viability and concentration of the resulting hepatocyte suspension can be determined with the trypan blue exclusion method in a hemocytometer as described in section 3.1. Therefore, triplicate samples of varying cell numbers (from  $10^4$  to  $4 \times 10^5$ ) were prepared from the resulting hepatocyte suspension of three different rat perfusions. DNA was extracted with the High Pure PCR Template Preparation Kit and quantified with the RediPlate 96 PicoGreen dsDNA Microplate Assay as described in the previous paragraphs. Figure 3.3.2 shows a plot of DNA content ( $\mu$ g DNA) as a function of hepatocyte number. Each data point corresponds to the mean value of 9 samples (3 samples x 3 rat perfusions) and the error bars represent the standard deviation. A straight line was fitted to the data with linear regression (Excel) and the slope represents the cellular DNA content. As shown in the plot, each rat hepatocyte contains  $7.73 \times 10^{-6}$   $\mu$ g DNA. This number was used to convert the normalized PCR data (Ad copies per  $\mu$ g DNA) to Ad copies per cell, as required by the mathematical model presented in Chapter 4.

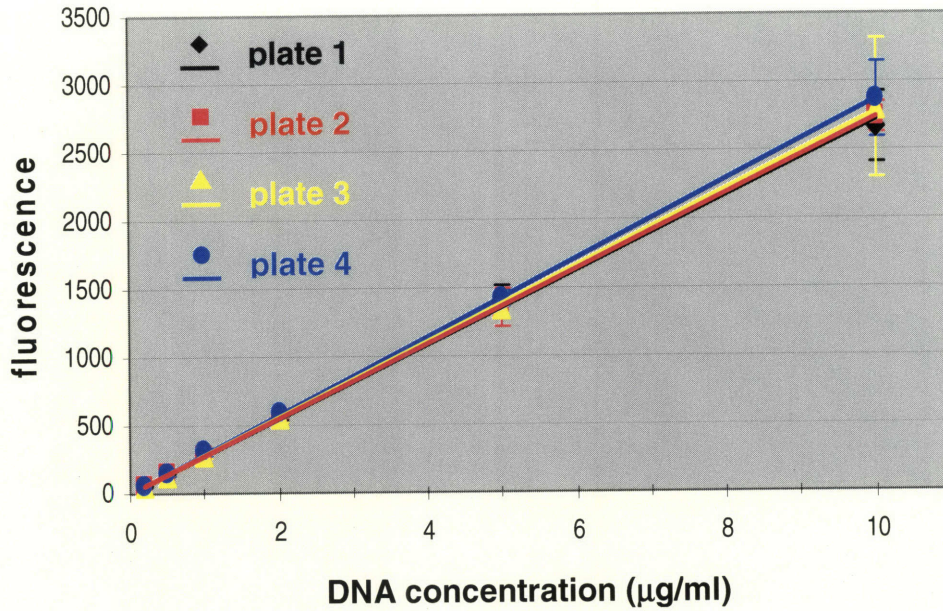


**Figure 3.3.1.** Dynamic range, sensitivity and reproducibility of RediPlate 96 PicoGreen dsDNA assay. Calf thymus DNA dilutions ranging from 0.2 to 10 µg/ml were assayed in triplicates. Fluorescence was measured with a microplate reader. The fluorescence signals were plotted against the DNA concentration after subtracting background fluorescence. Four different experiments are shown. The symbols represent the mean data values and the error bars the standard deviation. The lines represent the standard curves (linear regression with Excel).

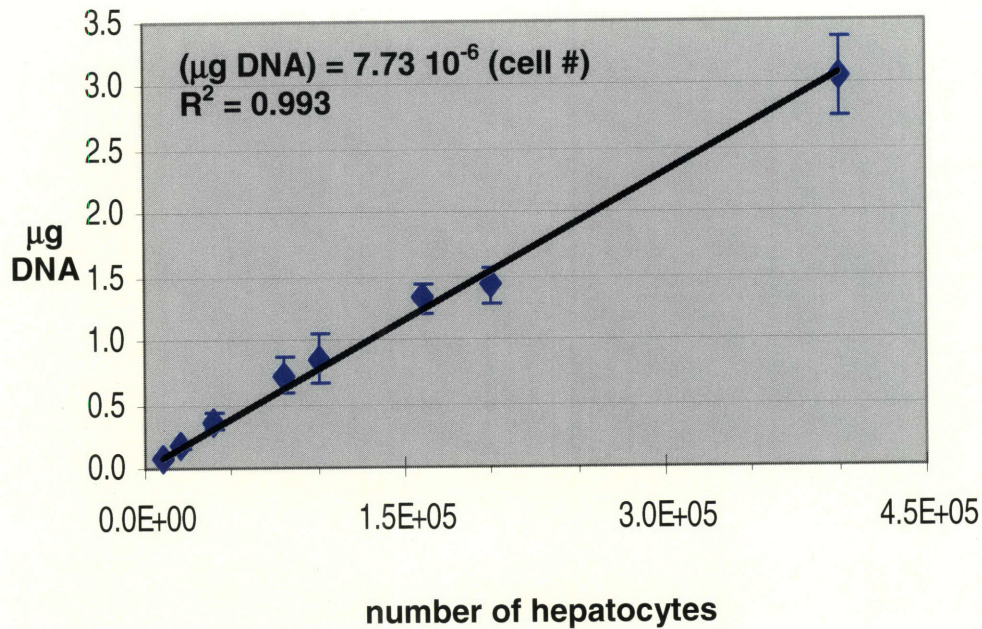


**Figure 3.3.2.** Rat hepatocyte DNA content measurements. Samples of varying cell numbers were prepared after rat liver perfusion and hepatocyte isolation. DNA was extracted and quantified with the Rediplate 96 PicoGreen dsDNA Microplate Assay (standard curves were derived from a series of calf thymus DNA dilutions). Fluorescence was measured with a microplate reader and the DNA content of each sample was determined from the standard curve by interpolation. The DNA content is plotted here as a function of cell number. The data points represent the mean values of 9 samples (3 samples x 3 rat perfusions) and the error bars the standard deviation. The straight line corresponds to the linear regression with Excel.

## 3.4. Quantitative real time TaqMan<sup>®</sup> PCR

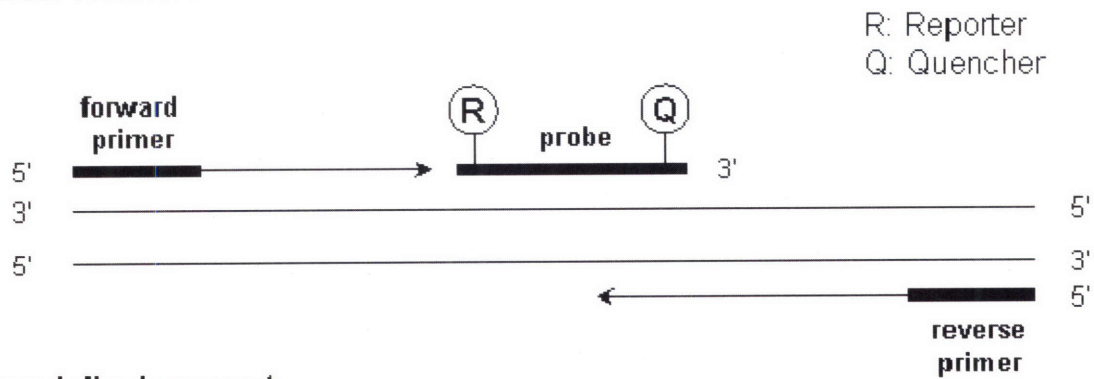
### 3.4.1 Introduction

Quantitative real-time PCR has been applied extensively in the field gene therapy in the last 10 years to assess the transfer of gene delivery vectors and track their distribution in vivo as well as to accurately determine viral vector titers (Heid et al. 1996, Becker et al. 1999, Hackett et al. 2000, Ma et al. 2001, Senoo et al. 2000). The advantages of this quantitative method include a large dynamic range (up to 7 orders of magnitude), reproducibility, accuracy and sensitivity, as well as high sample throughput.

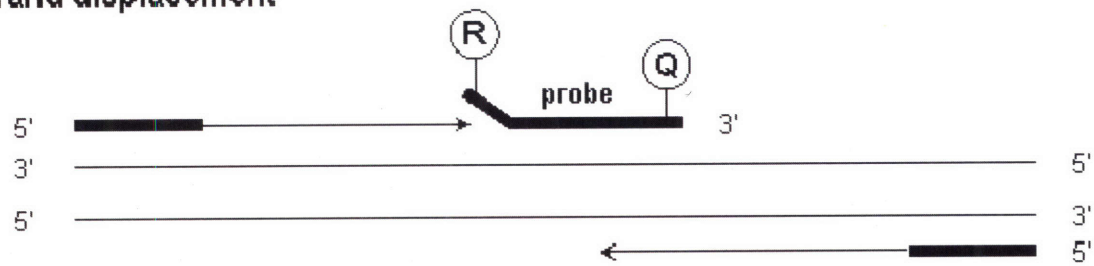
The TaqMan PCR assay is based on the use of a dual-labeled fluorogenic probe that hybridizes to the target DNA sequence between the forward and reverse primer sites. The probe contains a fluorescent dye at the 5' end (FAM, 6-carboxyfluorescein), which serves as a reporter and another at the 3' end (TAMRA, 6-carboxy-tetramethyl-rhodamine) that serves as a quencher. When the probe is intact, the emission spectrum of FAM is absorbed by TAMRA (fluorescence energy transfer phenomenon) due to the proximity of the two dyes. During PCR, the primers and probe anneal to the target DNA sequence (if it is present in the sample) and the polymerization (primer elongation) step begins. As the primer upstream of the probe is extended, the 5' to 3' nucleolytic activity of the AmpliTaq Gold DNA polymerase cleaves the probe, thus separating the two dyes and increasing the fluorescence emission of the reporter (Figure 3.4.1) while polymerization of the strand proceeds. This process occurs in every PCR cycle and therefore the accumulation of the PCR product can be detected by monitoring the increase in emission intensity (Heid et al. 1996, Applied Biosystems 2000, 2002).

The PCR reaction takes place in a 96-well plate placed inside a Sequence Detection System (the ABI Prism 7700 system was used in this study). Light from an argon ion laser is distributed to the 96 wells through a multiplexed array of optical fibers and excites the fluorescent dyes in each well for 25 msec. The resulting emissions (500-660 nm) are collected every 7 sec by the optical fibers and directed to a spectrograph with a CCD camera (Figure 3.4.2). The fluorescent signals are subsequently analyzed and the data processed with the Sequence Detection Software (Applied Biosystems 2000). A value  $\Delta R_n$  is calculated which represents the normalized fluorescence emission intensity of the reporter (i.e. divided by the fluorescence emission intensity of a passive reference dye) at any given time during the PCR reaction,  $R_n^+$ , minus the normalized emission intensity of the reporter before the PCR reaction,

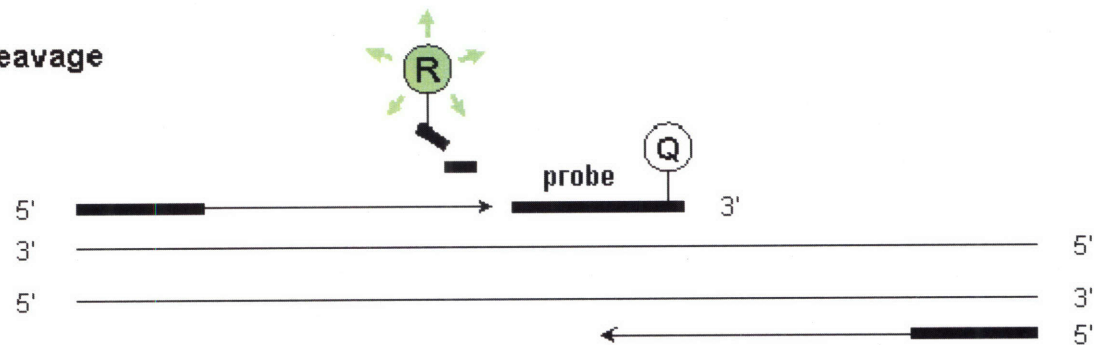
### primer extension



### strand displacement



### cleavage



### strand extension completed

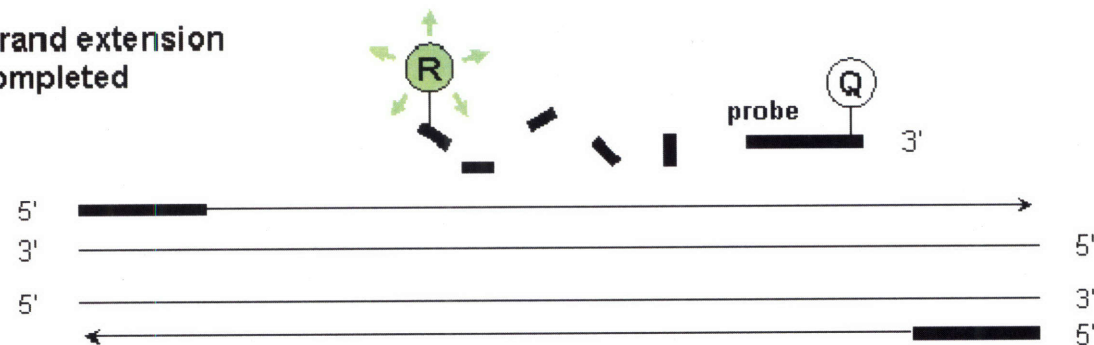


**Figure 3.4.1.** Schematic of real-time TaqMan PCR method.



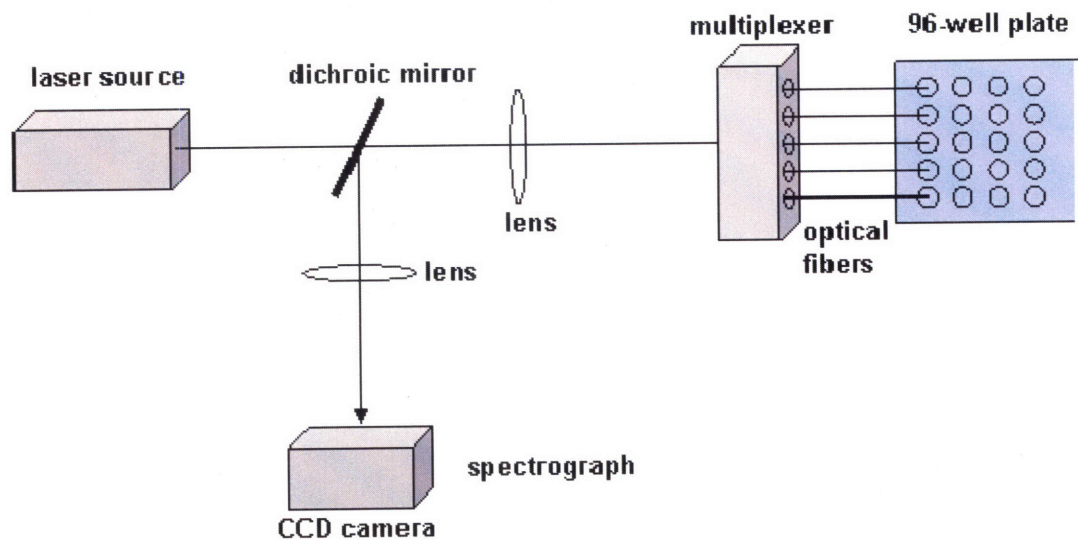


**Figure 3.4.2.** Schematic of fluorescence detection system

$R_n^-$  ( $\Delta R_n = R_n^+ - R_n^-$ ). An amplification plot is created where  $\Delta R_n$  is plotted as a function of time represented by cycle number (Figure 3.4.3a). The initial PCR cycles where the fluorescent signal is below the detection limit, define the baseline of the amplification graph. When sufficient PCR product has accumulated, the signal can be detected above the baseline as it continues to increase proportionally to the increase in PCR product. Eventually the reaction will reach a plateau due to the insufficient quantities of DNA polymerase and other reagents. A fixed threshold is assigned arbitrarily based on the baseline data variation. Then, the cycle number where the plot crosses the threshold value is defined as the threshold cycle  $C_T$ . The value of  $C_T$  can be used to determine the quantity of the DNA template in a sample of interest and is inversely related to the number of template copies. The lower the  $C_T$  value is, the greater the initial quantity of DNA template is because it takes fewer PCR cycles to reach the threshold level of fluorescence. By plotting the  $C_T$  values vs. the initial template quantities for a series of dilutions of the DNA template, a standard curve can be constructed. Given the  $C_T$  of an unknown sample, its initial quantity can be determined from the standard curve by interpolation (Figure 3.4.3b).

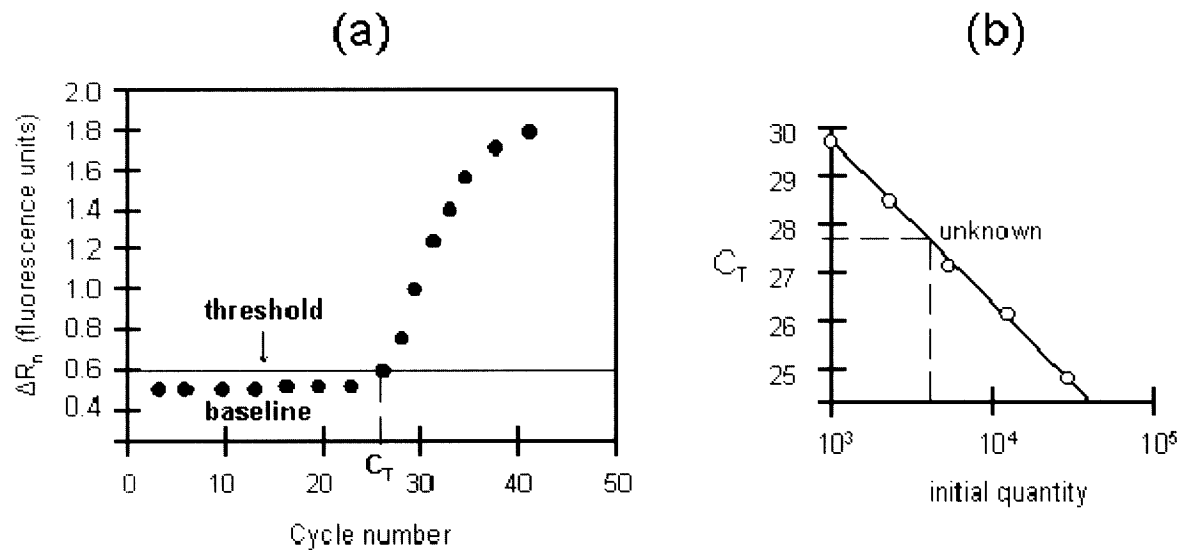


**Figure 3.4.3.** (a) Example of an amplification plot generated by the Sequence Detection Software from the fluorescence emission data collected during each PCR cycle. (b) Example of a standard curve plot for the quantification of an unknown sample.

### **3.4.2 TaqMan PCR Assay Design and Optimization for Quantification of Adenoviral Vector Gene Delivery**

#### Primer and probe design

The TaqMan primers and fluorogenic probe for the quantification of Ad vector levels (H5.010 CMV EGFP) were designed with the Primer Express<sup>®</sup> software (Applied Biosystems) using the default values for the design parameters. The Ad sequence was provided by the vector supplier (Vector Core, UPenn). Although the search for a primer/probe set was confined to the sequence that encodes for the EGFP gene, the entire Ad vector genome sequence was imported in Primer Express<sup>®</sup> in order to test for possible non-specific hybridization to Ad DNA regions other than EGFP, which could result in mispriming and would compromise the efficiency

of the PCR reaction. The results of the software search were examined according to specific guidelines that take into account the nucleotide composition and the melting temperatures of the oligonucleotide sequences in order to ensure optimum performance of the assay (Applied Biosystems 2001). Eventually, the TaqMan primers **5'-GGGCACAAGCTGGAGTACAAC-3'** (forward) and **5'-GTGGCGGATCTTGAAGTTCAC-3'** (reverse) and the fluorogenic probe **FAM-5'-CCGACAAGCAGAAGAACGGCATCA-3'-TAMRA** were selected. These primers amplify a 96 bp DNA fragment on the EGFP gene.

#### PCR reagents and amplification reaction conditions

The amplification reactions were performed with reagents from Applied Biosystems according to the manufacturer's directions. A 50µl reaction contained 25µl of 2X TaqMan Universal PCR Master Mix, 5µl of forward primer (300nM\*), 5µl of reverse primer (300nM\*), 5µl of probe (250nM) and 10µl of the DNA sample. The TaqMan Universal PCR Master Mix contains TaqMan buffer A (1X), MgCl<sub>2</sub> (5mM), dUTP (400µM), dATP, dCTP, dGTP (200µM each), AmpliTaq Gold DNA polymerase (0.025U/µl), AmpErase UNG (0.01U/µl) and glycerol (8%). The concentrations in parentheses refer to the final concentration of each reagent in the 50µl PCR reaction mixture. Thermocycling was performed in an ABI Prism 7700 Sequence Detection System. The samples were subjected to 50°C for 2 min (UNG enzyme incubation to degrade carryover contamination) and 95°C for 10 min (AmpliTaq Gold enzyme activation) and then to 45 cycles of 95°C for 15 sec (denaturing step) and 60°C for 1 min (annealing/extension step) with continuous monitoring of fluorescence emission. The data were processed with the SDS software (Applied Biosystems).

\*Note: primer concentrations determined after optimization.

#### Primer concentration optimization

The optimal concentrations of forward and reverse primer were identified experimentally by independently varying the concentration levels from 50nM to 900nM (Table 3.1) and running amplification reactions with a fixed amount of target DNA template. Optimal PCR performance is



achieved by selecting the primer concentrations that provide the lowest  $C_T$  and highest  $\Delta R_n$  (PE Biosystems 1999).

The adenoviral vector that has been used throughout this thesis for gene delivery to hepatocyte cultures served as the target DNA template for this optimization experiment. The Ad was pre-treated with proteinase K to prevent any interference of the viral capsid components with the activity of the DNA polymerase or its accessibility to the Ad DNA (Ma et al. 2001). The Ad was incubated with proteinase K at 37°C for 30min. This was followed by a 20min incubation at 95°C to inactivate the proteinase K. The amount of template used was  $2.6 \times 10^8$  Ad genome copies (10ng DNA) per PCR reaction (Note: the initial Ad genome concentration was determined with  $OD_{260}$  spectrophotometer measurements by the vector supplier). The concentration of the TaqMan probe was set to 250nM as recommended by the manufacturer. All primer combination reactions were run in triplicates as well as the No Template Control (NTC).

**Table 3.1.** Primer optimization matrix.

Reverse Primer (nM)	Forward Primer (nM)		
	50	300	900
50	50/50	300/50	900/50
300	50/300	300/300	900/300
900	50/900	300/900	900/900

Table 3.2 shows the results for all nine primer concentration combinations. The combination of 50nM forward and reverse primer gave both the lowest  $\Delta R_n$  and highest  $C_T$  values. All other primer combinations that contained a 50nM concentration of either the forward or the reverse primer resulted in reduced  $\Delta R_n$  and slightly increased  $C_T$  values. Finally, all primer combinations that contained at least 300nM forward and reverse primer gave both the highest  $\Delta R_n$  and the lowest  $C_T$  values; therefore any of these combinations will provide optimal PCR performance. A concentration of 300nM for both primers was selected for all subsequent PCR experiments for the quantification of Ad vector gene delivery in hepatocyte cultures.

**Table 3.2.** Primer concentration optimization results

<b>Forward/Reverse primer (nM)</b>	$\Delta R_n^*$	<b>mean</b>	<b>standard deviation</b>	<b>C<sub>T</sub></b>	<b>mean</b>	<b>standard deviation</b>
<b>NTC**</b>	0.00 -0.05 -0.01	-0.02	0.02	45 45 45	45.00	0.00
<b>50/50</b>	0.06 0.05 0.06	0.06	0.00	18.41 18.67 18.26	18.45	0.21
<b>50/300</b>	0.38 0.36 0.33	0.36	0.03	17.21 17.32 17.98	17.50	0.42
<b>300/50</b>	0.32 0.38 0.42	0.37	0.05	17.09 16.71 16.60	16.80	0.26
<b>50/900</b>	0.50 0.44 0.45	0.47	0.03	16.62 16.93 16.87	16.81	0.16
<b>900/50</b>	0.43 0.48 0.41	0.44	0.03	16.27 16.16 16.38	16.27	0.11
<b>300/300</b>	1.32 1.20 1.16	1.23	0.08	15.92 15.97 15.76	15.88	0.11
<b>300/900</b>	1.25 1.31	1.28	0.04	15.62 15.60	15.61	0.01
<b>900/300</b>	1.13 1.17 1.20	1.17	0.03	15.68 15.84 15.74	15.75	0.08
<b>900/900</b>	1.28 1.42 1.24	1.32	0.09	15.22 15.27 15.28	15.26	0.03

\* $\Delta R_n$  values correspond to the final measurements of PCR run (45<sup>th</sup> cycle).

\*\* **NTC**: no template control

### Sensitivity and dynamic range of the PCR assay

In theory, a single copy of a target DNA sequence can be detected with the real time TaqMan PCR method under optimal conditions. However, several parameters such as the primer and probe concentrations or the nature and purity of the DNA template can affect the sensitivity of the assay. To determine the detection limit and the dynamic range with the above-mentioned primers/probe set, the Ad-EGFP vector was used as the PCR template. After treatment with proteinase K, a series of 10-fold dilutions of the vector were prepared and PCR was performed in triplicates. As shown in the amplification plot in Figure 3.4.4, as few as 10 Ad copies could be detected with the assay (Note: the assay could detect 2 Ad copies per reaction in 4 out of 6 replicates). The linear range for quantification was between 10 and  $10^8$  Ad copies per PCR reaction – 7 orders of magnitude wide (Figure 3.4.5). The coefficient of variation of  $C_T$  values was less than 2%.

The ability of the assay to distinguish differences of 2-fold and 50% in Ad vector levels among samples was also tested. Figure 3.4.6a presents a  $[C_T]$  vs. [template quantity] plot for the above mentioned serial dilutions (the fitted standard curve is also shown) as well as samples containing  $2 \times 10^2$ ,  $3 \times 10^2$ , ...,  $2 \times 10^5$ ,  $3 \times 10^5$  Ad copies (red square symbols). All data points represent the mean values of triplicate PCR reactions and the error bars the  $\pm$  standard deviation. Figure 3.4.6b shows a log-log plot of the template quantity of the samples determined by interpolation using the standard curve versus the expected template quantity. The  $C_T$  values are also shown in the table in figure 3.4.6c. The results indicate that the assay is capable of distinguishing 2-fold differences (between  $10^3$  -  $2 \times 10^3$ ,  $10^4$  -  $2 \times 10^4$ ,  $10^5$  -  $2 \times 10^5$  Ad copies; not so sensitive between 100-200 copies) as well as 50% differences (between 200 – 300,  $2 \times 10^3$  -  $3 \times 10^3$ ,  $2 \times 10^4$  -  $3 \times 10^4$ ,  $2 \times 10^5$  -  $3 \times 10^5$  copies).

### Specificity of PCR assay

The specificity of the primers/probe set was confirmed by performing PCR with a different adenoviral vector as a template, a vector carrying the gene for  $\beta$ -galactosidase (vector H5.010CMVLacZ, Vector Core, UPenn) instead of EGFP. The two vectors are identical except for the transgene that they deliver. PCR reactions were carried out in triplicates for samples containing  $2 \times 10^7$  copies of Ad-LacZ with or without Ad-EGFP at ratios of 1:1 and 1: $10^4$ . The results are summarized in Table 3.3. Two of the replicates containing only Ad-LacZ template

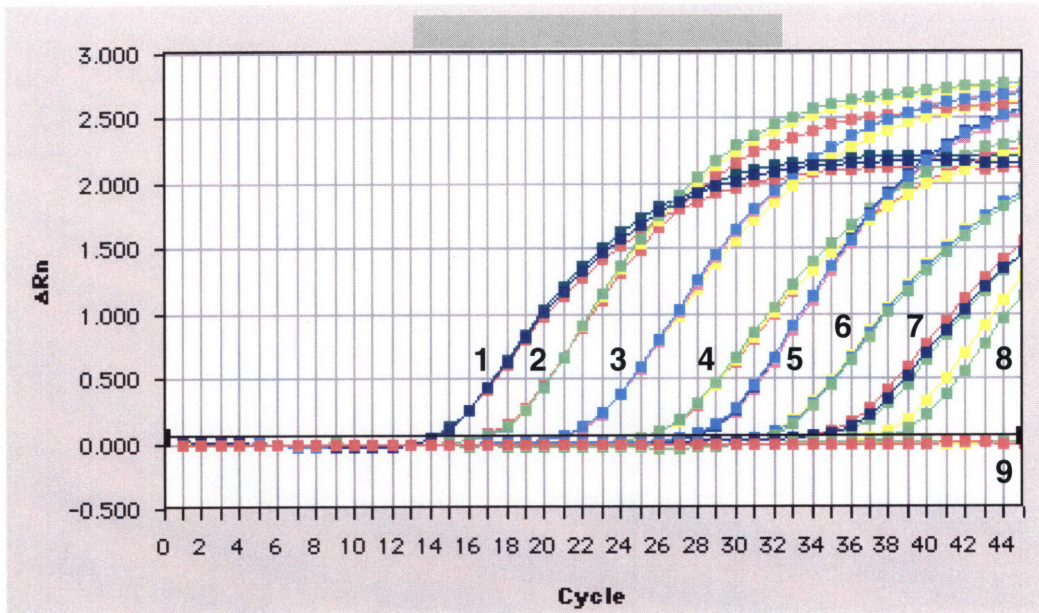


**Figure 3.4.4.** Amplification plot generated by the ABI Prism 7700 Sequence Detection System for a series Ad-EGFP vector dilutions. Curves 1 to 9 correspond to  $10^8$ ,  $10^7$ ,  $10^6$ ,  $10^5$ ,  $10^4$ ,  $10^3$ ,  $10^2$ , 10 and 0 (no template control) Ad copies respectively. Triplicate samples are shown. The horizontal line at  $\Delta Rn = 0.07$  represents the threshold.

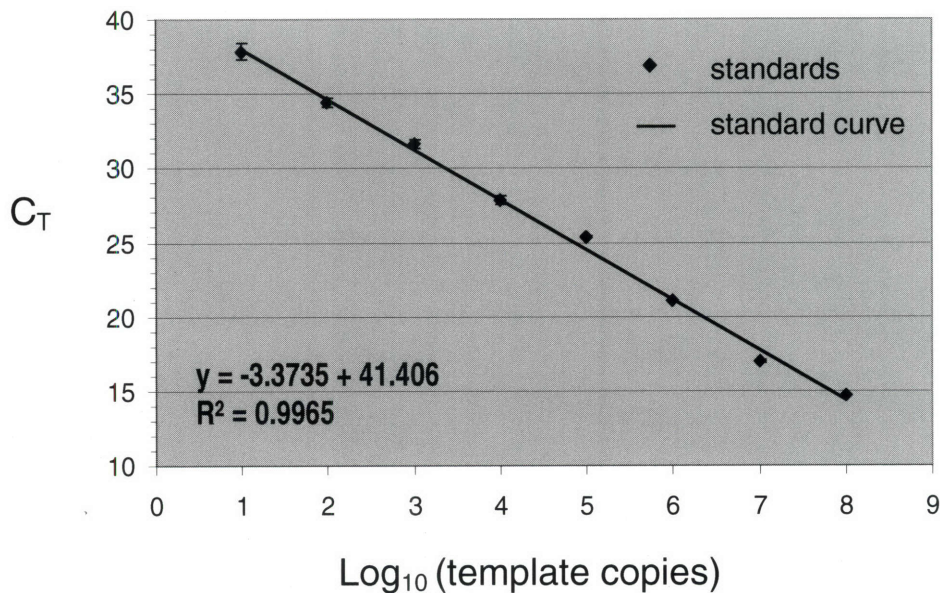
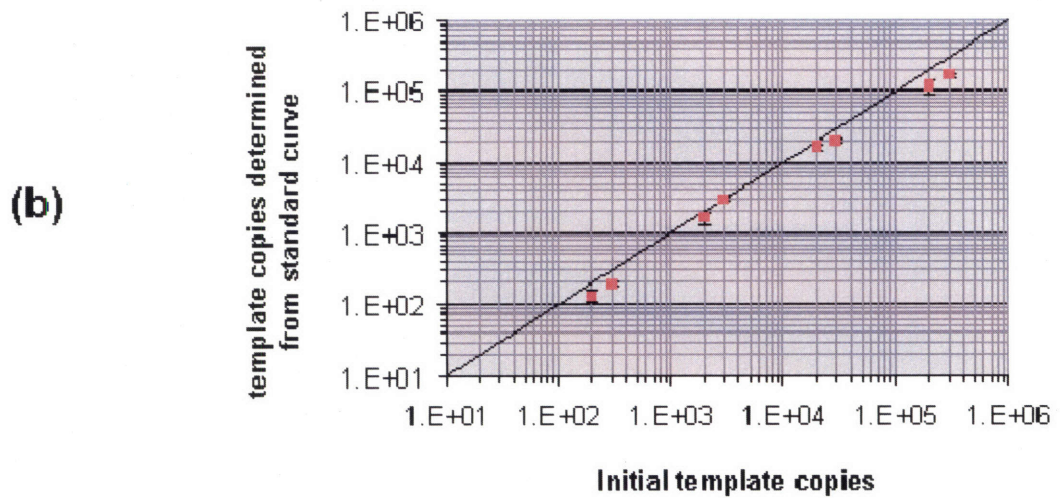
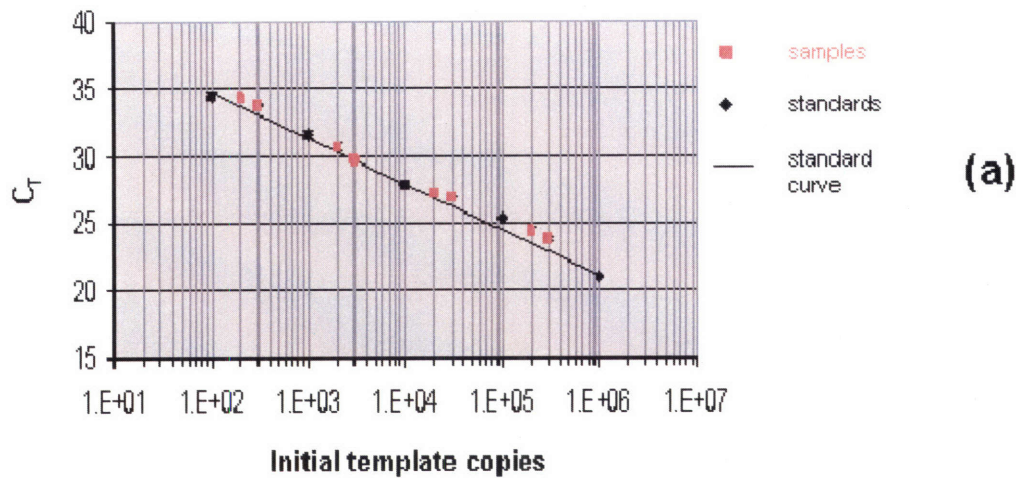


**Figure 3.4.5.** Dynamic range of TaqMan PCR assay for Ad-EGFP vector. Cycle number  $C_T$  is plotted against the initial Ad template quantity. All points represent the mean of triplicate PCR reactions  $\pm$  the standard deviation. The standard curve is shown as a solid line.



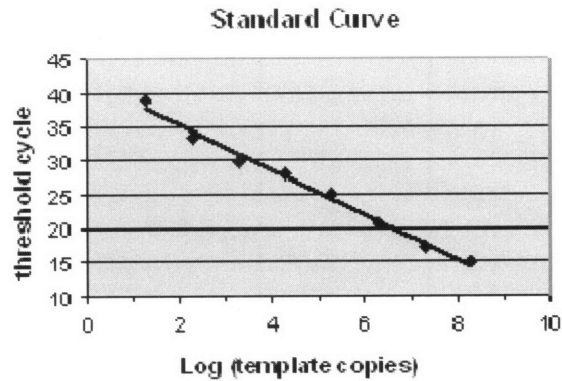


(c)

Initial Ad Template copies	Average $C_T$	Standard deviation
100	34.44	0.29
200	34.29	0.31
300	33.74	0.09
$10^3$	31.62	0.34
$2 \times 10^3$	30.62	0.27
$3 \times 10^3$	29.71	0.12
$10^4$	27.83	0.30
$2 \times 10^4$	27.20	0.13
$3 \times 10^4$	26.91	0.07
$10^6$	25.39	0.04
$2 \times 10^6$	24.36	0.31
$3 \times 10^6$	23.80	0.14

**Figure 3.4.6.** Ability of TaqMan PCR assay to determine 2-fold and 50% differences in Ad template concentration. a) Plot of the threshold cycle versus initial template copy number, (b) log-log plot of Ad template quantity determined with interpolation from standard curve versus actual template quantify. (c) Table of  $C_T$  values.

**Table 3.3.** Specificity of PCR assay. Amplification in the presence of Ad-βgal template.



Sample	C <sub>T</sub>	mean	standard deviation	Copy #	mean	standard deviation
<b>Ad-βgal (2x10<sup>7</sup> copies)</b>	45.00	44.09	1.58	0.13	0.36	0.41
	42.27			0.83		
	45.00			0.13		
<b>Ad-βgal/Ad-EGFP 1:10<sup>-4</sup></b>	31.13	31.14	0.03	1.80E+03	1.79E+03	37.56
	31.11			1.82E+03		
	31.17			1.75E+03		
<b>Ad-βgal/Ad-EGFP 1:1</b>	17.07	17.27	0.17	2.92E+07	2.56E+07	3.11E+06
	17.35			2.41E+07		
	17.38			2.36E+07		

failed to amplify; the third replicate had a C<sub>T</sub> value above 42 cycles, which corresponds to a template copy number outside the linear range for quantification (see standard curve inset). Additionally, the presence of 2x10<sup>7</sup> copies of Ad-LacZ had a negligible effect (less than 1.3-fold difference in measured concentration) on the amplification of 2x10<sup>3</sup> and 2x10<sup>7</sup> copies of Ad-EGFP.

As mentioned earlier, this TaqMan assay was developed to quantify Ad gene delivery in hepatocyte cultures (i.e. detect Ad in a background of genomic DNA). In order to ensure that the

excess genomic DNA would not interfere with the quantification of the vector, a control experiment was performed where DNA extracted from primary rat hepatocytes was mixed with Ad-EGFP vector of known quantities and amplified with TaqMan PCR<sup>1</sup>. Figure 3.4.7 shows a plot of the standard curve (10 to 10<sup>8</sup> copy number range) as well as the C<sub>T</sub> values for the samples containing Ad in the presence of cellular DNA (red squares). The results indicate that the presence of 25ng of hepatocyte genomic DNA per reaction had a negligible effect over a range of 10<sup>2</sup> to 10<sup>7</sup> Ad copies and therefore did not affect the efficiency of the PCR assay.

### Reproducibility of PCR assay

In all further PCR experiments, serial dilutions of the Ad-EGFP vector (ranging from 10<sup>2</sup> to 10<sup>7</sup> Ad copies) were included as standards for the detection and quantification of Ad DNA in hepatocyte cultures. In these experiments the slopes of the standard curves were comparable within a very narrow range; the average slope value was -3.44 and the coefficient of variation was less than 1% (12 PCR runs included). All triplicate amplifications resulted in very similar C<sub>T</sub> values with coefficient of variation that did not exceed 1%. All hepatocyte culture samples were assayed in triplicate and the Ad copy number was determined from the standard curve by interpolation. The mean Ad copy number values were calculated and the assay was repeated for samples for which the coefficient of variation exceeded 10%.

In conclusion, the above-mentioned experiments established the specificity, sensitivity (10 copies, 2-fold and 50% difference), dynamic range (6-7 log decades), precision (<2% CV of C<sub>T</sub> values) and reproducibility of the designed TaqMan PCR assay as well as the ability to detect the Ad-EGFP vector in the context of rat hepatocyte DNA. These attributes make this method a valuable means for the quantitative analysis of the main experiments in this thesis, which aim at the comparison of Ad gene delivery in two different types of hepatocyte culture. In addition to this, the primers/probe set designed here is specific to the EGFP gene not the Ad vector; therefore this assay could be directly applied to the quantification of gene delivery with different types of vectors.

---

<sup>1</sup> Note: primary hepatocytes were harvested from a male Fisher rat and DNA was extracted with the High Pure PCR Template Preparation Kit (Roche). The DNA content was quantified with the Rediplate 96 PicoGreen dsDNA Microplate assay (for details refer to section 3.3).

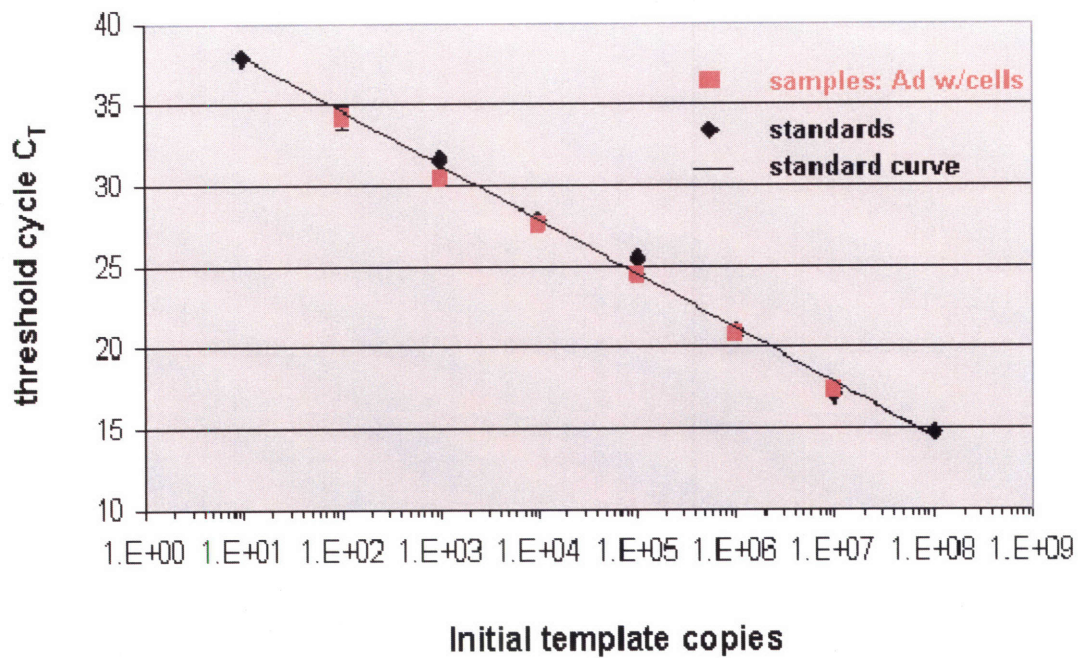


**Figure 3.4.7.** Specificity of PCR assay. Amplification of Ad-EGFP in the presence of hepatocyte genomic DNA (25ng/reaction).



## 3.5 RNA Extraction and Total RNA Quantification

### 3.5.1 RNA Extraction and Purification

#### Hepatocyte Monolayer Cultures

The hepatocytes were lysed and homogenized directly in the culture plates with 1 ml Trizol Reagent (Invitrogen) per well after the HGM medium had been removed. The homogenized samples were stored in microcentrifuge tubes at  $-80^{\circ}\text{C}$  until further processing to isolate the RNA. The RNA isolation process involved the addition of chloroform to each sample followed by centrifugation to separate the solution in three phases: an upper aqueous phase (RNA), an interphase (DNA) and a lower organic phase (protein). The aqueous phase was transferred to a fresh tube. The detailed instructions of the Trizol Reagent protocol were followed for the execution of the above-mentioned steps. The RNA samples were then purified with the RNeasy Mini Kit (Qiagen). During this process each sample is mixed with an equal volume of 70% ethanol and applied to an RNeasy mini column. The RNA binds to the silica-gel membrane in the column, is washed from contaminants with a special buffer and eventually is eluted with 30 $\mu\text{l}$  RNase-free water. These bind, wash and elution steps are performed by centrifugation. The purified RNA samples were stored at  $-80^{\circ}\text{C}$  until total RNA quantification and real-time RT-PCR analysis. Before performing these assays all samples were treated with RNase-free DNase I (Invitrogen) according to the manufacturer's protocol.

The interphase that formed during the Trizol-chloroform centrifugation of each sample was also transferred into a fresh tube for the purification of the DNA.

#### Liver Microreactor Cultures

The silicon scaffolds containing the hepatocyte tissue were removed from the microreactor chambers and were placed in microcentrifuge tubes in 1 ml Trizol Reagent. The cells were mechanically lysed with a syringe and a 24-gauge needle to ensure that the hepatocyte tissue inside the scaffold channels was thoroughly homogenized. The silicon scaffolds were then removed and the RNA was isolated and purified as described in the previous paragraph.

### **3.5.2 DNase Treatment of RNA Samples**

All RNA samples were treated with RNase-free DNase I (Invitrogen) to eliminate any potential contamination with DNA, which might interfere with the quantification of total RNA. 1µl RNA sample (2µl for liver microreactor samples) was mixed with 1µl 10X DNase I Reaction Buffer, 1µl DNase I (1U/µl), and DEPC-treated water to a total volume of 10µl. The mixture was incubated for 15 min at room temperature. Then the DNase I was inactivated with 1µl of 25 mM EDTA solution and incubation at 65°C for 10 min. Each sample was diluted with 39µl TE buffer to a total volume of 50µl before total RNA quantification.

### **3.5.3 Quantification of Total RNA Content in Hepatocyte Culture Samples**

After RNA isolation and purification followed by treatment with DNase I, the samples (hepatocyte monolayer cultures and tissue-engineered microreactors) were assayed for total RNA content with the RediPlate™ 96 RiboGreen® RNA Quantitation Kit (Molecular Probes). This assay is based on the ability of the nucleic acid stain RiboGreen to bind to RNA and subsequently emit bright green fluorescence. The stain is predispensed in the wells of a 96-well microplate and is dissolved in TE buffer before the addition of the RNA samples; fluorescence is measured in a fluorescence microplate reader using excitation at 485 nm and detection at 530 nm. The fluorescence of the sample of interest is compared to that of a standard curve of RNA. The kit contains rRNA standards from *E. coli*. The assay has a linear range of 3-200 ng in a 200 µl assay volume according to the manufacturer. This method for RNA concentration quantification was chosen over the more commonly used measurements of absorbance at 260 nm, because of its advantages of higher sensitivity, accuracy and dynamic range, as well as the ability for processing multiple samples at the same time.

The RediPlate RiboGreen assay was applied to all RNA samples that were also assayed for EGFP mRNA levels with quantitative real-time RT-PCR. A standard curve was prepared for each microplate. In order to ensure accurate RNA quantification of the rat hepatocyte samples with this assay, the standard curve derived with the *E. coli* rRNA standards provided in the kit was compared to a standard curve derived from a series of dilutions of Rat Total RNA (Ambion) treated with DNase I ranging from 0.01 to 1µg/ml (2 to 200 ng in a 200 µl assay volume). All standards were assayed in triplicates. There was no significant difference between the *E. coli*

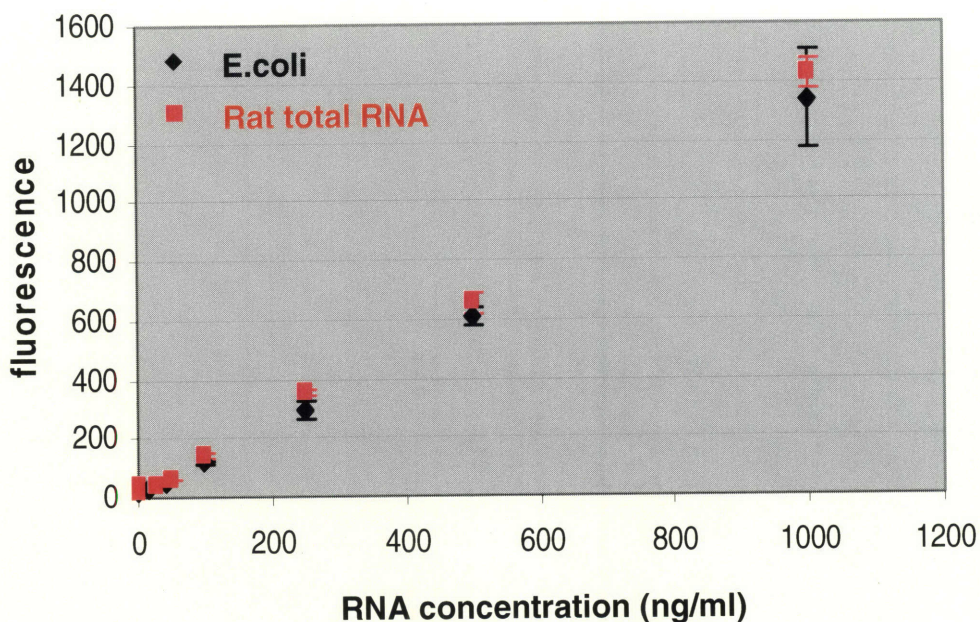


**Figure 3.5.1.** RediPlate 96 RiboGreen RNA Quantitation assay. Comparison of standard curves prepared with *E.coli* rRNA (included in the Rediplate kit) and Rat total RNA dilutions. Fluorescence was measured with a microplate reader. The fluorescence signals are plotted against the RNA concentration. All standards were assayed in triplicates. The symbols represent the mean values and the error bars the standard deviation.

and the Rat RNA standard curves (Figure 3.5.1). Therefore all subsequent plates were run with the standards included in the kit.

The slopes of the standard curves among different microplates were comparable within a narrow range – the coefficient of variation was less than 3% (n=6). All hepatocyte samples were assayed in triplicate and the total RNA content was determined from the standard curve by interpolation. The mean values were used for further calculations (to determine the volume of each sample needed for the reverse transcription reaction).

### **3.5.4 Cellular RNA Content Measurements for Rat Hepatocytes**

To determine the RNA content of a rat hepatocyte (for data normalization purposes), samples of hepatocytes were needed containing known numbers of cells. After each rat liver perfusion and hepatocyte isolation though, the cell viability and concentration of the resulting hepatocyte suspension can be determined with the trypan blue exclusion method in a hemocytometer as described in section 3.1. Therefore, triplicate samples of varying cell numbers (from  $10^4$  to  $4 \times 10^5$ ) were prepared from the resulting hepatocyte suspension of a rat perfusion. RNA was extracted as described in Section 3.5.1 and quantified with the RediPlate 96 RiboGreen RNA Quantitation Kit as described in Section 3.5.3. Figure 3.5.2 shows a plot of RNA content ( $\mu\text{g}$  RNA) as a function of hepatocyte number. Each data point corresponds to the mean value of 3 samples and the error bars represent the standard deviation. A straight line was fitted to the data with linear regression (Excel) and the slope represents the cellular RNA content. As shown in the plot, each rat hepatocyte contains  $4.8 \times 10^{-5}$   $\mu\text{g}$  RNA. This number was used to convert the normalized RT-PCR data (EGFP RNA copies per  $\mu\text{g}$  RNA) to EGFP mRNA copies per cell.

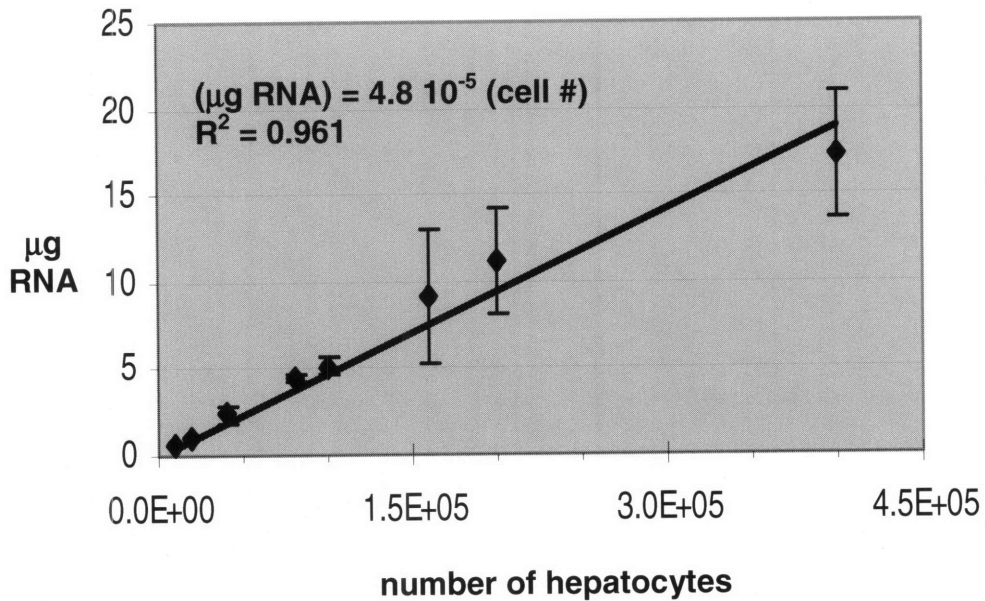


**Figure 3.5.2.** Rat hepatocyte RNA content measurements. Samples of varying cell numbers were prepared after rat liver perfusion and hepatocyte isolation. RNA was extracted and quantified with the Reditplate 96 RiboGreen RNA Quantitation Kit. Fluorescence was measured with a microplate reader and the RNA content of each sample was determined from the standard curve by interpolation. The RNA content is plotted here as a function of cell number. The data points represent the mean values of 3 samples and the error bars the standard deviation. The straight line corresponds to the linear regression with Excel.

## 3.6 Quantitative real-time RT-PCR

### 3.6.1 Introduction

Real-time PCR is the method of choice for gene quantification because of its significant advantages, as presented in Section 3.4 of this chapter. With the addition of a reverse transcription (RT) step before the PCR reaction, it has also become one of the most widely used methods for detecting and quantifying gene expression and comparing mRNA levels in different sample populations. There are several factors that make the quantification of RNA with RT-PCR significantly more complex than the quantification of genomic DNA. These include the inherent variability of RNA extracted from biological samples and its instability and most importantly the efficiency of the RT reaction. Due to the exponential nature of PCR, even minor experimental variations can lead to large changes in the final amplified product; therefore every step must be carefully designed and controlled. The additional step of reverse transcription, during which the RNA is converted into a cDNA template, is critical for the overall sensitivity, accuracy and reproducibility of the assay. The amount of produced cDNA must accurately represent the amount of input RNA. The efficiency of the RT reaction depends on the enzyme, the type of primers that prime the cDNA synthesis as well as the abundance of template (Bustin et al., 2005; Wong and Medrano, 2005; Bustin, 2002; Huggett et al., 2005).

In order to minimize these errors and correct for sample-to-sample variation, it is essential to apply a normalization strategy. An endogenous cellular RNA is amplified simultaneously with the target RNA and is used as a reference against which the target RNA values are normalized. The choice of the reference gene is a challenging issue itself and depends on the experimental system studied. Ideally, that gene should be expressed at constant levels independently of the experimental treatment.

In this thesis, real-time RT-PCR was applied for the quantification of EGFP expression after AdEGFP infection in rat hepatocyte monolayer and microreactor cultures. These *in vitro* systems were established from relatively homogeneous hepatocyte populations isolated from rat livers; therefore the variability among biological samples should not be a significant issue, although there could be differences between monolayer and microreactor cultures. Ribosomal RNA (18S rRNA) was selected for normalization since it has been shown to be a reliable control in rat liver compared to housekeeping genes such as  $\beta$ -actin and GAPDH (Sivaraman et al., 2005; Bustin, 2000). Other reports also suggest the use of rRNA as the most reliable strategy

for accurate RNA quantification (Bustin, 2002; Bustin et al, 2005). Normalization against total RNA concentration is another option provided that total RNA levels can be accurately measured.

It is possible to obtain absolute quantification of the target RNA. However, the preparation of standard curves from *in vitro* transcribed RNA requires a lot of effort and presents many problems. DNA standards can also be used; there is no control for the efficiency of the reverse transcription though (Applied Biosystems: User Bulletin #2, Relative Quantitation of Gene Expression, 2001). Another option is relative quantification, where RNA quantity is expressed relative to a basis sample (calibrator). The calibrator becomes the 1x sample and all other samples are expressed as an n-fold difference relative to the calibrator. In that case the results can be analyzed with the Comparative C<sub>T</sub> (2<sup>-ΔΔC<sub>T</sub></sup>) Method (Livak and Schmittgen, 2001). According to this method, the amount of target RNA, normalized to an endogenous reference and relative to a calibrator is given by the equation:

$$\text{amount of target} = 2^{-\Delta\Delta C_T}$$

$$\Delta\Delta C_T = \Delta C_{T,q} - \Delta C_{T,cb}$$

where ΔC<sub>T,q</sub> is the difference in threshold cycles between target (EGFP) and reference (18S) for any sample and ΔC<sub>T,cb</sub> is the difference in threshold cycles between target (EGFP) and reference (18S) for the calibrator sample. The comparative C<sub>T</sub> method is applicable only if the amplification efficiency of the target and the reference genes are approximately equal; therefore a validation experiment is required before using this method. This experiment is presented in the data analysis section.

The RT and PCR reactions were performed in a two-step assay following protocols and using reagents established by Applied Biosystems. The TaqMan PCR amplifications were performed with the ABI Prism 7700 Sequence Detection System. Random hexamers were used as the primer for the RT reaction in order to produce cDNA templates for both the target mRNA and the reference rRNA.

The general procedure for the real-time RT-PCR experiments consisted of the following steps: (a) RNA isolation and characterization, (b) DNase treatment, (c) reverse transcription, (d) PCR and (e) data normalization and analysis. These steps are described in detail in the following section.

### **3.6.2 Quantitative real-time RT-PCR Assay Design for Quantification of EGFP mRNA Levels after Ad Vector Gene Delivery**

#### (a) Template preparation (RNA isolation and characterization)

RNA was isolated from hepatocyte monolayer and microreactor cultures with Trizol Reagent (Invitrogen) and purified with the RNeasy mini kit (Qiagen). In the final step of this procedure the RNA was eluted with 30µl RNase-free water. The total RNA content of each sample was measured with the RediPlate™ 96 RiboGreen® RNA Quantitation Kit (Molecular Probes). These procedures are described in detail in Section 3.5.

#### (b) DNase Treatment

Before the reverse transcription reaction all RNA samples were treated with RNase-free DNase I (Invitrogen) to eliminate any potential contamination with DNA, which would lead to inaccurate quantification of mRNA levels. Monolayer cultures: the RNA samples were initially diluted 4 times; then 400 ng RNA were mixed with 1µl 10X DNase I Reaction Buffer, 1µl DNase I (1U/µl), and DEPC-treated water to a total volume of 10µl. Microreactor cultures: 200 ng RNA were mixed with 1.5µl 10X DNase I Reaction Buffer, 1.5µl DNase I (1U/µl), and DEPC-treated water to a total volume of 15µl. The mixtures were incubated at room temperature for 15 min. Then the DNase I was inactivated with 1µl of 25 mM EDTA solution (1.5µl for microreactor samples) and incubation at 65°C for 10 min.

#### (c) Reverse Transcription (cDNA synthesis)

The reverse transcription reactions were performed with reagents from Applied Biosystems according to the manufacturer's directions. Monolayer cultures (400ng RNA): each RT reaction had a total volume of 40µl and was prepared by mixing the 11µl RNA sample (volume after DNase treatment) with a 29µl RT mix. The RT mix contained 4µl of 10X RT buffer, 8.8µl MgCl<sub>2</sub> (5.5mM), 8µl dNTPs mixture (500µM each), 2µl Random Hexamers (2.5 µM), 0.8µl



RNase Inhibitor (0.4 U/ $\mu$ l), 2.5 $\mu$ l MultiScribe Reverse Transcriptase (3.125U/ $\mu$ l) and 2.9 $\mu$ l RNase-free water. The concentrations in parentheses refer to the final concentration of each reagent in the 40 $\mu$ l RT reaction mixture. Microreactor cultures (200ng RNA): each RT reaction had a total volume of 50 $\mu$ l and was prepared by mixing the 16.5 $\mu$ l RNA sample (volume after DNase treatment) with a 33.5 $\mu$ l RT mix. The RT mix contained 5 $\mu$ l of 10X RT buffer, 11 $\mu$ l MgCl<sub>2</sub>, 10 $\mu$ l dNTPs mixture, 2.5 $\mu$ l Random Hexamers, 1 $\mu$ l RNase Inhibitor, 3.125 $\mu$ l MultiScribe Reverse Transcriptase and 0.875 $\mu$ l RNase-free water. The final reagent concentrations were the same as in the monolayer culture samples. Since 18S rRNA was selected as the endogenous reference for normalization, a higher concentration of MultiScribe reverse transcriptase was applied (Applied Biosystems: TaqMan® Gold RT-PCR Kit, Protocol, 2002).

The reactions were incubated at 25<sup>o</sup>C for 10 min (hexamer incubation), then at 37<sup>o</sup>C for 60 min (reverse transcription) and at 95<sup>o</sup>C for 5 min (reverse transcriptase inactivation). After thermal cycling all cDNA samples were stored at -20<sup>o</sup>C.

RT reactions without reverse transcriptase (minus RT controls) were also prepared for each sample. The minus RT controls can account for any residual DNA contamination, since any PCR amplification in these samples would be attributed to genomic DNA templates.

#### (d) Real-Time PCR Data Acquisition

The amplification reactions for the EGFP cDNA template were performed with the same set of primers and TaqMan probe (FAM/TAMRA) as described in Section 3.4.2. The 18S cDNA template was detected and amplified with a pre-designed set of primers and TaqMan probe provided by Applied Biosystems (Eukaryotic 18S rRNA Endogenous control, Pre-Developed TaqMan Assay Reagents). The amplicon generated is 187 bp in length and the primer and probe sequences are conserved among several eukaryotic organisms including rat. The TaqMan probe contains the VIC™ dye as the reporter and TAMRA as the quencher.

The two templates were amplified in separate reactions and each sample was assayed in triplicate. In the case of the EGFP template, the 50 $\mu$ l PCR reaction contained 25 $\mu$ l of 2X TaqMan Universal PCR Master Mix, 5 $\mu$ l of forward primer (300nM), 5 $\mu$ l of reverse primer (300nM), 5 $\mu$ l of probe (250nM) and 10 $\mu$ l of the cDNA sample. In the case of the 18S template, the 50 $\mu$ l PCR reaction contained 25 $\mu$ l of TaqMan Universal PCR Master Mix (2X), 2.5 $\mu$ l of the primer and probe mix, 12.5 $\mu$ l RNase-free water and 10 $\mu$ l of the cDNA sample. cDNA samples

were diluted before PCR (100x for monolayer samples and 40x for microreactor samples). The quantity of cDNA sample added in each PCR reaction corresponds to 1 ng total RNA (except when specified otherwise).

Thermocycling was performed in an ABI Prism 7700 Sequence Detection System. The samples were subjected to 50°C for 2 min (UNG enzyme incubation to degrade carryover contamination) and 95°C for 10 min (AmpliTaQ Gold enzyme activation) and then to 45 cycles of 95°C for 15 sec (denaturing step) and 60°C for 1 min (annealing/extension step) with continuous monitoring of fluorescence emission. The data were processed with the SDS software (Applied Biosystems). The theoretical and experimental details of real-time TaqMan PCR are described in detail in Section 3.4.

(e) Data Normalization and Analysis

**Comparative C<sub>T</sub> Method:**

Before using the Comparative C<sub>T</sub> Method for RT-PCR data analysis, a validation experiment was performed to ensure that the amplification efficiencies of the EGFP and 18S templates were similar. Serial dilutions of a cDNA sample were assayed in triplicate for the EGFP and 18S templates with real-time PCR and the difference in threshold cycles ΔC<sub>T</sub> was calculated (the sample was isolated from a hepatocyte monolayer culture that had been infected with AdEGFP at a concentration of 6.4x10<sup>7</sup> i.p./ml for 24 hr). The results are shown in Table 3.3 below:

**Table 3.3:** Validation experiment for Comparative C<sub>T</sub> Method.

<b>Input Amount ng Total RNA</b>	<b>EGFP Average C<sub>T</sub></b>	<b>18S Average C<sub>T</sub></b>	<b>ΔC<sub>T</sub> EGFP – 18S</b>
<b>1</b>	30.55±0.03	19.35±0.13	11.20±0.14
<b>0.5</b>	31.88±0.17	20.38±0.07	11.50±0.18
<b>0.1</b>	34.18±0.13	22.86±0.21	11.31±0.25
<b>0.05</b>	34.96±0.22	23.79±0.13	11.18±0.25
<b>0.01</b>	37.62±0.26	26.27±0.07	11.35±0.27

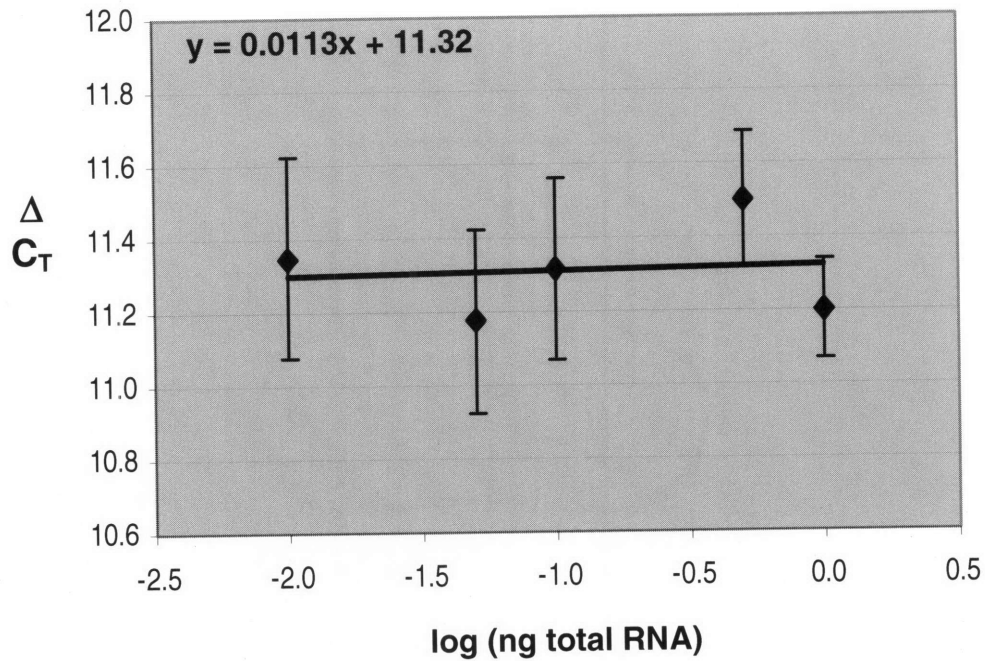
Figure 3.6.1 shows a plot of  $\Delta C_T$  versus the log (input amount of RNA). If the absolute value of the slope in the plot is  $<0.1$  then the  $2^{-\Delta\Delta C_T}$  method can be used for the relative quantification of EGFP mRNA levels in the experiments of this thesis. The slope in figure 3.6.1 was determined from linear regression with Excel and is equal to 0.0113, which is below the required limit.

Table 3.4 illustrates how the relative EGFP mRNA levels are calculated with the Comparative  $C_T$  Method. This example shows the results for three hepatocyte monolayer cultures infected with AdEGFP for 24 hr at three different concentrations:  $C_0$  (sample A),  $C_0/2$  (sample B) and  $C_0/10$  (sample C), where  $C_0=6.4 \times 10^7$  i.p./ml. The  $C_T$  values for the EGFP and 18S templates are used to calculate  $\Delta C_T$ ,  $\Delta\Delta C_T$  and  $2^{-\Delta\Delta C_T}$  (the amount of EGFP mRNA normalized to 18S and relative to the calibrator). The calibrator in this case is the sample exposed to the highest Ad concentration  $C_0$  (sample A).

**Table 3.4:** Relative Quantification with the Comparative  $C_T$  Method.

Sample (initial Ad conc.)	EGFP Average $C_T$	18S Average $C_T$	$\Delta C_T$ EGFP – 18S	$\Delta\Delta C_T$ $\Delta C_T - \Delta C_{T,A}$	EGFP <sub>N</sub> Rel. to A
<b>A (<math>C_0</math>)</b>	30.67±0.13	19.93±0.08	10.74±0.15	0.00±0.15	1.00 (0.90-1.11)
<b>B (<math>C_0/2</math>)</b>	33.56±0.03	19.74±0.08	13.82±0.08	3.08±0.08	0.12 (0.11-0.13)
<b>C (<math>C_0/10</math>)</b>	37.22±0.04	19.64±0.13	17.58±0.14	6.84±0.14	$8.7 \times 10^{-3}$ (7.9-9.6) $\times 10^{-3}$

These results indicate that sample B contains 8.3x less EGFP mRNA than sample A and sample C contains 115x less EGFP mRNA than A.



**Figure 3.6.1.** Relative amplification efficiency of 18S and EGFP templates. Serial dilutions of a cDNA sample (ranging from 0.01 to 1 ng input amount of total RNA) were assayed with real-time TaqMan PCR for the EGFP and 18S templates. This figure shows a plot of the difference in threshold cycles  $\Delta C_T$  versus the log input amount of total RNA. The data points represent the difference of the average  $C_T$  values and the error bars the standard deviation of the difference. The straight line corresponds to the linear regression with Excel. The cDNA sample was prepared from a hepatocyte monolayer culture that had been infected with AdEGFP at a concentration of  $6.4 \times 10^7$  i.p./ml for 24 hr.

**Simplified Comparative  $C_T$  Method ( $2^{-\Delta C'_T}$  Method):**

As described previously, the total RNA content of all experimental samples studied was quantified with the RiboGreen assay. Then, the PCR amplification reactions were set up using cDNA derived from the same amount of input RNA. This way the PCR results were already normalized to an external measurement (total RNA). In this case it is possible to apply a simplified version of the Comparative  $C_T$  Method (Livak and Schmittgen, 2001), where the amount of target RNA relative to a calibrator is given by the equation:

$$\text{amount of target} = 2^{-\Delta C'_T}$$

$$\Delta C'_T = C_{T,q} - C_{T,cb}$$

where  $C_{T,q}$  is the threshold cycle of the target (EGFP) for any sample and  $C_{T,cb}$  is the threshold cycle of the target (EGFP) for the calibrator sample. Table 3.5 shows the application of this simplified method to the example presented in Table 3.4:

**Table 3.5:** Relative Quantification with the Simplified Comparative  $C_T$  Method.

Sample (initial Ad conc.)	EGFP Average $C_T$	$\Delta C_T$ $C_T - C_{T,A}$	EGFP Rel. to A
<b>A (<math>C_0</math>)</b>	30.67±0.13	0.00±0.13	1.00 (0.91-1.09)
<b>B (<math>C_0/2</math>)</b>	33.56±0.03	2.89±0.03	0.135 (0.132-0.137)
<b>C (<math>C_0/10</math>)</b>	37.22±0.04	6.55±0.04	$1.06 \times 10^{-2}$ (1.03-1.10) $\times 10^{-2}$

These results indicate that sample B contains 7.4x less EGFP mRNA than sample A and sample C contains 94x less EGFP mRNA than A, values that are comparable to those derived in Table 3.4.

### Absolute Quantification of EGFP mRNA:

The levels of EGFP expression can also be quantified in terms of the number of cDNA copies with a standard curve prepared from a series of dilutions of the Ad vector, as described in Section 3.4. Again, since the PCR amplification reactions were set up using cDNA derived from the same amount of input RNA the results are already normalized against total RNA concentration. Table 3.6 shows the results for the example presented in Table 3.4:

**Table 3.6:** Absolute Quantification with Standard Curve Method.

<b>Sample (initial Ad conc.)</b>	<b>EGFP Average <math>C_T</math></b>	<b>Average copy # per ng RNA</b>
<b>A (<math>C_0</math>)</b>	30.67±0.13	910.0±82.0
<b>B (<math>C_0/2</math>)</b>	33.56±0.03	124.5±2.4
<b>C (<math>C_0/10</math>)</b>	37.22±0.04	10.1±0.3

According to the results sample B contains 7.3x less EGFP mRNA than sample A and sample C contains 90x less EGFP mRNA than A. These values are very similar to the ones derived with the Simplified Comparative  $C_T$  Method.

In conclusion, all three methods for the analysis of RT-PCR data produce comparable results for the experiments in this thesis, the simplified Comparative  $C_T$  Method being perhaps the easiest to apply.

## **3.7 Miniaturized Spectrometer System for Detection and Quantification of EGFP Expression in Microreactor Cultures**

### ***3.7.1 Introduction***

The design of the microreactor chamber allows the passage of light through the silicon scaffold channels as described in Chapter 2. Based on this characteristic, a fiber optic spectrometer system was built by Dr Karel Domansky to measure EGFP expression in microreactor cultures infected with an Ad gene delivery vector, by directing light of the appropriate wavelength into the microreactor chamber and detecting the emission of green fluorescence (Figure 3.7.1a) (Domansky et al., 2004). As illustrated in the schematic (Figure 3.7.1b), light from an LS-1 Tungsten Halogen Source (Ocean Optics) passes through a bandpass excitation filter (470/40nm), and travels via an optical fiber to the lower part of the microreactor chamber and through the hepatocyte tissue inside the silicon scaffold channels. The light exiting the upper part of the microreactor chamber is directed with the help of a collimator through a longpass emission filter (495nm) which filters out the excitation light, and is transmitted through an optical fiber to a USB2000 Fiber Optic Spectrometer (Ocean Optics). The spectrometer is a linear CCD-array detector responsive from 200 to 1100nm and is directly connected to a computer equipped with the OOIBase32 Spectrometer Operating Software (Ocean Optics). The software collects and processes the spectral data and displays them in real-time. In the experiments that will be presented in this thesis, the dark signal (background noise recorded by blocking the path of the excitation light immediately after the light source) was subtracted from the EGFP spectrum for every measurement. Integration time was set to 30sec and the displayed data were the average of two spectra.

This setup provides a non-invasive way to detect EGFP expression in the microreactor cultures and to follow the changes in expression with time by monitoring the emitted spectra at various times after infection with the Ad gene delivery vector, as presented in the following section. The spectrometer measurements were performed without disrupting the continuous medium flow in the microreactor system and typically lasted only a few minutes.

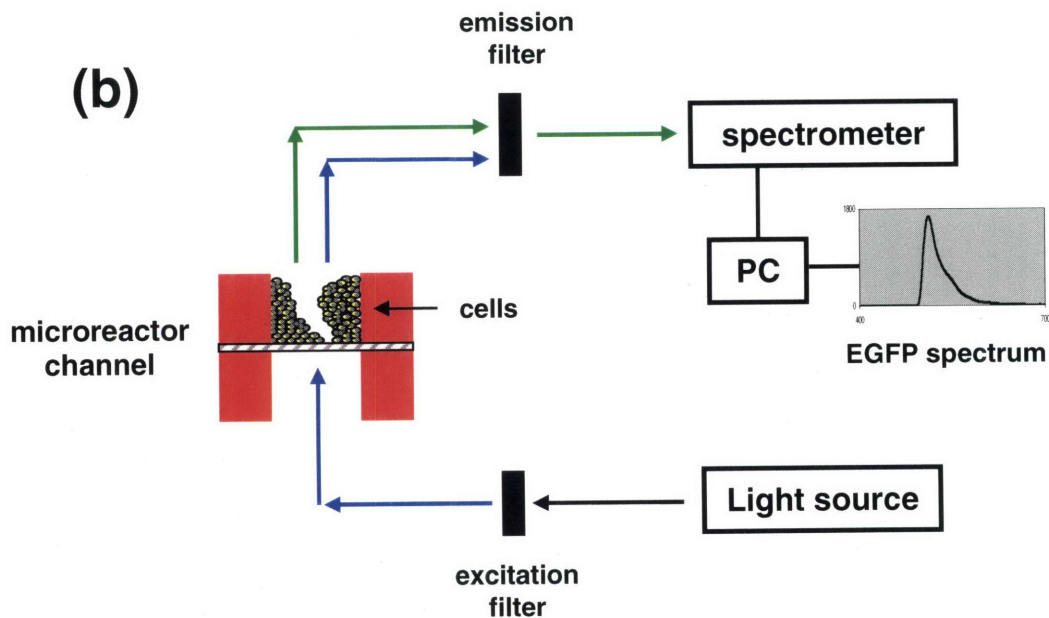
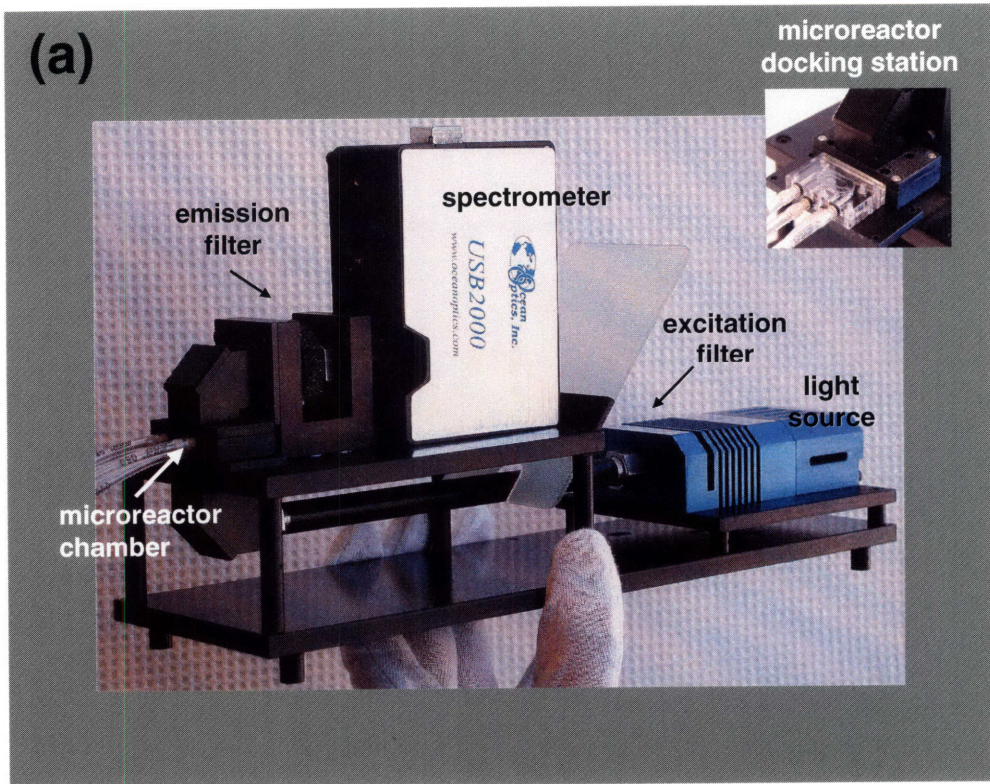


**Figure 3.7.1 (a)** Miniaturized Fiber Optic Spectrometer System (photograph by Karel Domansky). **(b)** Schematic of the spectrometer setup for EGFP detection in the microreactor cultures.



### **3.7.2 Detection of EGFP expression with the Spectrometer**

All the spectrometer data presented in Chapter 5 were obtained with the instrument shown in Figure 3.7.1. However, the first experiments to evaluate and optimize this technique were performed with the older version of the microreactor culture system (stainless steel chamber, Figure 2.2a). The original configuration of the fiber optic spectrometer adapted to that system is shown in Figure 3.7.2.

The example in Figure 3.7.3 illustrates the application of the spectrometer system for the detection of EGFP. One microreactor culture (graph a) was infected with the AdEGFP vector at a concentration of  $4 \times 10^6$  pfu/ml for 24 hours. The second (graph b) was not infected with Ad so as to serve as a control sample. The emission spectra were recorded for both microreactors immediately before the Ad infection ( $t=0$ ) and at different times afterwards. As shown in Figure 3.7.3, the intensity of the spectrum increased with time in the infected microreactor, whereas it remained practically unchanged in the control.

### **3.7.3 Monitoring the time course of EGFP expression in microreactor cultures with spectrometer measurements**

The increasing spectrum intensity levels reflect the increasing levels of produced EGFP protein as a result of Ad gene delivery in the hepatocyte cultures. Therefore, these measurements provide the means for tracking the changes in EGFP expression with time. The intensity values at 509nm (wavelength corresponding to the EGFP emission spectrum maximum) were used as a measure of EGFP expression. For each microreactor the intensity value at time  $t=0$  ( $I_{t=0}$ ) was subtracted from the value measured at any time  $t$  ( $I_t$ ). Intensity was plotted as a function of time  $t$ .

Figure 3.7.4 shows results of spectrometer measurements performed in five experiments (5 different rat liver perfusions). The time course of EGFP expression is plotted for several microreactor cultures infected with AdEGFP at a concentration of  $4 \times 10^6$  pfu/ml for 24h. Control cultures were prepared in every experiment; since all controls showed no change in spectrum intensity with time only one sample is included in the plot (pink triangles). Additionally, one

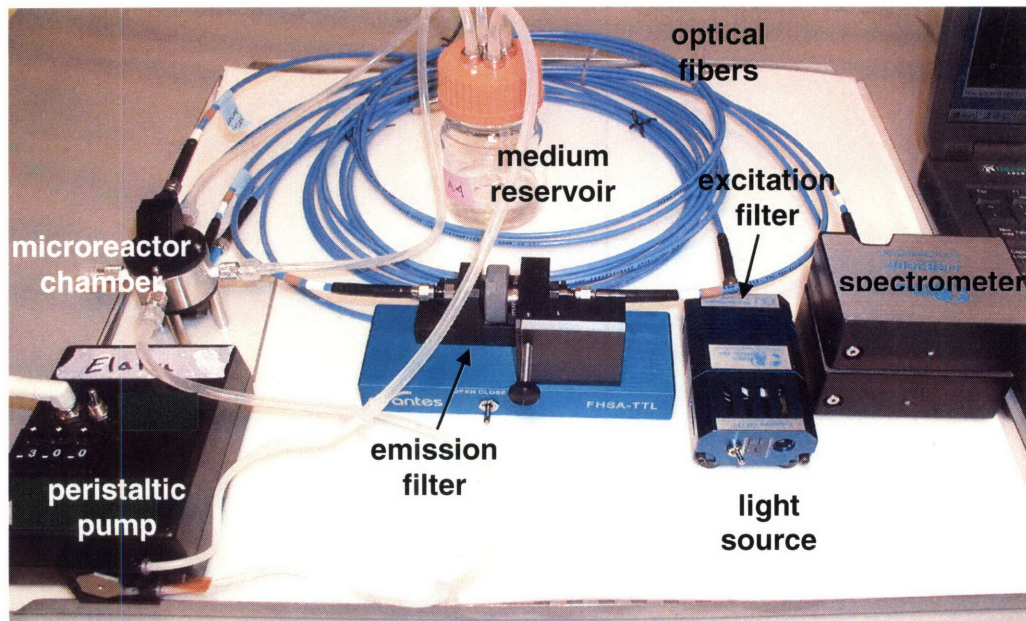


**Figure 3.7.2** Original configuration of the Miniaturized Fiber Optic Spectrometer System adapted to the older version of the microreactor culture system (stainless steel chamber). Photograph by Karel Domansky.

microreactor culture was infected with an Ad vector carrying the gene for  $\beta$ -galactosidase (Ad $\beta$ -gal) at the same conditions as the AdEGFP vector. No change in intensity was observed after infection (black triangles). Consequently, the increase in intensity observed in the cultures infected with AdEGFP was solely the result of EGFP expression and not of any other effect caused by the interaction of the Ad particles with the hepatocyte tissue. Based on the results presented in this plot, EGFP expression increases rapidly after Ad infection and reaches maximum levels around 50-70h after the beginning of Ad infection, then slowly decreases with time. EGFP expression was followed until  $t=11$  days in some microreactor cultures.

The experiments presented in Figures 3.7.3 and 3.7.4, were performed with the original version of the microreactor system (stainless steel chamber). Similar results were obtained for the polycarbonate microreactors.

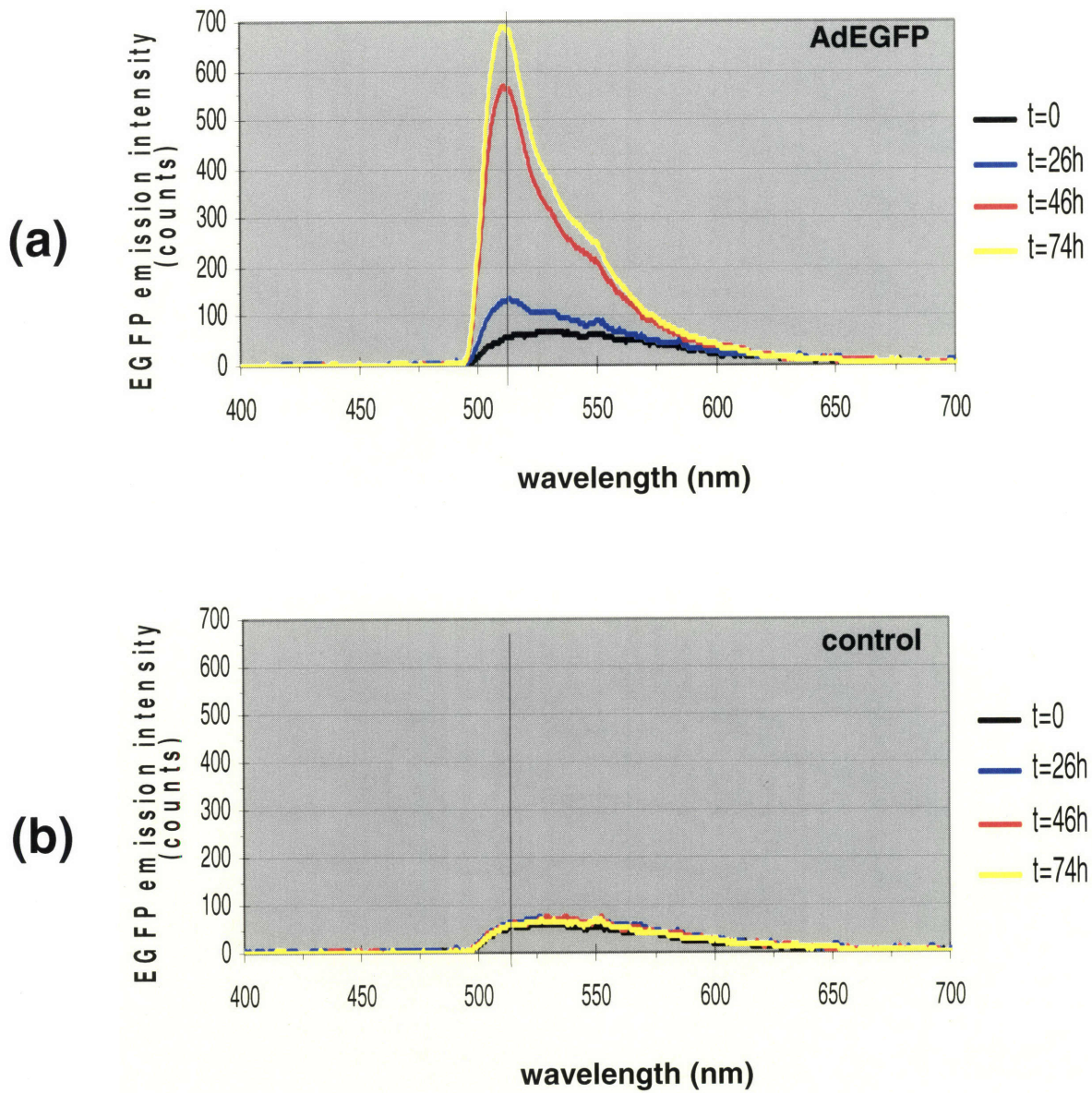


**Figure 3.7.3** Detection of EGFP expression in hepatocyte microreactor cultures with the miniaturized spectrometer system. The graphs show the EGFP emission spectra recorded at different times after the beginning of Ad infection (t=0): **(a)** microreactor culture infected with AdEGFP at a concentration of  $4 \times 10^6$  pfu/ml for 24h, **(b)** control microreactor culture (not infected with Ad).



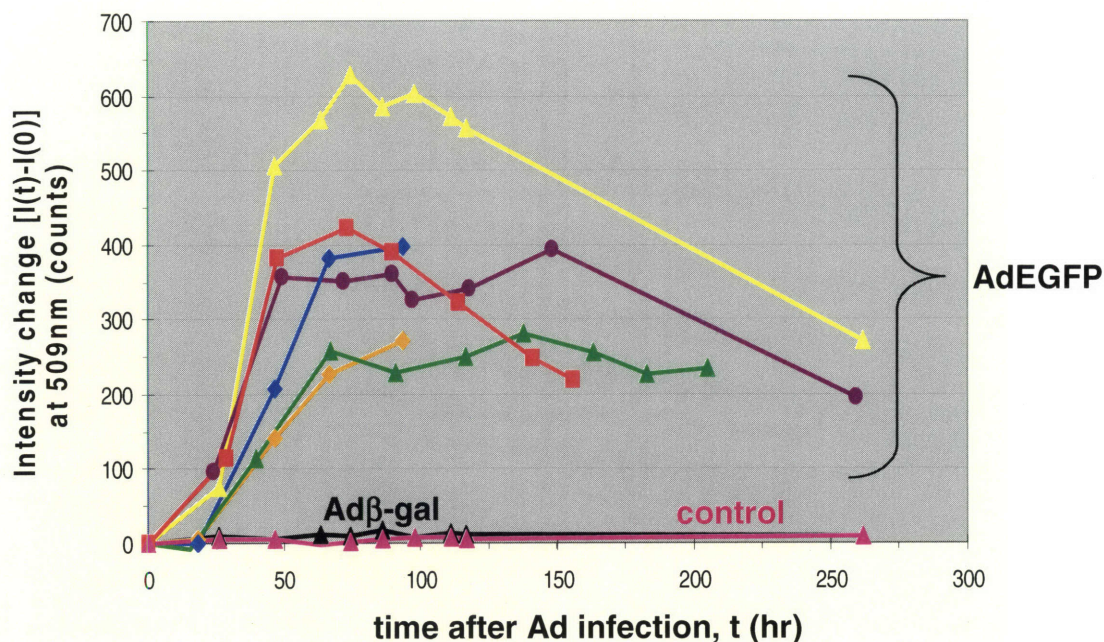


**Figure 3.7.4** Time course of EGFP expression in hepatocyte microreactor cultures after infection with an Ad gene delivery vector. Microreactor cultures were infected with AdEGFP at a concentration of  $4 \times 10^6$  pfu/ml for 24 hours. EGFP expression was detected with the spectrophotometer. The EGFP emission spectra were recorded at different times after the beginning of the Ad infection ( $t=0$ ). The intensity ( $I_t$ ) at 509nm (EGFP emission maximum) was selected as a means for quantifying the levels of EGFP expression. This graph shows the intensity change ( $I_t - I_{t=0}$ ) at 509nm plotted against the time  $t$  after the beginning of the Ad infection. Results from five experiments (different rat liver perfusions) are presented. Two controls are included: one microreactor culture infected with Ad $\beta$ -gal (black triangles) and one not infected at all (pink triangles).

Note: the data presented as yellow and pink triangles correspond to the microreactor cultures shown in Figure 3.7.3 (a) and (b) respectively.

### **3.7.4 Quantification of EGFP expression with spectrometer measurements**

It is not possible to quantitatively compare the EGFP intensity levels among the samples shown in Figure 3.7.4 because these values are not normalized to the total number of cells present in each microreactor. The difference in intensity values could be a result of the cell number variability. However, if the hepatocytes are harvested at the end of each experiment and the total DNA is extracted and quantified, then quantitative information about gene delivery efficiency can be extracted from spectrometer measurements. The change in the EGFP expression levels as a function of Ad concentration can then be measured and compared to the change in EGFP mRNA levels as well as to the change in the cellular uptake of Ad particles. This approach was followed in the microreactor experiments presented in Chapter 5. In these experiments hepatocyte DNA was extracted and quantified as described in Section 3.3.

## **3.8 Two-Photon Laser Scanning Fluorescence Microscopy in Microreactor Cultures**

### **3.8.1 Introduction**

The basic characteristic of the microreactor is that it allows the culture of hepatocytes in a 3D tissue environment. Therefore, a non invasive, in situ imaging method with three-dimensional resolution was needed to detect AdEGFP delivery to the tissue structures inside the microreactor channels. Two-photon excitation microscopy can satisfy these requirements.

Two-photon excitation first appeared as a theoretical concept in the 1930s and was proved experimentally three decades later (Masters and So, 2004); however, it was introduced in laser scanning microscopy for biological and other applications relatively recently (Denk et al., 1990). Two-photon excitation is the result of the simultaneous absorption of two photons in a single (quantitized) event. In conventional fluorescence microscopy a fluorophore molecule is excited by the absorption of a single photon of a particular wavelength (e.g. 350nm) and returns to the ground state by emitting a single photon of lower wavelength. In two-photon microscopy, the same fluorophore is excited by the simultaneous absorption of two photons of longer wavelength (700nm), each of which by itself does not have sufficient energy to cause the transition to the excited state (Sheppard and Shotton, 1997); the resulting emission however is the same (Figure 3.8.1a). Since two photons have to be absorbed the rate of absorption and consequently of the resulting fluorescence emission depends on the square of the excitation intensity. This property is responsible for the several advantages of two-photon microscopy.

The extremely high laser powers required for two-photon excitation events to happen can be achieved with mode-locked (or pulsed) lasers, where, although the average laser power is low, the power at the peak of the pulse is very high. Moreover, as the laser beam focuses on the sample, the density of the photons increases and at the focal point it becomes high enough to generate two-photon excitation (Figure 3.8.1b). Consequently, fluorescent emissions result only from the focal point. Since there are no out-of-focus emissions, there is no need for a confocal aperture to obtain 3D resolution, in contrast to confocal microscopy (in fact 3D resolution is identical to that of an ideal confocal microscope) and, photobleaching and photodamage of the sample are minimized. Furthermore, attenuation of the excitation beam by out-of-focus absorption does not occur, allowing increased depth penetration in the sample (Piston, 1999; Denk et al., 1995). This is also enhanced by the fact that high wavelength light is used (red or near infrared).

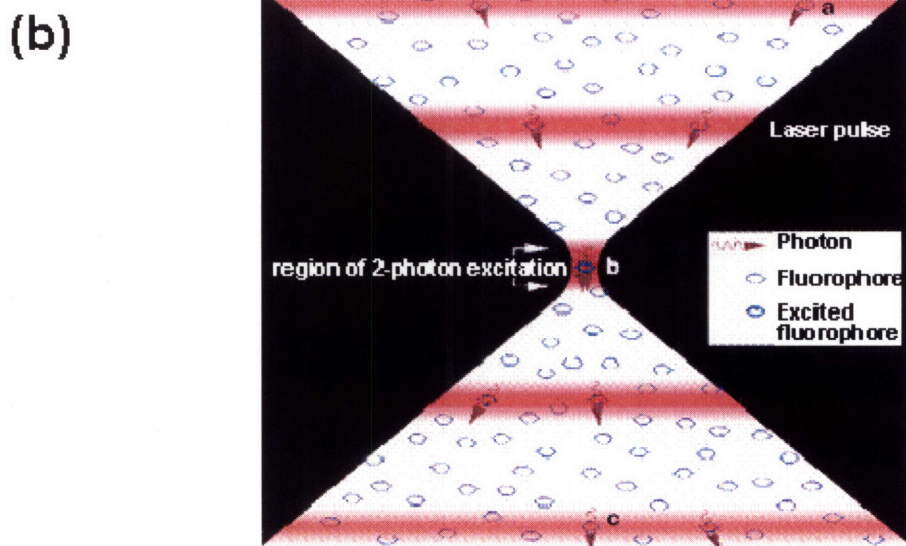
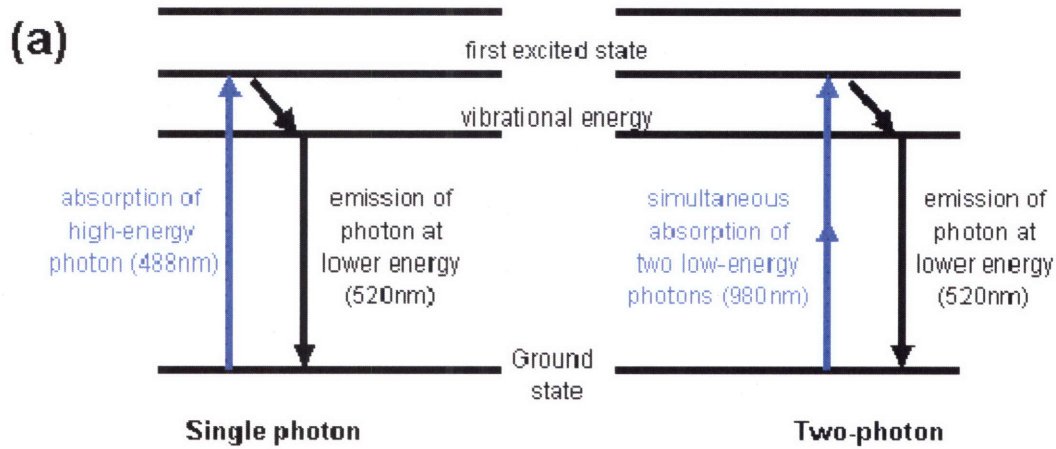


**Figure 3.8.1** (a) Single photon vs two-photon excitation of a fluorophore. (b) Demonstration of the 2-photon excitation event that occurs at the focal point due to the extremely high photon density (image from Piston D.W., 1999. Imaging living cells and tissues by two-photon excitation microscopy. *Trends in Cell Biology*, Vol. 9: 66-69).

In this thesis, two-photon laser scanning fluorescence microscopy was applied for the detection of EGFP expression in hepatocyte microreactor cultures after AdEGFP infection. A protocol was developed for quantitative assessment of gene delivery efficiency, cell viability and the spatial distribution of Ad-infected hepatocytes.

### ***3.8.2 Two-photon imaging in Hepatocyte Microreactor Cultures: Detection of EGFP expression; spatial distribution and temporal variations.***

#### **Experimental procedures**

The application of 2-photon microscopy for the detection of Ad gene delivery in hepatocyte microreactor cultures was initially demonstrated with the original configuration of the microreactor system (stainless steel chamber, Figure 2.2a). Microreactors seeded with day 3 spheroids were infected with an adenovirus vector carrying the gene for EGFP driven by the CMV promoter. The Ad vector used in the experiments described in this section was provided by Dr Jack Wands (Liver Research Center, Brown University). The Ad was introduced inside the microreactor reservoir on day 3 after seeding at a concentration of  $4 \times 10^6$  pfu/ml. (Note: this value is based on the infectious titer of the original Ad preparation as measured by the vector supplier.) The virus circulated for 24 h and was subsequently washed from the system.

***Two-photon imaging:*** The expression of EGFP in hepatocytes cultured inside the microreactor channels was detected with a two-photon laser scanning fluorescence microscope built by Dr Peter So's lab (Department of Mechanical Engineering, MIT). Two-photon imaging involved the acquisition of a stack of xy planes, each plane corresponding to different depth or z distance from the surface of the silicon scaffold advancing in increments of  $1 \mu\text{m}$  (as illustrated in the schematic part of Figure 3.8.2). Images were obtained using a mode-locked Titanium-Sapphire tunable femto second laser (Coherent Inc.) with 150 fsec pulse width with a 76 MHz repetition rate. The power of incident light was regulated with a Glan-Thompson polarizer and was typically measured to be 65 mW before entering the Axiovert 5100 TV microscope optics (Carl Zeiss Inc.). An excitation wavelength of 840nm was typically used to maximize the adsorption cross section for EGFP. A galvanometer-driven x-y scanner (Cambridge Technology) provided raster scanning of the sample to generate a two-dimensional image within a focal plane at a speed of 6-10 s per frame. A piezoelectronic driver (Physik Instruments) was used to precisely control the distance between the objective lens and the sample for depth profiling. The



maximum imaging depth was defined by the working distance of the microscope objective. The original version of the microreactor chamber was designed to have a 0.980 mm distance between the silicon scaffold surface and the lens to enable imaging of the hepatocyte tissue deep inside the channels. Images were taken using a 20X Achroplan water immersion objective lens (Carl Zeiss Inc.) with a numerical aperture of 0.5 and a working distance of 2 mm. Chromatic selection of green fluorescent light was achieved with a dichroic filter set using a bandpass filter centered at  $525 \pm 25$  nm. EGFP emission was detected with a single photon counting system using a R5600-P photomultiplier tube (Hamamatsu). A 100 MHz single photon counting discriminator (F100T, Advanced Research Instruments) converted single photon bursts into TTL pulses, which were counted via computer.

A control experiment was performed to calibrate the extent of spectral loss of intensity as a function of sample depth due to light scattering. Green fluorescent beads were embedded in a matrix of agarose (10%) and lipid (5%) to simulate optical conditions found within a cell mass and imaged under the above mentioned conditions. Approximately 50% of intensity was lost within a depth of 60  $\mu\text{m}$  (Powers et al, 2002).

### **Detection of EGFP expression and spatial distribution**

Figure 3.8.2 shows 2-photon imaging data from two microreactor cultures, one infected with AdEGFP and a control. The samples were imaged approximately 70 hours after the beginning of Ad infection. Each of the four columns of panels contains sequential images (xy planes) corresponding to a microreactor channel; each plane is 10 $\mu\text{m}$  deeper than the one above it. Only part of a channel cross section can be seen in each panel. The yellow lines outline the channel boundaries. The first three columns correspond to three different channels in the microreactor that was infected with Ad. The last column corresponds to one channel inside the control microreactor culture. The bright colored areas represent EGFP-expressing cells. Fluorescence emission due to EGFP expression was clearly detected throughout the depth of the tissue imaged (100 $\mu\text{m}$ ) and was significantly higher than the hepatocyte auto-fluorescence levels displayed in the control culture. These data demonstrate the accessibility of the 3D hepatocyte tissue structures to in situ fluorescence microscopy and therefore the possibility to obtain spatial information about EGFP expression under defined Ad delivery conditions.

### **Temporal variations in EGFP expression**

Figure 3.8.3a shows two-photon imaging data from a microreactor culture infected with Ad. In this experiment EGFP expression was monitored in specific channels at three different

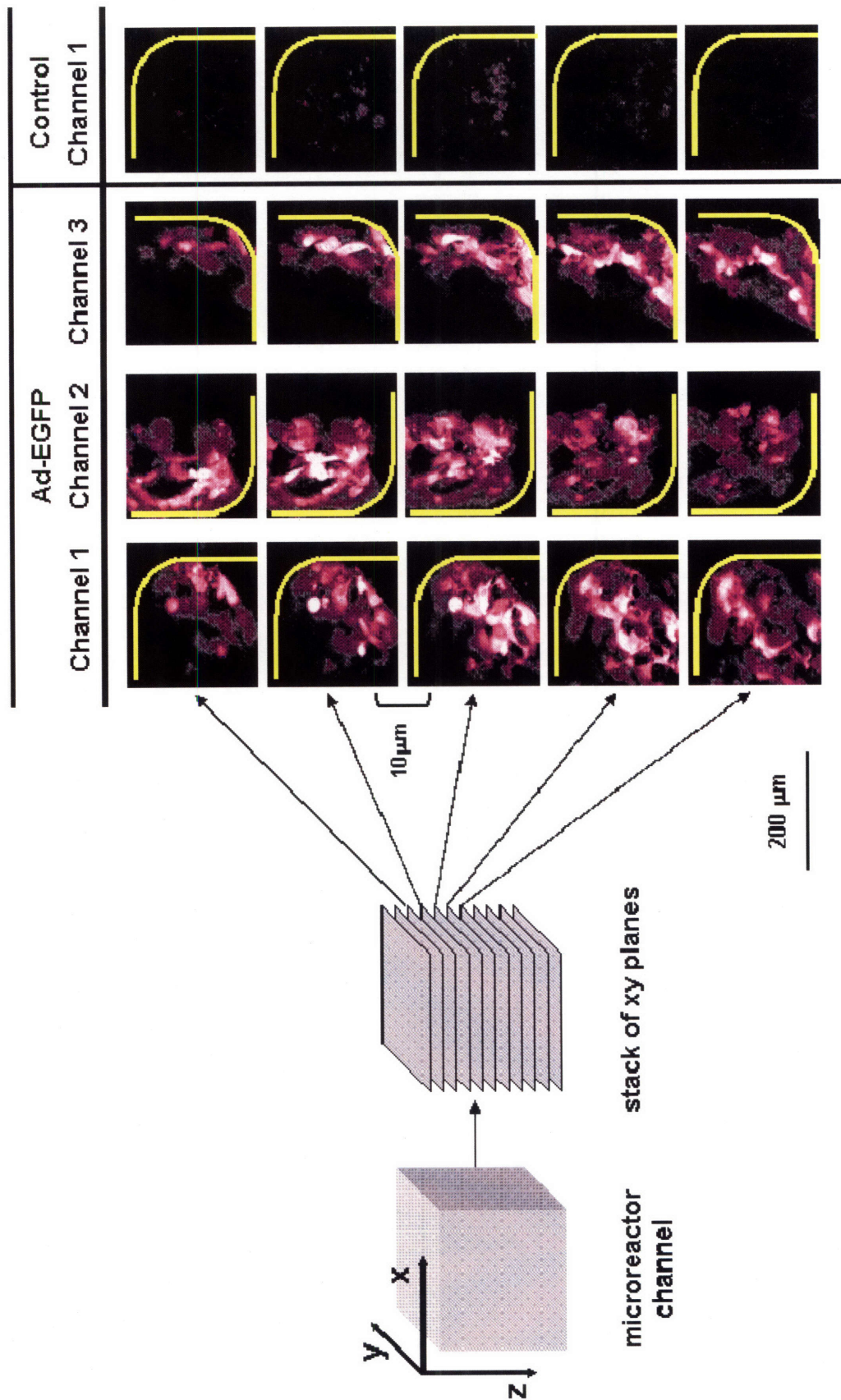


**Figure 3.8.2** Detection of EGFP expression in hepatocyte microreactor cultures with two-photon laser scanning fluorescence microscopy. Microreactor cultures were infected with Ad-CMV-EGFP at a concentration of  $4 \times 10^6$  pfu/ml for 24h. Two-photon imaging was performed ~70h after the Ad infection. This figure shows data from two microreactor cultures, one infected with AdEGFP and a control. Each of the four columns of panels contains sequential images (xy planes) corresponding to a microreactor channel. Only part of a channel cross section can be seen in each panel. The yellow lines outline the channel boundaries. The first three columns correspond to three different channels in the microreactor that was infected with Ad. The last column corresponds to one channel inside the control microreactor culture. The bright colored areas represent EGFP-expressing cells.

time points after Ad infection ( $t = 21, 64, 93\text{h}$ ). The data presented in this figure correspond to a single channel. The same three sequential planes ( $10\mu\text{m}$  apart) are shown for each time point. Total EGFP expression in that microreactor was also followed with time with spectrometer measurements. Figure 3.8.3b shows the EGFP spectrum intensity change ( $I_t - I_{t=0}$ ) at  $509\text{nm}$  plotted as a function of time after the beginning of Ad infection. The green circles mark the time points when two-photon imaging was also performed. As described in section 3.7 EGFP expression increases rapidly 24-70h after Ad infection reaching a maximum which gradually declines after a few days. This trend is captured in the two-photon data as an increase in brightness from the early to the later time points. These results demonstrate the ability to obtain temporal information about gene expression with two-photon microscopy.

Additionally, two-photon imaging data also reveal morphological structures of the hepatocyte tissue inside the microreactor channels. In channels 1 and 2 of Figure 3.8.2 the tissue cross section consists of several layers of hepatocytes spanning a distance from the walls to the middle of the channel; the gaps observed inside the tissue mass (especially for channel 2) might be conduits for medium flow. In channel 3 the tissue cross section is thinner and the cells spread along the wall. Note that only part of a channel cross section can be seen in each panel. In Figure 3.8.3 the hepatocytes span the middle of the channel diagonally and also spread along the wall.

### ***3.8.3 Two-photon imaging of EGFP expression in Hepatocyte Microreactor Cultures: Quantification of Ad gene delivery efficiency in terms of % EGFP-expressing cells.***

The results presented in the previous section offer qualitative information about Ad gene delivery in the microreactor system. However, as mentioned earlier, one of the goals in this thesis was to develop quantitative methods to analyze the barriers to gene delivery in 3D hepatocyte tissue. For that purpose, a two-photon imaging protocol was developed to (a) measure the efficiency of Ad gene delivery by quantifying the percentage of hepatocytes expressing EGFP, (b) determine the effect of Ad delivery to cell viability by quantifying the percentage of dead hepatocytes and (c) determine the distribution of Ad-infected cells throughout the depth of the tissue inside the silicon scaffold channels. To detect and quantify the total number of cells (EGFP and non-EGFP expressing) as well as the number of dead cells with two-photon microscopy, the microreactor cultures were incubated with two nucleic acid



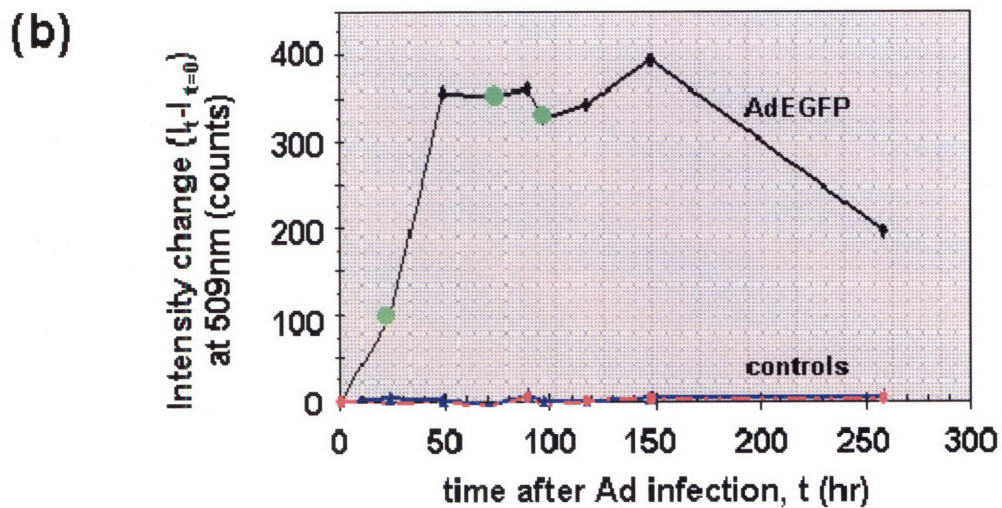
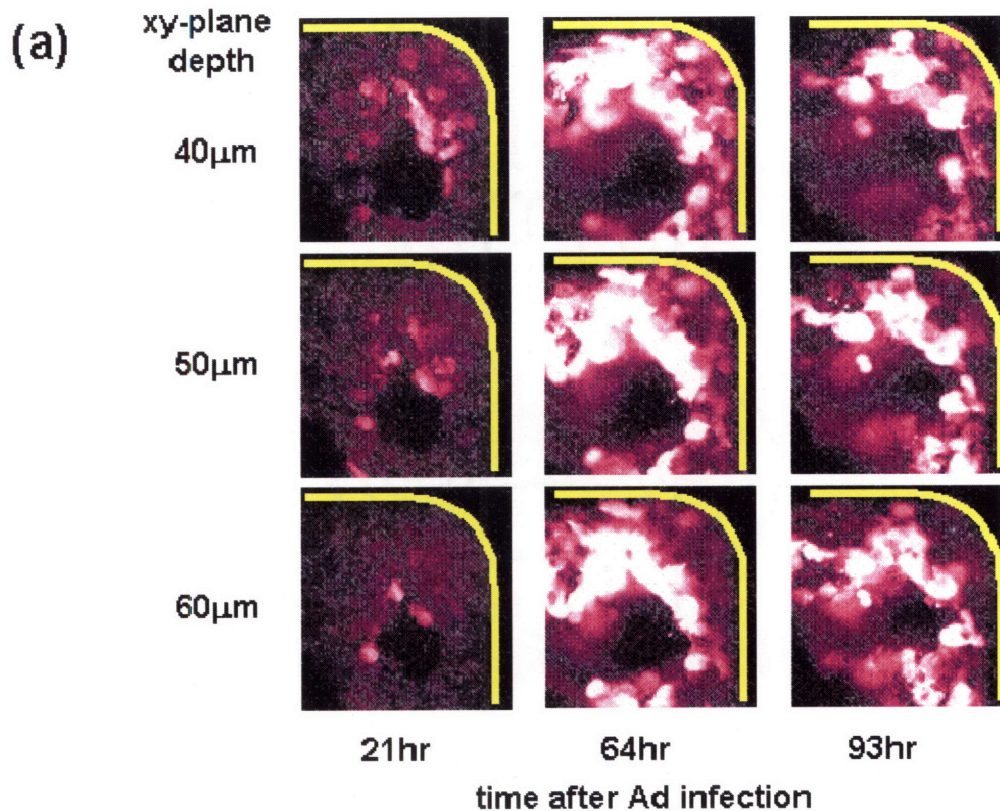


**Figure 3.8.3 (a)** Two-photon imaging of a single channel in a hepatocyte microreactor at different times (21, 64 and 93h) after Ad infection ( $4 \times 10^6$  pfu/ml for 24h). Three sequential xy planes (at 40, 50 and 60 $\mu$ m depth from the silicon scaffold surface) are shown for each time point. Only part of a channel cross section can be seen in each panel. The yellow lines outline the channel boundaries. The bright colored areas correspond to EGFP-expressing cells. **(b)** Time course of total EGFP expression in the above-mentioned microreactor (2 controls included). The green circles mark the time points when two-photon imaging was also performed.

stains: Ethidium Homodimer 1, which stains the nuclei of dead cells fluorescent red and Hoechst 33342, which stains the nuclei of living cells fluorescent blue.

### **Experimental procedures**

These experiments were carried out with the polycarbonate chamber version of the microreactor system. Microreactor cultures were infected with AdEGFP (vector described in section 3.2) for 24h at concentrations ranging from  $4 \times 10^5$  to  $4 \times 10^6$  pfu/ml. (Note: these values are based on the infectious titer of the original Ad preparation as measured by the vector supplier.)

***Nuclear counterstaining:*** The microreactor cultures were stained with ethidium homodimer 1 and Hoechst approximately 70h after the beginning of the Ad infection, in preparation for imaging with two-photon fluorescence scanning microscopy. Initially, the medium in the reservoir was replaced with fresh HGM containing ethidium homodimer-1 at a concentration of  $6 \mu\text{M}$ ; the solution was left to flow through the system for 30 minutes. The medium was then replaced with HGM containing Hoechst 33342 at a concentration of  $15 \mu\text{g/ml}$  which ran through the microreactor system for 60 minutes. Longer times are required for counterstaining of the microreactor cultures in comparison to the monolayer cultures to ensure efficient penetration of the dyes through the three-dimensional tissue structures located inside the microreactor channels.

***Two-photon imaging:*** The samples were imaged with the two-photon laser scanning fluorescence microscope system at the Center for Biological Imaging of the University of Pittsburgh. Images were obtained using a mode-locked titanium-sapphire ultrafast tunable laser system (Coherent Mira Model 900-F; Coherent, Inc., Santa Clara, CA). The power of incident light was typically  $\sim 450\text{mW}$  outside the laser cavity and was regulated with a custom-built input power attenuator (neutral density attenuator filter) before entering the Olympus IX70 inverted microscope optics (Olympus America, Inc.). An excitation wavelength of  $820\text{nm}$  was selected to adequately detect all fluorophores of interest, Hoechst, EGFP and Ethidium Homodimer 1. The system also comprised Olympus Fluoview confocal scanning electronics and external photomultiplier detection systems. Scanning speed was set at 16 s per frame. xy image planes were acquired at  $2 \mu\text{m}$  z-axis intervals. A piezoelectronic driver was used to precisely control the distance between the objective lens and the sample for depth profiling. Images were taken using a 20X Olympus LMPlan IR objective lens (Olympus America, Inc.) with a numerical

aperture of 0.4. Each microreactor channel was scanned twice; the first time for EGFP and Ethidium Homodimer detection with a dichroic filter set (Chroma Technology Corp.) comprising a HQ535/50m filter (green emission), a 565dclp dichroic mirror and a HQ610/75m filter (red emission); the second time for Hoechst detection with a dichroic filter set using a bandpass filter centered at  $450 \pm 25$  nm (blue emission).

***Environmental Control System (ECS):*** When cell cultures are removed from the controlled environment of the incubator they are inevitably exposed to non optimal conditions. The temperature decreases and the pH increases to non physiological levels within 10min; exposure to these conditions for prolonged periods of time can be detrimental to the culture. During the two-photon microscopy experiments at least three channels were imaged in each microreactor. Each channel was scanned twice and the thickness of the imaged tissue was typically 100 $\mu$ m. Given the scanning speed (16s per frame) and the distance between consecutive frames (2 $\mu$ m), the duration of imaging for each microreactor was at least 90min.

In order to maintain the culture conditions at physiological levels ( $T \sim 37^{\circ}\text{C}$ ,  $\text{pH} \sim 7.4$ ) during imaging, the microreactors were connected to a portable environmental control system (ECS, shown in Figure 3.8.4a). The ECS was built by Dr. Karel Domansky and is designed to maintain the temperature and pH of the microreactor culture by controlling the temperature and pH of the medium flowing into the chamber (Domansky et al., 2004). A portion of the tubing connected to the upper inlet of the chamber is enclosed in a cartridge equipped with heating panels. A temperature sensor measures the temperature of the medium exiting the microreactor chamber,  $T_{\text{outlet}}$ . These measurements are transmitted to a controller/heater device and compared to a setpoint value ( $T_{\text{setpoint}}$ ).  $T_{\text{setpoint}}$  is the value of the temperature of the medium exiting the chamber when the temperature inside the chamber ( $T$ ) is at  $37^{\circ}\text{C}$ . The difference between  $T_{\text{setpoint}}$  and  $T_{\text{outlet}}$  is used to control the rate of heat transfer to the medium flowing through the cartridge. The pH was controlled by continuous flow of a mixture of air and 8.5%  $\text{CO}_2$  through the cartridge. (Note: only the portion of the tubing enclosed in the cartridge is gas permeable.) Calibration experiments were performed to determine  $T_{\text{setpoint}}$  using a microreactor chamber equipped with a temperature sensor. The change in temperature  $T$  inside the chamber as a function of time after the microreactor was removed from the incubator and connected to the ECS is shown in Figure 3.8.4b. The change in medium pH with time was also measured with an inline pH probe connected at the chamber outlet and is shown in Figure 3.8.4c. The temperature and pH stabilized at  $37^{\circ}\text{C}$  and 7.55 respectively after approximately 15-20min. The

cartridge and the microreactor chamber were attached on a Plexiglas sheet and mounted on a stainless steel platform designed to fit the microscope stage.

### **Two-photon image processing and analysis with the MetaMorph software**

The raw data of each two-photon scan consisted of a stack of xy-planes (z-stack). Each plane (image) was processed as follows: The three wavelength components (Hoechst, EGFP and Ethidium Homodimer) were initially separated and subjected to a low pass filter to smooth out noise and other areas containing high spatial frequency data. The green component was subtracted from the red component to eliminate the effect of EGFP bleed-through to the Ethidium Homodimer channel. The three processed components (blue, green and red-green z-stacks) were combined to create an overlay z-stack. As mentioned earlier, each microreactor channel was scanned twice; the EGFP and Ethidium Homodimer components were acquired with the first scan and Hoechst with the second. Whenever the images of the 2 scans were slightly displaced the color alignment feature of the software was applied.

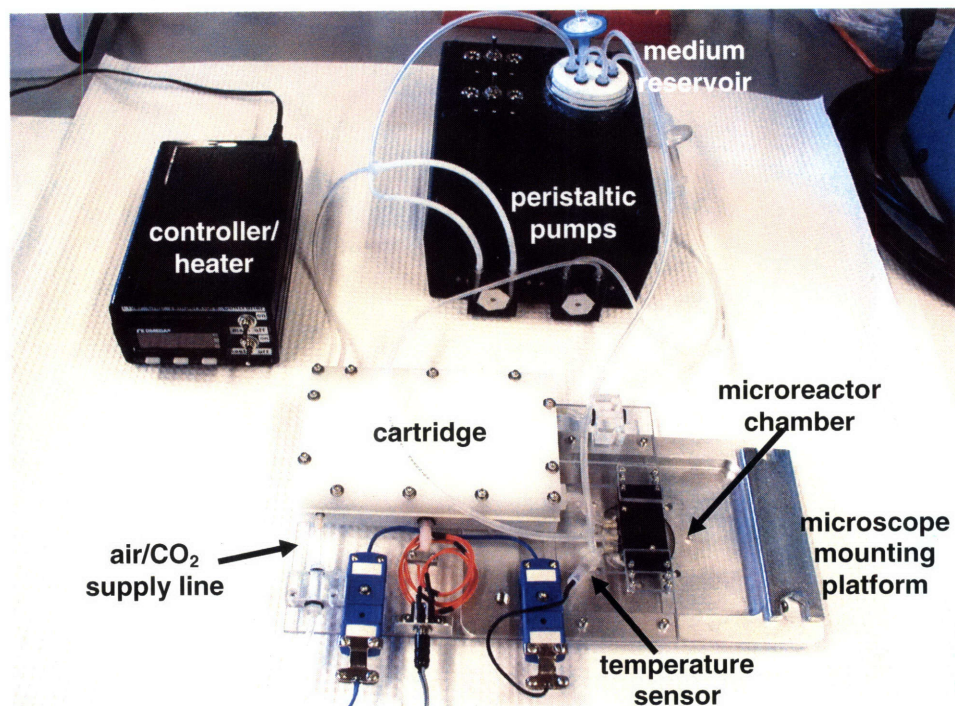
The 3D reconstruction module of the MetaMorph software was used to create a 3D model from each processed z-stack. The 3D model consists of a series of angled top views of the microreactor channel which, when viewed in quick succession, enhance the visualization of the details of the 3D tissue architecture. The view at a 0° angle is equivalent to the projection of all the xy-planes of the z-stack on a single plane.

Figure 3.8.5 shows two-photon imaging data from microreactor cultures infected with AdEGFP at a concentration of  $4 \times 10^6$  pfu/ml for 24h. The cultures were stained with Hoechst and Ethidium Homodimer and imaged ~70h after the beginning of the Ad infection. The data were processed as described above. Three-color overlay images from three microreactor channels are presented. The first four rows of panels consist of four xy-planes (at 10µm distance from each other) selected from each channel. In the last row, each panel shows the projection, on a single plane, of all xy-planes of the respective channel (0° angle view of the 3D reconstructed model). The white squares outline the channel boundaries. The blue- and red-stained nuclei correspond to live and dead cells respectively and the green fluorescent areas to EGFP-expressing cells.

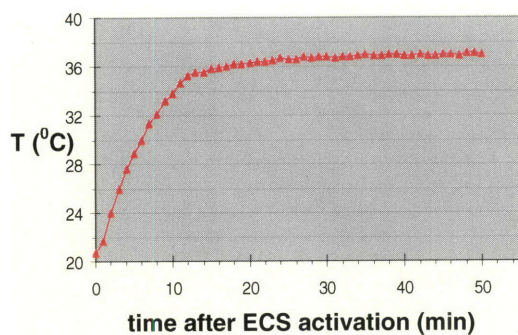
***Quantification of gene delivery efficiency and cell viability:*** To quantify the percentage of EGFP-expressing cells (gene delivery efficiency) and live cells (cell viability) in each imaged channel (z-stack), the total number of live cells was determined by counting the Hoechst-stained



(a)



(b)



(c)

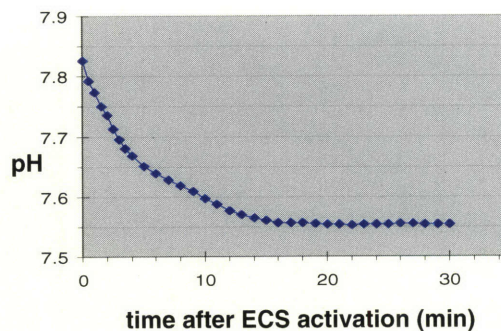


**Figure 3.8.4** (a) Environmental Control System (ECS) (photograph by Dr. Karel Domansky). (b) Plot of the temperature  $T$  inside the microreactor chamber as a function of time after the microreactor was removed from the incubator and connected to the ECS. (c) Plot of the medium pH at the microreactor chamber outlet as a function of time after the microreactor was removed from the incubator and connected to the ECS.



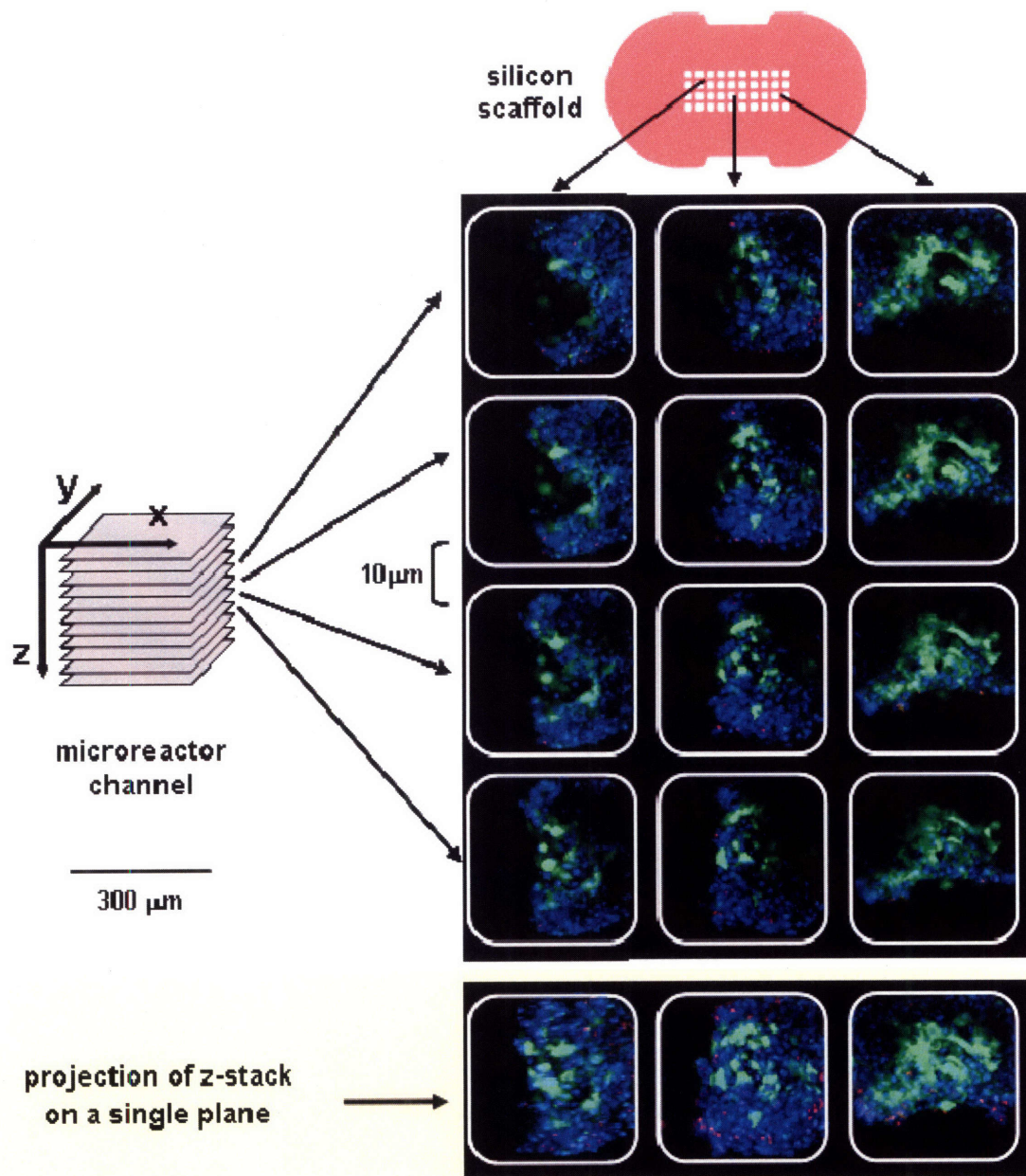


**Figure 3.8.5** Two-photon imaging of hepatocyte tissue in microreactor cultures infected with AdEGFP and stained with Hoechst and Ethidium Homodimer 1. Microreactor cultures were infected with AdEGFP at a concentration of  $4 \times 10^6$  pfu/ml for 24h. The cultures were stained with  $15 \mu\text{g/ml}$  Hoechst (blue) and  $6 \mu\text{M}$  Ethidium Homodimer (red) and imaged with 2-photon laser scanning fluorescence microscopy  $\sim 70$ h after the beginning of the Ad infection. This figure shows processed data from three microreactor channels. The white squares outline the channel boundaries. The blue- and red-stained nuclei correspond to live and dead cells respectively and the green fluorescent areas to EGFP-expressing cells. The first four rows of panels consist of consecutive xy-planes ( $10 \mu\text{m}$  apart) in each channel. In the last row, each panel shows the projection, on a single plane, of all xy-planes that are part of the z-stack of the respective channel.

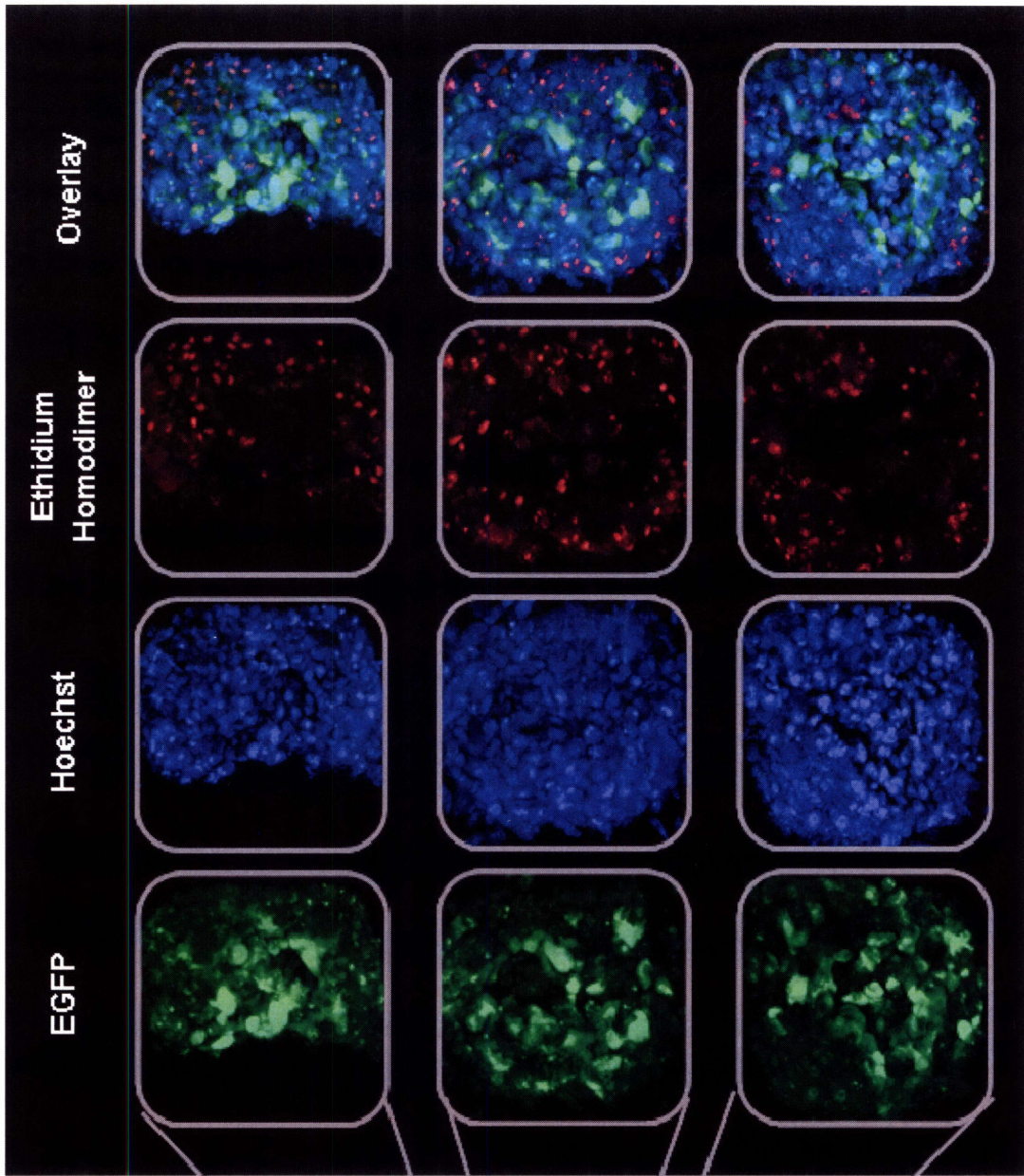
nuclei, the number of dead cells by counting the Ethidium Homodimer-stained nuclei and the Ad infected cells by counting the number of green fluorescent cells. Cell counting was performed manually with the help of the 'object counting' function provided in the MetaMorph software. To facilitate this procedure single-plane projections of the z-stacks were used. To avoid underestimating the cell count due to overlap, each z-stack was divided to sub-stacks; the xy-planes of each sub-stack were projected to a single plane and the counts of all sub-stacks were combined in the end.

The data in Figure 3.8.6 were obtained from the same experiment as those in Figure 3.8.5. Separate single-plane projections of the blue, green and red z-stacks as well as of their overlays are shown for three microreactor channels. The separated color images were used to facilitate counting of the live, dead and EGFP-expressing cells. Quantitative results are presented in Chapter 5.

***Spatial distribution of EGFP-expressing and dead cells inside microreactor channels:*** To determine whether there was variation in the distribution of EGFP-expressing cells and dead cells as a function of the depth z inside the microreactor channels, each z-stack (corresponding to a 100µm tissue sample) was divided into two sub-stacks (A: 0-50µm and B: 50-100µm). The percentage of EGFP-expressing cells as well as that of dead cells was quantified separately for each sub-stack. Average values from several microreactor channels were determined for A and B and were compared. The results are presented in Chapter 5.

**Figure 3.8.6 (on the following page).** Two-photon imaging in microreactor cultures for quantification of gene delivery efficiency. Microreactor cultures were infected with AdEGFP at a concentration of  $4 \times 10^6$  pfu/ml for 24h. The cultures were stained with 15µg/ml Hoechst and 6µM Ethidium Homodimer and imaged with 2-photon laser scanning fluorescence microscopy ~70h after the beginning of the Ad infection. This figure shows processed data from three microreactor channels. The z-stacks for the blue, green and red components of each channel and their overlay were projected on single planes to produce the reconstructed top views of the imaged channels presented here. The grey squares outline the channel boundaries. The blue- and red-stained nuclei correspond to live and dead cells respectively and the green fluorescent areas to EGFP-expressing cells.





### 3.9 References

Applied Biosystems: ABI PRISM® 7700 Sequence Detection System, User's Manual (2000).

Applied Biosystems: Primer Express® Tutorial for Real Time Quantitative PCR Primer and Probe Design (2001).

Applied Biosystems: User Bulletin #2. Relative Quantitation of Gene Expression (2001).

Applied Biosystems: TaqMan® Gold RT-PCR Kit, Protocol (2002).

Applied Biosystems: TaqMan® Universal PCR Master Mix, Protocol (2002).

Applied Biosystems: Guide to Performing Relative Quantitation of Gene Expression Using Real-Time Quantitative PCR (2004).

Becker, K., Pan, D., Whitley, C.B. (1999). Real-Time Quantitative Polymerase Chain Reaction to Assess Gene Transfer. *Human Gene Therapy* **10**, 2559-2566.

Block, G.D., Locker, J., Bowen, W.C., Petersen, B.E., Katyal, S., Strom, S.C., Riley, T., Howard, T.A., Michalopoulos, G.K. (1996). Population Expansion, Clonal Growth, and Specific Differentiation Patterns in Primary Cultures of Hepatocytes Induced by HGF/SF, EGF and TGF $\alpha$  in a Chemically Defined (HGM) Medium. *The Journal of Cell Biology* **132** (6), 1133-1149.

Bustin, S.A. (2000). Absolute quantification of mRNA using real-time reverse transcription polymerase chain reaction assays. *Journal of Molecular Endocrinology* **25**, 169-193.

Bustin, S.A. (2002). Quantification of mRNA using real-time reverse transcription PCR (RT-PCR): trends and problems. *Journal of Molecular Endocrinology* **29**, 23-39.

Bustin, S.A., Benes, V., Nolan, T., Pfaffl, M.W. (2005). Quantitative real-time RT-PCR – a perspective. *Journal of Molecular Endocrinology* **34**, 597-601.

Davis, A.R., Meyers, K., Wilson, J.M. (1998). High-Throughput Method for Creating and Screening Recombinant Adenoviruses. *Gene Therapy* **5**, 1148-1152.

Davis, A.R., Wivel, N.A., Palladino, J.L., Tao, L., Wilson, J.M. (2001). Construction of Adenoviral Vectors. *Molecular Biotechnology* **18**, 63-70.

Denk, W., Strickler, J.H., Webb, W.W. (1990). Two-Photon Laser Scanning Fluorescence Microscopy. *Science*, **248**, 73-76

Denk W., Piston D.W., Webb W.W. (1995). Two-Photon Molecular Excitation in Laser-Scanning Microscopy. *Handbook of Biological Confocal Microscopy*, edited by J.B. Pawley, Plenum Press, 445-458

Domansky, K., Sivaraman, A., Griffith, L.G. (2004). Micromachined bioreactor for in vitro cell self-assembly and 3D tissue formation, *Lab-on-Chips for Cellomics: Micro and Nanotechnologies for Life Science*, Kluwer Academic Publishers, pp. 319-346,.

Graham, F.L., Smiley, J., Russell, W.C., Nairn, R. (1977). Characteristics of a Human Cell Line Transformed by DNA from Human Adenovirus Type 5. *Journal of General Virology* **36**, 59-74.

Hackett, N.R., El Sawy, T., Lee, L.Y., Silva, I., O'Leary, J., Rosengart, T.K., Crystal, R.G. (2000). Use of Quantitative TaqMan Real-Time PCR to Track the Time-Dependent Distribution of Gene Transfer Vectors in Vivo. *Molecular Therapy* **2** (6), 649-656.

Heid, C.A., Stevens, J., Livak, K.J., Williams, P.M. (1996). Real Time Quantitative PCR. *Genome Methods* **6**, 986-994.

Huggett, J., Dheda, K., Bustin, S., Zumla, A. (2005). Real-time RT-PCR normalization; strategies and considerations. *Genes and Immunity* **6**, 279-284.

Livak, K.J. and Schmittgen, T.J (2001). Analysis of Relative Gene Expression Data Using Real-Time Quantitative PCR and the  $2^{-\Delta\Delta C_T}$  Method. *Methods* **25**, 402-408.

Ma, L., Bluysen, H.A.R., De Raeymaeker, M., Laurysens, V., van der Beek, N., Pavliska, H., van Zonneveld, A-J., Tomme, P., van Es, H.H.G. (2001). Rapid determination of adenoviral vector titers by quantitative real-time PCR. *Journal of Virological Methods* **93**, 181-188.

Masters, B.R. and So, P.T.C. (2004). Antecedents of Two-Photon Excitation Laser Microscopy. *Microscopy Research and Technique* **63**, 3-11.

PE Biosystems: Sequence Detection Systems Quantitative Assay Design and Optimization (1999).

Piston D.W. (1999). Imaging living cells and tissues by two-photon excitation microscopy. *Trends in Cell Biology*, **9**, 66-69

Powers, M.J., Domansky, K., Kaazempur-Mofrad, M.R., Kalezi, A., Capitano, A., Upadhyaya, A., Kurzawski, P., Wack, K.E., Beer-Stolz, D., Kamm, R., Griffith, L.G. (2002). A Microfabricated Array Bioreactor for Perfused 3D Liver Culture. *Biotechnology and Bioengineering* **78** (3), 257-269.

Powers, M.J., Janigian, D.M., Wack, K.E., Baker, C.S., Beer-Stolz, D., Griffith, L.G. (2002). Functional Behavior of Primary Rat Liver Cells in a Three-Dimensional Perfused Microarray Bioreactor. *Tissue Engineering* **8** (3), 499-513.

Seglen, P.O. (1976). Preparation of isolated liver cells. *Methods in Cell Biology* **13**, 29-83.

Senoo, M., Matsubara, Y., Fujii, K., Nagasaki, Y., Hiratsuka, M., Kure, S., Uehara, S., Okamura, K., Yajima, A., Narisawa, K. (2000). Adenovirus-Mediated in Utero Gene Transfer in Mice and Guinea Pigs: Tissue Distribution of Recombinant Adenovirus Determined by Quantitative TaqMan-Polymerase Chain Reaction Assay. *Molecular Genetics and Metabolism* **69** , 269-276.

Sheppard C.J.R. and Shotton D.M. (1997). *Confocal Laser Scanning Microscopy*. BIOS Scientific Publishers Limited, 87-90

Sivaraman, A., Leach, J.K., Townsend, S., Iida, T., Hogan, B.J., Stolz, D.B., Fry, R., Samson, L.D., Tannenbaum, S.R., Griffith, L.G. (2005). A Microscale In Vitro Physiological Model of the

Liver: Predictive Screens for Drug Metabolism and Enzyme Induction. *Current Drug Metabolism* **6**, 569-592.

Wong, M.L., and Medrano, J.F. (2005). Real-time PCR for mRNA quantitation. *BioTechniques* **39**, 75-85.

Wu F.J., Friend J.R, Hsiao C.C., Zilliox M.J., Ko W.-J., Cerra F.B., Hu W.-S., 1996. Efficient Assembly of Rat Hepatocyte Spheroids for Tissue Engineering Applications. *Biotechnology and Bioengineering*, Vol. **50**, pp. 404-415

# **CHAPTER 4**

## **Quantitative Analysis of Ad Gene Delivery in Hepatocyte Monolayer Cultures**



## 4.1 Introduction

This chapter presents the quantitative analysis of adenoviral vector gene delivery to hepatocyte monolayer cultures. It is divided into two parts. The first part addresses the extracellular mass transfer and cellular uptake of the AdEGFP vector. A mathematical model is developed to describe these processes and the Ad uptake rate constant  $k_u$  is determined by fitting to experimental results using the model.

The second part examines the events following the Ad internalization, namely the transgene (EGFP) expression (DNA transcription and mRNA translation). Protein expression is detected with fluorescence microscopy and the gene delivery efficiency is quantified in terms of the percentage of Ad-infected cells. The mRNA levels of the transgene are measured with quantitative real-time RT-PCR.

## 4.2 Extracellular Mass Transfer and Cellular Uptake of AdEGFP Vector

### 4.2.1 Mathematical Model description

In vitro Ad gene delivery experiments are typically performed by overlaying the vector-containing medium on top of a cell monolayer adhering to the surface of a tissue culture plate. The Ad particles immediately above the cells are taken out of the medium by adsorption to the cell surface and internalization, creating a concentration gradient in the vertical ( $x$ ) direction. Additionally, the gravitational force acting on the viral particles causes them to sediment. Therefore, the Ad particles suspended in the medium are subject to three processes: diffusion, sedimentation and uptake by the cells (Figure 4.1a). The application of the conservation equation for Ad particles in the medium (control volume) and at the interfaces where  $x=0$  and  $x=L$  (Figure 4.1b) leads to the derivation of the following governing equation and boundary conditions that describe Ad mass transfer in this system (detailed derivation in Appendix 4.1):

$$\frac{\partial C}{\partial t} = u_s \frac{\partial C}{\partial x} + D \frac{\partial^2 C}{\partial x^2} \quad (1)$$

$$u_s C + D \frac{\partial C}{\partial x} = k_u C \quad \text{at } x = 0 \quad (2)$$

$$u_s C + D \frac{\partial C}{\partial x} = 0 \quad \text{at } x = L \quad (3)$$

Additionally, the initial Ad concentration in the cell culture medium is uniform, therefore the initial condition is:

$$C = C_0 \quad \text{at } t = 0 \quad (4)$$

$C$  is the concentration of infectious adenovirus in the medium (Ad particles/cm<sup>3</sup>),  $t$  is time (s),  $u_s$  is the sedimentation velocity (cm/s),  $D$  is the diffusion coefficient of Ad in the medium (cm<sup>2</sup>/s),  $k_u$

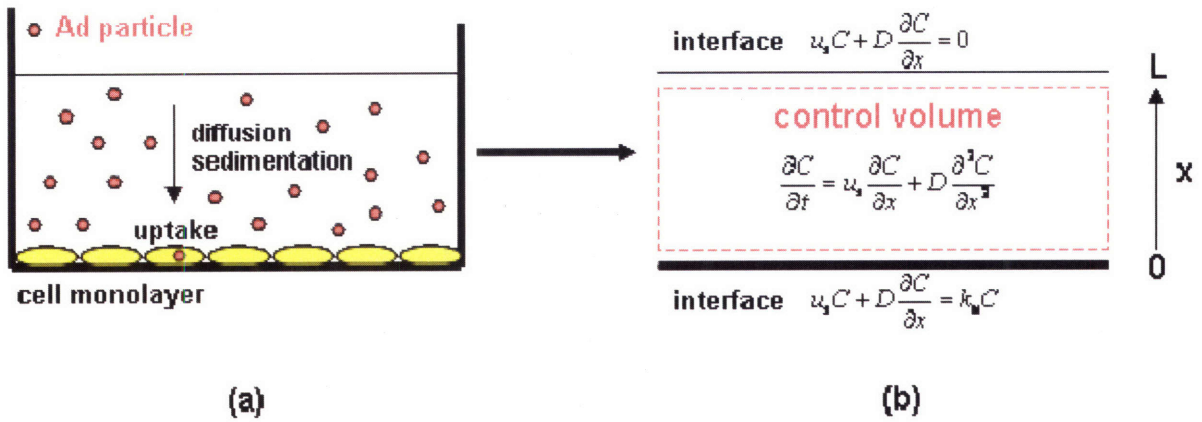


**Figure 4.1:** (a) Schematic of Ad gene delivery in tissue culture well, (b) governing equation and boundary conditions for Ad mass transfer

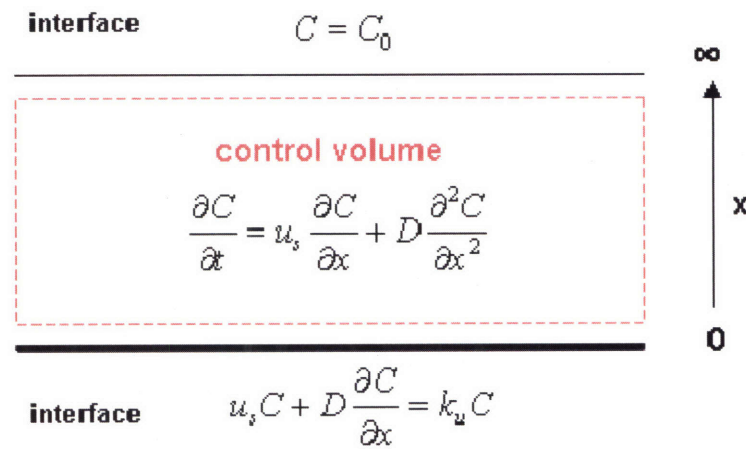


**Figure 4.2:** Revised governing equation and boundary conditions for Ad mass transfer

is the Ad uptake rate constant (cm/s) and L is the depth of the liquid film above the cell monolayer (cm).  $C_0$  is the initial Ad concentration. A list of the mathematical model parameters including their values is presented in Table 4.1. Table 4.2 contains a list of the variables.

The cell monolayer is considered uniform and any edge effects at the walls of the tissue culture plate are assumed negligible, therefore the problem is one-dimensional.

The first term on the right hand side of Equation 1 describes the process of sedimentation, which is included in the conservation equation as a convective flux. The sedimentation velocity,  $u_s$ , represents the velocity of an Ad particle when the gravitational force is balanced by the forces due to buoyancy and drag, and can be expressed as:

$$\mathbf{u}_s = \mathbf{s} \cdot \mathbf{g} = 7.4 \times 10^{-8} \text{ cm / s}$$

where  $s$  is the Ad sedimentation coefficient and  $g$  the gravitational acceleration. In the experiments described in this chapter  $s$  can be assumed constant and independent of concentration given that the Ad solution is very dilute (volume fraction of Ad particles in medium  $< 3.5 \times 10^{-8}$ ).

The second term on the right hand side of Equation 1 describes the process of diffusion. The Ad particles are assumed to be spherical with a diameter of 100nm (March et al, 1995) and therefore their diffusion coefficient in cell culture medium can be evaluated with the Stokes-Einstein equation (Deen 1998):

$$\mathbf{D} = \frac{\kappa T}{6\pi\mu r} = 6.5 \times 10^{-8} \text{ cm}^2 / \text{s}$$

where  $\kappa$  is Boltzmann's constant,  $T$  is the medium temperature,  $\mu$  is the medium viscosity and  $r$  is the Ad radius.

**Table 4.1:** Parameters in mathematical model for Ad mass transfer in monolayer hepatocyte cultures.

Parameter	Symbol	Value	Reference
gravitational acceleration	g	981 cm/s <sup>2</sup>	-
Ad sedimentation coefficient	s	750 S*	Nyberg-Hoffman et al., Nature Medicine 3 (7), 1997
sedimentation velocity	u <sub>s</sub>	7.4 x 10 <sup>-8</sup> cm/s	u <sub>s</sub> = s g
Boltzmann's constant	κ	1.38 x 10 <sup>-16</sup> cm <sup>2</sup> g s <sup>-2</sup> K <sup>-1</sup>	-
culture medium temperature	T	310 K	-
culture medium viscosity	μ	0.007 g.cm <sup>-1</sup> s <sup>-1</sup>	assumed equal to the viscosity of water at 37 <sup>o</sup> C
Ad particle radius	r	50 nm	see section 1.5
Ad diffusion coefficient in cell culture medium	D	6.5 x 10 <sup>-8</sup> cm <sup>2</sup> /s	calculated with Stokes-Einstein equation (Deen 1998)
depth of cell culture medium layer	L	0.2 cm	calculated from surface area (3.8cm <sup>2</sup> ) and medium volume (0.75cm <sup>3</sup> ) per culture well
surface area per cell in monolayer culture	A	1.7 x 10 <sup>-5</sup> cm <sup>2</sup>	determined by measuring the average cellular area on phase-contrast microscope images of hepatocyte cultures
Ad uptake rate constant	k <sub>u</sub>	cm/s	determined by fitting experimental data to mathematical model
initial Ad concentration in medium**	C <sub>0</sub>	Ad particles/ml	determined by fitting experimental data to mathematical model

\* 1S (Svedberg) = 10<sup>-13</sup>s

\*\* refers to infectious Ad particles

**Table 4.2:** Variables in mathematical model for Ad mass transfer in monolayer hepatocyte cultures.

Variable	Symbol
Ad concentration in medium (particles/ml)*	C
time after start of Ad infection (s)	t
distance from cell monolayer surface (cm)	x
number of Ad particles taken up by cell monolayer	$N_{Ad}$
Number of cells per culture plate well	n

\* refers to infectious Ad particles

Equation 2 states that the Ad flux at the cell monolayer surface ( $x=0$ ) should be equal to the Ad uptake rate by the cells. The uptake rate is assumed to follow first order kinetics and  $k_u$  is the rate constant. Equation 3 is a no flux boundary condition at the surface of the medium ( $x=L$ ).

The mean displacement of an Ad particle by diffusion for time  $t$  can be calculated with the following equation (Einstein, 1956):

$$\lambda(t) = \sqrt{2Dt}$$

Given that the maximal time period for Ad exposure in the experiments described in this thesis is 24 hours, the maximum mean displacement will be:

$$\lambda \approx 0.1\text{cm}$$

which is half the depth  $L$  of the Ad containing medium (0.2 cm). Therefore it can be reasonably assumed that the Ad concentration at  $x=L$  will not change significantly during the infection process and the second boundary condition (Equation 3) can be replaced with:

$$C = C_0 \quad \text{at } x = \infty \quad (3a)$$

(semi-infinite domain, Figure 4.2). This change allows for an analytical closed form solution of the mathematical model to be obtained using the method of the Laplace transform.

The total number of Ad particles taken up by the cells in a tissue culture plate well during the time of exposure to Ad,  $N_{Ad}$ , can be derived as the integral with time of the Ad flux at the  $x=0$  boundary:

$$N_{Ad} = \int_0^{\tau} nA(\text{flux})_{x=0} dt = nA \int_0^{\tau} k_u C_{x=0} dt \quad (5)$$

where  $n$  is the number of cells per well,  $A$  is the cellular area and  $\tau$  is the duration of the Ad infection. (Note: the flux at  $x=0$  is equal to the Ad uptake rate as shown in Equation 2)

The derivation of the analytical solution for the system of equations 1, 2, 3a and 4 is described in detail in Appendix 4.2. The total number of Ad particles taken up into the cells per well at a given time is given by the following equation:

$$N_{Ad} = nAC_0 \left\{ \frac{u_s}{2} t + \sqrt{\frac{Dt}{\pi}} \exp\left(-\frac{u_s^2}{4D} t\right) + \left[ \frac{u_s}{2} t + D \frac{k_u^2 + (k_u - u_s)^2}{2k_u u_s (k_u - u_s)} \right] \cdot \text{erf}\left(\frac{u_s}{2\sqrt{D}} \sqrt{t}\right) + \frac{D}{2} \frac{2k_u - u_s}{k_u (k_u - u_s)} \left[ \exp\left[\frac{k_u (k_u - u_s)}{D} t\right] \cdot \text{erfc}\left(\frac{2k_u - u_s}{2\sqrt{D}} \sqrt{t}\right) - 1 \right] \right\} \quad (6)$$

If the contribution of sedimentation is assumed negligible compared to that of diffusion ( $u_s = 0$ ), the above equation is reduced to:

$$N_{Ad} = nAC_0 \left\{ 2\sqrt{\frac{Dt}{\pi}} + \frac{D}{k_u} \left[ \exp\left(\frac{k_u^2 t}{D}\right) \cdot \text{erfc}\left(k_u \sqrt{\frac{t}{D}}\right) - 1 \right] \right\} \quad (7)$$

Equation 7 can also be derived from the analytical solution of the system of equations (1), (2), (3a) and (4) without the sedimentation terms (Appendix 4.3).

In order to roughly determine the relative significance of Ad sedimentation compared to diffusion, a “Peclet” number can be calculated:

$$Pe = \frac{u_s \lambda(t)}{D}$$

where  $\lambda(t)$  is the mean displacement by diffusion for time  $t$ . The values for the Pe number range from 0.03 ( $t=2h$ ) to 0.1 ( $t=24h$ ) indicating that for short durations of Ad infection the rate of diffusion is much faster than the rate of sedimentation.

Figure 4.3a shows the predictions of the 2 mathematical models (equation 6 - diffusion/sedimentation and equation 7 – diffusion) for the uptake of Ad particles by the cell monolayer.  $N_{Ad}$ , normalized to the monolayer surface area ( $nA$ ) and the initial Ad concentration in the cell culture medium ( $C_0$ ), is plotted as a function of the duration of Ad infection ( $t$ ) for varying values of the uptake rate constant  $k_u$  ranging from  $5 \times 10^{-8}$  to  $5 \times 10^{-5}$  cm/s. As expected, the number of Ad particles taken up by the cell monolayer increases with increasing  $k_u$  values and increasing time of exposure to the Ad vector. Another observation is that the contribution of the sedimentation term to the mathematical model predictions appears insignificant as expected from the estimations of the Pe number; therefore it will not be included in the analysis that follows. For values of  $k_u$  even further below  $5 \times 10^{-8}$  cm/s the  $N_{Ad}$  curve tends to overlap with the one for  $k_u=0$ . As the uptake rate constant increases above the value of  $5 \times 10^{-5}$  cm/s the curves tend to overlap. At that point the uptake rate is very fast relative to diffusion and the Ad vector transfer process is entirely controlled by diffusion. Under these conditions equation 2 can be replaced with the fast-reaction boundary condition,  $C=0$  at  $x=0$  and therefore the uptake rate constant does not enter the mathematical model. The solution of the model in that case is as follows (Appendix 4.4):

$$N_{Ad} = 2nAC_0 \sqrt{\frac{Dt}{\pi}} \quad (8)$$

Figure 4.3b shows a plot similar to the one in Figure 4.3a for Ad uptake predictions with the diffusion model for varying  $k_u$  values (Equation 7) as well as for the fast-reaction boundary condition (Equation 8).



The Ad concentration profile in the medium (diffusion model) is given by the following equation:

$$C(x, t) = C_0 \left\{ \operatorname{erf} \left( \frac{x}{2\sqrt{Dt}} \right) + \exp \left[ \frac{k_u}{D} (x + k_u t) \right] \cdot \operatorname{erfc} \left( \frac{x}{2\sqrt{Dt}} + k_u \sqrt{\frac{t}{D}} \right) \right\} \quad (9)$$

Figure 4.4 shows the predicted Ad vector concentration profiles in cell culture medium for different  $k_u$  values. At 2 hours after the beginning of Ad infection a distinct concentration gradient has already formed for uptake rate constant values higher than  $5 \times 10^{-8}$  cm/s and becomes more pronounced as the  $k_u$  value increases. This indicates that under these conditions the uptake process is faster than diffusion, which is consistent with the fact that viral infection in standard culture systems is generally diffusion limited. The concentration at the top of the medium ( $x=L=0.2$  cm) is not affected significantly by the cellular uptake throughout a 24hr exposure to Ad.

#### **4.2.2 Experimental Approach to Evaluate the Uptake Rate Constant $k_u$ .**

The mathematical model describes the Ad vector mass transfer and uptake processes in a standard 2D hepatocyte culture system was developed for the purpose of determining a characteristic parameter that quantifies the efficiency of Ad gene delivery. That parameter is the uptake rate constant,  $k_u$ , and it represents the ability of the target cells to bind and internalize the Ad vector. An equivalent parameter will be estimated in Chapter 5 for the case of the 3D tissue-engineered liver microreactor system. The ultimate goal of this comparative analysis will be to illustrate in a quantitative way the effect of a more organotypic in vitro hepatocyte culture on the efficiency of Ad gene delivery.

The experimental approach that was designed in order to determine the unknown rate constant  $k_u$ , consisted of measurements of the number of Ad particles ( $N_{Ad}$ ) taken up by hepatocyte monolayer cultures exposed to varying initial Ad concentrations ( $C_0$ ) for varying amounts of time ( $t$ ). Then the unknown parameter was evaluated by curve-fitting the experimental results with the analytical solution derived from the mathematical model (equation 7).

The experimental procedures were described in detail in Chapter 3 (Materials and Methods). Briefly, monolayer cultures of primary rat hepatocytes were established on collagen-coated 12-well plates at a density of  $3 \times 10^5$  cells per well and incubated in HGM for 24 hours. Then ( $t = 0$ ) the medium in each well was replaced with 750  $\mu$ l HGM containing Ad5-CMV-EGFP at three different concentrations:  $4 \times 10^5$ ,  $2 \times 10^6$  and  $4 \times 10^6$  infectious particles (i.p.) /ml. These Ad concentrations are based on the infectious titer of the original Ad preparation as measured by the vector supplier and correspond to MOI values of 1, 5 and 10 respectively. At specified time points ( $t = 2, 4, 8, 12$  and 24h), the Ad infection was terminated. The hepatocytes were then either harvested immediately for DNA extraction (data set 1) or cultured in HGM until  $t=48$ hr when they were harvested for DNA extraction (data set 2). Triplicate wells were prepared for each initial Ad concentration, time point condition and data set. DNA was extracted from each sample and quantified with the RediPlate 96 PicoGreen Microplate Assay. The number of Ad particles internalized by the cell monolayer in each sample,  $N_{Ad}$ , was determined by quantifying the number of Ad genomic copies with quantitative real-time TaqMan PCR. The PCR results were normalized to the DNA content for each sample.

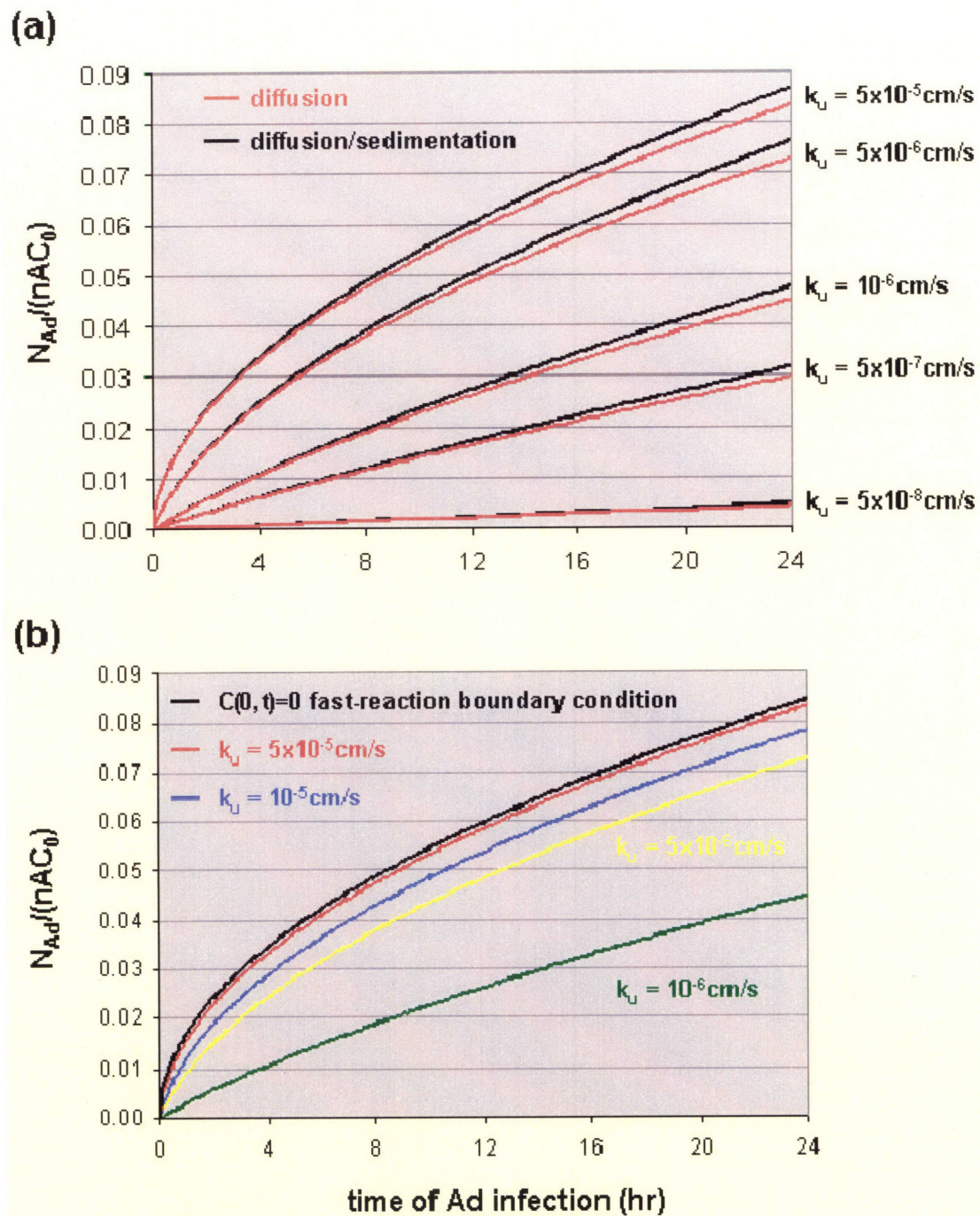


**Figure 4.3.** Mathematical model predictions for the uptake of Ad particles by the cell monolayer,  $N_{Ad}$  (normalized to the cell monolayer surface area,  $nA$ , and the initial Ad concentration in the cell culture medium,  $C_0$ ) as a function of the duration of Ad infection for varying values of the uptake rate constant  $k_u$ . **(a)** Effect of sedimentation on Ad uptake. The black curves correspond to the diffusion/sedimentation model. The red curves correspond to the diffusion model. **(b)** Diffusion model with fast-reaction boundary condition (black curve) and with flux=(uptake rate) boundary condition for varying rate constant values.



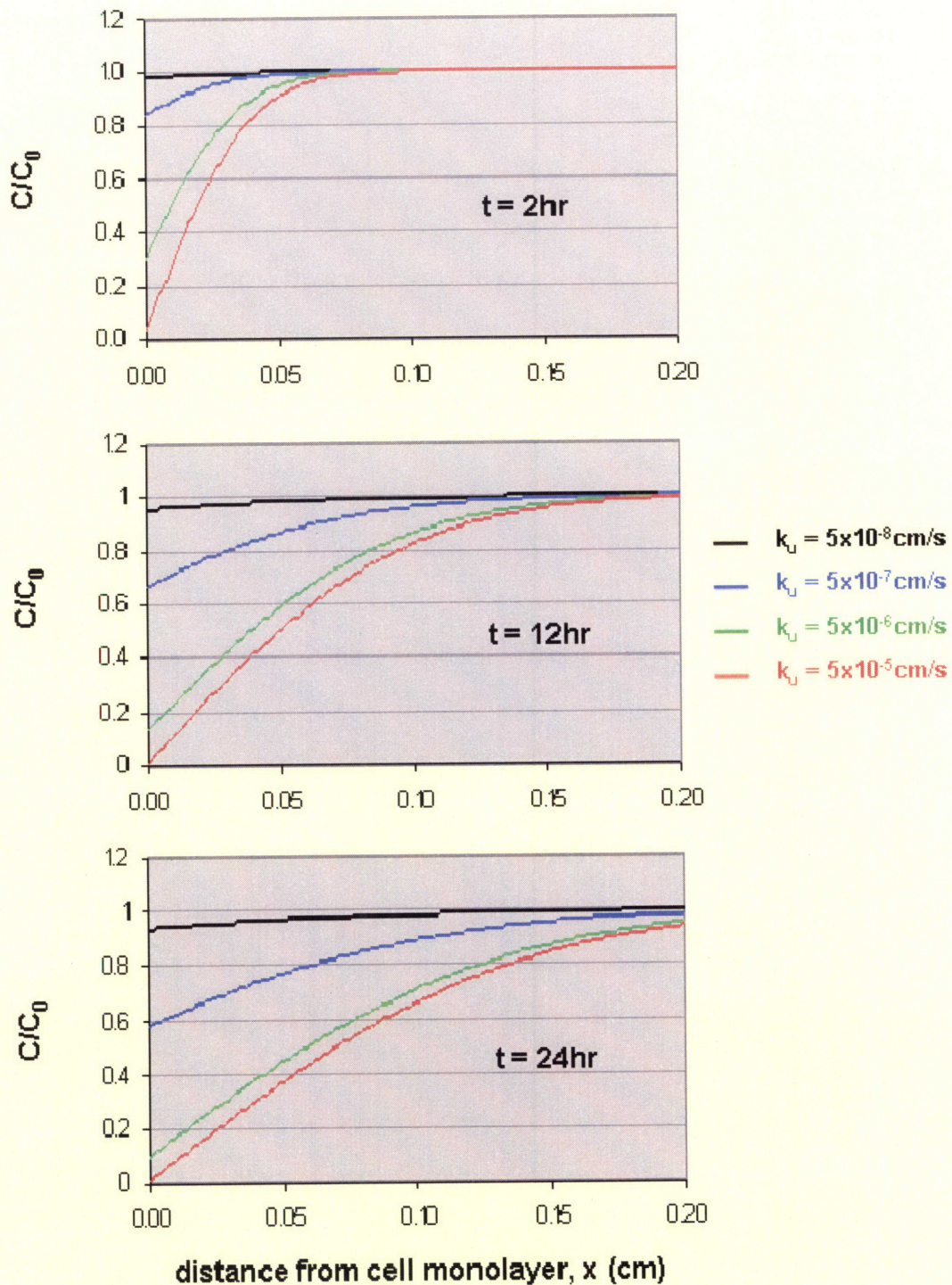


**Figure 4.4.** Adenoviral vector concentration profiles in cell culture medium after 2, 12 and 24 hours of hepatocyte monolayer exposure to Ad, as predicted by the diffusion-uptake mathematical model (equation 8) for varying uptake rate constant ( $k_u$ ) values.

### **4.2.3 Experimental Results and Analysis**

#### **Adenoviral vector uptake in monolayer hepatocyte cultures**

Incubation of the hepatocyte cultures with Ad5-CMV-EGFP led to the internalization of the vector and the transfer of the viral genome into the cell nucleus and subsequently the expression of EGFP. Figure 4.5 shows results from two experiments (different rat perfusions). The normalized Ad uptake ( $N_{Ad}/n$ ) is plotted as a function of the time the cell monolayers were exposed to the Ad vector and for three different initial Ad concentrations spanning one order of magnitude,  $C_0$ ,  $C_0/2$ ,  $C_0/10$ .  $C_0$  is equal to  $4 \times 10^6$  i.p./ml (or pfu/ml) according to the infectious titer as measured by the vector supplier. The closed symbols correspond to data set 1 (DNA harvested immediately after termination of Ad infection). The open symbols correspond to data set 2 (DNA harvested at  $t = 48$  hr). All data points represent the mean values of two experiments performed in triplicate and the error bars represent the standard deviation.

As expected, the average number of Ad particles taken up by the cells increased with increasing time of exposure and increasing concentration of Ad in the medium, and appeared to approach a plateau at longer times. From the comparison of the two data sets we concluded that the number of intracellular Ad genome copies did not change significantly between the termination of infection and  $t = 48$  hr when transgene (EGFP) expression reached maximum levels. Consequently, there was no significant degradation of the internalized vector genome over this time. This information was important to have for the experimental analysis in the microreactor cultures (Chapter 5), where the cells were harvested at the time of maximum EGFP expression for DNA and RNA extraction, as well as for the analysis of EGFP expression data and their normalization to the Ad vector uptake results.



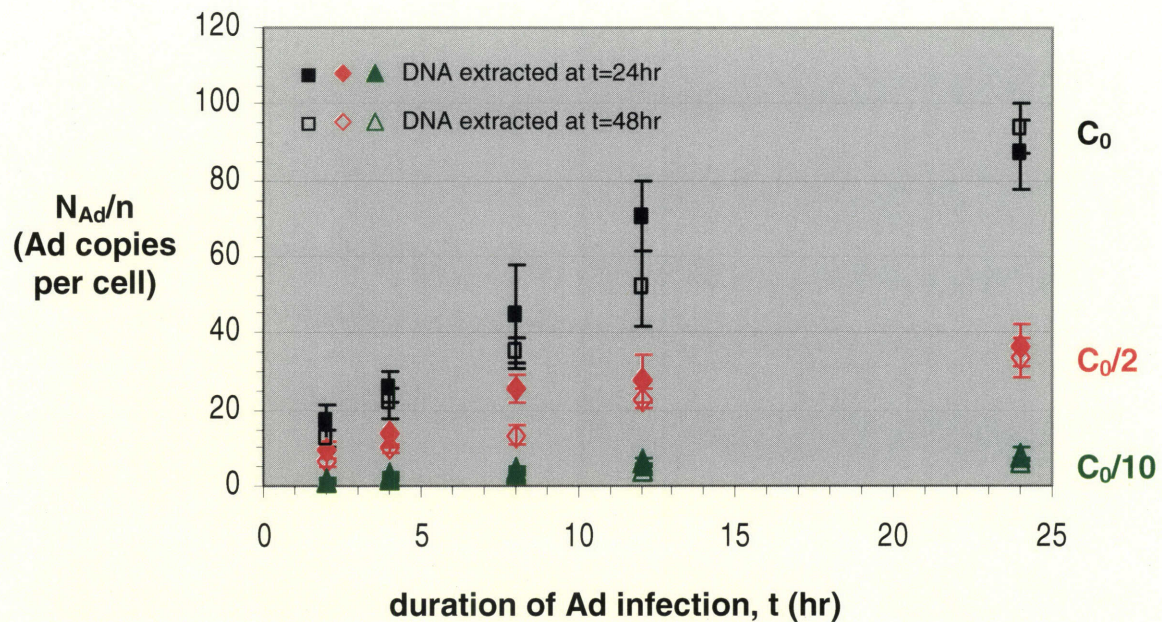


**Figure 4.5.** Experimental results for adenoviral vector uptake in monolayer hepatocyte cultures. Primary rat hepatocytes were seeded on collagen-coated 12-well plates at a density of  $3 \times 10^5$  cells per well, cultured for 24hr in HGM, then incubated with Ad5-CMV-EGFP at three concentrations ( $C_0$ ,  $C_0/2$  and  $C_0/10$ ) for varying amounts of time (ranging from 2hr to 24hr). Two sets of triplicate samples were prepared for each condition. In the first set, the cells were harvested immediately after the end of Ad infection. In the second set the cells were cultured in HGM until  $t = 48$ hr and subsequently harvested. DNA was extracted from all samples. Total DNA content was measured with the Rediplate 96 PicoGreen DNA Quantification Kit. The number of Ad genome copies was quantified with real-time TaqMan PCR. This graph shows the number of Ad copies normalized to cell number and plotted against time of infection. All data points represent the mean values of two experiments (different rat liver perfusions) performed in triplicate  $\pm$  the standard deviation of the mean. Closed symbols correspond to samples where cells were harvested immediately after termination of Ad infection. Open symbols correspond to samples where the cells were harvested at  $t=48$ hr.

### Initial Ad concentration, $C_0$ : real infectious Ad titer vs. plaque assay measurements

Another important observation arising from the results in Figure 4.5 was that the Ad uptake per cell greatly exceeded the maximum expected values (MOI). For example, according to the infectious titer of the Ad preparation measured by the vector supplier,  $C_0 = 4 \times 10^6$  i.p./ml. The total medium volume per well was  $750 \mu\text{l}$ , therefore the total number of infectious Ad particles per well was equal to  $3 \times 10^6$ ; given that there were  $3 \times 10^5$  cells per well, the maximum expected number of internalized Ad particles per cell ( $N_{\text{Ad}}/n$ ) was 10 (MOI=10). However, after 24 hours of exposure to Ad of initial concentration equal to  $C_0$ ,  $N_{\text{Ad}}/n$  was almost an order of magnitude higher (Figure 4.5).

This discrepancy is the result of the methods used to determine the infectious titer of Ad preparations. Whereas the internalized Ad particles were measured in this thesis with quantitative real-time PCR, a very sensitive and accurate method, the Ad infectious titer was quantified with the plaque-forming assay. As described in Section 3.2, this method measures the number of plaques formed after the infection of 293 cells with dilutions of the Ad preparation. Although it is the predominant technique used in Ad production laboratories, the plaque assay can significantly underestimate the actual infectious particle concentration, depending on the conditions under which it is performed, such as the total volume of the Ad-containing medium above the 293 cell monolayers as well as the duration of the infection. As shown in the mathematical model developed in this chapter, the process of Ad delivery is diffusion limited. If the plaque-assay experiments do not allow sufficient time for the Ad vectors to diffuse through the liquid film and reach the monolayer surface, then the concentration of infectious viral particles will inevitably be underestimated. The inability of this assay to accurately measure infectious titers has been documented in literature and alternative approaches have been proposed (Mittereder et al., 1996, Nyberg-Hoffman et al., 1997; Shabram and Aguilar-Cordova, 2000); however it still remains the prevalent method for this type of measurements.

According to the plaque assay protocol that was followed by our vector suppliers, the 293 cells were cultured in 6-well plates (surface area per well =  $9.5 \text{ cm}^2$ ). The volume of the Ad-containing medium solution was 1 ml per well; therefore the depth of the liquid film above the cells was equal to 0.105 cm. Since the duration of the infection was 3 to 4 hours, the mean displacement of an Ad particle by diffusion would be:

$$\ell = \sqrt{2Dt} = \mathbf{0.037 \text{ to } 0.043 \text{ cm}}$$



which is much smaller than the depth of the liquid film. This means that the Ad vectors at a distance greater than 0.037 or 0.043 cm (i.e. the majority of the vectors) did not have sufficient time to reach the cell monolayer and interact with it.

#### Estimation of parameters $k_u$ and $C_0$ with nonlinear least squares curve fitting.

It is obvious from Equation 7 that an accurate knowledge of the initial Ad concentration  $C_0$  is essential in order to reliably determine the value of the uptake rate constant with nonlinear least squares curve fitting. Since this was not the case in our experiments as explained in the previous section,  $C_0$  was also considered as an unknown parameter in the analysis of the experimental data. Both  $k_u$  and  $C_0$  were fitted to the data with equation 7. For that purpose the optimization toolbox of the software package MatLab was applied and specifically the function *lsqcurvefit*, which solves nonlinear curve-fitting (data-fitting) problems in the least squares sense. The medium-scale Levenberg-Marquardt algorithm was chosen with a termination tolerance on the vector  $x = [C_0, k_u]$  set to  $\text{ToIX} = 10^{-9}$  and the default settings for all other optimization parameters. Data set 1 was used ( $N_{Ad}/n$  versus  $t$ ). Since  $N_{Ad}/n$  is linearly proportional to the initial concentration  $C_0$  (Equation 7), the data for initial concentrations  $C_0/2$  and  $C_0/10$  were multiplied by a factor of 2 and 10 respectively and the unknown parameters were fitted to all the data together. The algorithm converged to the parameter values:  **$C_0 = 6.4 \times 10^7$  i.p./ml and  $k_u = 9 \times 10^{-6}$  cm/s** with the value of the squared 2-norm of the residual (resnorm) equal to 451. The computed values of  $C_0$  and  $k_u$  are also shown in Figure 4.6, where data set 1 (symbols) and the mathematical model correlation (solid lines) were plotted.

According to these results, the initial Ad concentration was more than an order of magnitude higher than the one calculated from the infectious titer measurements with the plaque assay ( $4 \times 10^6$  i.p./ml). In fact, this value is much closer to the total Ad particle concentration ( $6.8 \times 10^7$  p./ml) as calculated from the genomic titer of the Ad preparation. The genomic titer is typically measured with optical absorbance at 260 nm ( $\text{OD}_{260}$ ) and one absorbance unit is equivalent to approximately  $10^{12}$  Ad vector particles; this is a widely accepted method for quantifying total particle concentration. Therefore, according to our results the majority of Ad particles in the vector preparation were infectious. Similar observations were made when an alternative approach that circumvents the diffusion limitations of the plaque assay was applied for titer measurements (Nyberg-Hoffman et al., 1997; Shabram and Aguilar-Cordova, 2000).

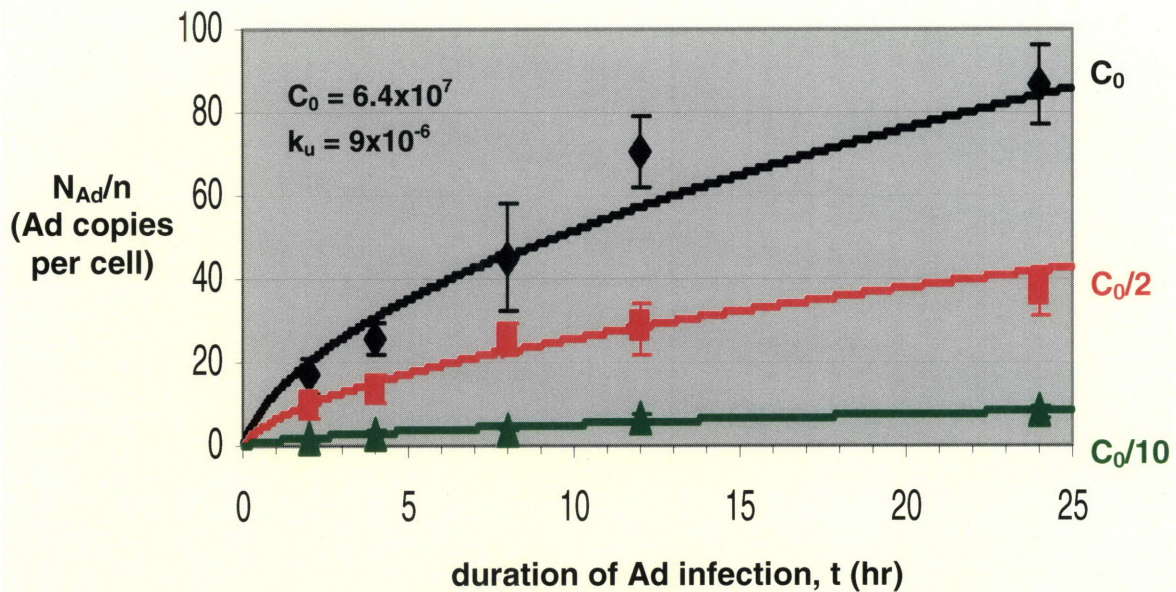


**Figure 4.6.** Mathematical model correlation to the experimental results for adenoviral vector uptake in monolayer hepatocyte cultures. The diffusion/uptake model (Equation 7) was used to fit the initial Ad concentration in the cell culture medium,  $C_0$ , and the Ad uptake rate constant,  $k_u$ , to the experimental data described in Figure 4.5. (Note: the data corresponding to the samples where cells were harvested immediately after termination of Ad infection were used). The graph shows the number of Ad copies normalized to cell number and plotted against time of infection. All data points represent the mean values of two experiments (different rat liver perfusions) performed in triplicate  $\pm$  the standard deviation of the mean. The solid lines represent the mathematical model correlation performed with a nonlinear least squares method implemented in MATLAB's Optimization Toolbox.

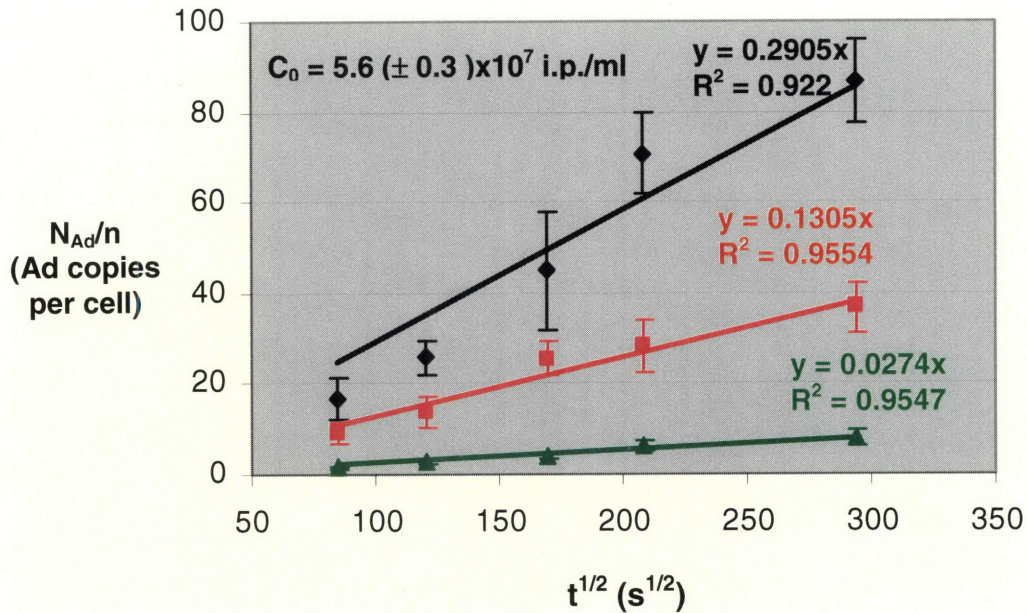
A minimum boundary on the concentration  $C_0$  can be estimated by fitting this parameter to the data with the fast-reaction boundary condition mathematical model (Equation 8) for all starting concentrations used experimentally. In this case, the experimental results for  $N_{Ad}/n$  (data set 1) were plotted against the square root of time  $t$  (Figure 4.7); a straight line was fitted to each of the three data series ( $C_0$ ,  $C_0/2$ ,  $C_0/10$ ) with linear least squares regression (Excel) and  $C_0$  was determined from the slopes. The average value was calculated as  $C_0 = 5.6 (\pm 0.3) \times 10^7$  i.p./ml. For this value the squared 2-norm of the residuals was calculated as  $\text{resnorm} = 572$ , which is higher compared to the value obtained with the diffusion model correlation. Consequently the diffusion model provides a better fit for the experimental data. Therefore the initial Ad concentration  $C_0$  is bound by this value and the genomic titer:

$$5.6 \times 10^7 \text{ i.p./ml} < C_0 < 6.8 \times 10^7 \text{ i.p./ml}$$

The lowest possible value for the uptake rate constant  $k_u$  can be calculated by assuming the initial concentration  $C_0$  is equal to the maximum possible value i.e. the genomic titer and fitting  $k_u$  to the data. In that case  $k_u = 5.6 \times 10^{-6}$  cm/s and value of the squared 2-norm of the residuals was calculated as  $\text{resnorm} = 410$ . Therefore:

$$k_u > 5.6 \times 10^{-6} \text{ cm/s}$$

The values that were determined by fitting both parameters to the data are within these boundaries.



$$\frac{N_{Ad}}{n} = \left( 2A \sqrt{\frac{D}{\pi}} C_0 \right) \sqrt{t}$$

**Figure 4.7.** Fast-reaction boundary condition model correlation to the experimental results for adenoviral vector uptake in monolayer hepatocyte cultures. Equation 8 (shown above) was used to fit the initial Ad concentration in the cell culture medium,  $C_0$ , to the experimental data described in Figure 4.5. (Note: the data corresponding to the samples where cells were harvested immediately after termination of Ad infection were used). The graph shows the number of Ad copies normalized to cell number and plotted against the square root of time. All data points represent the mean values of two experiments (different rat liver perfusions) performed in triplicate  $\pm$  the standard deviation of the mean. The solid lines represent the mathematical model correlation performed with linear least squares regression in Excel.  $C_0$  was estimated from the slope for each data series ( $C_0$ ,  $C_0/2$ ,  $C_0/10$ ) and an average value was calculated.

## 4.3 Transgene (EGFP) Expression

As previously described, there are many steps involved in the process of gene delivery. In the first part of this chapter, the attention was focused on the extracellular transfer and the cellular uptake of the Ad vector. Understanding the mechanisms that control these steps is an essential part of gene therapy research. However, the efficiency of gene delivery is ultimately determined by the end result, the successful production of the desired protein. In the second part of this chapter, the focus moves on to the detection and quantification of EGFP expression on monolayer hepatocyte cultures infected with the AdEGFP vector. Two different types of measurements are presented. The first involves the detection of EGFP protein with fluorescence microscopy and the quantification of gene delivery efficiency in terms of the percentage of EGFP-expressing cells; the second involves the application of Real-Time RT-PCR to measure the mRNA levels of EGFP. The EGFP expression measurements were made 48 hours after the Ad infection, when the EGFP expression reaches maximum levels in the hepatocyte monolayer cultures.

### ***4.3.1 Quantification of AdEGFP Gene Delivery Efficiency and Cell Viability with Fluorescence Microscopy.***

The experimental procedures for the hepatocyte monolayer culture and the Ad infection were presented in section 4.1.2 and were described in detail in Chapter 3 (Materials and Methods). Triplicate wells were prepared for each initial Ad concentration ( $C_0$ ,  $C_0/2$  and  $C_0/10$ , where  $C_0 = 6.4 \times 10^7$  i.p./ml as determined in section 4.1.3) and time point condition ( $t = 2, 4, 12$  and 24 hours). After the Ad infection, the hepatocytes were cultured in HGM until  $t=48$ hr when they were counterstained with Ethidium Homodimer-1 and Hoechst 33342 for fluorescence imaging. 5-6 different regions were chosen for imaging in each triplicate well group. For each region separate images were acquired with a FITC filter for EGFP (green), a DAPI filter for Hoechst (blue) and a Rhodamine filter for Ethidium Homodimer (red). The three images were combined in a three-color overlay. (More details about the staining and imaging procedures are presented in Chapter 3.)

Figure 4.8 shows six fluorescence micrographs of hepatocyte monolayers infected with the Ad vector. Each panel is an overlay of the green, blue and red images of a specific region



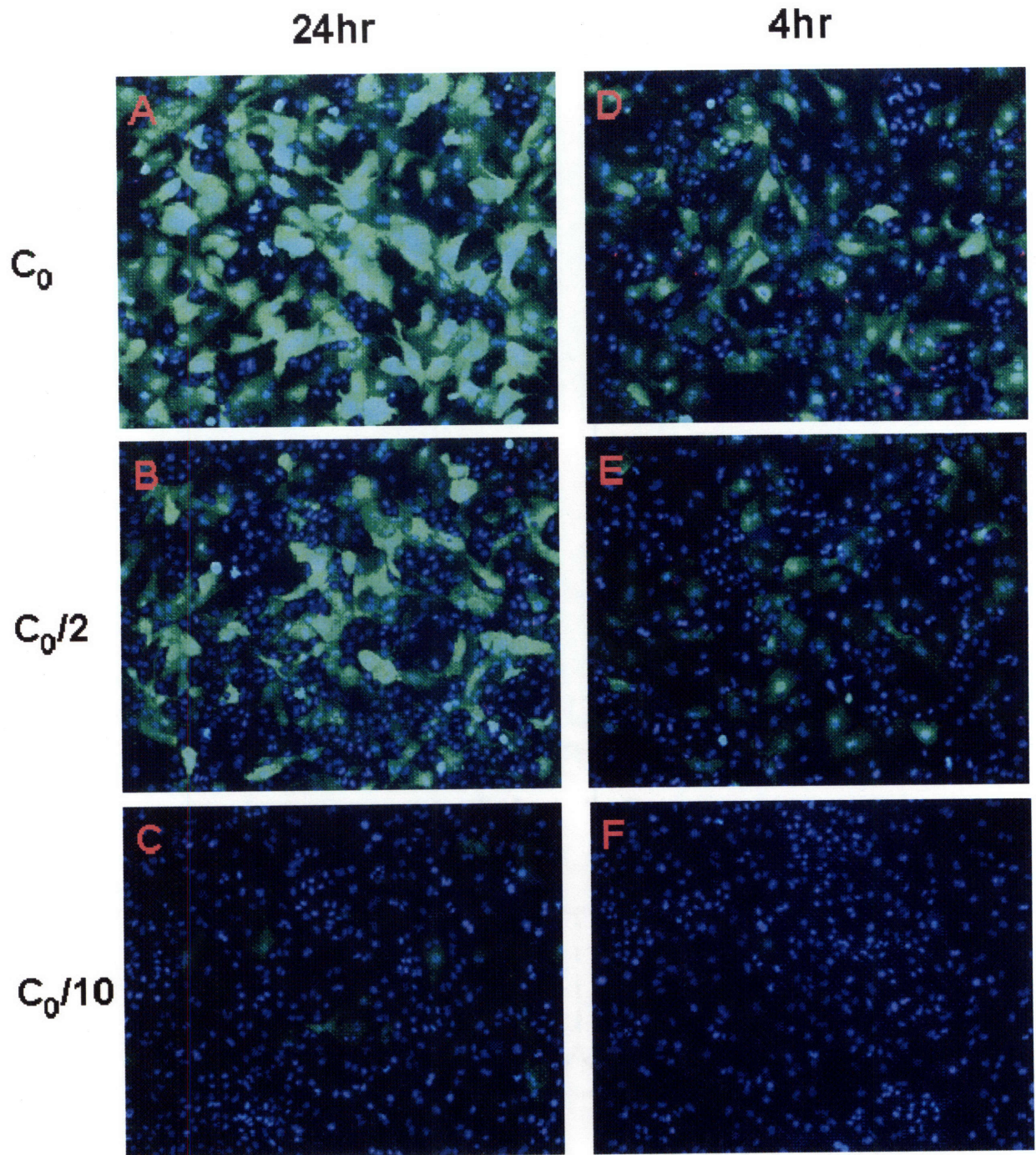


**Figure 4.8.** Fluorescence micrographs of hepatocyte monolayers infected with Ad5-CMV-EGFP. The cells were stained with Hoechst 33342 and Ethidium Homodimer 1 and imaged at  $t=48\text{hr}$  with a 10X dry objective lens. Panels **A**, **B** and **C** correspond to a 24hr Ad infection at concentrations of  $C_0$ ,  $C_0/2$  and  $C_0/10$  respectively. Panels **D**, **E** and **F** correspond to a 4hr Ad infection at concentrations of  $C_0$ ,  $C_0/2$  and  $C_0/10$  respectively. Each panel shows an overlay of the green, blue and red images captured. ( $C_0 = 6.4 \times 10^7$  i.p/ml)

on a cell culture well. The images were captured with a 10X dry objective lens. Panels A, B and C correspond to a 24 hr infection at concentrations of  $C_0$ ,  $C_0/2$  and  $C_0/10$  respectively. Panels D, E and F correspond to a 4 hr infection at concentrations of  $C_0$ ,  $C_0/2$  and  $C_0/10$  respectively. The observation of these images leads to the following conclusions: as the initial concentration of Ad in the medium decreases, the percentage of hepatocytes that express EGFP and the levels of EGFP expression in these cells decrease as well; secondly, as the duration of the Ad infection decreases so does EGFP expression. These qualitative observations are in agreement with the results for the cellular uptake of the Ad vector presented in the first part of this chapter.

Quantitative information for the Ad gene delivery efficiency was obtained from the fluorescence micrographs in terms of the percentage of the hepatocytes expressing EGFP. For that purpose, the number of live cells on each imaged region was determined by counting manually the number of blue nuclei (Hoechst), the number of dead cells was determined by counting the number of red nuclei (Ethidium Homodimer) and the number of EGFP-expressing cells was determined by counting the number of green fluorescent cells. Then the gene delivery efficiency was calculated as follows:

$$\text{gene delivery efficiency} = \frac{\text{\# of EGFP}^+ \text{ cells}}{\text{\# of live cells}} 100\%$$

In Figure 4.9A, gene delivery efficiency (% EGFP-expressing cells) is plotted as a function of the time the hepatocyte monolayers were exposed to the Ad vector and for three different initial Ad concentrations. Each data point represents the mean value of 5-6 imaged regions  $\pm$  the standard deviation of the mean. The number of hepatocytes with detectable levels of EGFP expression (under the conditions of image acquisition applied in this experiment) increased with time of infection and Ad concentration. At the highest Ad concentration ( $C_0$ ) the percentage of cells with detectable levels of EGFP approached 100%, even for relatively short duration of infection such as 4 hours. However, it must be emphasized that there was a significant difference in the fluorescence intensity (i.e. levels of EGFP) between the time points of 24 and 4 hours, as demonstrated in Panels A and D of Figure 4.8, a difference which could reflect the different number of Ad vectors internalized by the cell monolayer (see Figure 4.6).

Additionally, the percentage of dead cells on the monolayer cultures was calculated as a measure of the toxicity of the Ad infection and is presented in Figure 4.9B. The viability fell to 80% in the case of the highest Ad concentration and longer times of infection. However, it must



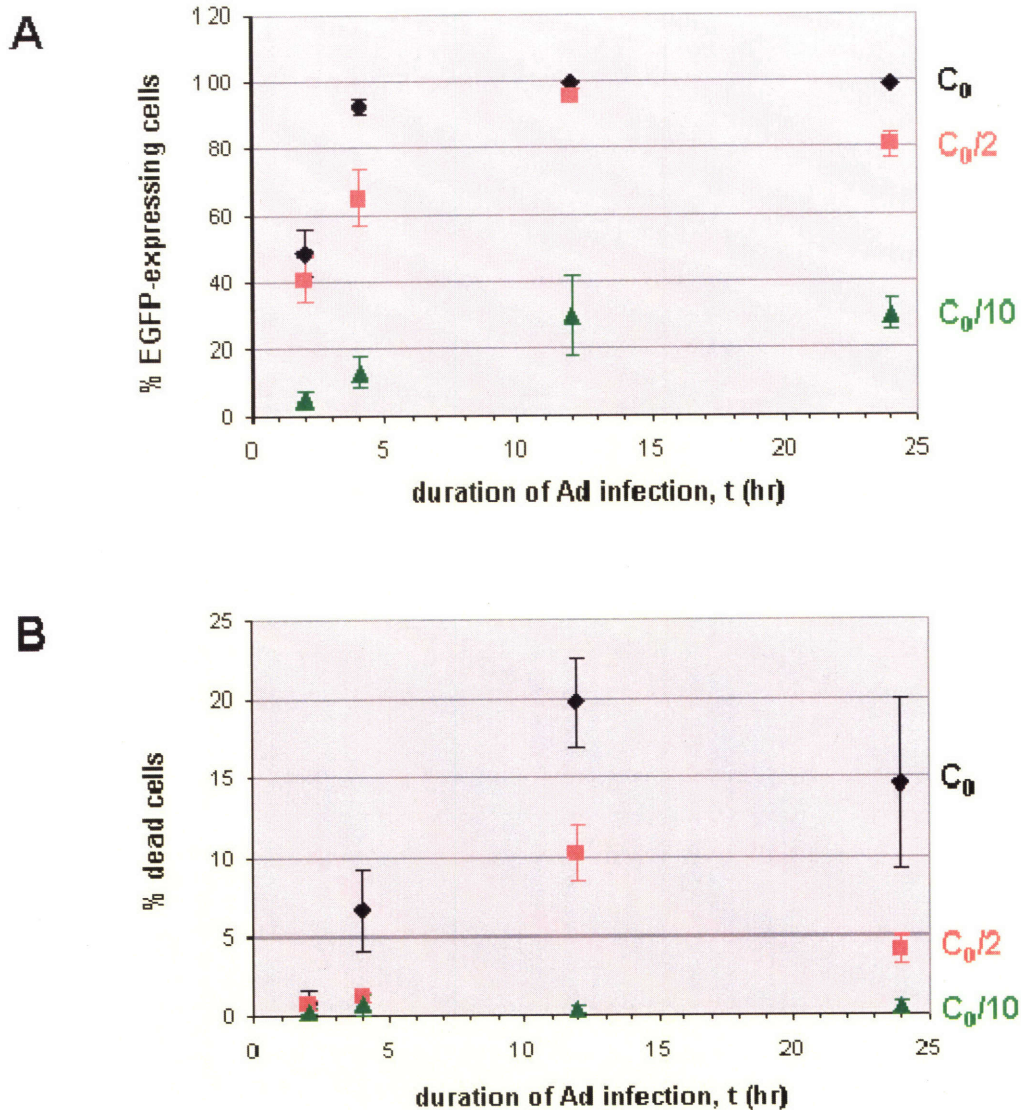


**Figure 4.9.** Quantification of Ad gene delivery efficiency and cell viability in monolayer hepatocyte cultures with fluorescence imaging. The cells were incubated with Ad5-CMV-EGFP at three concentrations ( $C_0$ ,  $C_0/2$  and  $C_0/10$ ) for varying amounts of time (ranging from  $t=2$ hr to 24hr). Triplicate samples were prepared for each condition. After the end of Ad infection the cells were cultured in HGM until  $t = 48$ hr and subsequently counterstained with Hoechst 33342 and Ethidium Homodimer-1 for fluorescence imaging. Images were acquired from 5-6 different regions in each triplicate group. The number of live cells was determined by the count of Hoechst-stained nuclei, the number of dead cells by the count of Ethidium-stained nuclei and the number of EGFP-expressing cells by the count of green fluorescent cells. **Graph A** shows the % EGFP-expressing cells plotted against time of infection. **Graph B** shows the % dead cells on the hepatocyte monolayers plotted against time of infection. All data points represent the mean values of the imaged regions  $\pm$  the standard deviation of the mean. ( $C_0 = 6.4 \times 10^7$  i.p./ml)

be noted that these numbers do not take into account the number of cells that might have died and detached from the monolayers before the time of the fluorescence imaging.

#### **4.3.2 Quantification of EGFP mRNA Levels with Real-Time TaqMan RT-PCR.**

The same procedures for Ad infection in monolayer cultures as described earlier were followed in these experiments as well. Triplicate wells were prepared for each initial Ad concentration ( $C_0$ ,  $C_0/2$  and  $C_0/10$ , where  $C_0 = 6.4 \times 10^7$  i.p./ml as determined in section 4.1.3) and time point condition ( $t = 2, 4, 8, 12$  and  $24$  hours). After the Ad infection, the hepatocytes were cultured in HGM until  $t=48$ hr when they were harvested in Trizol reagent for RNA extraction (data set 4). RNA was isolated and purified, and the total RNA content of each sample was measured. The same amount of RNA (400 ng) was used for all reverse transcription reactions. The quantity of cDNA sample amplified in each PCR reaction corresponded to 1 ng input total RNA. For each sample the target gene (EGFP), as well as an endogenous reference gene (18S rRNA) were amplified with quantitative real-time TaqMan PCR. The results were analyzed with the Comparative  $C_T$  Method, which calculates the EGFP mRNA levels normalized to 18S and relative to a calibrator. One of the three cultures infected with Ad for 24 hr at concentration  $C_0$  was selected as the calibrator sample. Additionally, the data were analyzed with the Standard Curve method to determine the number of EGFP cDNA copies present in each sample; in this case EGFP expression was normalized to the amount of total RNA. All experimental procedures and data analysis methods are described in detail in Chapter 3 (sections 3.5 and 3.6).

Control hepatocyte monolayer samples that were not infected with Ad showed no PCR amplification as expected. The minus RT controls for Ad-infected samples (in which the reverse transcriptase is omitted from the RT reaction) also tested negative; consequently there were no DNA contaminants present in the RNA template samples.

Figure 4.10 shows the normalized EGFP mRNA levels relative to the calibrator ( $2^{-\Delta\Delta C_T}$ ) calculated with the Comparative  $C_T$  Method. EGFP expression is plotted on a logarithmic scale against the time the hepatocyte monolayers were exposed to the Ad vector, and for the three different Ad concentrations. Each data point represents the mean value of three samples. The error bars correspond to the standard deviation of the mean. The results indicate that there is some variability among samples subjected to the same Ad infection conditions reflected in the error bars on the plot. However, the real-time RT-PCR assay could clearly detect the effect of

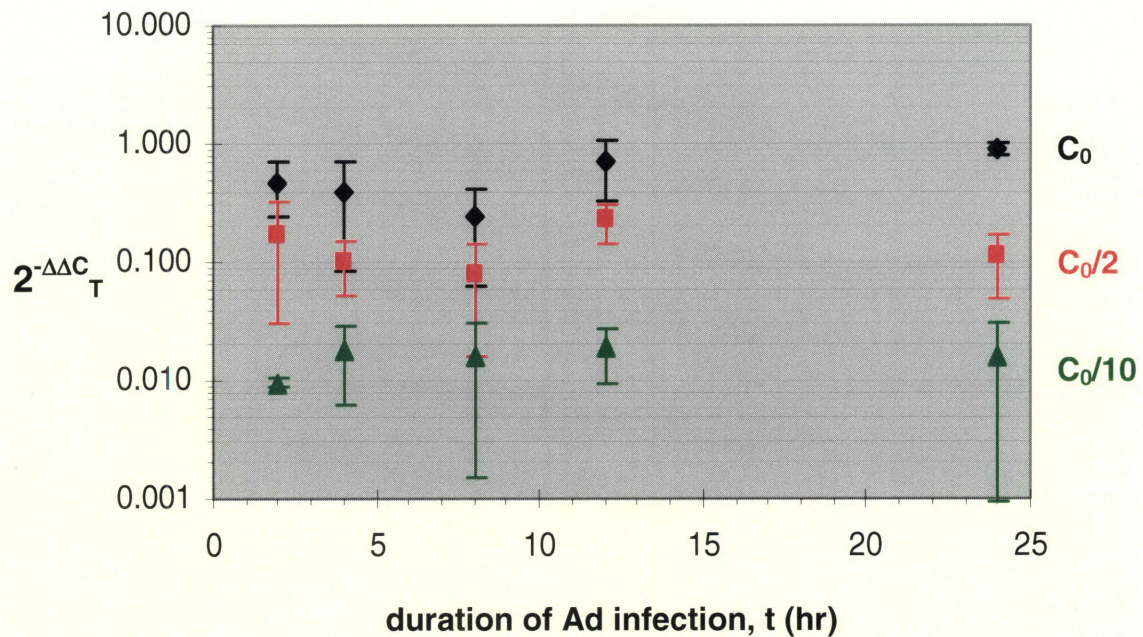


**Figure 4.10.** Quantification of EGFP mRNA levels after AdEGFP vector infection in monolayer hepatocyte cultures with real-time RT-PCR. Primary rat hepatocytes were seeded on collagen-coated 12-well plates at a density of  $3 \times 10^5$  cells per well, cultured for 24hr in HGM, then incubated with Ad5-CMV-EGFP at three concentrations ( $C_0$ ,  $C_0/2$  and  $C_0/10$ , where  $C_0 = 6.4 \times 10^7$  i.p./ml) for varying amounts of time  $t$  (ranging from 2hr to 24hr). Triplicate samples were prepared for each condition. The cells were harvested at  $t = 48$ hr for RNA extraction. Total RNA content was measured with the Rediplate 96 RiboGreen RNA Quantification Kit. 400ng RNA were used for cDNA synthesis by reverse transcription. EGFP mRNA and 18S rRNA (endogenous reference) were amplified with real-time TaqMan PCR in separate reactions (1ng input total RNA per reaction). The PCR data were analyzed with the Comparative  $C_T$  Method. This graph shows the EGFP mRNA levels normalized against the 18S levels and relative to a calibrator sample ( $2^{-\Delta\Delta C_T}$ ) plotted against time of infection. The calibrator sample was one of the 3 cultures infected with Ad for 24hr at concentration  $C_0$ . All data points represent the mean values of three samples and the error bars correspond to the standard deviation of the mean.



the increasing Ad concentration on the levels of EGFP expression, which was observed qualitatively with fluorescence imaging of the monolayer cultures (Figure 4.8). The increase in mRNA levels with Ad concentration is also in agreement with the trend observed for the Ad vector uptake measurements (Figure 4.6).

Similar results were obtained with the Standard Curve method (Figure 4.11). EGFP expression normalized against total RNA (cDNA copies/ng RNA) is plotted here on a linear scale versus the duration of Ad infection. Monolayer cultures infected with the highest Ad concentration  $C_0$  show a trend of increasing levels of EGFP expression with time of infection as expected from the fluorescence microscopy and Ad vector uptake data. However, the data for the Ad concentration of  $C_0/2$  show an unexpected decrease in mRNA levels at the 24hr time point, a result that is probably due to an experimental error and is not supported by the fluorescence and Ad uptake data. The mRNA expression at the lowest Ad concentration,  $C_0/10$ , does not show any significant trend with infection time; however, at that level of expression the cDNA copies before PCR amplification are in the order of 50, which is close to the sensitivity limit of the assay.

The ratio of mRNA levels divided by the intracellular Ad levels can be calculated as a measure of transgene expression efficiency relative to Ad uptake, a quantity that will be a basis for comparison with the gene delivery results in the hepatocyte microreactor cultures. The data presented in Figure 4.11 were converted to cDNA copies per cell with the conversion factor determined in Section 3.5 and then divided with the data presented in Figure 4.5 (Ad genomic copies per cell – data set 2 corresponding to DNA extraction at t=48h). The results are shown in Figure 4.12. All data points represent the ratio of the mean values ( $m_1/m_2$ ). The error bars represent the standard deviation of the quotient ( $s$ ) calculated from the standard deviations ( $s_1$  and  $s_2$ ) and the mean values ( $m_1$  and  $m_2$ ) of the two quantities with the following formula:

$$s = \frac{m_1}{m_2} \sqrt{\left(\frac{s_1}{m_1}\right)^2 + \left(\frac{s_2}{m_2}\right)^2} \quad (10)$$

Ideally, EGFP expression efficiency relative to intracellular Ad genomic levels should be independent of the experimental conditions (duration of infection, initial Ad concentration), given that the transgene expression is driven by a constitutive promoter (CMV). In other words, one would expect the mRNA levels to increase with the number of intracellular transgene copies. Figure 4.12 indicates that for the majority of experimental conditions, the EGFP expression

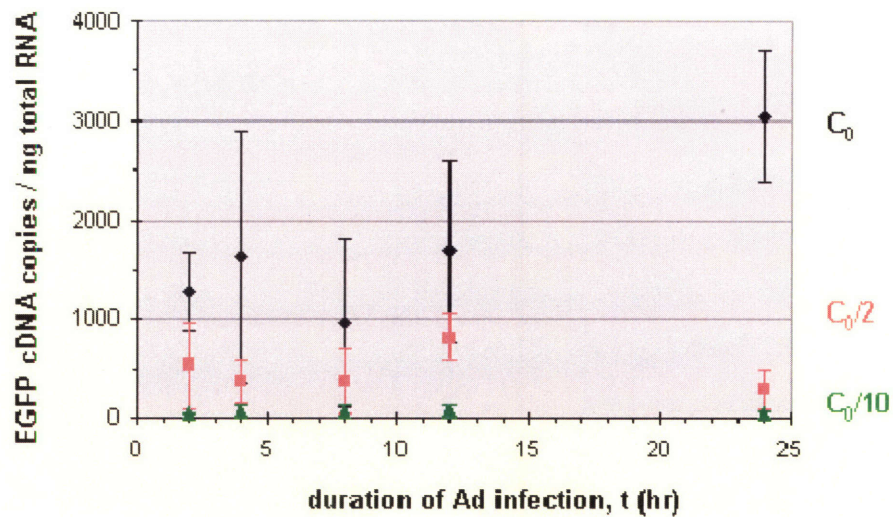


**Figure 4.11.** EGFP mRNA levels normalized against total RNA. The data were obtained as described in Figure 4.10 and were analyzed with the Standard Curve Method. The standards were prepared from serial dilutions of Ad genomic DNA. The number of EGFP cDNA copies present in each sample (corresponding to 1 ng input total RNA) were determined from the standard curve with interpolation. This graph shows the normalized EGFP expression levels plotted against time of infection. All data points represent the mean values of three samples and the error bars correspond to the standard deviation of the mean.

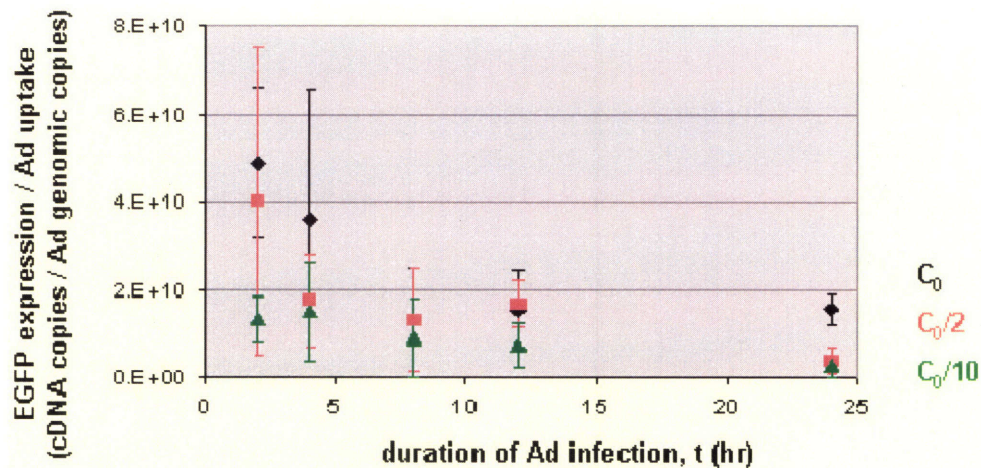


**Figure 4.12.** EGFP expression efficiency relative to Ad vector uptake. The data presented in Figure 4.11 were converted to cDNA copies per cell and were normalized against the Ad vector uptake data (Ad genomic copies/cell) presented in Figure 4.5 (data set 2: DNA extracted at  $t=48h$ ). All data points represent the ratio of the mean values and the error bars correspond to the standard deviation of the quotient.

relative to Ad uptake levels lay within a narrow range of values with an average of  $1.2 \times 10^{10}$  mRNA copies per Ad genomic copy and a standard deviation of  $5 \times 10^9$ . Three data points (corresponding to short infection times) display higher average values as well as large standard deviations. This is due to the relatively high average expression levels measured for these data points (in comparison to the Ad uptake levels) as well as the high degree of variability among the triplicate samples. It seems unlikely that this deviation has any biological significance. It could be argued that high levels of intracellular Ad copies (resulting from longer Ad exposure at high concentrations) might be toxic to the hepatocyte cultures or trigger gene silencing mechanisms, leading to lower levels of mRNA transcription. However, if that was the case then other data points should also have higher expression levels (e.g. 24h infection at  $C_0/10$  and 8h infection at  $C_0/2$ ). Additionally, the fluorescence microscopy data does not support that hypothesis. In conclusion, within the limits of experimental error, the results suggest no significant trend in EGFP mRNA expression levels relative to Ad vector uptake.

The sample variability exhibited in the RT-PCR experiment compared to the Ad vector uptake results (also obtained with PCR) is most likely caused by the inherent variability of the reverse transcription step, as explained in the introduction of section 3.6. The RT was carried out using random hexamers as primers for cDNA synthesis, in order to create both EGFP mRNA and 18S rRNA templates. However, ribosomal RNA is present at much higher levels than the target mRNA in total RNA preparations. This could affect the sensitivity and accuracy of quantification due to disproportionate priming of the 2 templates, especially at the low levels of expression corresponding to the lowest Ad concentration.

The sensitivity and accuracy of the EGFP expression quantification could be improved by modifying the RT-PCR assay to use EGFP-specific primers for cDNA synthesis. In that case it would not be possible to normalize EGFP levels against an endogenous gene such as 18S and apply the Comparative  $C_T$  Method. However, combined with total RNA measurements and the Standard Curve analysis method (or the Simplified Comparative  $C_T$  method), this alternative approach could provide more sensitive mRNA quantification.

## 4.4 References

Deen, W.M. (1998). *Analysis of Transport Phenomena*. Oxford University Press, p.19.

Einstein, A. (1956). *Investigations on the Theory of the Brownian Movement*. Dover Publications, p.81.

Mittereder, N., March, K.L., Trapnell, B.C. (1996). Evaluation of the Concentration and Bioactivity of Adenovirus Vectors for Gene Therapy. *Journal of Virology*, 7498-7509.

Nyberg-Hoffman, C., Shabram, P., Li, W., Giroux, D., Aguilar-Cordova, E. (1997). Sensitivity and reproducibility in adenoviral infectious titer determination. *Nature Medicine* 3 (7), 808-811.

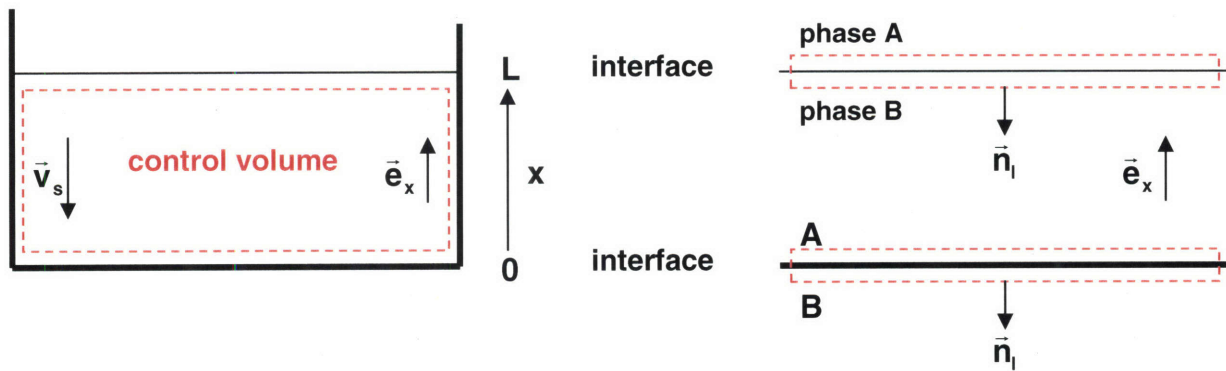
Shabram, P., Aguilar-Cordova, E. (2000). Multiplicity of Infection/Multiplicity of Confusion. *Molecular Therapy* 2 (5), 420-421.



## APPENDIX 4.1

### Mathematical Model for Ad Mass Transfer to Monolayer (2D) Hepatocyte Cultures: Derivation of Ad Conservation Equation and Boundary Conditions.

The control volume of the system is defined as the Ad-containing liquid film above the cell monolayer. The boundaries of the control volume correspond to the cell monolayer at  $x=0$  and the liquid-air interface at  $x=L$ . Any edge effects at the walls of the culture well are considered negligible. Additionally the cell monolayer is assumed to be flat and uniformly distributed on the surface of the culture well. Therefore this system can be mathematically described as one-dimensional diffusion and sedimentation with a heterogeneous reaction at the  $x=0$  boundary.



- $\bar{e}_x$                       unit vector
- $\bar{v}_s = -u_s \bar{e}_x$         sedimentation velocity
- $\bar{n}_i = -\bar{e}_x$               unit vector normal to interfacial surface

The basic form of the conservation equation for Ad particles at any interior point of the control volume is (Deen, 1998, Table 2.1):

$$\begin{aligned} \frac{\partial C}{\partial t} &= -\bar{\nabla} \cdot \bar{N} \\ &= -\bar{\nabla} \cdot (C\bar{v} + \bar{J}) \end{aligned}$$

$N$  is the total flux,  $Cv_s$  is the convective flux (sedimentation) and  $J$  the diffusive flux of Ad.

By substituting for:

$$\begin{aligned}\bar{\mathbf{v}} &= -\mathbf{u}_s \bar{\mathbf{e}}_x \\ \bar{\mathbf{J}} &= -\mathbf{D} \bar{\nabla} \mathbf{C} \\ \bar{\nabla} &= \bar{\mathbf{e}}_x \frac{\partial}{\partial x}\end{aligned}$$

the Ad conservation equation can be written as:

$$\frac{\partial \mathbf{C}}{\partial t} = \mathbf{u}_s \frac{\partial \mathbf{C}}{\partial x} + \mathbf{D} \frac{\partial^2 \mathbf{C}}{\partial x^2}$$

The basic form of the conservation equation for Ad particles at an interface is (Deen, 1998, Table 2.1):

$$\left[ (\bar{\mathbf{N}} - \mathbf{C} \bar{\mathbf{v}}_i)_B - (\bar{\mathbf{N}} - \mathbf{C} \bar{\mathbf{v}}_i)_A \right] \cdot \bar{\mathbf{n}}_i = \mathbf{R}$$

where  $\mathbf{v}_i$  is the interfacial velocity,  $\mathbf{n}_i$  is the unit vector normal to the interfacial surface pointing from phase A toward phase B, and  $\mathbf{R}$  is the rate of formation.

For the interface at  $x=0$  there is no flux in phase B,  $\mathbf{v}_i=0$  (stationary interface) and  $\mathbf{R}=-k_u \mathbf{C}$ . Therefore the above-mentioned equation can be written as:

$$-\bar{\mathbf{N}} \cdot \bar{\mathbf{n}}_i = -k_u \mathbf{C}$$

$$\Rightarrow \mathbf{u}_s \mathbf{C} + \mathbf{D} \frac{\partial \mathbf{C}}{\partial x} = k_u \mathbf{C}$$

Similarly, for the interface at  $x=L$  there is no flux in phase A,  $v_1=0$  and  $R=0$ . Then:

$$\vec{N} \cdot \vec{n}_1 = 0$$

$$\Rightarrow \boxed{u_s C + D \frac{\partial C}{\partial x} = 0}$$

Therefore the complete system of equations (including the initial condition) that describe the mass transfer of Ad in the monolayer cell culture system is written as:

$$\boxed{\begin{aligned} \frac{\partial C}{\partial t} &= u_s \frac{\partial C}{\partial x} + D \frac{\partial^2 C}{\partial x^2} \\ u_s C + D \frac{\partial C}{\partial x} &= k_u C \quad \text{at } x = 0 \\ u_s C + D \frac{\partial C}{\partial x} &= 0 \quad \text{at } x = L \\ C &= C_0 \quad \text{at } t = 0 \end{aligned}}$$

## APPENDIX 4.2

### Mathematical Model for Ad Mass Transfer to Monolayer (2D) Hepatocyte Cultures: Analytical Solution.

The mathematical model equations describing the processes of diffusion, sedimentation and uptake of Ad particles in the hepatocyte culture system are as follows:

$$\begin{aligned}\frac{\partial C}{\partial t} &= u_s \frac{\partial C}{\partial x} + D \frac{\partial^2 C}{\partial x^2} \\ C(x,0) &= C_0 \\ u_s C(0,t) + D \frac{\partial C}{\partial x}(0,t) &= k_u C(0,t) \\ C(\infty,t) &= C_0\end{aligned}$$

Substituting for  $\Theta=C/C_0$ :

$$\begin{aligned}\frac{\partial \Theta}{\partial t} &= u_s \frac{\partial \Theta}{\partial x} + D \frac{\partial^2 \Theta}{\partial x^2} \\ \Theta(x,0) &= 1 \\ u_s \Theta(0,t) + D \frac{\partial \Theta}{\partial x}(0,t) &= k_u \Theta(0,t) \\ \Theta(\infty,t) &= 1\end{aligned}$$

Applying the Laplace transform:

$$\bar{\Theta}(x, s) = L\{\Theta(x, t)\} = \int_0^{\infty} e^{-st} \Theta(x, t) dt$$

the transformed mathematical model can be written as:

$$D \frac{d^2 \left( \bar{\Theta} - \frac{1}{s} \right)}{dx^2} + u_s \frac{d \left( \bar{\Theta} - \frac{1}{s} \right)}{dx} - s \left( \bar{\Theta} - \frac{1}{s} \right) = 0$$

$$D \frac{d \bar{\Theta}}{dx} (0, s) = (k_u - u_s) \bar{\Theta} (0, s)$$

$$\bar{\Theta} (\infty, s) = \frac{1}{s}$$

The general solution of the above differential equation is:

$$\bar{\Theta} - \frac{1}{s} = c_1 e^{\lambda_1 x} + c_2 e^{\lambda_2 x}$$

where  $\lambda_1$  and  $\lambda_2$  are the roots of the characteristic equation:

$$D \lambda^2 + u_s \lambda - s = 0$$

$$\lambda_1 = \frac{-u_s + \sqrt{u_s^2 + 4Ds}}{2D} > 0$$

$$\lambda_2 = \frac{-u_s - \sqrt{u_s^2 + 4Ds}}{2D} < 0$$

and  $c_1$  and  $c_2$  are constants to be determined from the boundary conditions. From the second boundary condition ( $x \rightarrow \infty$ ) and since  $\lambda_1 > 0$ ,  $c_1$  has to be equal to zero. Then from the first boundary condition:

$$c_2 = -\frac{1}{s} \frac{\frac{k_u - u_s}{\sqrt{D}}}{\sqrt{s + \frac{u_s^2}{4D} + \frac{2k_u - u_s}{2\sqrt{D}}}}$$

Therefore the solution of the Laplace transformed model can be written as follows:

$$\bar{\Theta}(x, s) = \frac{1}{s} - \frac{1}{s} \frac{\frac{k_u - u_s}{\sqrt{D}}}{\sqrt{s + \frac{u_s^2}{4D} + \frac{2k_u - u_s}{2\sqrt{D}}}} e^{-\left(\sqrt{s + \frac{u_s^2}{4D} + \frac{2k_u - u_s}{2\sqrt{D}}}\right) \frac{x}{\sqrt{D}}}$$

which can be simplified with the following substitutions:

$$a = \frac{k_u - u_s}{\sqrt{D}}, \quad b = \frac{u_s^2}{4D}, \quad c = \frac{x}{\sqrt{D}}, \quad d = \frac{2k_u - u_s}{2\sqrt{D}}$$

$$\bar{\Theta} = \frac{1}{s} - \frac{1}{s} \left\{ a \cdot e^{-c\sqrt{b}} \cdot \left[ \frac{e^{-c\sqrt{s+b}}}{\sqrt{s+b+d}} \right] \right\}$$

The inverse Laplace transform of the above is  $\Theta(x, t)$ . This operation cannot be easily performed directly with Laplace transform tables or with programs such as Matlab or Mathematica. In order to find the solution, the following Laplace-transform theorems were used:

**s – shift theorem**

$$L^{-1}\{F(s+b)\} = e^{-bt}f(t) \quad \text{where} \quad f(t) = L^{-1}\{F(s)\}$$

**multiplication by  $\frac{1}{s}$  theorem**

$$L^{-1}\left\{\frac{G(s)}{s}\right\} = \int_0^t g(\tau) d\tau \quad \text{where} \quad g(t) = L^{-1}\{G(s)\}$$



Therefore, if

$$F(s+b) = \frac{e^{-c\sqrt{s+b}}}{\sqrt{s+b+d}} \longrightarrow F(s) = \frac{e^{-c\sqrt{s}}}{\sqrt{s+d}}$$

$$G(s) = a \cdot e^{-c\sqrt{b}} \cdot F(s+b)$$

then

$$\bar{\Theta}(s) = \frac{1}{s} - \frac{G(s)}{s} \xrightarrow[\text{transform}]{\text{inverse Laplace}} \Theta(x,t) = 1 - \int_0^t g(\tau) d\tau \quad (1)$$

where

$$\begin{aligned} g(t) &= a \cdot e^{-c\sqrt{b}} \cdot L^{-1}\{F(s+b)\} \\ &= a \cdot e^{-c\sqrt{b}} \cdot e^{-bt} \cdot f(t) \end{aligned}$$

and  $f(t)$  can be determined as the inverse Laplace transform of  $F(s)$  with Matlab's Symbolic Math Toolbox:

$$f(t) = \frac{1}{\sqrt{\pi t}} \cdot e^{-\frac{c^2}{4t}} - d \cdot e^{cd+d^2t} \cdot \text{erfc}\left(\frac{c}{2\sqrt{t}} + d\sqrt{t}\right)$$

where  $\text{erfc}$  is the complementary error function. Note that  $f(t)$  and  $g(t)$  are also a function of  $x$  since  $c$  is a function of  $x$ .

The last step to obtain the concentration profile  $\Theta(x,t)$  is the integration of  $g(t)$  with respect to the time  $t$  (see equation 1). The function  $g(t)$  can be written as:

$$\mathbf{g}(t) = \mathbf{a} \cdot \mathbf{e}^{-c\sqrt{b}} \left[ \Phi_1(t) - \mathbf{d} \cdot \mathbf{e}^{cd} \Phi_2(t) \right]$$

where

$$\Phi_1(t) = \frac{1}{\sqrt{\pi t}} \cdot \mathbf{e}^{-bt - \frac{c^2}{4t}}$$

$$\Phi_2(t) = \mathbf{e}^{(d^2 - b)t} \cdot \operatorname{erfc} \left( \frac{c}{2\sqrt{t}} + d\sqrt{t} \right)$$

Then (from Matlab's Symbolic Math Toolbox):

$$\int_0^t \Phi_1 dt = \frac{1}{2\sqrt{b}} \cdot \left\{ \mathbf{e}^{c\sqrt{b}} \cdot \left[ \operatorname{erf} \left( \sqrt{bt} + \frac{c}{2\sqrt{t}} \right) - 1 \right] + \mathbf{e}^{-c\sqrt{b}} \cdot \left[ \operatorname{erf} \left( \sqrt{bt} - \frac{c}{2\sqrt{t}} \right) + 1 \right] \right\}$$

The solution to the integral of  $\Phi_2$  cannot be found with programs like Matlab, Mathematica or integration properties and it is possible that an analytical solution does not exist. This presents an obstacle for the derivation of the concentration profile  $C(x,t)$  and consequently the equation for the number of Ad particles taken up by the hepatocyte monolayers,  $N_{Ad}(t)$  (equation 5 in Chapter 4):

$$N_{Ad}(t) = nAk_u \int_0^t C(0,t) dt = nAk_u C_0 \int_0^t \Theta(0,t) dt \quad (2)$$

This equation is needed to fit the uptake rate constant  $k_u$  to the experimental data  $N_{Ad}(t)$ . As is obvious, the expression for the concentration at the cell monolayer,  $\Theta(0,t)$  would be enough for the data analysis.

$$\begin{aligned} \Theta(0,t) &= 1 - \left[ \int_0^t \mathbf{g}(x,\tau) d\tau \right]_{x=0} \\ &= 1 - \frac{\mathbf{a}}{\sqrt{b}} \cdot \operatorname{erf}(\sqrt{bt}) + \mathbf{ad} \cdot \left[ \int_0^t \Phi_2(x,\tau) d\tau \right]_{x=0} \end{aligned} \quad (3)$$

In order to evaluate the behavior of the integral of  $\Phi_2$  at  $x=0$  the following theorem can be used (Bender and Orszag, 1978):

To determine the leading behavior of integral  $I(x) = \int_a^b f(x,t) dt$  as  $x \rightarrow 0$

If  $f(x,t) \sim f(0,t)$  for  $x \rightarrow 0$  uniformly for  $a \leq t \leq b$ , that is if  $\lim_{x \rightarrow 0} \frac{f(x,t)}{f(0,t)} = 1$  uniformly in  $t$

Then:  $\int_a^b f(x,t) dt \approx \int_a^b f(0,t) dt$  for  $x \rightarrow 0$

provided that the right side of this relation is finite and non zero.

Therefore

$$\left[ \int_0^t \Phi_2(x, \tau) d\tau \right]_{x=0} \approx \int_0^t \Phi_2(0, \tau) d\tau$$

provided that

$$\lim_{x \rightarrow 0} \frac{\Phi_2(x,t)}{\Phi_2(0,t)} = 1 \quad \text{uniformly in } t$$

$$\Lambda(x,t) = \frac{\Phi_2(x,t)}{\Phi_2(0,t)} = \frac{\text{erfc}\left(\frac{c}{2\sqrt{t}} + d\sqrt{t}\right)}{\text{erfc}(d\sqrt{t})} \quad \text{where} \quad c = \frac{x}{\sqrt{D}}, \quad d = \frac{2k_u - u_s}{2\sqrt{D}}$$

To determine if the limit of  $\Lambda(x,t)$  when  $x \rightarrow 0$  is equal to 1, a 3-dimensional plot was created using Matlab. Whereas parameters  $D$  and  $u_s$  are known (see Chapter 4), the value of the uptake rate constant  $k_u$  is not. Therefore, graphs of  $\Lambda$  versus  $x$  and  $t$  were created for values of  $k_u$  ranging from  $5 \times 10^{-8}$  to  $5 \times 10^{-5}$  cm/s. Similar behavior was observed in all cases. Figure 1 shows

two graphs for  $k_u=5 \times 10^{-6}$  cm/s. Graph A shows the behavior of function  $\Lambda$  for the full range of axes  $x$  and  $t$ . To examine what happens near  $t=0$ ,  $\Lambda$  is plotted with  $t$  ranging from 0 to  $10^{-10}$  s and  $x$  from 0 to  $10^{-8}$  cm (graph B). In conclusion, the function  $\Lambda$  is bound by 1 at  $x=0$  and the above mentioned theorem can be used. Then:

$$\int_0^t \Phi_2(0, \tau) d\tau = \int_0^t e^{(d^2-b)\tau} \cdot \operatorname{erfc}(d\sqrt{\tau}) d\tau$$

$$= \frac{1}{d^2-b} \left[ e^{(d^2-b)t} \cdot \operatorname{erfc}(d\sqrt{t}) - 1 \right] + \frac{d}{d^2-b} \frac{1}{\sqrt{b}} \cdot \operatorname{erf}(\sqrt{bt})$$

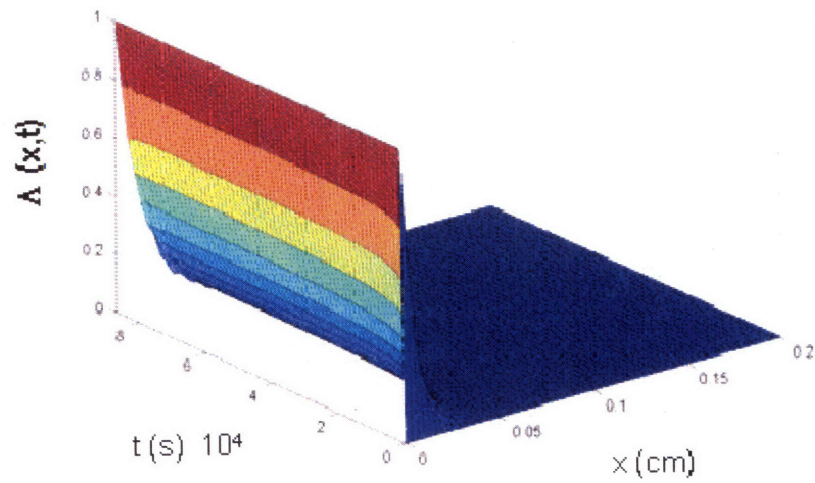
(derived using integration by parts, the expression for the derivative of the complementary error function  $\frac{d}{dz} \operatorname{erfc}(z) = -\frac{2}{\sqrt{\pi}} \cdot e^{-z^2}$  and Matlab's Symbolic Math Toolbox).

Then,  $\Theta(0,t)$  is determined with equation (3) and can be integrated to give the expression for  $N_{Ad}(t)$  (equation 2):

$$N_{Ad}(t) = nAC_0 \left\{ \frac{u_s t + \sqrt{Dt}}{\sqrt{\pi}} \cdot e^{-\frac{u_s^2}{4D}t} + \left[ \frac{u_s t + D}{2k_u u_s (k_u - u_s)} \right] \cdot \operatorname{erf} \left( \frac{u_s}{2\sqrt{D}} \sqrt{t} \right) + \right.$$

$$\left. + \frac{D}{2k_u (k_u - u_s)} \left[ e^{\frac{k_u(k_u - u_s)}{D}t} \cdot \operatorname{erfc} \left( \frac{2k_u - u_s}{2\sqrt{D}} \sqrt{t} \right) - 1 \right] \right\}$$

graph A



graph B

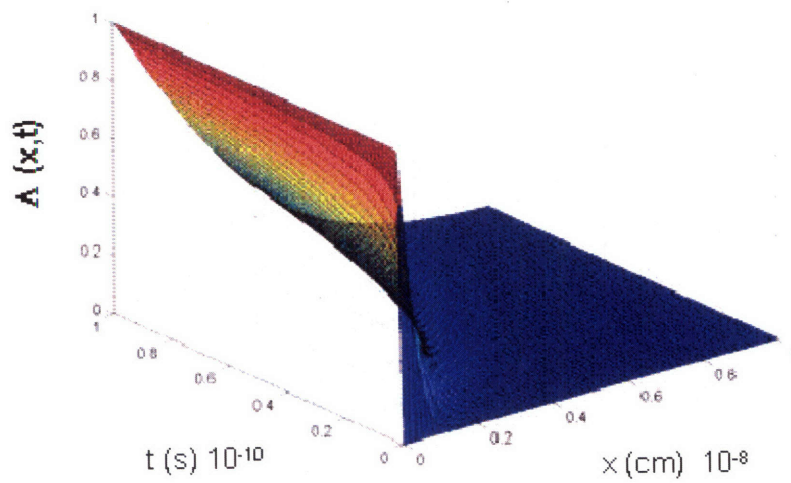


**Figure 1.** Surface plot of the function  $\Lambda(x,t)$  for  $k_v = 5 \times 10^{-6}$  cm/s to determine the behavior of  $\Lambda$  as  $x \rightarrow 0$ ; **graph A:** full range of axes  $x$  [0-0.2cm] and  $t$  [0-86400s]; **graph B:** axes range:  $x$  [0- $10^{-8}$ cm],  $t$  [0- $10^{-10}$ s].

## APPENDIX 4.3

### Mathematical Model for Ad Mass Transfer to Monolayer (2D) Hepatocyte Cultures without Sedimentation: Analytical Solution.

The mathematical model equations when the process of sedimentation is assumed negligible are reduced to the following:

$$\begin{aligned}\frac{\partial C}{\partial t} &= D \frac{\partial^2 C}{\partial x^2} \\ C(x,0) &= C_0 \\ D \frac{\partial C}{\partial x}(0,t) &= k_u C(0,t) \\ C(\infty,t) &= C_0\end{aligned}$$

Following the same procedure as in Appendix 4.2, the Laplace-transformed model can be written as:

$$\begin{aligned}\frac{d^2\left(\bar{\Theta} - \frac{1}{s}\right)}{dx^2} - \frac{s}{D}\left(\bar{\Theta} - \frac{1}{s}\right) &= 0 \\ D \frac{d\bar{\Theta}}{dx}(0,s) &= k_u \bar{\Theta}(0,s) \\ \bar{\Theta}(\infty,s) &= \frac{1}{s}\end{aligned}$$

The solution of the differential equation is:

$$\bar{\Theta}(x,s) = \frac{1}{s} - \frac{1}{s} \cdot \frac{\frac{k_u}{\sqrt{D}}}{\sqrt{s} + \frac{k_u}{\sqrt{D}}} e^{-\sqrt{s} \frac{x}{\sqrt{D}}}$$

In this case, the inverse Laplace transform can be determined directly with Matlab's Symbolic Math Toolbox and therefore the concentration profile can be derived as:

$$C(x, t) = C_0 \left[ \operatorname{erf} \left( \frac{x}{2\sqrt{Dt}} \right) + e^{\frac{k_u(x+k_u t)}{D}} \cdot \operatorname{erfc} \left( \frac{x}{2\sqrt{Dt}} + k_u \sqrt{\frac{t}{D}} \right) \right]$$

The equation for the uptake of Ad particles can then be derived from:

$$N_{Ad}(t) = nA k_u \int_0^t C(0, t) dt$$

$$N_{Ad}(t) = nAC_0 \left\{ 2\sqrt{\frac{Dt}{\pi}} + \frac{D}{k_u} \left[ \exp \left( \frac{k_u^2 t}{D} \right) \cdot \operatorname{erfc} \left( k_u \sqrt{\frac{t}{D}} \right) - 1 \right] \right\}$$



## APPENDIX 4.4

### Mathematical Model for Ad Mass Transfer to Monolayer (2D) Hepatocyte Cultures with Diffusion and Fast-Reaction Boundary Condition: Analytical Solution.

The mathematical model equations when the process of sedimentation is assumed negligible and the reaction rate is fast enough to assume that the Ad concentration at the surface of the cell monolayer approaches zero, are reduced to the following:

$$\begin{aligned}\frac{\partial C}{\partial t} &= D \frac{\partial^2 C}{\partial x^2} \\ C(x,0) &= C_0 \\ C(0,t) &= 0 \\ C(\infty,t) &= C_0\end{aligned}$$

Following the same procedure as in Appendix 4.2, the Laplace-transformed model can be written as:

$$\begin{aligned}\frac{d^2\left(\bar{\Theta} - \frac{1}{s}\right)}{dx^2} - \frac{s}{D}\left(\bar{\Theta} - \frac{1}{s}\right) &= 0 \\ \bar{\Theta}(0,s) &= 0 \\ \bar{\Theta}(\infty,s) &= \frac{1}{s}\end{aligned}$$

The solution of the differential equation is:

$$\bar{\Theta}(x,s) = \frac{1}{s} - \frac{1}{s} \cdot e^{-\sqrt{s} \cdot \frac{x}{\sqrt{D}}}$$

The inverse Laplace transform can be determined directly with Matlab's Symbolic Math Toolbox and therefore the concentration profile can be derived as:

$$C(x, t) = C_0 \operatorname{erf}\left(\frac{x}{2\sqrt{Dt}}\right)$$

The equation for the uptake of Ad particles can then be derived from:

$$N_{Ad}(t) = nA k_u \int_0^t C(0, t) dt$$

$$N_{Ad} = 2nAC_0 \sqrt{\frac{Dt}{\pi}}$$

# **CHAPTER 5**

## **Quantitative Analysis of Ad Gene Delivery in Hepatocyte Microreactor Cultures**

## 5.1 Introduction

This chapter presents the quantitative analysis of adenoviral vector gene delivery to hepatocytes cultured in the microreactor system. Like Chapter 4 it is divided into two parts. The first part addresses the extracellular mass transfer and cellular uptake of the AdEGFP vector. A simplified mathematical model is developed to describe these processes based on qualitative observations and quantitative results obtained with two-photon laser scanning fluorescence microscopy, as well as on quantitative real-time PCR data. The lower and upper boundaries for the Ad uptake rate constant  $k_{3D}$  are then determined by fitting to experimental results using the model.

The second part examines the events following the Ad internalization, namely the transgene (EGFP) expression (DNA transcription and mRNA translation). Protein levels are quantified with fluorescence emission intensity measurements using a custom-made miniaturized spectrometer and mRNA levels are measured with quantitative real-time RT-PCR. Finally, gene delivery efficiency is also quantified in terms of the percentage of Ad-infected cells via the detection of EGFP expression with two-photon microscopy.

## 5.2 Extracellular Mass Transfer and Cellular Uptake of AdEGFP Vector

Ad gene delivery in hepatocyte monolayer cultures is a process that can be adequately described with a one-dimensional mathematical model comprising Ad diffusion and cellular uptake, as demonstrated in Chapter 4; moreover, the expression of the transgene (EGFP) can be easily detected with fluorescence microscopy. The liver microreactor however is a complex three-dimensional culture system with continuous medium flow. The adenoviral vector is introduced in the medium reservoir at specific concentrations and circulates continuously in the system for a defined amount of time. During the Ad infection the Ad particles flow into the microreactor chamber and through the silicon scaffold channels, where they interact with the hepatocyte tissue and are internalized by the cells. Figure 5.1 shows a schematic of this process.

A rigorous mathematical model for the mass transfer of the Ad vector would have to assume a specific tissue geometry representative of the average microreactor channel (for

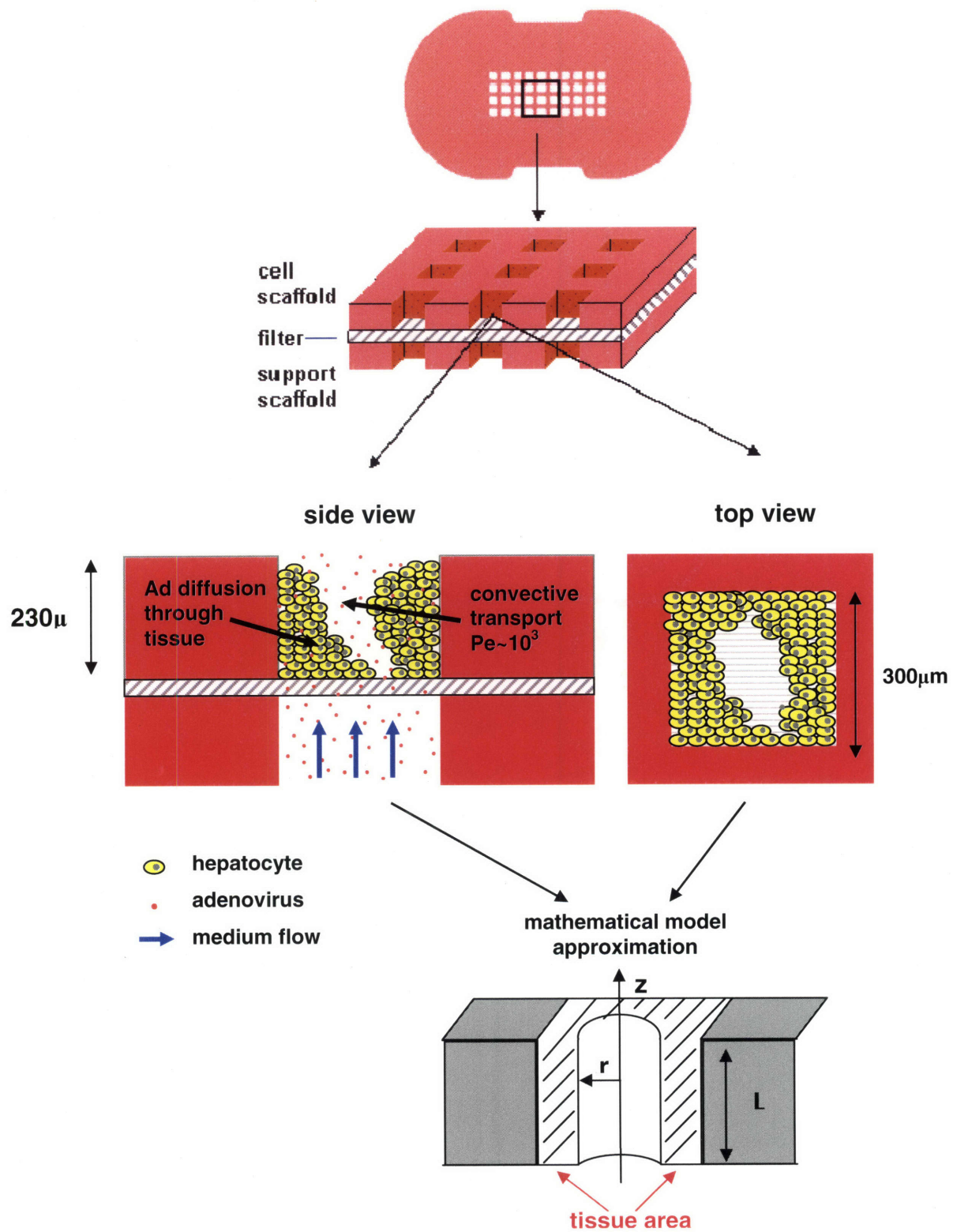


**Figure 5.1.** Schematic of hepatocyte tissue structures and adenoviral vector mass transfer processes inside the microreactor channels.

example a cylindrical fluid flow conduit in the center of the channel) and comprise the following processes: convective transport of Ad in the z direction (Peclet number in the order of  $10^3$ ), diffusion to the tissue in the r direction, diffusion and reaction (cellular uptake) inside the tissue. The model combined with experimental data for the Ad uptake (real-time PCR) as a function of initial Ad concentration would be applied to estimate the Ad uptake rate constant,  $k_{3D}$ . It is obvious that this is a complex mathematical problem. For example the rate of diffusion of the Ad particles in the tissue depends on how compact the structure of the tissue is and whether there are smaller fluid flow conduits running through it. The extraction of intact tissue units from the scaffold for sectioning and histology to examine the tissue morphology is very impractical and the material of the scaffold itself (silicon) cannot be sectioned. The alternative approach is via the in situ detection of EGFP expression and spatial distribution of EGFP-expressing cells with a fluorescence microscopy technique.

### ***5.2.1 Tissue morphology and spatial distribution of Ad-infected hepatocytes in microreactor cultures.***

Conventional fluorescence microscopy cannot be applied to three-dimensional samples. Figure 5.2a shows a fluorescence micrograph of an entire microreactor (40 channels) infected with Ad at an initial concentration of  $3.2 \times 10^7$  i.p./ml for 24h. The image was taken at ~70h after the beginning of infection (when EGFP expression reaches maximum levels; see section 5.3.1) with a FITC filter set and a 5X dry objective lens focusing at the top of the silicon scaffold. Obviously there are hepatocytes expressing EGFP; however there is no 3D resolution and no possibility to probe deep inside the tissue.

This issue was addressed with the application of two-photon laser scanning fluorescence microscopy, a technique that allows non-invasive, in situ imaging of tissues with three-dimensional resolution. The theoretical background and the experimental details of this method are described in detail in Chapter 3 (section 3.8). Preliminary experiments demonstrated the ability to detect EGFP inside the tissue and provided qualitative information about the spatial distribution of expressing cells (section 3.8.2, Figures 3.8.2-3.8.3). EGFP was detected throughout the channel cross section and the 60 to 100 $\mu$ m-deep sections that were imaged. Moreover, gene expression changes with time could also be followed by imaging the same microreactor channels at different times.



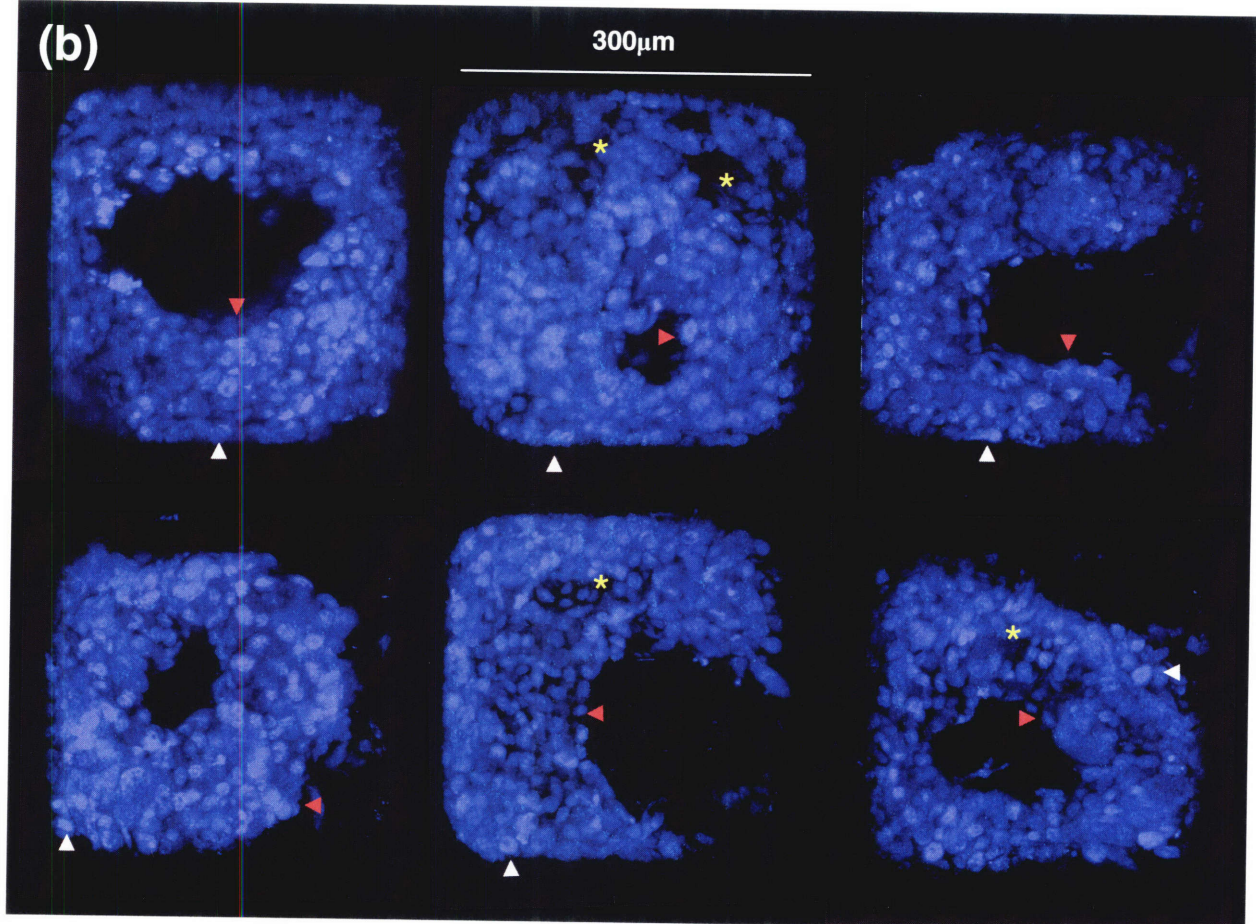
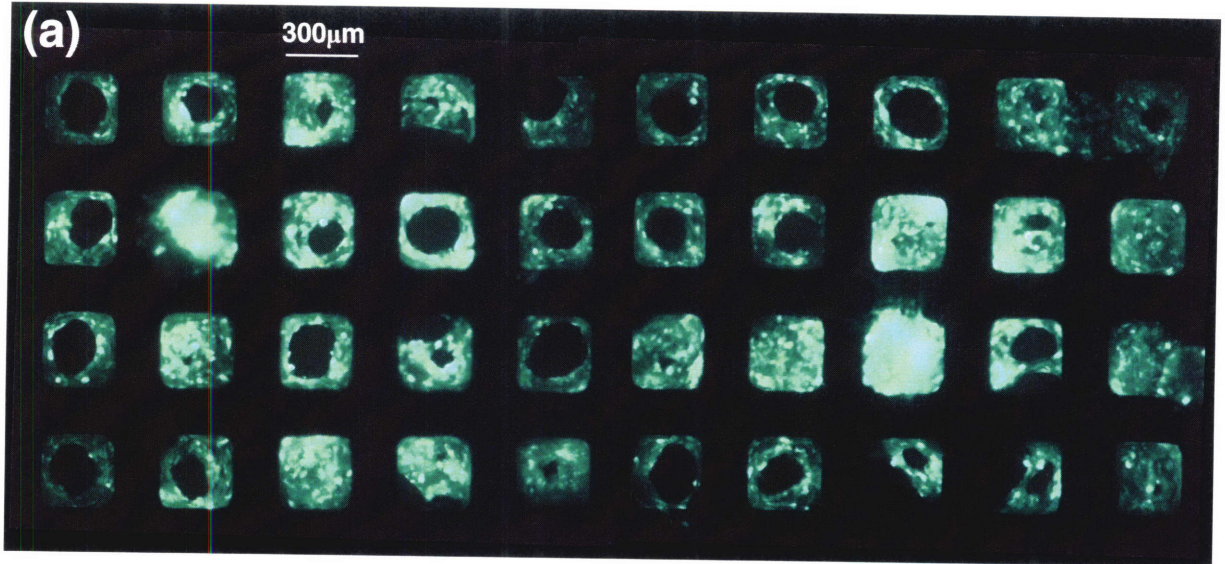


**Figure 5.2.** Morphology of hepatocyte tissue in microreactor channels. (a) Fluorescence micrograph of entire microreactor infected with AdEGFP for 24h at a concentration of  $3.2 \times 10^7$  i.p./ml. (b) Two-photon micrographs of microreactor channels stained with Hoechst 33342. The red arrows point to cells that are 50-100 $\mu$ m deeper inside the channel than those marked by white arrows. The yellow stars mark the position of smaller fluid flow conduits in the tissue.



To obtain quantitative information about the spatial distribution of Ad-infected cells, a protocol was developed which included nuclear counterstaining with Hoechst 33342 and Ethidium Homodimer 1, to detect the number of live and dead cells respectively and distinguish between EGFP expressing and non-expressing cells. These experiments were performed with a different two-photon imaging system for enhanced resolution. The data were processed with the MetaMorph software and the different categories of cells (live, dead, EGFP-expressing) were counted. Section 3.8.3 contains a detailed description of the experimental procedures as well as the data analysis, and Figures 3.8.5 and 3.8.6 demonstrate examples of the results.

The observation of 3D-reconstructed models of several microreactor channels (from two-photon imaging data) provided information about the morphology of the tissue. Some examples are presented in Figure 5.2b. This figure shows top view images of 3D-reconstructed models for six microreactor channels. The hepatocytes were incubated with Hoechst to stain the nuclei. A prevalent feature is the formation of a central fluid flow conduit; it is not cylindrical however, but has a shape that rather resembles a conical section with the apex pointing away from the top of the cell scaffold and towards the filter. This cannot be visualized in these 2D images, but certain features are marked. The red arrows point to cells that are 60-100 $\mu$ m deeper inside the channel than the cells marked with white arrows. Secondary medium flow conduits were also observed in some cases, usually in channels containing higher numbers of cells. These are marked in Figure 5.2b with yellow stars.

The spatial distribution of EGFP-expressing cells and dead cells was quantified as a function of the channel depth, in order to detect a potential gradient in the Ad concentration in the z-direction. Microreactors were infected with Ad at a concentration of  $4 \times 10^6$  pfu/ml (based on the infectious titer measured by the Ad vector supplier) for 24h; the cells were stained with Hoechst and ethidium homodimer and imaged ~70h after the beginning of infection. Two-photon imaging data from two microreactors and six channels (3 per microreactor) were used. Each channel was imaged at a depth of 100 $\mu$ m and was divided into two sections, A (0-50 $\mu$ m) and B (50-100 $\mu$ m). The percentage of EGFP-expressing cells and dead cells was calculated in each section by counting the number of blue, green and red cells. The results are shown in Table 5.1. The mean values of all 6 channels were calculated and are shown in the table as well as the standard deviations. There is no significant difference between the mean values for the % EGFP-expressing cells (i.e. the gene delivery efficiency levels) in the two sections; the same applies to the mean values for the % dead cells (i.e. cell toxicity levels). Comparison between

the two means in each case was performed by Student's *t*-test for two samples with unequal variances. Statistical significance was determined at the <0.05 level.

**Table 5.1:** Spatial distribution of EGFP-expressing and dead cells in microreactor channels as a function of channel depth.

depth z channel	% EGFP-expressing cells		% dead cells	
	1-50 $\mu$ m	50-100 $\mu$ m	1-50 $\mu$ m	50-100 $\mu$ m
1	50.0	21.4	29.2	7.8
2	40.3	60.6	10.2	21.7
3	27.3	30.0	26.4	13.2
4	29.1	37.0	8.6	6.9
5	29.6	32.2	12.4	10.6
6	24.5	32.9	6.0	16.4
<b>mean</b>	<b>33.5</b>	<b>35.7</b>	<b>15.5</b>	<b>12.8</b>
<b>standard deviation</b>	9.7	13.3	9.8	5.6

Based on these results it can be assumed that the Ad concentration does not vary significantly as a function of depth *z* inside the microreactor channels.

The observation of combined 3-color images (Hoechst-EGFP-Ethidium Homodimer) did not provide conclusive information on whether all the cells in the tissue are accessible to the Ad particles. At depths greater than 100 $\mu$ m and positions away from the main fluid flow conduit the detection of EGFP-expression and Hoechst staining becomes increasingly difficult, possibly due to limitations of the imaging technique (loss of emission intensity because of light scattering). To circumvent this problem, a simplified approach was followed in order to develop a mathematical model for the estimation of the Ad uptake rate constant,  $k_{3D}$ . Two limiting cases were examined. The first one assumes that all the cells in each microreactor channel are exposed to the same Ad concentration; in this case a lower limit for  $k_{3D}$  is estimated. The second case assumes that only the cells at the tissue-medium interface have access to the Ad vector (i.e. the tissue is compact); in this case the upper limit for  $k_{3D}$  is determined.

### 5.2.2 Mathematical Model Description.

The total number of Ad particles taken up by the hepatocytes in the microreactor culture during the time of Ad infection,  $N_{Ad}$ , is derived as the integral with time of the Ad flux at the tissue surface:

$$N_{Ad} = \int_0^{\tau} A \cdot (\text{flux})_{\text{cell surface}} dt \quad (1)$$

where  $A$  is the total surface area ( $\text{cm}^2$ ) that is exposed to the Ad and  $\tau=24\text{h}$  is the duration of infection. The flux at the tissue surface is equal to the Ad uptake rate:

$$(\text{flux})_{\text{cell surface}} = k_{3D} C \quad (2)$$

where  $k_{3D}$  is the uptake rate constant ( $\text{cm/s}$ ) and  $C$  the Ad concentration in the medium (infectious Ad particles/ $\text{cm}^3$ ). The Ad concentration in the medium is assumed constant throughout the depth ( $z$ -dimension) and cross section ( $r$ -dimension) of each channel and is the same inside all channels of the microreactor. Therefore  $C$  is a function of time  $t$  only.

The Ad concentration is expected to decrease with time as a result of the Ad uptake by the cells. A simple calculation was performed to estimate the effect of Ad uptake based on the experimental results presented in Figure 5.4a. If the initial Ad concentration is  $6.4 \times 10^7$  i.p./ml, the total number of infectious Ad particles in the circulating medium at the beginning of the infection ( $t=0$ ) is  $1.28 \times 10^9$  (the total medium volume is 20ml). Assuming an uptake of 600 Ad particles per cell by the end of the infection (a value that corresponds approximately to the maximum uptake levels observed, Figure 5.4a) and an average of 40,000 cells in the microreactor, the total number of Ad particles removed from the medium due to uptake by the tissue will be  $2.4 \times 10^7$ . This corresponds to a decrease of less than 2% in the Ad concentration. Consequently, the effect of the Ad uptake on the Ad concentration in the circulating medium is not significant and can be neglected.

Before solving the mathematical model with the assumption that the concentration remains constant with time ( $C(t)=C_0$ ), other factors were taken into consideration. Adenoviral vectors are relatively stable at  $37^\circ\text{C}$  and therefore any loss of infectivity during the 24h infection was considered negligible. Another possibility is the adsorption of the Ad vector on the microreactor system surfaces. As described in Chapter 2, the microreactor system consists of several components, including the chamber, the medium reservoir, an extensive network of

tubing and the crossflow filter. The materials of these components were originally selected for low cell toxicity and low levels of protein adsorption. To determine whether there was significant adsorption of Ad particles, the Ad concentration in the circulating medium was monitored with time during the Ad infection of microreactor cultures.

**Adsorption of Ad particles on microreactor system surfaces:** Microreactor cultures were infected with Ad at three concentrations ( $C_0$ ,  $C_0/2$  and  $C_0/10$ , where  $C_0=6.4 \times 10^7$  i.p./ml) for 24h. Samples were collected from the medium reservoir at different times during the Ad infection ( $t = 0, 1, 3, 5, 8, 20$  and 24h). The number of Ad particles in each sample was determined by measuring the number of Ad genomic copies with quantitative real-time TaqMan PCR. This method quantifies the total (infectious and non-infectious) Ad particle concentration. The ratio of genomic titer over infectious titer is  $\sim 1.06$  and therefore  $C_{0, \text{genomic}} = 6.8 \times 10^7$  p./ml as determined in Chapter 4.

Figure 5.3 shows a graph of the total number of Ad particles in the medium plotted as a function of time for the three different initial concentration values. The data points represent the mean values of 4 or 5 microreactor samples from two experiments (different rat liver perfusions) and the error bars correspond to the standard deviation of the mean. The results indicate a marked decrease in the concentration of Ad particles with time. Within 24h, the concentration decreased on average by 55%, 30% and 65% for initial Ad concentrations of  $C_0$ ,  $C_0/2$  and  $C_0/10$  respectively ( $C_0=6.4 \times 10^7$  i.p./ml).

To reflect this change in concentration with time in the mathematical model, the adsorption of Ad particles on microreactor system surfaces is assumed to follow first order kinetics. Then the mass balance for Ad in the medium takes the form of the following differential equation:

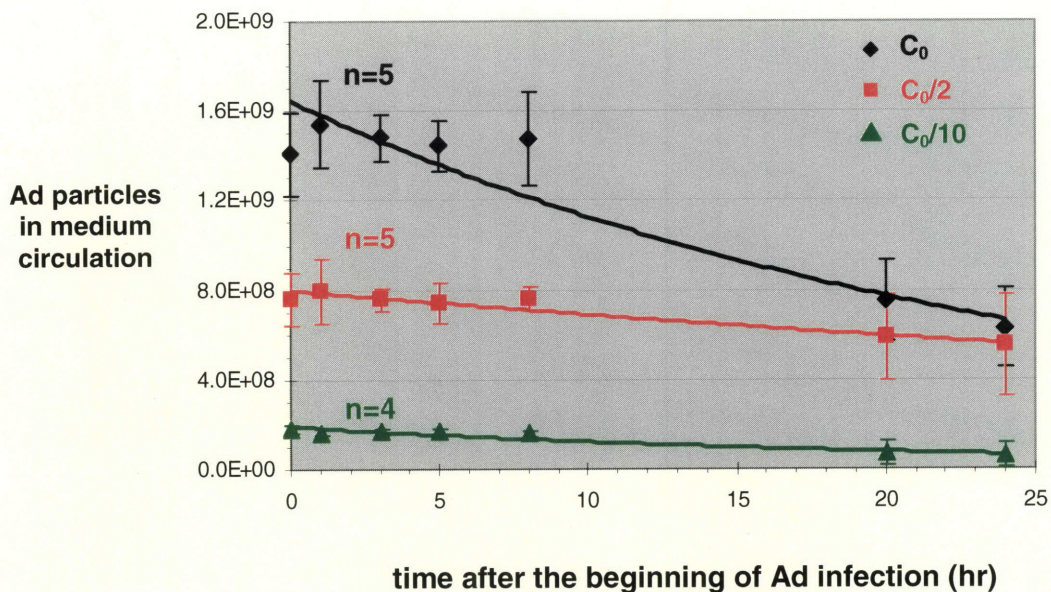
$$\frac{dC}{dt} = -k_A C$$

where  $k_A$  is the adsorption rate constant. The solution of this equation, subject to the initial condition:

$$C = C_0 \quad \text{at } t = 0$$

is derived as:

$$C = C_0 e^{-k_A t} \quad (3)$$



$$\begin{aligned}
 \text{--- } Y &= 1.65 \times 10^9 e^{-0.0379X} & k_A &= 0.0379 \text{ h}^{-1} \\
 \text{--- } Y &= 8.00 \times 10^8 e^{-0.0148X} & k_A &= 0.0148 \text{ h}^{-1} \\
 \text{--- } Y &= 1.92 \times 10^8 e^{-0.0444X} & k_A &= 0.0444 \text{ h}^{-1}
 \end{aligned}$$

**Figure 5.3.** Adsorption of Ad vector on microreactor system surfaces during Ad infection of hepatocytes. Microreactor cultures were infected with Ad at three concentrations ( $C_0$ ,  $C_0/2$  and  $C_0/10$ , where  $C_0=6.4 \times 10^7$  i.p./ml) for 24h. The circulating medium was sampled at different times during the infection and the number of Ad particles (infectious and non infectious) was quantified with real-time TaqMan PCR. The adsorption rate constant  $k_A$  was fitted to the data separately for each initial Ad concentration using Equation (3). This graph shows the total number of Ad particles in the medium plotted against time after the beginning of the Ad infection. All data points represent the mean values of two experiments (different rat liver perfusions) each performed in duplicate or triplicate  $\pm$  the standard deviation of the mean. The solid lines represent the exponential least squares regression with Excel.

The adsorption rate constant  $k_A$  was fitted to the experimental data shown in Figure 5.3 separately for each initial Ad concentration using Equation (3). The solid lines in the graph represent the exponential least squares regression with Excel. The fitted  $k_A$  values are also shown in Figure 5.3. The mean of these three values was calculated and used in the mathematical model for Ad uptake:

$$k_A = 0.0324 \text{ h}^{-1}$$

After combining equations (1), (2) and (3), the number of Ad particles taken up by the microreactor culture after time  $t$ , is given by the following equation:

$$N_{Ad} = Ak_{3D}C_0 \frac{1 - e^{-k_A t}}{k_A}$$

For the above value of  $k_A$  and  $t=24\text{h}$ :

$$N_{Ad} = 17Ak_{3D}C_0 \quad (4)$$

Therefore the Ad uptake rate constant  $k_{3D}$  can be determined by fitting to the experimental data presented in Figure 5.3 with equation (4).  $A$  is the total surface area which is exposed to the Ad vector. As described earlier in this section, two limiting cases were examined: (A) all cells in the microreactor are equally exposed to the Ad containing medium, (B) only the cells at the tissue-medium interface have access to the Ad particles. The first case provides the lower limit for the Ad uptake constant,  $k_{3D,L}$ , whereas the second one provides the upper limit,  $k_{3D,U}$ .

**(A) Lower limit for the Ad uptake constant in microreactor cultures,  $k_{3D,L}$ :** In this case all hepatocytes in each microreactor channel are assumed to be equally exposed to the Ad vector. Then the surface area  $A$  is given by the following equation:

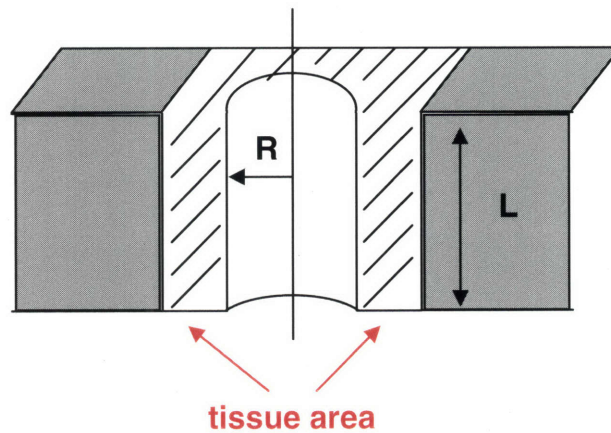
$$A = n \times A_{\text{cell}}$$

$n$  is the total number of cells in the microreactor and  $A_{\text{cell}}$  is the surface area of each cell. Assuming that each hepatocyte is a cube with length of  $25\mu\text{m}$ , then  $A_{\text{cell}}=3,750\mu\text{m}^2$ . Equation (4) then becomes:

$$\frac{N_{\text{Ad}}}{n} = 17A_{\text{cell}} k_{3\text{D},\text{L}} C_0 \quad (5)$$

The uptake rate constant  $k_{3\text{D},\text{L}}$  can be determined by plotting  $N_{\text{Ad}}/n$  (number of Ad particles internalized by the hepatocytes after a 24h infection, normalized to cell number) as a function of the initial Ad concentration  $C_0$ , and fitting a straight line through the experimental data (with intercept = 0).  $k_{3\text{D},\text{L}}$  can then be calculated from the value of the slope.

**(B) Upper limit for the Ad uptake constant in microreactor cultures,  $k_{3\text{D},\text{U}}$ :** In this case the assumption is that only the hepatocytes at the tissue-medium interface are exposed to the Ad vector. As discussed earlier in this chapter, the tissue geometry inside each microreactor channel can be approximated to be such that a cylindrical medium flow conduit is formed in the center of the channel as shown in the schematic below:



In that case the area  $A$  in equation (4) is the area of the cylinder multiplied by the number of channels:

$$A = 40 \times (2\pi RL)$$



where  $L=230\mu\text{m}$  is the depth of the channel and  $R$  is the radius of the cylinder. Edge effects at the top and bottom side of the tissue are assumed negligible.  $R$  depends on the thickness of the tissue area and therefore on the number of cells inside the channel and is calculated as:

$$R = \sqrt{\frac{(\text{channel volume}) - (\text{tissue volume})}{\pi L}}$$

The channel has a square cross section  $300\mu\text{m}$  wide, therefore  $(\text{channel volume})=2.07 \times 10^7 \mu\text{m}^3$ . The tissue volume is the product of the number of cells in the channel and the cell volume. Assuming that each hepatocyte is a cube with length of  $25\mu\text{m}$ , then  $(\text{cell volume})=15,625 \mu\text{m}^3$ . The average number of cells per channel can be calculated by dividing the total number of cells,  $n$ , with the number of channels in the microreactor (40). Equation (4) becomes:

$$\frac{N_{\text{Ad}}}{A} = 17k_{3\text{D,U}} C_0 \quad (6)$$

The uptake rate constant  $k_{3\text{D,U}}$  can be determined by plotting  $N_{\text{Ad}}/A$  (number of Ad particles taken up by the hepatocytes after a 24h infection, normalized to total surface area) as a function of the initial Ad concentration  $C_0$ , and fitting a straight line through the experimental data (with intercept = 0).  $k_{3\text{D,U}}$  can then be calculated from the value of the slope.

### **5.2.3 Experimental Results and Analysis.**

The Ad vector uptake in microreactor cultures was quantified with real-time PCR. Microreactor cultures were infected with Ad at three concentrations ( $C_0$ ,  $C_0/2$  and  $C_0/10$ , where  $C_0=6.4 \times 10^7$  i.p./ml) for 24h. The cells were harvested ~70h after Ad infection for DNA extraction. Total DNA content was measured with the Rediplate 96 PicoGreen DNA Quantification Assay. The number of Ad genome copies was quantified with real-time TaqMan PCR. Figure 5.4a shows a graph of the number of Ad copies normalized to cell number and plotted against the initial Ad concentration. All data points represent the mean values of two experiments (different rat liver perfusions) performed in duplicate or triplicate  $\pm$  the standard deviation of the mean. The Ad uptake increased linearly as a function of concentration. The normalized Ad uptake data

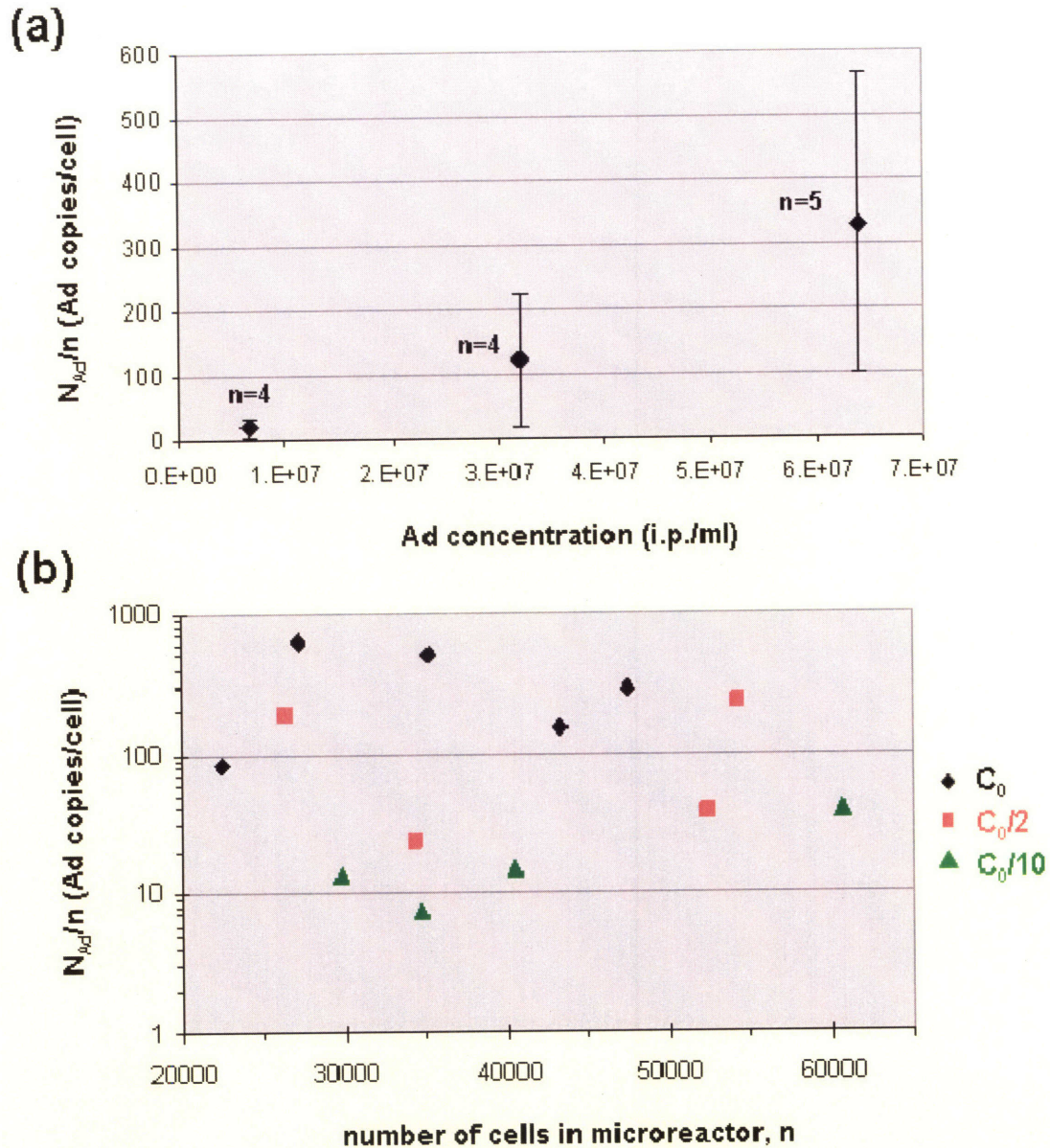


**Figure 5.4.** Quantification of Ad vector uptake in hepatocyte microreactor cultures with real-time PCR. Microreactor cultures were infected with Ad at three concentrations ( $C_0$ ,  $C_0/2$  and  $C_0/10$ , where  $C_0=6.4 \times 10^7$  i.p./ml) for 24h. The cells were harvested ~70h after Ad infection for DNA extraction. Total DNA content was measured with the Rediplate 96 PicoGreen DNA Quantification Kit. The number of Ad genome copies was quantified with real-time TaqMan PCR. **(a)** This graph shows the number of Ad copies normalized to cell number and plotted against Ad concentration. All data points represent the mean values of two experiments (different rat liver perfusions) performed in duplicate or triplicate  $\pm$  the standard deviation of the mean. **(b)** This graph shows the number of Ad copies normalized to cell number and plotted against the total cell number, n. Each data point corresponds to one of the microreactor samples shown in graph (a).

(Ad copies/cell) for the individual microreactor samples were also plotted (on a logarithmic scale) against the total cell number (Figure 5.4b). Each data point corresponds to a different microreactor sample. By examining each group of data corresponding to a different initial Ad concentration separately, it appears that, overall, the distribution of data is random and does not follow any particular trend. For example, if the Ad uptake rate constant  $k_{3D}$  was equal to the lower limit (all cells exposed to Ad), the normalized Ad uptake would be expected to increase with cell number. This is observed in the low Ad concentration group, but not in the other 2 groups. If  $k_{3D}$  was equal to the upper limit (only cells at tissue-medium interface exposed to Ad), the Ad uptake would be expected to decrease with increasing cell number. Higher cell number in the microreactor channels means smaller surface area,  $A$ , exposed to the Ad vector. Such a trend is not obvious in any data group either. Therefore, the actual value of  $k_{3D}$  probably corresponds to an intermediate state, where the hepatocytes at the tissue-medium interface are exposed to higher Ad concentration levels than the cells deeper in the tissue.

**Estimation of lower limit for the Ad uptake constant,  $k_{3D,L}$ :** Figure 5.5a shows a plot of  $N_{Ad}/n$  as a function of the initial concentration  $C_0$ . Equation (5) was used to fit  $k_{3D,L}$  to the experimental data described above. All data points represent the mean values of 4 or 5 microreactor samples from two experiments (different rat liver perfusions) and the error bars correspond to the standard deviation of the mean. The solid line corresponds to the linear least squares regression performed in Excel. The rate constant value calculated from the slope is:

$$k_{3D,L} = 0.0076 \text{ cm/s}$$

**Estimation of upper limit for the Ad uptake constant,  $k_{3D,U}$ :** Figure 5.5b shows a plot of  $N_{Ad}/A$  as a function of the initial concentration  $C_0$ . Equation (6) was used to fit  $k_{3D,U}$  to the experimental data described above. The average cell number per microreactor in these experiments was  $n=40,000$ . This corresponds to a cylinder radius  $R=85\mu\text{m}$  and a total surface area  $A=0.05\text{cm}^2$ . All data points represent the mean values of 4 or 5 microreactor samples from two experiments (different rat liver perfusions) and the error bars correspond to the standard deviation of the mean. The solid line corresponds to the linear least squares regression performed in Excel. The rate constant calculated from the slope is:

$$k_{3D,U} = 0.204 \text{ cm/s}$$



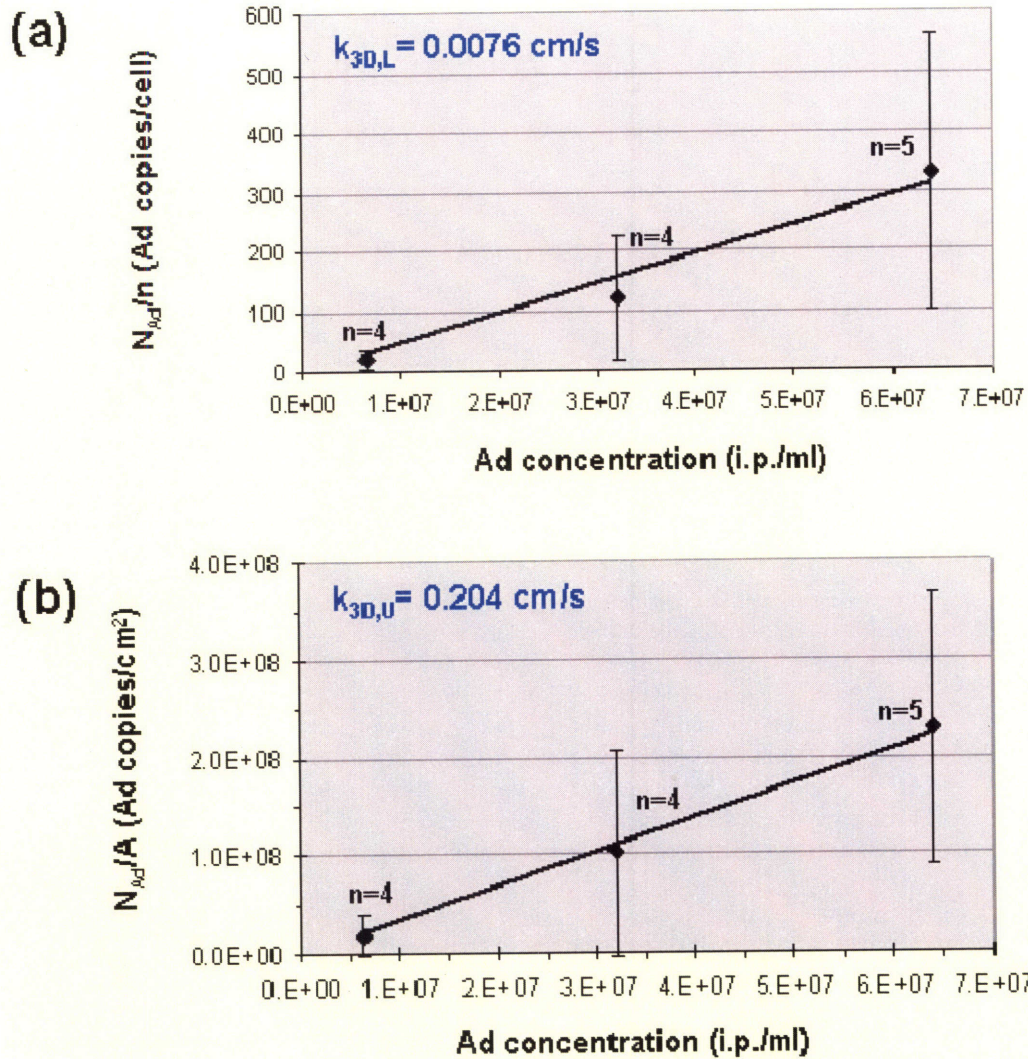


**Figure 5.5.** Mathematical model correlation to the experimental results for Ad vector uptake in hepatocyte microreactor cultures. **(a)** Lower boundary for the Ad uptake rate constant  $k_{3D,L}$ . Equation (5) was used to fit  $k_{3D,L}$  to the experimental data described in Figure 5.4. The graph shows the number of Ad copies ( $N_{Ad}$ ) normalized to cell number ( $n$ ) and plotted against the Ad concentration  $C_0$ . **(b)** Upper boundary for the Ad uptake rate constant  $k_{3D,U}$ . Equation (6) was used to fit  $k_{3D,U}$  to the experimental data. The graph shows the number of Ad copies ( $N_{Ad}$ ) normalized to the tissue area exposed to the Ad vector ( $A$ ) and plotted against the Ad concentration  $C_0$ . All data points represent the mean values of two experiments (different rat liver perfusions) performed in duplicate or triplicate  $\pm$  the standard deviation of the mean. The solid lines represent the mathematical model correlation performed with linear least squares regression in Excel.

A similar uptake rate constant value is obtained if a different value of A is calculated for each microreactor.

In conclusion, although the exact value of the Ad uptake rate constant in hepatocyte microreactor cultures,  $k_{3D}$ , could not be estimated, a simplified mathematical model was developed based on qualitative and quantitative experimental data to determine its lower and upper boundaries:

$$\mathbf{0.0076\text{ cm/s} < k_{3D} < 0.204\text{ cm/s}}$$

$k_{3D}$  lies within a range of approximately one order of magnitude. The efficiency of Ad uptake in the microreactor cultures appears significantly higher than in the hepatocyte monolayer cultures, since  $k_{3D}$  is at least three orders of magnitude higher than  $k_{2D}$  (estimated as  $\sim 10^{-5}$  cm/s).

## 5.3 Transgene (EGFP) Expression

As described in Section 4.3, the levels of expression of the transgene (*egfp*) transferred into the target cells by the vector (Ad) are what ultimately determines the efficiency of gene delivery. In the experiments presented in this section gene expression was quantified as a function of the initial Ad concentration in the medium. EGFP expression was detected and monitored with time with a miniaturized spectrometer system especially designed for the microreactor cultures, and quantified in terms of fluorescence intensity levels. As in the case of the hepatocyte monolayer cultures, quantitative real-time RT-PCR was applied to measure the EGFP mRNA levels. Additionally, EGFP protein was detected with a fluorescence microscopy technique, in particular two-photon scanning fluorescence microscopy, and gene delivery efficiency was quantified in terms of the percentage of EGFP-expressing cells. These measurements were made approximately 70 hours after the Ad infection, when EGFP expression reaches maximum levels in the microreactor cultures.

### ***5.3.1 Quantification of EGFP expression with the Miniaturized Spectrometer System***

The design and principle of operation of the spectrometer system have been described in detail in Chapter 3 (section 3.7). Briefly, the EGFP protein produced in the hepatocytes cultured inside the silicon scaffold channels is excited by a light beam passing through the microreactor. The emission spectrum is detected by a fiber optic spectrometer and recorded at different time points after the beginning of Ad infection. The spectral data are processed with special software. The spectrum intensity at 509nm is used as a measure of EGFP expression levels to plot the time course of expression. As shown in Chapter 3, in microreactor cultures EGFP expression reaches maximum levels around 50-70h after the beginning of Ad infection and then gradually declines.

In the experiments described earlier in this chapter (section 5.2) EGFP expression was monitored with the spectrometer until  $t \sim 70$ h when the hepatocytes were harvested for DNA extraction. Total DNA content for each microreactor was measured with the Rediplate 96 PicoGreen DNA Quantification Assay and converted to cell number. The spectrometer data were normalized against cell number. Figure 5.6 shows a graph of the normalized EGFP emission intensity at  $t \sim 70$ h (counts/cell) plotted as a function of Ad concentration (i.p./ml). All



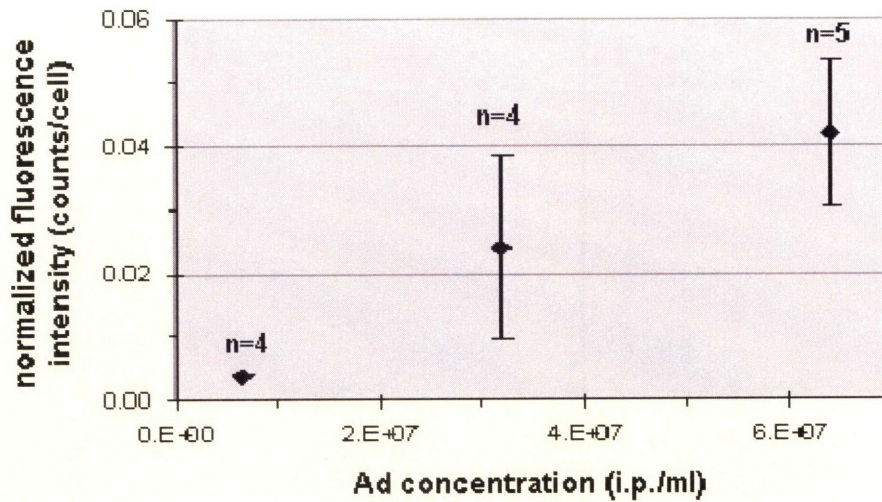


**Figure 5.6.** Quantification of EGFP expression levels in microreactor cultures with the spectrometer system. Microreactor cultures were infected with Ad at three concentrations ( $C_0$ ,  $C_0/2$  and  $C_0/10$ , where  $C_0=6.4 \times 10^7$  i.p./ml) for 24h. The change in EGFP expression with time was monitored by measuring fluorescence emission with the spectrometer. The cells were harvested after the last measurement (~70h) for DNA extraction. Total DNA content was measured with the Rediplate 96 PicoGreen DNA Quantification Assay and converted to cell number. This graph shows fluorescence emission intensity at ~70h after Ad infection normalized to cell number and plotted against Ad concentration. All data points represent the mean values of 4-5 microreactor samples from two experiments (different rat liver perfusions)  $\pm$  the standard deviation of the mean.

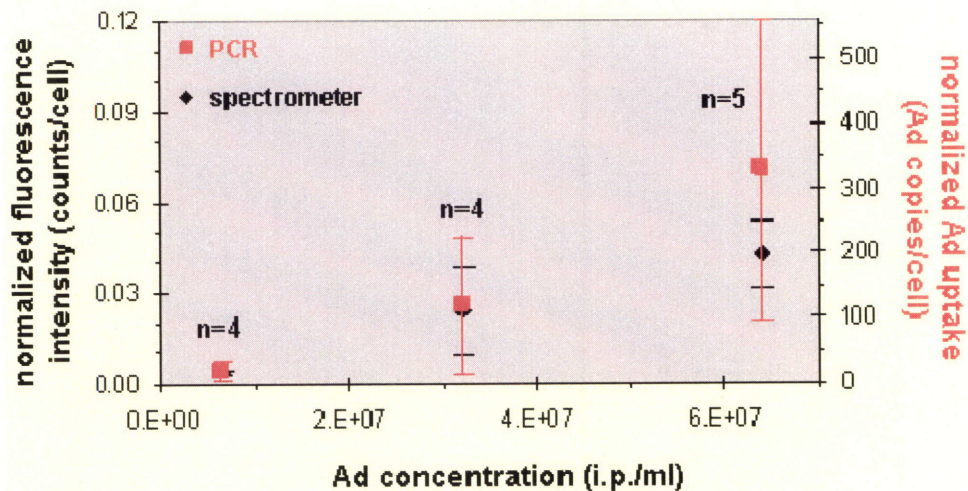


**Figure 5.7.** Comparison of the dependence of EGFP expression and Ad vector uptake on Ad concentration. This graph shows the normalized EGFP fluorescence intensity data at t~70h (Figure 5.6) and the normalized Ad copy number data (Figure 5.4a) quantified with the spectrometer and PCR respectively, and plotted against the Ad concentration. All data points represent the mean values of 4-5 samples  $\pm$  the standard deviation of the mean.



data points represent the mean values of 4-5 microreactor samples from two experiments (different rat liver perfusions) and the error bars correspond to the standard deviation of the mean. The graph indicates that protein expression increased linearly with Ad concentration.

Figure 5.7 shows a comparison of these results to the Ad uptake data obtained with real-time PCR for the same microreactor samples (Section 5.2, Figure 5.4a). The two sets of data are plotted on two differently scaled y-axes in order to compare their relative dependence on Ad concentration. The graph indicates that the increase in Ad vector uptake with Ad concentration correlates with the increase in EGFP expression.

### **5.3.2 Quantification of EGFP mRNA Levels with Real-Time TaqMan RT-PCR.**

The same procedures for Ad infection in microreactor cultures as described earlier were followed in this experiment as well. Hepatocyte cultures were infected with AdEGFP at three different concentrations ( $C_0$ ,  $C_0/2$  and  $C_0/10$ , where  $C_0 = 6.4 \times 10^7$  i.p./ml) for 24 hours. Duplicate samples were prepared for each condition. The change in EGFP expression with time was followed with spectrophotometer measurements. The cells were harvested in Trizol Reagent for RNA extraction at approximately  $t=70$ h (time point of maximum EGFP expression attained). RNA was isolated and purified, and the total RNA content of each sample was measured. The same amount of RNA (200 ng) was used for all reverse transcription reactions. The quantity of cDNA sample amplified in each PCR reaction corresponded to 1 ng input total RNA. For each sample the target gene (EGFP), as well as an endogenous reference gene (18S rRNA) were amplified with quantitative real-time TaqMan PCR. The results were analyzed with the Comparative  $C_T$  Method, which calculates the EGFP mRNA levels normalized to 18S and relative to a calibrator. Additionally, the data were analyzed with the Standard Curve method to determine the number of EGFP cDNA copies present in each sample; in that case EGFP expression was normalized to the amount of total RNA. All experimental procedures and data analysis methods are described in detail in Chapter 3 (sections 3.5 and 3.6).

Control microreactor cultures that were not infected with Ad showed no PCR amplification. The minus RT controls for the Ad-infected samples (in which the reverse transcriptase is omitted from the RT reaction) tested negative as well.

Similar results were obtained with both data analysis methods. Figure 5.8 shows the EGFP mRNA levels normalized against total RNA calculated with the Standard Curve Method. EGFP expression (cDNA copies per ng total RNA) is plotted against initial Ad concentration.

Each data point represents the mean value of two samples. The error bars correspond to the difference from the mean. The results show a clear trend of increasing levels of EGFP expression with increasing Ad concentration. This is in agreement with the trend observed in the Ad vector uptake measurements (Figure 5.4a).

The ratio of mRNA levels divided by the intracellular Ad levels was calculated as a measure of transgene expression efficiency relative to Ad uptake, a quantity that will be a basis for comparison with the gene delivery results in the hepatocyte monolayer cultures (presented in Chapter 4). The data presented in Figure 5.8 were converted to cDNA copies per cell with the conversion factor determined in Section 3.5 and then divided with the respective Ad uptake data presented in Figure 5.4a (Ad genomic copies per cell). The results are shown in Figure 5.9. All data points represent the ratio of the mean values. The error bars represent the standard deviation of the quotient calculated with Equation 10 of Chapter 4. The microreactor culture results for EGFP expression, Ad uptake and their ratio for the three Ad vector concentrations used in this experiment are also summarized in Table 5.2:

**Table 5.2:** EGFP expression efficiency relative to Ad vector uptake in microreactor cultures.

<b>Initial Ad concentration (i.p./ml)</b>	<b>EGFP expression (cDNA copies/cell) n=2</b>	<b>Ad uptake (Ad copies/cell) n=5</b>	<b>EGFP expression/ Ad uptake (cDNA/Ad copies)</b>
<b>6.4x10<sup>7</sup></b>	(6.08 ± 0.52) x10 <sup>11</sup>	330.3 ± 231.6	(1.84 ± 1.30) x10 <sup>9</sup>
<b>3.2x10<sup>7</sup></b>	(5.23 ± 0.03) x10 <sup>11</sup>	120.5 ± 104.9	(4.34 ± 3.77) x10 <sup>9</sup>
<b>6.4x10<sup>6</sup></b>	(7.2 ± 0.4) x10 <sup>10</sup>	18.8 ± 14.3*	(3.82 ± 2.92) x10 <sup>9</sup>

\*n=4

The microreactor cultures that were infected with the highest concentration of Ad, display lower levels of relative EGFP expression, although the experimental error introduced by the variability in Ad uptake data is rather large and the difference does not appear significant. The average value of EGFP expression relative to Ad uptake for the microreactor cultures is 3.3x10<sup>9</sup> mRNA copies per Ad genomic copy with a standard deviation of 1.3x10<sup>9</sup>.

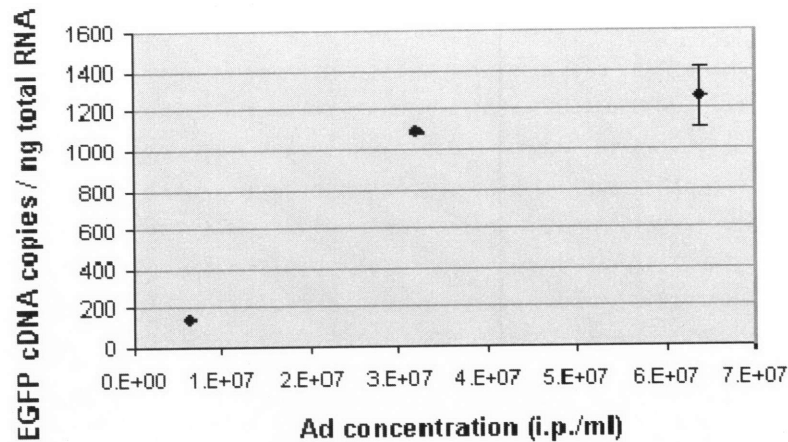


**Figure 5.8.** Quantification of EGFP mRNA levels after AdEGFP infection in hepatocyte microreactor cultures with real-time RT-PCR. Microreactor cultures were infected with Ad at three concentrations ( $C_0$ ,  $C_0/2$  and  $C_0/10$ , where  $C_0=6.4 \times 10^7$  i.p./ml) for 24h. Duplicate samples were prepared for each condition. The cells were harvested 70h after Ad infection for RNA extraction. Total RNA content was measured with the Rediplate 96 RiboGreen RNA Quantification Kit. 200ng RNA were used for cDNA synthesis by reverse transcription. The EGFP cDNA was quantified with real-time TaqMan PCR (1ng input total RNA per reaction). The data were analyzed with the Standard Curve Method. Standards were prepared from serial dilutions of Ad genomic DNA. The number of EGFP cDNA copies present in each sample (corresponding to 1 ng input total RNA) were determined from the standard curve with interpolation. This graph shows the EGFP expression levels normalized to total RNA plotted against Ad concentration. All data points represent the mean values of two samples  $\pm$  the error.

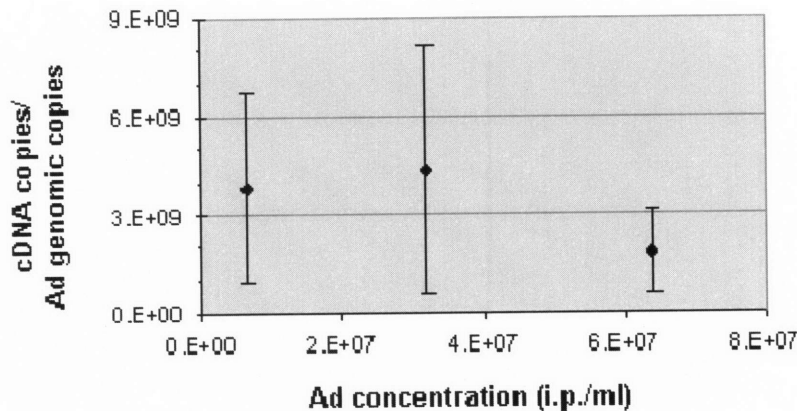


**Figure 5.9.** EGFP expression efficiency relative to Ad vector uptake in microreactor cultures. The data presented in Figure 5.8 were converted to cDNA copies per cell and were normalized against the Ad vector uptake data (Ad genomic copies/cell) presented in Figure 5.4a. All data points represent the ratio of the mean values and the error bars correspond to the standard deviation of the quotient.

### Comparison with spectrometer data (mRNA levels vs protein levels)

EGFP expression in the microreactor cultures that were subjected to RT-PCR, was also monitored with the spectrometer from the beginning of Ad infection ( $t=0$ ) until  $t\sim 70$ h, when the cells were harvested for RNA extraction. At that time EGFP expression had reached maximum levels. Figure 5.10 shows the fluorescence emission intensity normalized against cell number (determined from the total RNA measurements and the conversion factor calculated in section 3.5) plotted as a function of time after Ad infection. All data points represent the mean values of two microreactor samples. The error bars correspond to the difference from the mean. The spectrometer results at  $t\sim 70$ h (normalized fluorescence intensity) are compared with the RT-PCR results (normalized mRNA levels) in Figure 5.11. The two sets of data are plotted against Ad concentration on two differently scaled y-axes, in order to compare the relative increase of expression with Ad concentration. The graph indicates that the two measurements are in agreement and that the dependence of EGFP mRNA levels (transcription) on the Ad concentration correlates with that of EGFP protein levels (translation).

### ***5.3.3 Quantification of AdEGFP Gene Delivery Efficiency and Cell Viability with 2-photon microscopy***

The application of two-photon microscopy for the detection of EGFP expression in microreactor cultures was demonstrated earlier in this chapter (section 5.2). Two-photon imaging data were used to extract information about the tissue morphology as well as the Ad infection inside the microreactor channels (quantitative analysis of the spatial distribution of EGFP-expressing hepatocytes), in order to develop a mathematical model and estimate the Ad uptake rate constant. In the experiment presented in this section, two-photon imaging was applied to quantify Ad gene delivery efficiency and cell viability as a function of the initial Ad concentration in the circulating medium. Gene delivery efficiency was measured as the percentage of EGFP-expressing cells and cell viability as the percentage of live cells.

Microreactor cultures were infected with AdEGFP for 24h at three different concentrations  $4\times 10^5$ ,  $2\times 10^6$  and  $4\times 10^6$  pfu/ml. (Note: these values are based on the infectious titer of the Ad preparation as measured by the vector supplier.); control samples were not infected with Ad. Duplicate samples were prepared for each condition. The cells were stained with Ethidium Homodimer 1 and Hoechst 33342 approximately 70h after the beginning of the Ad

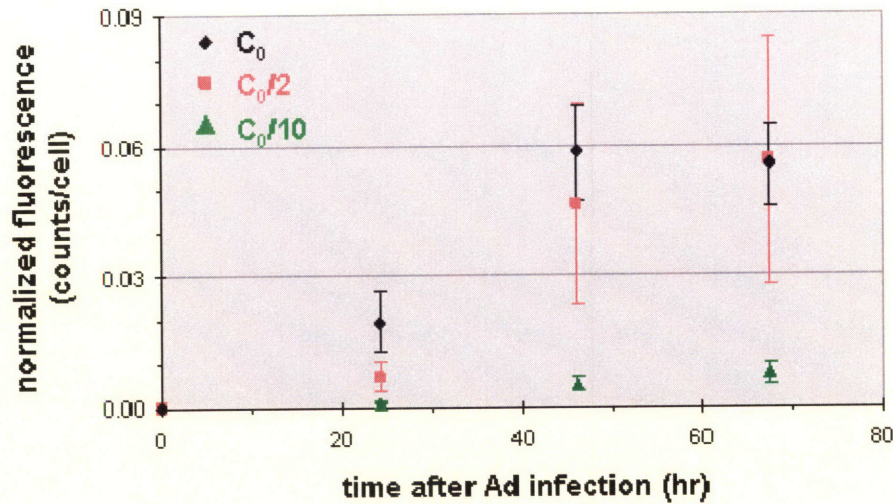


**Figure 5.10.** Quantification of EGFP expression levels with spectrometer measurements for the microreactor cultures presented in Figures 5.8 and 5.9. The change in EGFP expression with time was monitored by measuring fluorescence emission with the miniaturized spectrometer. The cells were harvested after the last measurement (~70h) for RNA extraction. Total RNA content was measured with the Rediplate 96 RiboGreen RNA Quantification Kit and converted to cell number. This graph shows the fluorescence emission levels normalized to cell number and plotted against time  $t$  after Ad infection. All data points represent the mean values of two samples  $\pm$  the error.

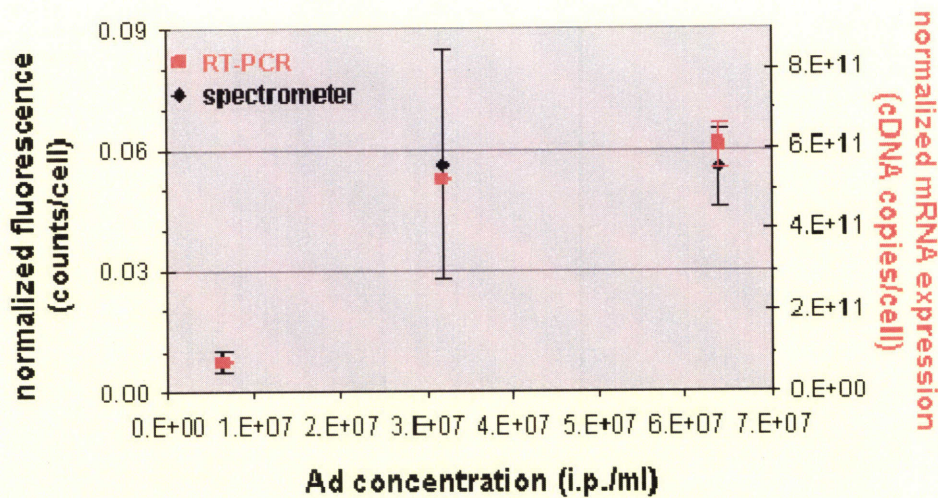


**Figure 5.11.** Comparison of EGFP expression measurements with the spectrometer and RT-PCR methods. This graph shows the normalized EGFP fluorescence emission data at  $t$ -70h (black diamonds, left y-axis) and the normalized EGFP mRNA expression data (red squares, right y-axis) quantified with the spectrometer and RT-PCR respectively, and plotted against the Ad concentration. All data points represent the mean values of two samples  $\pm$  the error.

infection and imaged with a two-photon laser scanning fluorescence microscope. During imaging the microreactors were connected to a portable environmental control system to maintain the temperature and pH at physiological levels. Images were acquired from three different channels in each microreactor. The two-photon imaging data were processed and analyzed with the MetaMorph software. To quantify the percentage of EGFP-expressing cells and live cells in each imaged channel, the total number of live cells was determined by counting the Hoechst-stained nuclei, the number of dead cells by counting the Ethidium Homodimer-stained nuclei and Ad infected cells by counting the number of green fluorescent cells. All experimental procedures and data analysis methods are described in detail in Section 3.8.3.

The two-photon experiments were performed with a different batch of adenoviral vector, therefore the real infectious titer was not known. As explained in Chapter 4 (section 4.1.3) the actual infectious titer can be different (higher) from the one measured with the plaque forming assay by the vector supplier. To determine the actual infectious Ad concentration in the medium circulation, the Ad vector uptake was also measured in these microreactors. After imaging, the hepatocytes were harvested for DNA extraction. The total DNA content of each sample was measured with the RediPlate 96 PicoGreen DNA Quantification Assay and the number of Ad genomic copies was quantified with real-time TaqMan PCR. The normalized Ad uptake (Ad genomic copies per cell) was calculated for each microreactor and the mean values of the duplicate samples are shown in Table 5.3. The real Ad concentration was then estimated from the graph in Figure 5.5a with interpolation. The uptake levels for the lowest Ad concentration (which are within the linear range) correspond to  $\sim 2 \times 10^7$  i.p./ml; this value is significantly higher than the vector supplier's measurement but still lower than the genomic titer ( $2.56 \times 10^7$  p/ml).

**Table 5.3:** Infectious Ad concentration determined from Ad vector uptake data.

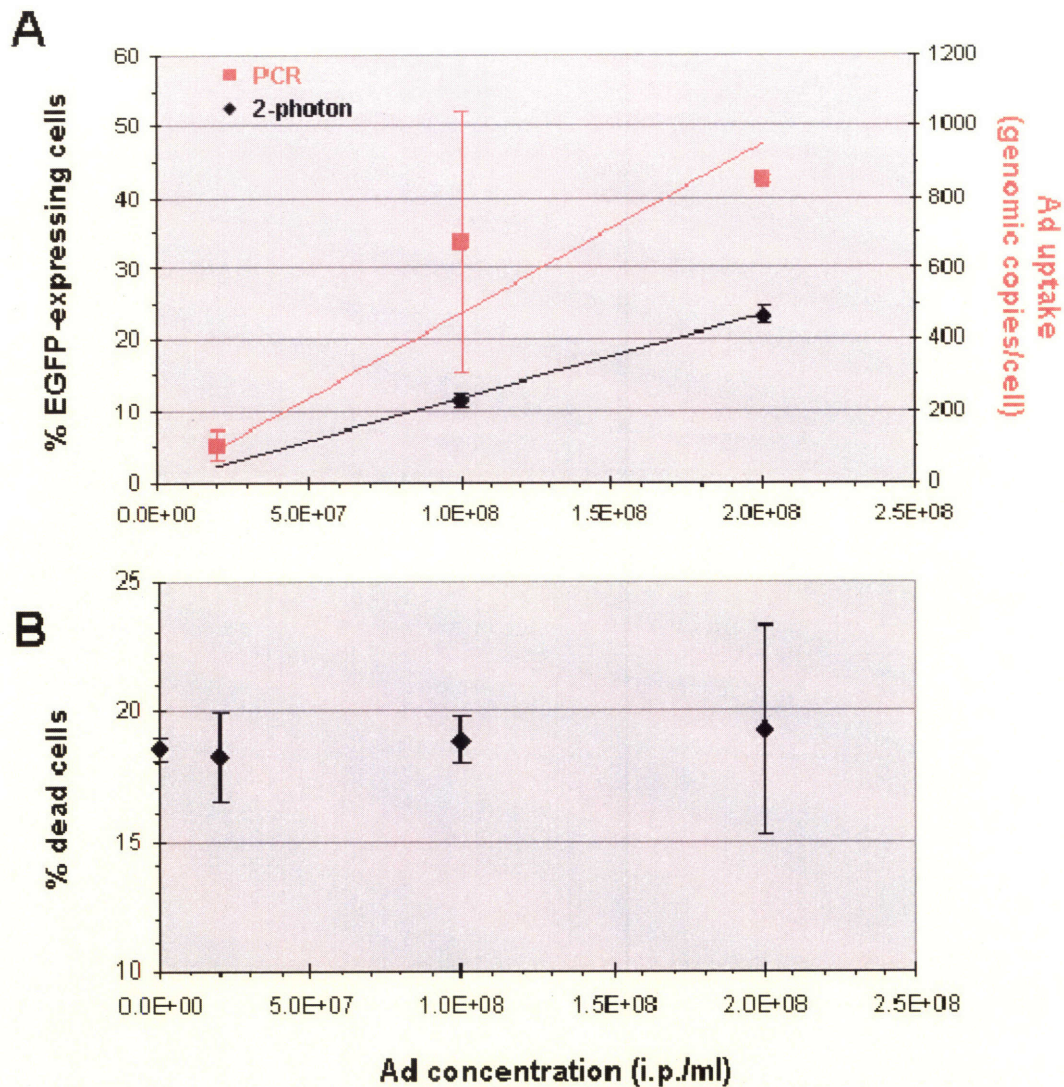
<b>initial Ad concentration according to supplier's titer (pfu/ml)</b>	<b>Ad uptake (Ad copies/cell) n=2</b>	<b>initial Ad concentration calculated from Figure 5.6 with interpolation (i.p./ml)</b>
<b><math>4 \times 10^5</math></b>	$103.4 \pm 43.4$	$2 \times 10^7$
<b><math>2 \times 10^6</math></b>	$672.6 \pm 367.7$	$1 \times 10^8$
<b><math>4 \times 10^6</math></b>	$849.5 \pm 11.6$	$2 \times 10^8$



Figure 5.12 shows the Ad gene delivery efficiency (% EGFP-expressing cells) and cytotoxicity (% dead cells) in microreactors, quantified with two-photon microscopy and plotted as a function of the initial Ad concentration in the medium. In graph A the 2-photon data are plotted together with the normalized Ad uptake results obtained with real-time PCR. The two sets of data are plotted in differently scaled y-axes to compare the relative change with Ad concentration. The percentage of EGFP-expressing cells increased linearly as did the number of internalized Ad copies per cell. However, for an increase in concentration of one order of magnitude, Ad uptake increased twice as much as the number of EGFP-expressing cells. This difference indicates that as the Ad concentration increases, the number of Ad infected cells with detectable levels of transgene expression increases as well as the number of internalized Ad particles in each infected cell. Cell viability was not affected by the Ad infection and remained at levels similar to the control cultures for the range of Ad concentration values studied (Graph B).

These results show the ability to quantify gene delivery efficiency in the three-dimensional microreactor cultures with two-photon microscopy. However, they cannot be compared with the respective results in monolayer hepatocyte cultures (Section 4.2.1) because they are obtained with different imaging methods and instruments. In both cases the quantification of the number of EGFP-positive cells depends on the threshold above which fluorescence emission can be detected, which is determined by the optics configuration and the detection system of each instrument. Additionally, in the microreactor there is loss of emission intensity with increasing sample depth, which affects the outcome of these measurements. Therefore, comparative analysis can only be performed when studying the efficiency of different gene delivery vectors.





**Figure 5.12.** Quantification of Ad gene delivery efficiency and cell viability in liver microreactor cultures with two-photon microscopy. The cultures were incubated with AdEGFP at three concentrations ( $C_0$ ,  $C_0/2$  and  $C_0/10$ , where  $C_0=2 \times 10^8$  i.p./ml) for 24hr. Duplicate samples were prepared for each condition. Approximately 70h after the beginning of Ad infection the cells were counterstained with Hoechst 33342 and Ethidium Homodimer-1 for imaging. Images were acquired from 3 different channels in each microreactor. The number of live cells was determined by the count of Hoechst-stained nuclei, the number of dead cells by the count of Ethidium-stained nuclei and the number of EGFP-expressing cells by the count of green fluorescent cells. **Graph A** shows the % EGFP-expressing cells (as well as the normalized Ad vector uptake) plotted against the initial Ad concentration. **Graph B** shows the % dead cells plotted against the initial Ad concentration. All data points represent the mean values of two microreactors  $\pm$  the difference from the mean.

# **CHAPTER 6**

## **Conclusions and Future Directions**

## 6.1 Summary of Results - Conclusions

In vitro systems currently used for gene delivery experiments often fail to reliably predict in vivo responses to gene delivery vectors, a phenomenon that to large extent could be the result of the inability to recreate key features of the in vivo environment.

The main objective of this thesis was to compare the gene delivery efficiency of an adenoviral vector (Ad5-CMV-EGFP) in standard 2D hepatocyte culture and in the Tissue-Engineered Liver Microreactor. The latter is a culture system designed to facilitate the morphogenesis of three-dimensional tissue-like structures from isolated liver cells under continuous perfusion and maintain cell viability and hepatic functionality for long-term culture periods. Quantitative assays were developed based on Real-Time PCR and RT-PCR to measure the levels of Ad vector uptake and transgene expression. Additionally, the Ad mass transport was mathematically modeled in both systems to estimate the Ad uptake constant as a basis for comparison of delivery efficiency. This parameter was found to be significantly higher in the microreactor system (about three orders of magnitude), suggesting a more efficient mechanism of Ad internalization.

Research studies in the past few years have shown that Ad uses different mechanisms to infect hepatocytes in vitro and in vivo. In vitro, Ad binds to the cells via the CAR receptor and is internalized via interactions with integrins. In vivo however Ad utilizes a different pathway. Evidence suggests that interactions with HSPG (heparan sulfate proteoglycans) enable liver transduction (Smith et al., 2003, Alemany and Curiel, 2001; Martin et al., 2003; Smith et al., 2002). Recent work has found that in vivo CAR is localized at the junctions between hepatocytes (lateral surface) and is not accessible to hepatic blood flow. Therefore the difference in Ad uptake efficiency we observed between the two in vitro systems could be the result of these different mechanisms of Ad uptake. However, there is no information at this point to indicate whether the Ad-HSPG interaction is more efficient than the Ad-CAR interaction.

Gene expression was measured in terms of transgene mRNA levels. The ratio of gene expression relative to Ad uptake was estimated as the basis for comparison of vector transcription efficiency. No significant difference was found between the 2 systems (ratios within the same order of magnitude) although experimental errors were relatively high probably due to the nature of the reverse transcription process. A more sensitive and accurate RT-PCR protocol is required to detect possible differences (or trends as a function of initial Ad concentration and/or duration of infection). These experiments provide some evidence that a more

physiological culture system can provide different information (potentially more relevant to the in vivo situation) compared to standard in vitro culture.

## **6.2 The Liver Microreactor as an In Vitro Assay for Gene Delivery**

The Tissue-Engineered Liver Microreactor is a promising platform for developing an alternative in vitro assay for gene delivery. It enables the formation of 3D perfused hepatic structures that resemble those of in vivo liver tissue and exhibit enhanced and sustained functional responses. Additionally its design allows the application of microscopy and spectroscopy for repeated in situ observation. Based on this characteristic, two assays were developed in this thesis for detection and quantification of gene delivery. The custom-designed spectrometer assay provides a means for non-invasively tracking the time course and levels of reporter gene expression by measuring fluorescence emitted by the cells cultured in the microreactor channels. This technique provides a convenient platform for comparative analysis of different vectors. The two-photon fluorescence scanning microscopy assay can be applied for detailed imaging of the hepatic tissue structures with 3-dimensional resolution. Combined with an environmental control system that maintains the temperature and pH at physiological levels this assay can be performed non-invasively to track the changes in transgene (EGFP) expression with time.

An important advantage of this system in comparison to standard hepatocyte culture is the maintenance of cell viability (for at least 3 weeks). Whereas monolayer hepatocyte culture deteriorates within a few days, long-term experiments can be performed in the microreactor. This aspect is of particular interest in cases where transgene expression following vector delivery is delayed (e.g. in the case of adeno-associated viral vectors).

The long-term maintenance of liver specific functions (such as the expression of hepatocyte-specific transcription factors) could be important in studying gene delivery vectors targeted to the liver via hepatocyte-specific promoters or receptors.

## 6.3 Future Directions

The difference observed in the efficiency of Ad gene delivery between the two in vitro systems poses an interesting question. Is there a mechanism of Ad internalization different than the CAR interaction involved in the case of the liver microreactor system? A potential approach to this question would be to determine the distribution of CAR in the tissue structures in the microreactor channels and whether it mimics that of in vivo tissue. Additionally, gene delivery experiments using an Ad vector with CAR ablation mutations could provide an answer. If hepatocyte transduction is not eliminated then another mechanism is involved.

The set of assays developed in this thesis provide a convenient platform for gene delivery studies comparing the efficiency of various vectors. Moreover, the advances in 2-photon imaging technology will facilitate the application of this technique and enable the development of more efficient protocols.

## 6.4 References

Alemanly, R. and Curiel D.T. (2001). CAR-binding ablation does not change biodistribution and toxicity of adenoviral vectors. *Gene Therapy*. **8**:1347–1353.

Au, T., Thorne, S., Korm, W.M., Sze, D., Kirn, D., Reid, T.R. (2007). Minimal hepatic toxicity of Onyx-015: spatial restriction of coxsackie-adenoviral receptor in normal liver, *Cancer Gene Therapy* **14**, 139–150.

Martin, K., A. Brie, P. Saulnier, M. Perricaudet, P. Yeh, and E. Vigne. 2003. Simultaneous CAR- and  $\alpha_V$  integrin-binding ablation fails to reduce Ad5 liver tropism. *Molecular Therapy* **8**:485–494.

Smith, T., N. Idamakanti, H. Kylefjord, M. Rollence, L. King, M. Kaloss, M. Kaleko, and S. C. Stevenson. 2002. In vivo hepatic adenoviral gene delivery occurs independently of the coxsackievirus-adenovirus receptor. *Molecular Therapy* **5**: 770–779.

Smith, T. A., N. Idamakanti, M. L. Rollence, J. Marshall-Neff, J. Kim, K. Mulgrew, G. R. Nemerow, M. Kaleko, and S. C. Stevenson. 2003. Adenovirus serotype 5 fiber shaft influences in vivo gene transfer in mice. *Human Gene Therapy*. **14**: 777–787.